DISSERTATION

NONSTATIONARY FLOOD RISK ASSESSMENT IN COASTAL REGIONS UNDER CLIMATE CHANGE

Submitted by

Mahshid Ghanbari

Department of Civil and Environmental Engineering

In partial fulfillment of the requirements

For the Degree of Doctor of Philosophy

Colorado State University

Fort Collins, Colorado

Spring 2021

Doctoral Committee:

Advisor: Mazdak Arabi

Robert Ettema
Russ Schumacher
Aditi Bhaskar

ABSTRACT

NONSTATIONARY FLOOD RISK ASSESSMENT IN COASTAL REGIONS UNDER CLIMATE CHANGE

Coastal cities are exposed to multiple flood drivers including high tide, storm surge, extreme rainfall, and high river flows. The occurrence of these flood drivers, either in isolation or in combination, can cause significant risk to property and human life. Climate change is placing greater pressure on coastal communities by increasing frequency and intensity of flood events through sea level rise (SLR) and more extreme rainfall and storm events. Therefore, effective adaptation strategies are essential to reduce future flood risk in exposed communities. The planning and implementation of effective adaptation strategies require a comprehensive understanding of future flood hazards and risks under future climate conditions and adaptation options.

The overarching goal of this dissertation is to improve the capacity to understand, estimate and mitigate future flood hazards and risks in coastal areas under uncertain climate change. To achieve this goal, first, a nonstationary mixture probability model was developed that enables simultaneous characterization of minor and major flood events under future sea level conditions. The probability model was used to estimate minor and major flooding frequency at 68 locations along the coasts of the Contiguous United States (CONUS). The results showed a significant increase in frequency of both minor and major flood events under future sea level conditions. However, the frequency amplification of minor and major flooding varied by coastal regions.

While regions in the Pacific and southeast Atlantic coast are likely to be exposed to higher frequency amplification in major flooding, the Gulf and northeast Atlantic coastal regions should expect the highest minor flood frequency amplification.

Second, the proposed mixture probability model was employed in a flood risk assessment framework to enable assessing future acute and chronic coastal flood risks under different SLR and adaptation levels. The HAZUS-MH flood loss estimation tool was used to estimate property damage. The application of the framework in Miami-Dade County revealed that as sea level rises, chronic risks from repetitive nonextreme flooding may exceed acute risks from extreme floods. Third, a nonstationary bivariate flood hazard assessment method was developed that enables estimation of future frequency of compound coastal-riverine flooding with consideration of impacts of climate change including SLR and variations in extreme river flows. The proposed method was employed at 26 paired tidal-riverine stations along the CONUS coast. Specifically, the joint return period of compound major coastal-riverine flooding, defined based on flood impact thresholds, was explored by mid-century. The results showed that under current climate conditions the northeast Atlantic and western part of the Gulf coasts are exposed to the highest compound major coastal-riverine flood probability. However, considering future SLR, emerging high compound major flooding probability was evident in the southeast Atlantic coast. The impact of changes in extreme river flows was found to be negligible in most of the locations. Finally, four stormwater intervention scenarios including gray (i.e., conventional centralized conveyance systems and water treatment plants) and green (i.e., decentralized infiltration measures) infrastructure systems, were assessed in New York City (NYC). The results revealed that in developed and urbanized cities like NYC, green systems should not be considered as a substitute for gray systems. Complementary benefits on flood and combined sewer outflow (CSO) reduction can be gained through integration of green and gray systems.

ACKNOWLEDGMENTS

First and foremost I would like to thank my advisor, Dr. Mazdak Arabi, for his dedicated support and guidance. Dr. Arabi continuously provided encouragement and was always willing and enthusiastic to assist in any way he could throughout the completion of my dissertation. I would also like to acknowledge and thank my committee members, Dr. Robert Ettema, Dr. Russ Schumacher, and Dr. Aditi Bhaskar, for their helpful and insightful comments. I also need to express my immense gratitude to Dr. Jayantha Obeysekera and Dr. William Sweet for always being available for help and for being such great sources of information and advice. I also would like to add my special thank to Dr. Jorge Ramirez, who is no longer with us but his memory will always be in my heart.

Without years of funding and support from National Science Foundation Grant No. 1444758 as part of the Urban Water Innovation Network (UWIN) the work presented in this dissertation would have not been possible. I would also like to thank my parents who have tirelessly supported my educational endeavors and thank them for the sacrifices they made so that I could be where I am today. I also would like to thank my friends for all of their support. And last but not least, I have to thank the love of my life, my husband Soheil, for standing by me and helping me accomplish this chapter of my life. Without his unconditional support and encouragement, this dissertation would not have been accomplished.

DEDICATION

To my husband, Soheil, and my parents for their unconditional love, constant support and encouragement.

TABLE OF CONTENTS

LIST OF TABLES

LIST OF FIGURES

CHAPTER 1.

INTRODUCTION

1.1. Research background

Floods are considered to be one of the most devastating and frequently occurring natural disasters responsible for significant annual economic losses, social and environmental damages, and loss of lives in the United States (NWS 2014; Walsh et al. 2014) and globally (Hallegatte et al. 2013; Hinkel et al. 2014). Coastal cities are more vulnerable to floods due to exposure to multiple flood drivers such as extreme coastal high tide, storm surge, and extreme rainfall and river flow (Lian et al. 2013; Moftakhari et al. 2017b). The occurrences of these flood drivers alone or in combination could cause significant damages and costs to coastal communities.

Climate change, which is leading to sea level rise (SLR) and extreme rainfall to increase, is putting greater pressure on coastal cities by increasing the frequency and intensity of flood events. Consequently, the annual damages caused by flooding events are becoming more extreme in recent decades (Hallegatte et al. 2011; Zheng et al. 2014). For example, extreme flooding in Houston and the surrounding area caused by Hurricane Harvey in August 2017, caused $125 billion in damage. Two more extreme floods caused by Hurricane Irma and Maria caused $140 billion in total damage in the same year. An extreme rainfall event that sparked extreme flooding in Maryland, in May 2018 caused a significant amount of damages (Link and Galloway 2019). The damages from tidal flooding (i.e., nuisance flooding) are also increasing across the United States (Jacobs et al. 2018; Moftakhari et al. 2017a). Thus, under climate change, a comprehensive nonstationary flood risk assessment is essential for management of flood risk by helping coastal planners and policymakers to understand future flood risk levels and their impacts.

SLR, which is one of the most perceivable effects of global warming is amplifying the frequency and intensity of coastal flooding (Rahmstorf and Coumou 2011) and is likely to exacerbate economic impacts of flooding due to increasing flood exposure in coastal cities (Nicholls and Tol 2006). Many coastal regions will be increasingly exposed to frequent tidal flooding as well as acute storm surge events as a result of SLR (Walsh et al., 2014; Ray & Foster, 2016). Thus, a coherent assessment of the chronic and acute impacts of SLR on coastal flooding is vital for the security of coastal communities.

SLR decreases the freeboard between local flood thresholds and high sea water levels (SWL) from tides and storm surges, which leads to increases in the frequency of both minor (Sweet et al., 2014; Moftakhari et al., 2015; Vandenberg-Rodes et al., 2016) and extreme flood events (Ezer and Atkinson, 2014; Kemp & Horton, 2013; Vousdoukas et al., 2017). Thus, in order to quantify coastal flooding risks under nonstationary sea-level conditions the effects of both frequent smaller high SWLs (i.e., minor flooding) and less frequent extreme SWLs (i.e., extreme flooding) must be reconciled. Development of effective adaptation strategies must take into account the cumulative losses from minor flooding as well as acute losses from major flooding. A challenge, however, is the inadequacy of widely used probability models in simultaneous characterization of both minor and major flooding under higher mean sea levels (MSL).

Various probabilistic methods are used in literature to characterize the likelihood of flooding under nonstationary conditions. Such as the nonstationary Generalized Extreme Value (GEV) distribution (Boettle et al. 2013; Menéndez and Woodworth 2010; Obeysekera et al. 2013; Salas and Obeysekera 2014) and generalized Pareto (GP) distribution (Méndez et al., 2006; Kyselý et al., 2010). However, using GEV and GP distribution only the tail of water level data can be characterized (Xu & Huang, 2008; Menéndez et al., 2008; Noto & La Loggia, 2009; Roth et al., 2012). As sea level rises, current local flood thresholds are likely to be exceeded more frequently during average high tides. Infrequent floodings which are mostly modeled by the upper tail of the sea-level distribution will become more frequent. Thus, in the absence of coastal adaptation measures, water level exceedances above the current coastal flood threshold cannot be characterized using models that characterize only the upper tail of the water level distribution. To address this gap, a statistically coherent mixture probability model is needed to characterize flood hazard under future SLR scenarios.

Flood hazard refers to the likelihood of a particular flood intensity at a specific site, whereas flood risk emerges from the interaction of flood hazard probability, exposed values, and their vulnerability (Crichton 1999; Merz et al. 2010). Thus, flood hazard probability is not the sole component of flood risk and information about exposure inventory (e.g., population, buildings, transport network, etc.), and the vulnerability of exposures to flooding hazards are also needed for estimating flood risk at a given location. It should be noted that the terms of "failure probability" (Moftakhari et al. 2017b) and "risk of failure" (Serinaldi 2015), which present the probability of observing at least one flooding event in a given design life are also used in literature for assessing flood risks.

Deployment of different flood adaptation strategies can alter elements of flood risk (Baxter 2013). For example, technical engineering measures such as forward pumps, sea walls, flood barriers, and levees lower flood probability. Other measures such as elevating houses and wet or dry flood proofing (Baxter 2013) can reduce flood risks by lowering the vulnerability of buildings (Kreibich et al. 2005; Kreibich and Thieken 2009). Although selecting the most efficient adaptation requires diligent planning, deployment of any of these measures ultimately leads to an increase in the SWL at which a community begins to flood (i.e., increase in the flood threshold).

Flood thresholds are established for many tide gauges and river stations in the U.S. by the National Oceanic and Atmospheric Administration (NOAA) (Sweet et al. 2018) and National Water Information System (NWIS) World Wide Web site (http://waterdata.usgs.gov/nwis) (NWS 2019), respectively. Flood categories based on exceedances over flood thresholds describe the severity of flood impact. Minor flooding refers to events with minimal or no property damage, moderate flooding is accompanied with some inundation of structures and roads and has relatively considerable damages to private and commercial property. As flood level increases to the major flood threshold, inundated area and infrastructure impact escalate significantly. Implementation of flood adaptation strategies enables societies to minimize the impact of flood events through increasing flood thresholds and reducing exposure or vulnerability.

Beside tidal flooding and storm surge events, coastal cities are exposed to heavy precipitation. The interaction among these flood drivers may cause a compound flood event (Moftakhari et al. 2017b; Wahl et al. 2015a) that could exacerbate flood impacts and cause huge social and economic losses (Hemmati et al. 2020; Zscheischler et al. 2018). The same meteorological system such as low atmospheric pressure and tropical cyclone can lead to storm surge and heavy precipitation events (Zheng et al. 2013, 2014). In regions where the flood level is influenced by both extreme sea levels (SLs) and rainfall, considering the co-occurrence of these flood drivers is important to predict the potential of high-impact compound flood events (Moftakhari et al. 2019). Ignoring the dependence between these flood events may substantially underestimate the flood risks at locations that flood hazard can be influenced by the interaction of inland and coastal flooding (Kew et al., 2013; Wahl et al., 2015; H. Moftakhari et al., 2019).

There is a rapidly growing literature concerning this interaction at local (Fang et al. 2020; Khanal et al. 2019; Moftakhari et al. 2017b; Orton et al. 2020), continental (Bevacqua et al. 2019a), and, global (Couasnon et al. 2020; Eilander et al. 2020; Ward et al. 2018) scale. However, a comprehensive assessment of the impact of climate change on this interaction, particularly the interaction of coastal and riverine flooding, has not been explored along the coastal U.S. This research gap is important due to several reasons.

First, as sea level rises due to climate change, the risks of compound flooding are likely to increase due to an increase in sea level exceedances over coastal flood threshold (Vandenberg-Rodes et al. 2016; Vousdoukas et al. 2017; Ghanbari et al. 2019) and also impeding a free river discharge to sea (Moftakhari et al. 2019). Thus, it is essential to consider future SLR projections in compound coastal-riverine flood hazard assessment. Climate change is also influencing extreme hydrological events regionally (Ahn and Palmer 2016; Peterson et al. 2008). Some areas have experienced an increase in the frequency of heavy precipitation and extreme streamflow events (Pryor et al. 2009; Groisman et al. 2001, 2005). Such changes in hydrological conditions have an immediate impact on the risks of urban and riverine flooding. With the increase of extreme streamflow frequencies, coastal regions threatened by SLR could experience exacerbation of consequence of compound flooding events. Therefore, consideration should be given to possible increase in co-occurrence of exceedances of high SLs or river flows.

Second, a comprehensive assessment of compound coastal-riverine flooding based on the definition of impact flood thresholds is lacking. Previous global and national studies on compound coastal-riverine flooding explore annual frequency without specific consideration of compound flood impacts in different locations. Since in many situations, there is no exact correspondence between the extremeness of flood events based on return periods and the impact they cause, assessment should be based on consequences rather than just probability (Hague et al. 2020). Considering just probability, a comparison of flooding impacts over large areas is difficult to obtain. However, using flood impact thresholds facilitates comparison between different regions. Thus, assessment of current and future frequency of compound flooding events, defined based on impact flood thresholds, is important to identify hot spot regions in terms of compound flood frequency amplification.

Urban flooding due to extreme precipitation also poses substantial threats to people and property across the world (Jha et al. 2012). As already mentioned, these threats can further compound by the co-occurrence of high sea level (SL) either from tide or storm surge events in coastal urban areas (Smith and Rodriguez 2017). To offset increased future urban and compound flood risks in cities, implementation of effective and viable stormwater management strategies is essential. Stormwater interventions play a critical role by protecting cities from flooding and water quality degradation, particularly when considering the impacts of climate change (Roy et al. 2008).

Stormwater interventions include gray infrastructure, green infrastructure, and hybrid systems (Zhang et al. 2017). Gray infrastructure, such as conveyance pipes, large centralized storage basins pump stations, and treatment facilities historically served society's needs for water security, public sanitation, and flood protection. Over recent decades, green infrastructure systems have emerged as a promising flood risk management alternative or complementary to gray infrastructure (Ferguson et al. 2013; Vogel et al. 2015).

Green systems are considered nature-based solutions that seek to preserve the site's pre-development hydrologic conditions or to reduce the impacts of post-development on urban hydrology (Li et al. 2019). They provide environmental and social co-benefits since they facilitate natural hydrologic and biogeochemical cycles in cities and densely developed urban regions.

Green and gray stormwater infrastructure is often referred as either this-or-that choice (Jayasooriya and Ng 2014; Li et al. 2019). However, there is another opportunity to incorporate their complementary functionality and to obtain the best of what systems can offer (Sanders and Grant 2020).

New York City (NYC) is one of the locations that is threatened by compound flooding from heavy precipitation and storm surge (Wahl et al. 2015a). Pressures on the city water systems are on the rise due to the increased frequency of extreme precipitation events, SLR, and land-use change (Karamouz et al. 2015; Yohe and Leichenko 2010). Several studies assess the effectiveness of adaptation strategies in reducing stormwater runoff and flood risks in NYC (e.g., Rosenzweig et al., 2011; Aerts et al., 2013; Zahmatkesh et al., 2015; Karamouz et al., 2019). However, an improved understanding of future urban and compound flood hazard and benefit that can be gained from implementation of combinations of different practices as a part of integrated water management still need to be investigated thoroughly to improve resiliency of NYC's water system under uncertain future.

1.2. Research objectives

The overall goal of this dissertation is to enhance the capacity to understand, estimate and mitigate future flooding hazards and risks in coastal areas with consideration of the impact of climate change including SLR and changes in extreme precipitation and river flows. Specifically, the objectives are to:

1. Develop a statistically coherent nonstationary mixture probability model for sea levels, which enables simultaneous assessment of minor and extreme coastal flooding under future sea level rise scenarios.

2. Incorporate the proposed mixture probability distribution in a risk assessment framework to simultaneously estimate acute and chronic flood risk in coastal regions under different sea level rise and adaptation level scenarios.

3. Develop a bivariate flood hazard assessment framework to estimate the joint return period of compound coastal-riverine flooding that accounts for sea level rise and changes in extreme river flows.

4. Examine the complementary and substitutive effect of green stormwater interventions on flood control and combined sewer outflow reduction under current and future storm scenarios in NYC.

Achieving these research objectives provides more accurate flood risk assessment under future climate conditions in coastal areas, which in turn could assist coastal planners and policy makers in their decision to adopt more efficient adaptation strategies to reduce the adverse effect of climate change. This could save billions of dollars that are and will be spent annually for damage repair and insurance claims and also enhance the quality of life as it would provide a safer living environment.

1.3. Significance of the dissertation

This dissertation is significant in several aspects of flood risk assessment and adaptation. First, it develops a coherent probability mixture model, which reconciles the probabilistic characteristics of the upper tail as well as the bulk of the sea level data. The novel probability mixture model allows to simultaneously investigate minor and extreme coastal flooding frequency under future SLR conditions. Second, the study provides a flood risk assessment framework for assessing chronic and acute flood risks in coastal cities under different SLR and adaptation levels. Simultaneous assessment of chronic and acute flood risk under future conditions is novel and enhances the capacity for more resilient coastal management. Third, it presents a copula-based bivariate flood hazard assessment framework that enables estimation of compound coastal-riverine flooding frequency under future climate conditions. The framework is the pioneer in assessment of compound coastal-riverine frequency that accounts for SLR and changes in extreme river flow.

1.4. Organization of the dissertation

This dissertation is organized into five chapters, including:

Chapter 1: presents a holistic research background and the main objectives and significance of this dissertation.

Chapter 2: develops a statistically coherent mixture Normal-Generalized Pareto distribution model which reconciles the probabilistic characteristics of the upper tail as well as the bulk of the sea level data. The performance validity of the mixture model was corroborated for 68 tidal stations along the coasts of the Contiguous United States with long-term observed data.

Chapter 3: implements the proposed mixture probability model in a coastal flood risk assessment framework to simultaneously estimate acute and chronic risk from minor and major flooding in coastal regions under different SLR and adaptation level scenarios. The application of the framework was demonstrated for Miami-Dade County.

Chapter 4: develops a bivariate compound flooding risk assessment method to estimate the joint return period of compound coastal-riverine flooding with consideration of SLR and changes in extreme river flows. The proposed compound flood risk assessment is conducted at 26 paired tidal-riverine stations along the coasts of the Contiguous United States with long-term observed data and impact flood threshold.

Chapter 5: identifies, models, and assesses different green and gray stormwater management intervention scenarios in New York City under current and future climate to understand benefit that can be gained from implementation of different practices, individually or in combination.

Chapter 6: presents the main findings of this research study and the summary of the work concluded, and provides recommendations for future work.

Two chapters of the dissertation have been published and one is in review as journal articles. The full references for the articles are:

- Ghanbari, M., Arabi, M., Obeysekera, J., & Sweet, W. (2019). A coherent statistical model for coastal flood frequency analysis under nonstationary sea level conditions. Earth's Future, 7(2), 162–177. https://doi.org/10.1029/2018EF001089
- Ghanbari, M., Arabi, M., and Obeysekera, J. (2020). "Chronic and Acute Coastal Flood Risks to Assets and Communities in Southeast Florida." *Journal of Water Resources Planning and Management*, 146(7). https://doi.org/10.1061/(ASCE)WR.1943-5452.0001245
- Ghanbari, M., Arabi, M., Kao, S. C., Obeysekera, J., & Sweet, W. (2021). Climate Change and Changes in Compound Coastal-Riverine Flooding Hazard Along the U.S. Coasts. Submitted to *Earth's Future*

CHAPTER 2.

A COHERENT STATISTICAL MODEL FOR COASTAL FLOOD FREQUENCY ANALYSIS UNDER NONSTATIONARY SEA LEVEL CONDITIONS

Highlights

Flood exposure is increasing in coastal communities due to rising sea levels. Understanding the effects of sea level rise (SLR) on frequency and consequences of coastal flooding and subsequent social and economic impacts are of utmost importance for policymakers to implement effective adaptation strategies. Effective strategies may consider impacts from cumulative losses from minor flooding as well as acute losses from major events. In the present study, a statistically coherent Mixture Normal-Generalized Pareto Distribution (GPD) model was developed, which reconciles the probabilistic characteristics of the upper tail as well as the bulk of the sea level data. The nonstationary sea level condition was incorporated in the mixture model using Quantile Regression method to characterize variable GPD thresholds as a function of SLR. The performance validity of the mixture model was corroborated for 68 tidal stations along the Contiguous U.S. (CONUS) coast with long-term observed data. The method was subsequently employed to assess existing and future coastal minor and major flood frequency. The results indicate that the frequency of minor and major flooding will increase along all CONUS coastal regions in response to SLR. By the end of the century, under the "Intermediate" SLR scenario, major flooding is anticipated to occur with return period less than a year throughout the coastal CONUS. However, these changes vary geographically and temporally. The mixture model was reconciled with the property exposure curve to characterize how SLR might influence Average Annual Exposure (AAE) to coastal flooding in twenty major CONUS coastal cities.

2.1. Introduction

The global mean sea level (MSL) has been increasing over the past decades (IPCC 2014). The rate of sea level rise (SLR) is anticipated to continue to accelerate globally and regionally over the 21st century (Howat et al., 2007; Rahmstorf, 2007; Sweet et al., 2017). Consequently, many coastal regions will be increasingly exposed to frequent coastal flood inundation (Walsh et al. 2014). Coastal communities are particularly vulnerable to SLR due to risks from acute storm surge as well as chronic tidal flooding events. The implications of SLR may include increases in severity and frequency of coastal flooding (Rahmstorf and Coumou 2011; Ray and Foster 2016), posing enormous socioeconomic implications in coastal cities (Hinkel et al., 2013; Aerts et al., 2014; Hallegatte et al., 2013). Thus, a coherent assessment of the chronic and acute impacts of SLR on coastal flooding is vital for security of coastal communities.

SLR reduces the freeboard between high water levels (either from tide or storm surge) and local flood thresholds, causing to increase the frequency of both minor (Sweet et al., 2014; Moftakhari et al., 2015; Vandenberg-Rodes et al., 2016; Dahl et al., 2017) and major (Kemp & Horton, 2013; Ezer & Atkinson, 2014; Vousdoukas et al., 2017) coastal flood events. Thus, quantification of risks from coastal flooding under nonstationary sea level conditions must reconcile the effects of both minor and major floods. Development of effective adaptation and mitigation strategies must take into account the cumulative losses from frequent smaller high-water levels (i.e., minor flooding) as well as acute losses from less frequent extreme high-water levels (i.e., major flooding). A challenge, however, is the inadequacy of widely used probability models in simultaneous characterization of both minor and major flooding under higher mean sea levels.

Literature is replete with probabilistic methods to characterize the likelihood of major flooding under nonstationary condition. Chief among these approaches are the nonstationary Generalized Extreme Value (GEV) distribution and Generalized Pareto Distribution (GPD). Nonstationarity of sea level conditions is typically taken into account by time-dependent distribution parameters for GEV (Boettle et al. 2013; Menéndez and Woodworth 2010; Obeysekera et al. 2013; Salas and Obeysekera 2014) or GP (Méndez et al., 2006; Kyselý et al., 2010) distributions. The increasing frequency of minor flooding due to SLR has motivated several recent studies (Sweet et al., 2014; Dahl et al., 2017; Moftakhari et al., 2017; Sweet et al., 2018). However, most of these previous studies model minor and major flood events separately.

Two important considerations must be addressed to fully characterize acute and chronic flooding risks in a statistically rigorous manner under nonstationary condition. First, using time as a covariate in nonstationary probability models poses planning and management challenges since future SLR projections are fraught with uncertainty. Considerable scientific discourse still remains how to statistically detect SLR acceleration over time (Nicholls & Cazenave, 2010; Haigh et al., 2014). Moreover, local factors such as land subsidence, changes in ocean circulation, and groundwater pumping may also considerably alter the rate of SLR in a region (Konikow, 2011; Ezer et al., 2013). In addition, selecting a meaningful SLR scenario is not a straightforward task and several factors should be weighed by policymakers and coastal planners to select an appropriate SLR such as the decision type, planning horizon and overall risk tolerance (Hall et al., 2016; Sweet et al., 2017). Thus, since extreme sea level data are correlated with MSL (Tebaldi et al., 2012) nonstationarity may be addressed in terms of changing in MSL instead of time.

Further, Extreme Value (EV) distributions are commonly used to characterize the tail of water level data (Xu & Huang, 2008; Menéndez et al., 2008; Noto & La Loggia, 2009; Roth et al., 2012; Niroomandi et al., 2018). However, with higher sea levels, current local flood thresholds are likely to be exceeded more frequently during average high tides. Flood events that are currently characterized as infrequent and are mostly modeled by the upper tail of the sea level distribution will become more frequent with SLR and will not be rare events anymore. Thus, in the absence of coastal adaptation measures, water level exceedances above the current flood threshold cannot be characterized using models that characterize only the upper tail of the water level distribution. This limitation impedes full characterization of risks from coastal flooding under nonstationary sea level conditions. Thus, requisite to a full characterization of flood risks is an approach that reconciles the probabilistic characteristics of the upper tail as well as the bulk of the sea level distribution (Stephens et al. 2018).

This study develops a statistically coherent nonstationary mixture probability model for sea water levels to facilitate coastal flood frequency analysis. Specifically, the objectives of the study are to: 1) develop and corroborate a nonstationary Mixture Normal-GPD probability model with changes in MSL as the covariate; 2) evaluate current and future coastal flood return periods for regions along the coastal Contiguous U.S. (CONUS); 3) investigate changes in the frequency of minor and major coastal flooding for the stations along the coastal CONUS; and 4) quantify current and future exposure to coastal flooding in twenty coastal cities in the CONUS. The new mixture probability model enhances the capacity to simultaneously investigate minor and major coastal flooding frequency under future SLR scenarios. The study also investigates the time to anticipated SLR levels on a decadal basis.

2.2. Materials and Methods

Current local flood thresholds will be exceeded more frequently under higher MSL, which can ultimately result in inadequacy of the extreme value distributions (Figure 2.1). We developed a nonstationary Mixture Normal-GPD model to enable full characterization of coastal flood frequency with SLR as the covariate. In the mixture model, the Normal distribution describes the bulk of daily maximum sea levels, while GPD characterizes the upper tail of the data. Nonstationarity was incorporated by expressing the location parameters of both Normal distribution and GP distribution as a function of SLR. The model was corroborated for 68 tidal monitoring locations along the coastal CONUS with long-term observed water level data. We used the mixture probability model to assess the effects of SLR on future coastal flood frequency along the coastal CONUS. Subsequently, we reconciled the model with exposure curve for coastal assets (i.e. property value of buildings) in twenty coastal cities to quantify the Average Annual Exposure (*AAE*) of assets to minor and extreme coastal flooding over a range of SLR levels. Finally, recent regional SLR projections were used to investigate how far in the future changes in frequency of coastal flooding may be realized.

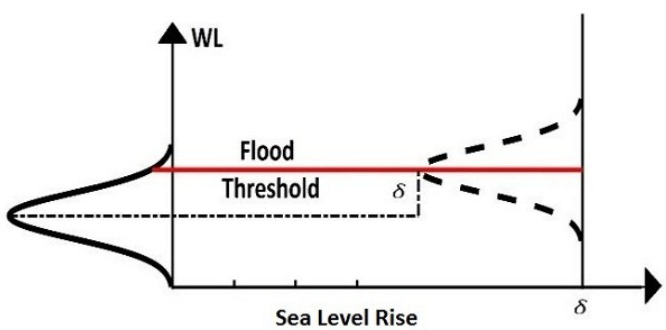

Figure 2.1. Schematic of changes in water level probability distribution with a δ increase in MSL

2.2.1. Tidal stations, study cities, and projected SLR scenarios

We used three sets of data in this study to estimate current and future coastal flood frequency and conduct property exposure analysis along the coastal CONUS. First, we used hourly observed sea level data from 68 stations with at least 30 years of data to develop and corroborate the mixture probability model. These stations are located along CONUS coasts, including northeast Atlantic, southeast Atlantic, Gulf, and Pacific coasts. The data represent Still Water Elevation (SWEL), which encompass both tide and storm components. All the hourly observed water level data are relative to the latest National Tidal Datum Epoch (NTDE), which references the 1983-2001 period with MHHW as the tidal datum except the data from two stations along the Gulf coast (Grand Isle and Rockport tidal stations), which are on the modified epoch. We modified the hourly time series correspond to these two stations to take the sea level data back onto the 1983-2001 epoch (Sweet et al., 2018).

Second, we selected twenty populated cities along the coastal CONUS, which cover a variety of geographic coastal regions (5 cities in each coastal region). All of the cities are highly exposed areas to coastal flooding in terms of infrastructure and other properties. For each city, we used cumulative property exposure values correspond to water level above mean higher high water (MHHW) from risk finder tool (https://riskfinder.climatecentral.org) provided by Climate Central (Climate Central 2016). We obtained the property exposure values for 10 different water level values (i.e., 1 to 10 ft above MHHW). Exposure values between these data points were modeled by a linear function.

Third, we used two regional SLR projections to perform a decadal assessment of expected time to certain changes in mean sea levels by 2100. We selected the “Intermediate Low” scenario, which corresponds to 0.5 m global SLR with 73% chance of being exceeded under RCP 4.5 climate change scenario. We simulated more accelerated SLR conditions using the "Intermediate" scenario with 1 m global SLR and 17% chance of being exceeded under RCP 8.5 climate change scenario (Kopp et al., 2014; Sweet et al., 2017). Antarctic ice sheet instability could transition to more extreme scenarios (i.e., Intermediate-High, High and Extreme) later in the century. However, those outcomes are less likely to occur. Thus, the results of the present study may be deemed as plausible but conservative estimates compared to other extreme SLR scenarios.

2.2.2. Minor, moderate, and major coastal flooding classification

To secure public safety and take steps to increase coastal cities preparedness level, three "official" coastal flood thresholds have been established by National Oceanic and Atmospheric Association (NOAA). Minor flooding (i.e., exceedances over minor flood threshold) refers to events that can cause minimal damage with public threat and inconvenience. Moderate coastal flooding (i.e., exceedances over moderate flood threshold) has relatively considerable damages to private and commercial property. Major flooding (i.e., exceedances over major flood threshold) is destructive and can cause extensive losses to life and property. These thresholds are defined observationally during flooding events and are available for less than half of NOAA tide gauges in the CONUS (NOAA 2014).

A recent study done by Sweet et. al (2018) found a common pattern between all "official" NOAA coastal flood thresholds based on the local tide range such that in the most cases minor, moderate and major coastal flooding begin about 0.5 m, 0.8 m and 1.2 m above the local diurnal tide range. Consequently, they estimate a "derived" set of flood threshold based on the statistical relationship (regression-based) for nearly all stations along the coastal CONUS. In this study, we used these set of "derived" coastal flood thresholds for each station as an approximation of minor, moderate and major flooding threshold, which are spatially consistent and can provide national coverage (Sweet et al., 2018).

2.2.3. Mixture Normal-GPD probability model

We developed a nonstationary mixture model that simultaneously characterize the bulk and upper tail of the sea water level distribution. The six parameter model represents extreme values by a GPD and bulk data by a Normal distribution. We estimated the parameters of the mixture model for the 68 tidal monitoring stations along the coastal CONUS.

2.2.3.1. Extreme Value Analysis (EVA)

EVA is commonly used to characterize extreme events with two primary methods for selecting extremes: Peak over threshold (POT) and block maxima method (e.g. annual maxima). The block maxima approach and corresponding probability models such as the GEV distribution can only consider one event per block (e.g. year). However, coastal flooding, particularly minor flooding events, may occur with multiple occurrences in a year (Moftakhari et al. 2015; Ray and Foster 2016). Hence, we used the POT method in the current study to consider multiple events per year. In this approach, a threshold is determined to describe statistical properties of events that exceed the threshold over a given period of time. The cumulative distribution (G) of the independent exceedances above the threshold follow the GPD is given by (Coles 2001):

$$G_{u,\alpha,\xi}(x) = \Pr(X \leq x \mid X > u) = \begin{cases} 1 - \left(1 + \xi \dfrac{x-u}{\alpha}\right)^{-\frac{1}{\xi}} & if\ \xi \neq 0 \\ 1 - \exp\left(-\dfrac{x-u}{\alpha}\right) & if\ \xi = 0 \end{cases} \tag{2.1}$$

where u, α and ξ denote the location, scale and shape of the GPD distribution.

2.2.3.2. Mixture Normal-GPD distribution

The bulk of daily maximum sea level closely follows a Normal distribution (Sweet & Park, 2014). Thus, using the idea of extreme value mixture model (Behrens et al. 2004) the GPD model for the data above the threshold is mixed with a Normal distribution for the data below the threshold to derive a single spliced distribution that coherently characterizes probability density of the entire range of sea level data. The cumulative distribution function of the mixture model is defined as (MacDonald et al. 2011):

$$F(x|\mu,\sigma,u,\alpha,\xi,\varphi) = \begin{cases} (1-\varphi)\ \dfrac{N\ (x|\ \mu,\sigma)}{N\ (u|\ \mu,\sigma)} & if\ x < u \\ (1-\varphi)+\varphi G(x|u,\alpha,\xi) & if\ x \geq u \end{cases} \tag{2.2}$$

where $N(x|\mu,\sigma)$ and $G(x|u,\alpha,\xi)$ are the Normal and conditional GPD cumulative distribution functions, respectively. Variables μ and σ represent mean and standard deviation of the Normal distribution, and φ denotes the probability of independent exceedances over threshold. Variable φ is the ratio of number of clusters above threshold to the total number of observations (Coles 2001). We used the Maximum Likelihood Estimation (MLE) in MATLAB (MathWorks®) to estimate parameters of the mixture model for the study locations.

2.2.4. Characterization of nonstationary sea water level

The effects of SLR must be considered in both components of the Mixture Normal-GPD model. Hence, in the proposed approach, the location parameter of the Normal distribution (μ) and the location parameter of the GPD (u) are expressed as functions of changes in MSL (δ). Climate change may also beget changes in storminess of events (i.e., the frequency and intensity of storms) that cause coastal flooding (Wolf and Woolf 2006) leading to changes in other parameters (e.g. scale and shape parameter) of water level distribution (Arns et al. 2017; Devlin et al. 2017; Wahl

2017). However, the changes in storminess were not included in this study for two reasons: (1) previous studies have observed that SLR have more immediate threat for the increase in exceedances over flood thresholds than possible changes in storm variability (Tebaldi et al., 2012; Church et al., 2013; Sweet & Park, 2014); (2) although increase in storminess could change extreme events accompanied with storm surge, as sea levels rise most of coastal floodings start at normal high tides, with no additional effect of severe weather such as storm or hurricane. The approach assumes that SLR will shift the current sea level distribution toward higher water level without any deformation of the distribution (Mudersbach & Jensen, 2010; Tebaldi et al., 2012; Le Cozannet et al., 2015). Thus, no additional covariate dependency was assumed for scale parameter of Normal component as well as scale and shape parameters of the GP component.

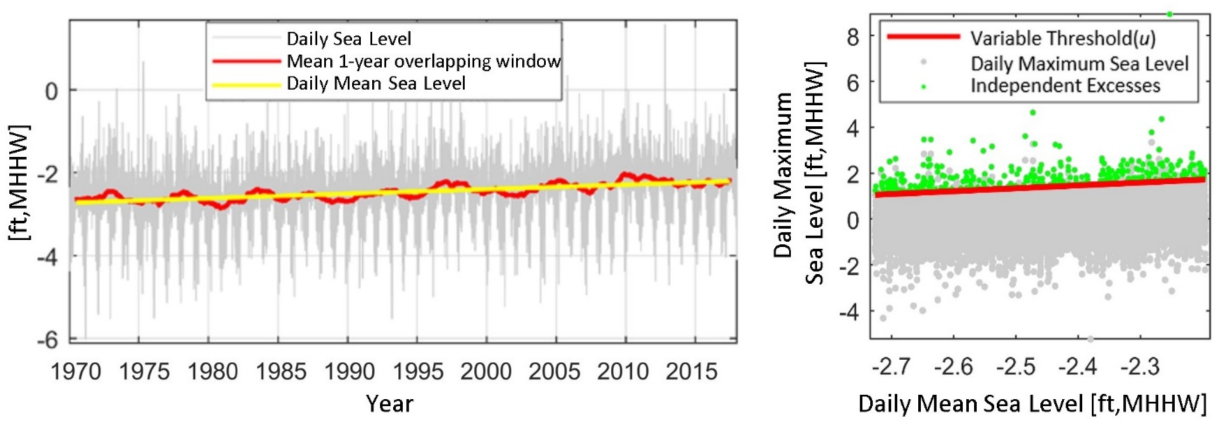

Figure 2.2. (Left Panel) Daily mean sea level calculated using linear function fitted to the daily sea levels, (Right panel) Variable threshold estimated using Quantile regression method and independent excesses over threshold (Battery (NY) tidal station)

The location parameter of GPD may be represented by either choosing a constant or a variable threshold. When a constant threshold is used, exceedances of the threshold occur more frequently in future years, which may violate the assumption of extreme value analysis (Coles 2001). Hence, we computed a variable GPD threshold using Quantile Regression method (Koenker & Hallock, 2001; Kyselý et al., 2010). The analysis determines the relationship between daily mean sea level (independent variable) and daily maximum sea level (response variable) data. Daily mean sea levels (DMSL) were computed from the linear model fitted to the daily sea levels (i.e., daily time series of mean of hourly observed water levels) (Figure 2.2, left panel). The linear model (Yellow line) was used instead of daily mean sea level time series, which was computed from the mean of daily values for 1-year overlapping windows centered at the indicated day (Red line), to remove the noise component in the time series and avoid having sample variability. We assume DMSL correspond to 183rd day of the year 2017 as current DMSL and present all the computed DMSLs as sum of current DMSL and changes in MSL ($DMSL_{current} + \delta$). Eventually, we calculated the GPD variable threshold as the 97% (Méndez et al., 2006; Sweet et al., 2014) quantile regression assuming linear dependence between daily maximum sea level and DMSL (Figure 2.2, right panel). The nonstationary characterization of GPD threshold includes two components and is a function of changes in MSL (δ) according to the following equation:

$$u = u(\delta) = \beta_1(DMSL_{current} + \delta) + \beta_0 = \beta_1\delta + (\beta_0 + \beta_1 \times DMSL_{current}) \tag{2.3}$$

where u denotes the value of the variable GPD threshold, $DMSL_{current}$ represents the daily mean sea level corresponding to the current (i.e., reference) year, β_1 and β_0 denote the slope and intercept coefficients of the quantile regression model, and δ represent change in mean sea level from the current level. Year 2017 is used as the reference year in the study. The quantile regression coefficients are assumed to remain constant over the range of mean sea levels.

The estimated slope coefficient (β_1) indicates the rate of change in the GPD threshold, which is used to characterize extremes, with changes in MSL. When β_1 is greater than 1, the changes in extreme values are greater than changes in MSL itself. Conversely, a β_1 value less than 1 points to smaller changes in extremes relative to changes in MSL.

The MLE technique requires independent observations of extremes for robust estimation of GPD parameters. Thus, a minimum time interval between water level extremes (i.e., threshold exceedances) must be identified such that the resulting sequences are statistically independent. In the current study, we employed a minimum of 3-day runs (Méndez et al., 2006; Sweet et al., 2014). The maximum of successive extremes within each cluster was used to estimate GPD parameters (Figure 2.2, right panel).

Similarly, the nonstationary component for the bulk of the distribution is incorporated by changing the location parameter of the Normal component of the distribution as follows:

$$\mu = \mu(\delta) = \mu_0 + \delta \tag{2.4}$$

where μ_0 represents the estimated Normal distribution location parameter computed from historical daily maximum sea level.

2.2.5. Coastal flood frequency and amplification factor

The relation between coastal flood level and return period will change under nonstationary conditions (Church et al., 2006; Lin et al., 2012), and subsequently, the frequency of exceedance of a given flood threshold will increase (Dahl et al. 2017). The annual frequency (expected number of days per year) of exceedances above coastal flooding thresholds (n_e) can be obtained from the mixture probability model as follows:

$$n_e = \frac{1}{T} = \begin{cases} n_y\left(1 - \left[\dfrac{(1-\varphi)}{1 + erf\left(\dfrac{u-\mu}{\sigma\sqrt{2}}\right)}\left(1 + erf\left(\dfrac{x-\mu}{\sigma\sqrt{2}}\right)\right)\right]\right) & x < u \\ \varphi n_y\left(1 + \xi\dfrac{x-u}{\alpha}\right)^{-\frac{1}{\xi}} & x \geq u \end{cases} \tag{2.5}$$

where n_y is the number of observations per year, T denotes the return period and *erf* is the error function.

While the frequency of coastal flooding increases with SLR, changes in the frequency of minor and major flooding may not be the same everywhere. Thus, the effect of SLR on changes in frequency of minor and major flooding across coastal regions in the CONUS were assessed using the flood frequency amplification factor (AF), which is defined as the ratio of current to future return period of a given water level under a specific SLR (Buchanan et al. 2017):

$$AF = \frac{T_0(x)}{T_\delta(x)} \tag{2.6}$$

where $T_0(x)$ is the current return period of water level (x), and $T_\delta(x)$ is the return period of water level (x) under a δ increase in MSL.

2.2.6. Average annual exposure to coastal flooding

Flood risk computation involves quantification of flood probability, assets (or other values) at risk, and vulnerability (Kron 2005; Merz et al. 2010). A widely-used risk indicator for flood risk assessment is the Average Annual Losses (*AAL*) (Kron 2005; Purvis et al. 2008). However, in this study, we used the exposure values as an approximation of damages due to many uncertainties in estimating damages across different types of flooding, especially indirect losses in the case of minor flooding. Thus, we estimated Average Annual Exposure (AAE) of property to “minor” and “moderate and major” coastal flooding in twenty major CONUS coastal cities. Here, we use the term “extreme” flooding to refer to “moderate and major” flooding since both flooding categories can cause considerable damage to property (NOAA 2014). *AAE* to minor and extreme (i.e., moderate and major) flooding is determined by:

$$AAE\ Extreme = \int_{0}^{1-F(Moderate\ Flood\ Threshold)} n_y * E\left(F^{-1}(1-p)\right)dp \tag{2.7.a}$$

$$AAE\ Minor = \int_{1-F(Moderate\ Flood\ Threshold)}^{1-F(Minor\ Flood\ Threshold)} n_y * E\left(F^{-1}(1-p)\right)dp \tag{2.7.b}$$

where E denotes the exposure function, and p represents the sea level exceedance probability. The *AAE* to minor and major flooding was computed for twenty cities along the coastal regions in CONUS for various SLR levels.

2.3. Results

The study reveals that minor and major flood frequency generally increase as sea level rises, however, these changes vary geographically along the coastal CONUS. Major flood frequency amplification is primarily governed by the value of shape parameter. In regions with negative or close to zero shape parameter (i.e., Pacific and Southeast Atlantic coasts) major flood frequency amplification is more sensitive to SLR and is higher than minor flood frequency amplification. On the contrary, locations with large positive shape parameter (i.e., Gulf and northeast Atlantic coasts) are anticipated to be exposed to higher frequency amplification in minor flooding. Considering regional SLR projections, events currently classified as major flooding are anticipated to occur with return period less than a year in all stations by the end of the century under Intermediate SLR scenario.

2.3.1. Parameters of the Mixture model by region

The mixture model parameter values for all 68 tidal stations were estimated using the MLE method and are summarized in Appendix A Table A1. The GPD shape parameter governs the qualitative behavior of GPD distribution (Coles 2001). When the shape parameter is positive ($\xi >$

0), the distribution is heavy-tailed and has no upper bound. Conversely, when $\xi < 0$ the distribution is thin-tailed and has upper limit equal to $x_{max} = u - \frac{\alpha}{\xi}$.

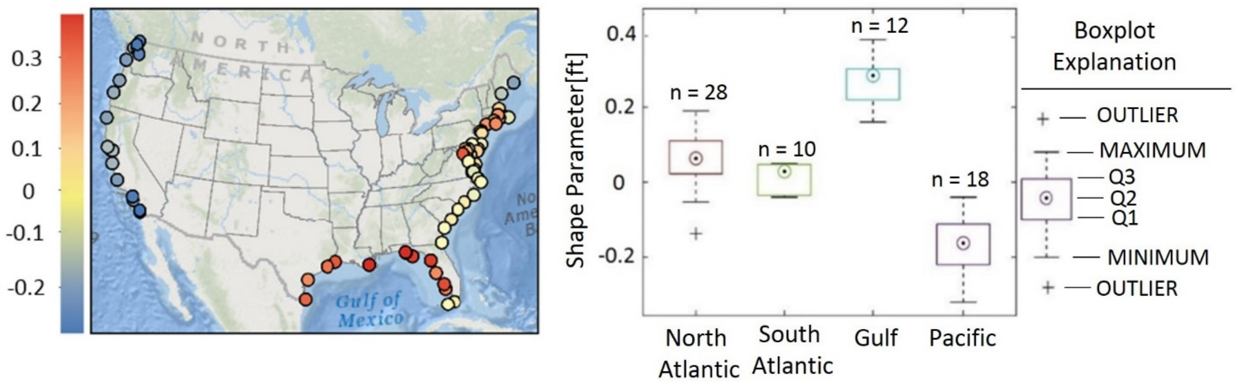

Figure 2.3. (Left) Geographical distribution of GPD shape parameter (Right) Boxplot of GPD shape parameter (Q1, Q2, and Q3 indicate lower quartile, median, and higher quartile respectively and n denotes the number of stations)

The estimated shape parameters for the stations along the coastal CONUS reveal important regional patterns (Figure 2.3). Figure 2.3 (right panel) presents the boxplot of GPD shape parameters in each region. From this boxplot, it can directly be observed that locations along Gulf and Pacific coasts have the highest and lowest GPD shape parameter respectively and the median is almost equal to zero for stations along the southeast Atlantic coasts. The shape parameters for stations along the Pacific coast region are negative ranging between -0.02 to -0.1 or highly negative with values less than -0.1. These stations historically do not experience tropical cyclone or hurricanes and have a very narrow continental shelf that limits storm surge potential. On the other hand, stations along the Gulf and northeast Atlantic regions are exposed to tropical cyclones and strong winter storms, respectively. The shape parameter for these stations is highly positive with values more than 0.1 or positive ranging between 0.02 to 0.1. Stations along southeast Atlantic region experience differing degrees of exposure to tropical storms with the shape parameter approximately zero with values in the range of -0.02 to 0.02. It is clear that different experience among stations in terms of historical exposure to extreme flooding can be reflected by GPD shape parameter (Buchanan et al., 2016).

Local characteristic of tidal stations could also affect the value of GPD shape parameter. For example, Key West and Vaca Key (Florida Keys) stations, which are located close to the margins of continental shelf zones, similar to the situation along the Southwestern Pacific coast, tend to be exposed to lower surge compared to stations that are located behind the wide shelves. Moreover, stations close to estuaries may be also exposed to relatively high storm surge or large riverine inputs (e.g. Washington DC station) (Tebaldi et al. 2012).

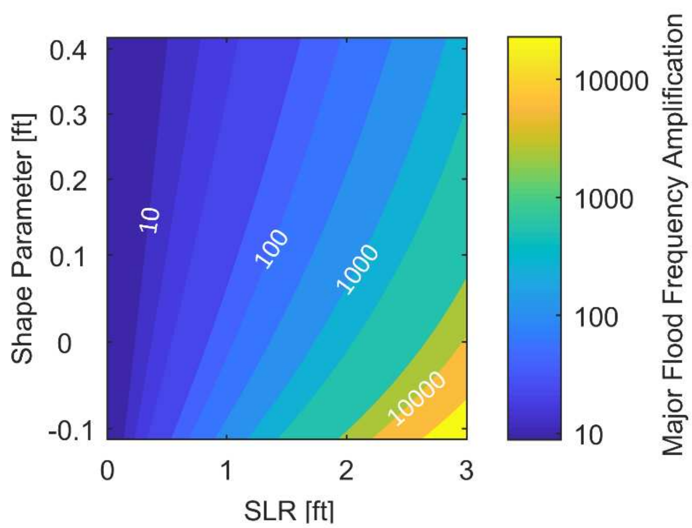

Figure 2.4. Sensitivity of major flood frequency amplification with SLR and the distribution shape parameter

The sensitivity of major flood frequency amplification to the shape parameter over a range of SLR levels is illustrated in Figure 2.4. Other parameters of the distribution and Quantile Regression coefficients were kept constant at: $u_0 = 1.8$; $\alpha = 0.4$; $\mu_0 = 0$; $\sigma = 0.8; \varphi = 0.02; \beta_1 = 1; \beta_0 = 7$. Generally, frequency amplification of major flooding is inversely related to the value of shape parameter. As shape parameter increases, major flooding frequency amplification tends to be smaller for changes in MSL. This response is governed by the effects of shape parameter on the tail of sea level distribution and the frequency of extreme flood levels. Distributions with $\xi > 0$ have relatively high frequency of extreme flood levels, while distributions with $\xi < 0$ have an upper bound of extreme flood levels. When shape factor is highly negative, e.g. for locations where currently major flooding does not occur or is highly unlikely, very large frequency amplifications may be computed.

Conversely, minor flooding frequency amplification is not sensitive to the value of shape parameter. The minor flood threshold typically is not located at the tail of the GPD and is not governed by shape parameter.

2.3.2. Current and future coastal flooding return period

Changes in the return period of future coastal flooding were assessed under different SLR levels in the study locations. The median of these changes by coastal regions is summarized in Figure 2.5. Figures A2 to A69 (panel E) in Appendix A provide the results of the analysis for each station. Generally, future return periods will become shorter as the sea level rises. A significant change is determined for study sites in the Pacific region. For example, 500-year flood will become a 10-year, yearly and monthly flood under 0.5, 1, and 2 ft SLR respectively. However, these changes in flood return period do not necessarily indicate higher exposure and risks in the future since return period alone does not provide sufficient information for risk management policies (Tebaldi et al. 2012). For example, the flood levels for the current 100-year event is about 3 ft for regions along the Pacific coast, posing little flood risks.

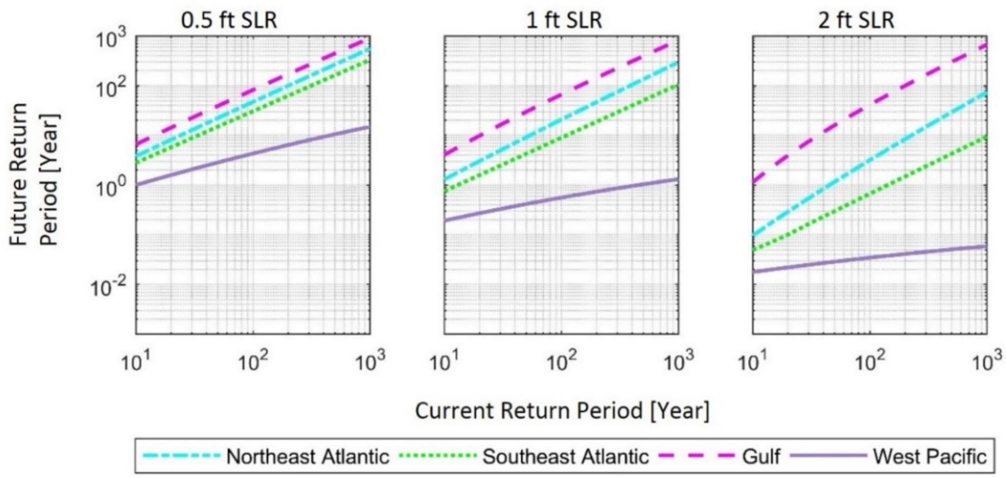

Figure 2.5. Current versus future coastal flood return period (Median value for each region)

To make this point clearer, Figure 2.6 depicts the estimated future return period for prevailing 100-year coastal flooding events under 0.5 ft (left panel) and 2 ft (right panel) SLR levels. Locations along the Gulf region will experience the highest 100-year depth. On the contrary, the smallest 100-year flood depths are estimated for locations along the Pacific coast, which historically have not been exposed to hurricane and tropical cyclone. A relation is evident between the future return period and current 100-year return level (Tebaldi et al. 2012), which express that changes in return period alone does not provide sufficient information for risk management policies.

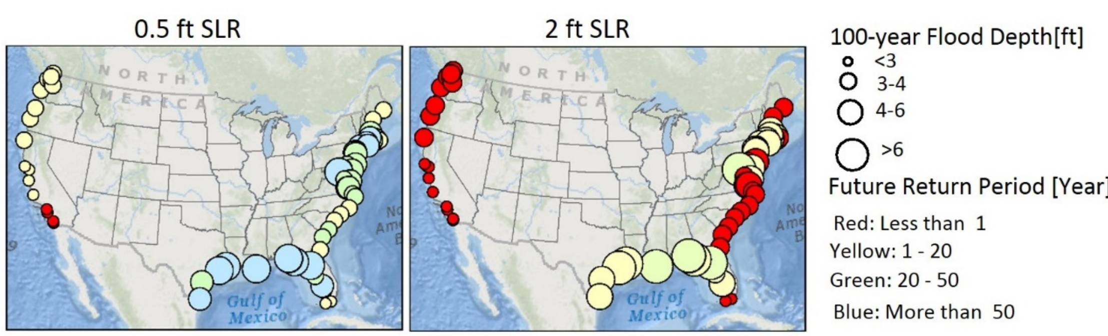

Figure 2.6. Future 100-year flood return period classified by current 100-year flood depth. The size and color represent the “Future return period” and the “depth” of current 100-year flood, respectively.

2.3.3. Current and future frequency of minor and major coastal flooding

For more practical use of future return period, we calculated the frequency of minor and major flooding (i.e., exceedances over 'derived' minor and major flood threshold respectively) for each station under current and future MSL values. Generally, as sea levels rise, the likelihood of flooding increases should the local flooding thresholds remain constant (Kruel, 2016; Dahl et al., 2017). Figure2.7 (top panels) shows estimated future return period for major flooding events, under the current MSL, 1 ft and 2 ft SLR. Under the current condition, major flooding events occur along the Gulf and northeast Atlantic coasts with a return period less than 100-year. With 1 ft SLR, the large majority of locations (except locations along the southwest Pacific with no exceedances above major flood threshold) tend to be exposed to major flooding with a return period of 1- 20 years. Under 2 ft SLR, should no interventions be implemented, major flooding will become commonplace with multiple annual occurrences in most of the CONUS coastal regions.

Annual Frequency (i.e., expected annual number of exceedances) of minor flooding is presented in Figure 2.7 (bottom panels). Annual frequency of minor flooding was computed instead of return period since multiple minor flooding events may occur within in a year (i.e. return period less than 1 year). Results show that minor flooding currently occurs with the expected number of 1 to 20 days per year in most stations along the Atlantic, Gulf, and Northwest Pacific coasts. Under the current MSL, the least frequency of exceedances is realized with expected annual exceedances of less than 1 day for stations along the southwest Pacific coast as well as the southwestern coast of Florida. However, 1 ft SLR will culminate in increased frequency of minor flooding to 20-50 days per year in a majority of the study locations. With no adaptations or interventions, 2 ft SLR will result in more than 150 days of minor flooding per year in all the locations.

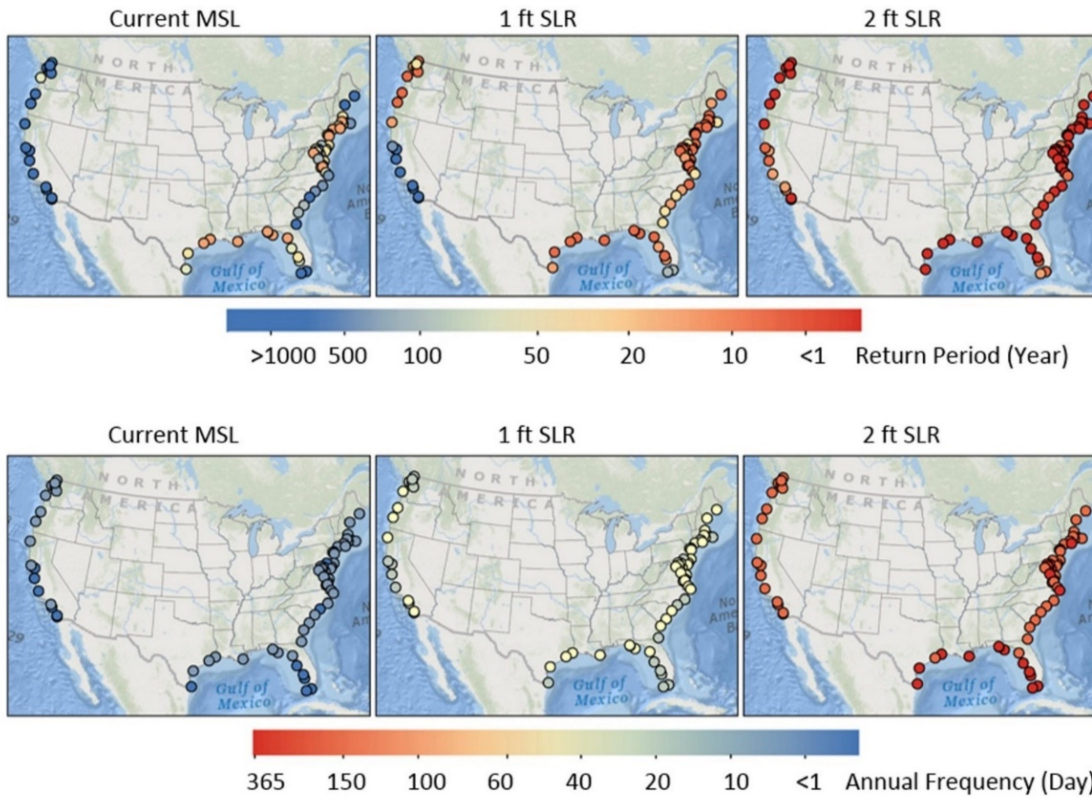

Figure 2.7. (Top panels) Return period of major coastal flooding; (Bottom panels) Expected annual frequency of minor coastal flooding

2.3.4. Frequency amplification of minor and major coastal flooding

Although the frequencies of minor and major flooding are forecasted to increase as a result of SLR, changes in their frequencies are not the same across regions. Thus, frequency amplification of minor and major coastal flooding were calculated for all sites to assess the effect of SLR on changes in the frequency of minor and major flooding separately across different coastal regions (Figure 2.8).

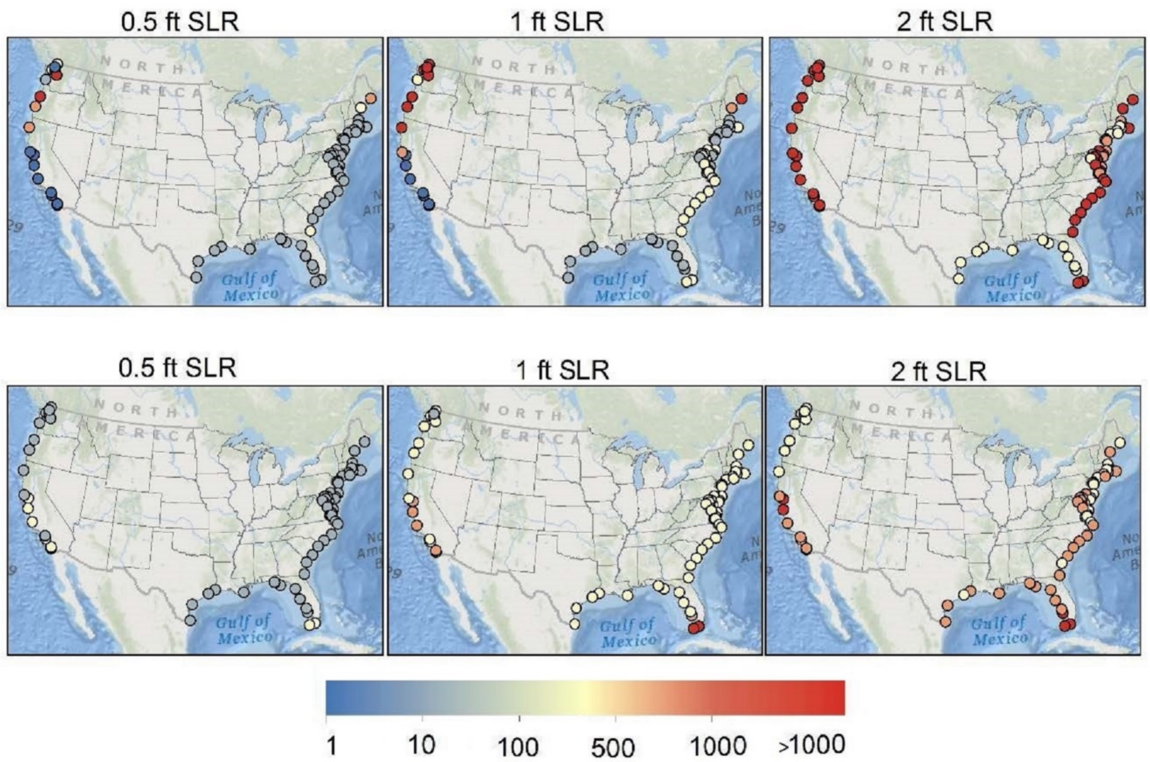

Figure 2.8. (Top panels) Major flood frequency amplification; (Bottom panels) Minor flood frequency amplification

The frequency amplification of major flooding in the locations along the northwest Pacific will increase substantially with 1 ft SLR. Although the region is not historically exposed to major flooding, the major flood threshold is anticipated to be exceeded by return period of less than 10 years under 1 ft increase in the MSL. With 2 ft SLR, major flood frequency amplification in southwest Pacific will also increase with more than three orders of magnitude. Thus, SLR 2 ft above the current MSL will beget striking amplification of major flooding frequency in all locations along the Pacific and southeast Atlantic. With 0.5 ft SLR, minor flood will become more frequent by up to ten-fold in all stations, except those located along southwest Pacific coast and Florida Keys stations with an estimated two orders of magnitude increase. Under 1 ft SLR, the highest amplification in minor flooding (more than 500 times) was found in Florida Keys stations.

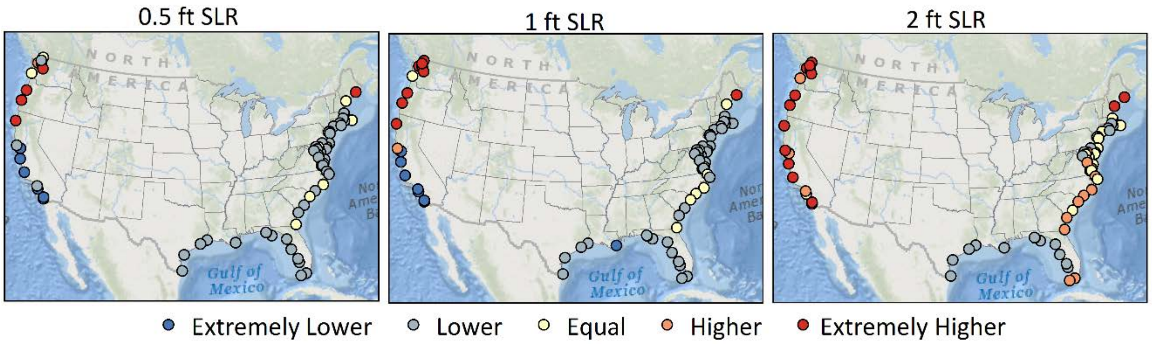

Figure 2.9. The ratio of frequency amplification of major to minor flooding

We calculated the ratio of major flood frequency amplification to minor flood frequency amplification to investigate patterns of change in flood frequency with SLR in the study regions. Results indicate varying trends by locations across the coastal CONUS (Figure 2.9). The frequency amplification of minor flooding is higher than major flooding in most of the study locations up to 1 ft SLR except locations along the northwest Pacific coast. Under 2 ft SLR, the frequency of major flooding will be amplified at higher rates in locations along the Pacific and southeast Atlantic coasts. Minor flooding frequency, on the other hand, tends to be higher along the Gulf and northeast Atlantic coasts. Thus, as sea level rises locations that historically are not exposed to major flooding are expected to experience higher frequency amplification in major flooding. Coastal areas with considerable historical major flooding will be likely exposed to higher frequency amplification in minor flooding.

2.3.5. Regional SLR scenarios for the United States

Observed and projected acceleration of SLR varies regionally across the coastal CONUS. Consequently, the indicated SLR levels in this study are expected to be realized over different time horizons in different coastal locations. Different SLR projections have been derived based on alternative climate scenarios although considerable debate still remains about the acceleration of SLR (Haigh et al., 2014; Dangendorf et al., 2017). Figure 2.10 (adapted from Sweet et al., 2017) illustrates the decade when the indicated SLR (0.5 ft, 1ft, and 2 ft) are anticipated to occur under "Intermediate Low" and "intermediate" SLR scenarios.

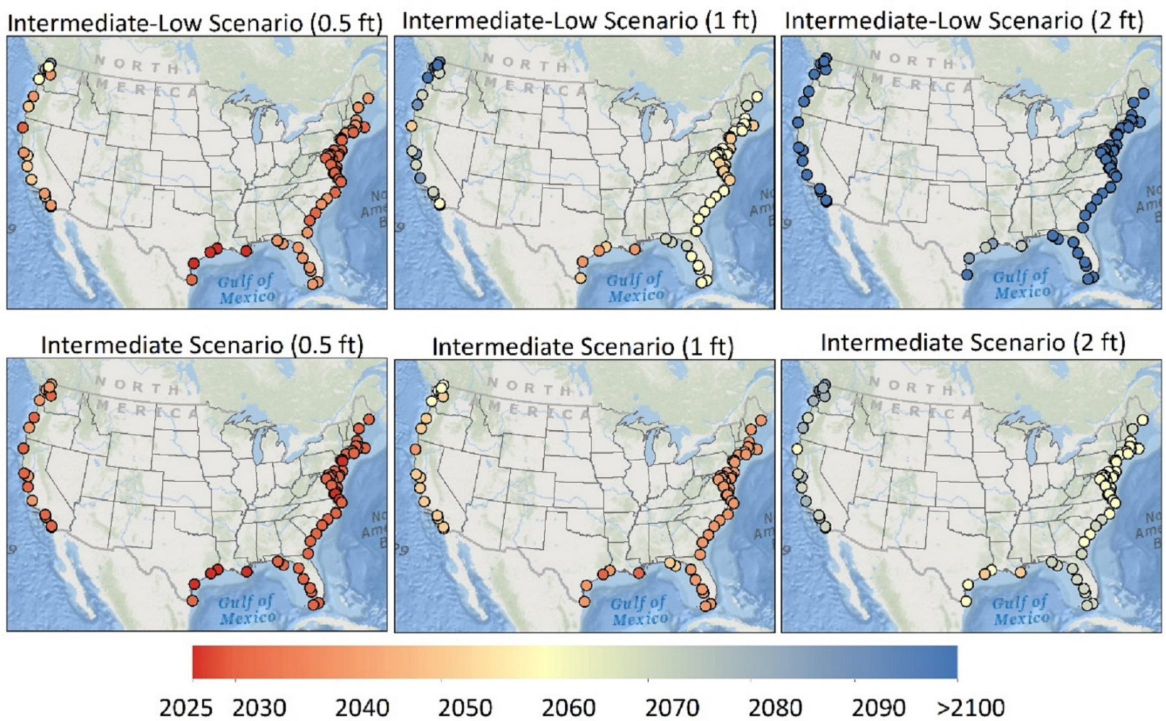

Figure 2.10. The decade when indicated SLR values are anticipated to occur under Intermediate Low and Intermediate SLR scenarios (Sweet et al. 2017)

The expected time to frequent destructive major floods with return period of 1 year under "Intermediate Low" and "Intermediate" SLR scenarios are illustrated in Figure 2.11. Under the "Intermediate-Low" scenario (Left panel), most of the stations (except stations along the west of the Gulf coast) will not experience yearly major flooding by the end of the century. However, under the "Intermediate" scenario major flooding will occur one or more times a year by approximately 2050-2060 in stations along the western Gulf and mid-Atlantic coasts, 2070-2080 in stations along southeast Atlantic (Except Florida Keys) and some stations along the northwest Pacific, and 2080-2090 in Florida Keys and stations along the southwest Pacific coasts. In general, under the “Intermediate” scenario events that are currently characterized as major flooding are anticipated to occur with return period less than a year in all stations by the end of the century.

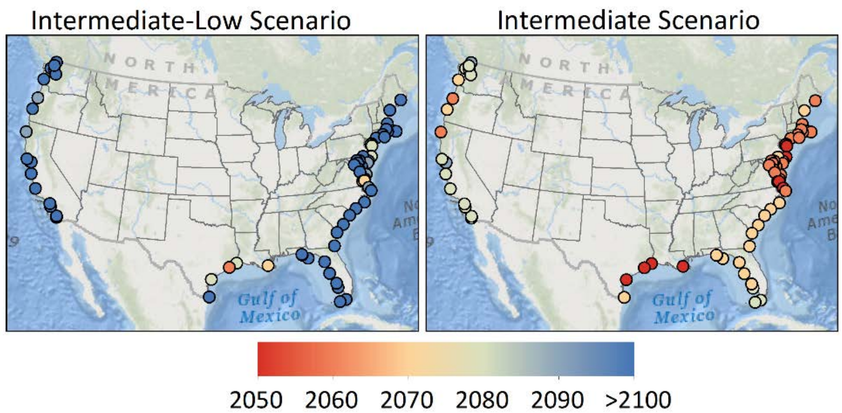

Figure 2.11. The decade when events currently characterized as major flooding are anticipated to occur with return period less than a year

2.3.6. Average annual exposure to coastal flooding

The *AAE* to minor and extreme flooding (i.e., Moderate and major flooding) for 20 populated coastal cities in the CONUS was computed under current condition and 3 different SLR levels (Figure 2.12). The *AAE* to both minor and extreme flooding is the highest in the New York City. Although the *AAE* currently is not a major concern for Miami, with 2 ft SLR Miami will encompass the second highest value of assets exposed to minor and extreme coastal flooding. This response can be attributed to less extreme water level variance in the Key West station (Church et al., 2013; Hunter, 2012), which is the closest station to Miami in this study.

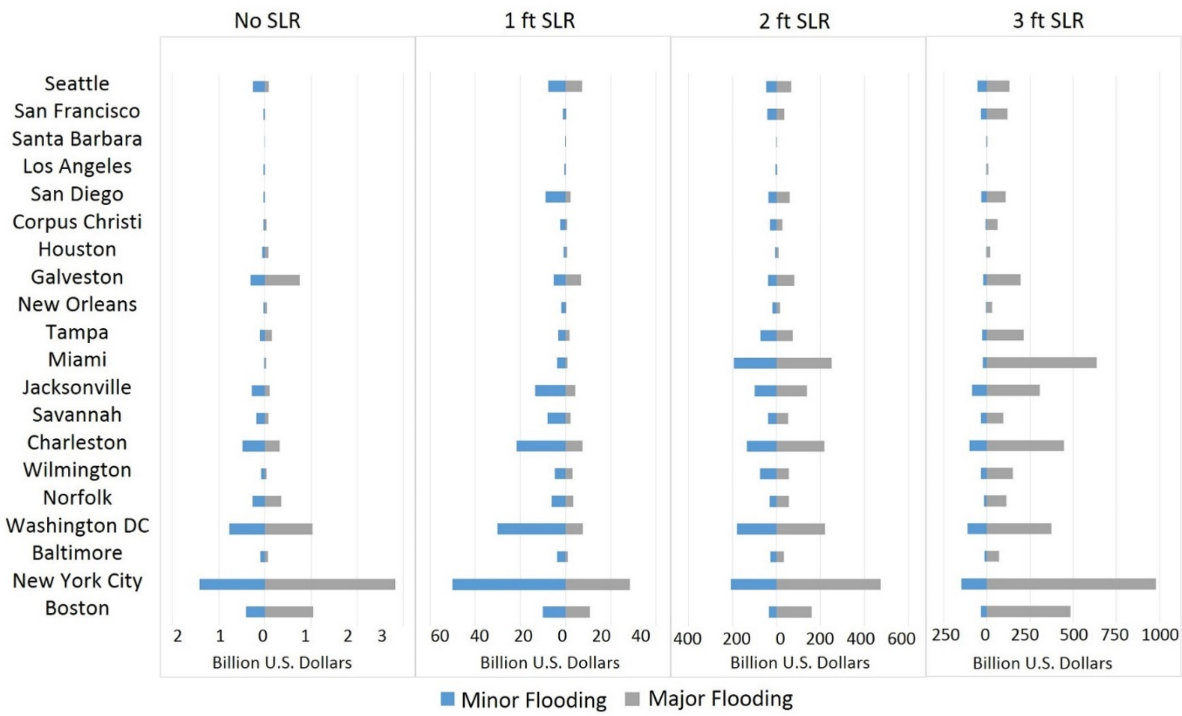

Figure 2.12. The *AAE* to minor and extreme flooding in 20 coastal cities along the coastal CONUS

The ratio of *AAE* to minor flooding to total *AAE* was calculated to explore regional trends in the contribution of each coastal flood category (Figure 2.13). Under prevailing MSL, extreme coastal flooding accounts for more than 50% of total *AAE* in the cities along the Gulf and northeast Atlantic (e.g. New Orleans and New York City). Minor flooding, however, contributes to more than 50% of total *AAE* in the study cities along the southeast Atlantic and Pacific (e.g. Jacksonville and Los Angeles). Under smaller amounts (up to 1 ft) of SLR, *AAE* will be primarily from minor flooding in all study cities. However, extreme flooding will dominate the coastal flooding *AAE* in most of the CONUS cities for SLR exceeding 2 ft.

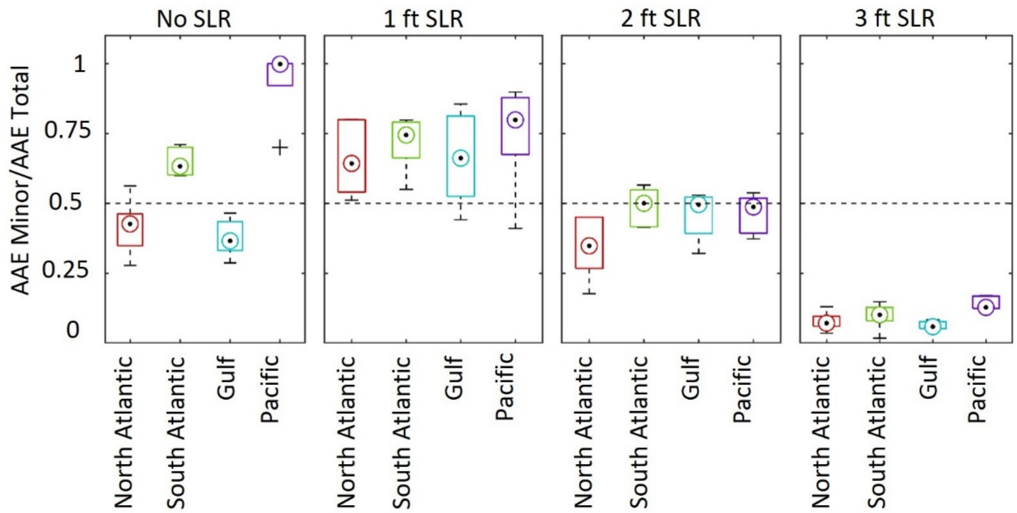

Figure 2.13. The ratio of *AAE* to minor flooding to total *AAE* for CONUS coastal regions

These responses can be explained by the components of the mixture probability model. With no rise in MSL, the tail of the sea level distribution (i.e., GPD) governs the contributions from both minor and extreme flooding. Thus, in locations with a positive GPD shape parameter contributions from acute *AAE* to extreme events exceed chronic *AAE* to minor flooding (i.e., cities along the Gulf coast). On the other hand, cumulative *AAE* from minor flooding is the dominant component of total *AAE* in the study locations with negative GPD shape parameters (i.e., cities along the Pacific coast) due to the thin-tailed distribution. With relatively small increases (e.g. up to 1 ft) in MSL, a substantial increase in annual exposure to minor flooding is evident. With up to 1f t SLR, minor flood threshold in all study cities will be smaller than the GPD threshold, and thus, exceedances of the minor flood threshold will be governed by the bulk of the Mixture distribution (i.e., Normal distribution component). Conversely, with SLR above 2 ft, moderate and major flood thresholds will also be shifted to the bulk of the water level distribution, which will lead to a greater portion of *AAE* from extreme flooding events.

Minor flooding can cause considerable indirect damages to assets and economic activities in cities, such as business interruption, road closure, traffic disruptions, economic losses, public inconvenience and long-term chronic degradation of infrastructure from increasing inundation of saltwater (e.g. Sweet et al.2014; Moftakhari et al. 2018). We do not consider these impacts in the current study. Moreover, repeated events of exposure to coastal flooding are assumed to be independent. Thus, the *AAE* used in this study may be viewed as a worst case risk estimate and is likely substantially larger than Average Annual Losses (Hallegatte et al. 2013). Detailed damage and restoration functions may be considered when actual losses are computed using the proposed mixture probability model and risk analysis approach. The nonstationary mixture model improves the capability to assess increasing coastal flood risks due to SLR. However, climate change may alter weather conditions that influence increased risks of pluvial flooding from heavy precipitation (Wahl et al., 2015; Moftakhari et al., 2017) in addition to storm surge. Further theoretical development is needed to reconcile these compounding effects in the analysis of risks to assets and communities in coastal region.

2.4 Conclusions

A nonstationary Mixture Normal-GPD probability distribution was developed to model coastal flooding frequency over a range of SLR levels. The model facilitates a coherent assessment of coastal flooding exposure to extreme events as well as minor but more frequent events. The model was parameterized for 68 tidal monitoring stations along the coastal CONUS. The results show a good fit between the model and observed sea level data in all study locations. Regional trends are evident in the estimated values of the mixture model parameters. Particularly, the distribution shape parameter, which governs the qualitative behavior of the models and risks to both chronic and acute flooding hazards, showed strong regional trends.

Model assessments reveal that all regions across coastal CONUS will experience significant increases in frequency of minor and major flooding over a range of future SLR levels. Under higher SLR scenarios (e.g. 2 ft SLR), infrequent major flooding is likely to occur multiple times per year in the majority of stations along Atlantic, Gulf, and northwest Pacific coasts. Similarly, minor flooding with exceedances of more than 150 days per year may also occur in most of the study locations. However, the frequency amplification of minor and major flooding varies by coastal regions. Pacific coast regions should expect the highest major flood frequency amplification followed by regions within the southeast Atlantic coast. These regions, especially within the Pacific coast, are most vulnerable to the amplification of major flooding frequency since under current MSL the major flood threshold is rarely or never exceeded. On the contrary, the Gulf and northeast Atlantic coastal regions are likely to be exposed to higher frequency amplification in minor flooding.

Flood frequency amplification would exacerbate inundation impacts over time and cause a considerable increase in *AAE* of property to coastal flooding. While the communities have primarily focused on mitigating acute damages from extreme events, under smaller amounts of SLR (i.e., up to 1 ft) the *AAE* to minor flooding will exceed those from extreme events in a majority of CONUS coastal regions. However, *AAE* will be mainly from extreme flooding should SLR exceed 2 ft.

The time to specific SLR scenarios varies regionally and by future climate scenarios. Subsequently, risks from minor and extreme coastal flooding will be influenced by these considerations. Planning and design of effective coastal flooding solutions must incorporate both chronic and acute risks from minor and extreme events from SLR. The mixture probability model and the coastal property exposure analysis presented in this study facilitate full characterization of risk mitigation strategies by representing their effects on flood thresholds in coastal regions. These solutions may include engineering solutions such as higher sea walls and forward pumps, or management solutions such as spatial zoning regulations and buildings codes. The analysis indicates that adaptation strategies must account for increasing frequency of unprecedented major flooding in the Pacific and southeast Atlantic regions. In the Gulf and northeast Atlantic coasts, effective infrastructural, policy and management strategies may also target enhanced long-term service reliability of flood control systems and their resiliency to the amplification of minor flooding.

CHAPTER 3.

CHRONIC AND ACUTE COASTAL FLOOD RISKS TO ASSETS AND COMMUNITIES IN SOUTHEAST FLORIDA

Highlights

Chronic and acute coastal flood risks in Miami-Dade County are assessed over the range of sea-level rise (SLR) scenarios for the coming decades. HAZUS-MH coastal flood hazard modeling and loss estimation tool are used to determine flood extent and depth and corresponding monetary losses to buildings associated with different sea water levels (SWLs). The frequency of SWLs is estimated using a nonstationary mixture Normal-Generalized Pareto distribution under current condition and future SLR scenarios. Also, the least adaptation level to cope with SLR-induced amplification of coastal flooding is assessed in terms of an increase in flood threshold. The results indicate that under current sea-level conditions, coastal flood risks are predominantly from exposure to acute extreme events. However, chronic risks from repetitive non-extreme flooding may exceed those from extreme floods under future SLR scenarios. Therefore, adaptation strategies may incorporate consideration about chronic flooding to avoid increasing cumulative losses under future SLR scenarios.

3.1. Introduction

Coastal flooding poses significant human, ecological, and economic risks in the United States (NWS 2014; Walsh et al. 2014) and globally (Hallegatte et al. 2013; Hinkel et al. 2014). Climate change increases the exposure of coastal communities to flooding due to the rising sea levels and possible increased storminess (Shepard et al. 2012; Ezer and Atkinson 2014; Rahmstorf

2017). Sea-level rise (SLR) decreases the freeboard between local flood thresholds and high water levels from tides and storm surges, which leads to increases in the frequency of both minor flooding (Sweet et al. 2014; Moftakhari et al. 2015; Vandenberg-Rodes et al. 2016) and extreme events (Ezer and Atkinson 2014; Kemp and Horton 2013; Vousdoukas et al. 2017). SLR has been shown to be the primary factor influencing the frequency and intensity of coastal events (Woodworth and Blackman 2004) and may be deemed as the chief manifestation of climate change impacts in coastal regions (Nicholls et al. 2007; Sweet and Park 2014).

Exposure to extreme coastal flooding and subsequent acute damages have been extensively investigated (Wahl et al. 2015; McInnes et al. 2016; Vousdoukas et al. 2017). However, chronic losses from frequent minor flooding events are largely neglected (Moftakhari et al. 2017; Hino et al. 2019). Recent studies have shown that the frequency and extent of minor flooding, also referred to as tidal or nuisance flooding, has been increasing in response to rising sea levels (Sweet and Park 2014; Moftakhari et al. 2015; Ray and Foster 2016; Dahl et al. 2017). Whilst damages from a single minor flooding event may be insignificant, the cumulative losses from repeated exposure of assets over a long planning period may be increasingly important (Moftakhari et al. 2018). Thus, implementation of effective SLR adaptation strategies is predicated upon an improved understanding of exposure and vulnerability to both minor and extreme coastal flooding (Purvis et al. 2008; Hallegatte et al. 2013; Aerts et al. 2014).

Extreme value distributions such as Generalized Extreme Value (GEV) or Generalized Pareto (GP) distributions are commonly used for frequency analysis of flood events (Boettle et al. 2013; Menéndez et al. 2008; Salas et al. 2018). However, under nonstationary sea-level conditions, they are not sufficient for full characterization of flood probability distributions (Sweet and Park 2014; Stephens et al. 2018; Ghanbari et al. 2019). Recently, Ghanbari et al. (2019) developed a coherent and statistically rigorous mixture probability model that represents the entire range of sea water level (SWL) values, encompassing both the bulk and the upper tail of the sea-level distribution. The mixture model uses the Normal distribution for the bulk data and the Generalized Pareto Distribution (GPD) for the upper tail values. The approach explicitly accounts for nonstationary sea-level conditions using SLR as a covariate. The nonstationary mixture model can be used to assess expected damages and other flood risk measures while considering both minor and extreme flooding over a range of sea-level rise scenarios.

The application of the mixture model in a screening-level flood risk assessment framework is demonstrated for Miami-Dade County, which encompasses one of the highest values of assets exposed to coastal flooding (Genovese et al. 2011; Hanson et al. 2011). The region covers approximately 6300 km^2 on Florida's southeastern coast with a population of approximately 2.8 million inhabitants in 2017. Approximately \$38B of property and 384 miles of roads lie 3 feet above the current mean sea-level (MSL) (Tompkins and DeConcini 2014). Communities, as well as economic and environmental sectors in low elevation and highly populated areas of Miami-Dade County are increasingly exposed and vulnerable to both minor and extreme coastal flooding due to SLR (Genovese et al. 2011; Spanger-Siegfried et al. 2017).

To date, evaluation of SLR impacts in Miami-Dade County has mostly emphasized extreme flooding driven by hurricanes and tropical cyclones (i.e., storm surge) (Genovese et al. 2011; Klima et al. 2012; Genovese and Green 2015). However, only a few studies have investigated the effects of SLR on chronic risk from minor flooding (Wdowinski et al. 2016; Moftakhari et al. 2017a). Recurrent minor flooding is already emerging as a new issue in some parts of the county (e.g., the City of Miami Beach). With the rising sea levels, many coastal cities in this region will face more frequent minor coastal floods per year (Sweet et al. 2014; Sweet and

Park 2014). Thus, a simultaneous assessment of chronic and acute risks from both frequent minor and extreme flooding under future SLR scenarios is vital to improve investments on flood adaptation strategies that would safeguard the Miami-Dade coastal region against the adverse effects of SLR.

Flood adaptation strategies in coastal regions are implemented under deep uncertainty about critical driving forces (e.g., SLR) and stakeholder preferences (e.g., climate policy targets). These uncertainties pose a challenge to coastal planners and decision makers (Kwakkel et al. 2015). Traditionally, it is assumed that the future can be predicted and in order to reduce vulnerability a restricted plan for the outlined future (i.e., static optimal plan) is developed (Dessai and Hulme 2007; Hallegatte et al. 2012; Walker et al. 2013). However, the strategy would fail if the future tends to be different from the hypothesized futures. A more prudent approach would be to use a dynamically robust plan that will be successful in a wide range of future scenarios with the flexibility to dynamically change adaptation over time as the future unfolds (Kwakkel et al. 2015; Haasnoot et al. 2013). To achieve this approach, several adaptation strategies should be evaluated against different SLR scenarios to develop robust decision-making processes (Lempert et al. 2006; Groves and Lempert 2007; Haasnoot et al. 2013).

This study aims to investigate the effects of SLR on chronic and acute coastal flood risks in Miami-Dade County by incorporating a nonstationary mixture probability model in a screening-level flood risk assessment framework. Specifically, the objectives of the study are to 1) evaluate exposure of the region to coastal flooding over a range of SLR conditions; 2) evaluate changes in chronic and acute coastal flood risks under different SLR scenarios; 3) estimate the SLR values up to which adaptation levels -- in terms of increase in a flood threshold -- could perform acceptably and meet the policy target; and 4) identify the minimum adaptation level that might be needed to maintain the current level of flood risk. The study estimates the vulnerability of the region to coastal flooding over the course of the 21st century and identifies areas where chronic and acute flood risks are potentially high. The results can provide managers and decision makers in Miami-Dade County with preliminary information about current and future coastal flood risks. The improved understanding of risks and adaptation levels enhances the capacity for resilient coastal management.

3.2. Materials and Method

The nonstationary mixture Normal-GPD probability model developed by Ghanbari et al. (2019) was used within a screening level risk assessment framework to simultaneously assess chronic and acute coastal flood risks under higher MSL conditions in Miami-Dade County. The flood extent and depth corresponding to different SWL values are estimated using HAZUS coastal flood hazard modeling and monetary losses to buildings were estimated using the HAZUS loss estimation tool. Adaptation levels in terms of increases in the flood threshold were evaluated over a range of continuous SLR values to support the development of robust decision-making processes. Three possible SLR scenarios were considered to perform an assessment of expected time to certain rises in MSL, including: “Intermediate-Low”, “Intermediate”, and “Intermediate-High” as defined in Sweet et al. (2017).

3.2.1. Sea water level data (SWL)

69 years of hourly SWL data at the Key West tidal station over the 1950-2018 period (https://tidesandcurrents.noaa.gov/) were used for coastal flood frequency analysis. The hourly sea-level data are reported relative to the latest National Tidal Datum Epoch (NTDE), which references the 1983-2001 period with mean higher high water (MHHW) as the tidal datum. It

should be noted that the Virginia Key and South Port Everglades tidal stations are closer to the County, however, both stations have been operational for less than 30 years. The datum for the Virginia Key tidal station was used to adjust SWL data in Key West tidal station (https://tidesandcurrents.noaa.gov/stations.html?type=Datums).

3.2.2. Losses to buildings from coastal flooding

HAZUS-MH, FEMA's standardized modeling tool for estimating potential losses from flood events, was used to estimate monetary losses to buildings associated with different SWLs. First, HAZUS coastal flood hazard modeling was used to determine flood extent and depth corresponding to different SWL exceedances above MHHW (i.e., 0.3 m to 3 m with equidistant steps of 0.3 m). Coastal flood hazard modeling in HAZUS is similar to that presently used by FEMA to produce coastal Flood Insurance Rate Maps (FIRMs) (Scawthorn et al. 2006a; b). The approach considers lands that are adjacent to the sea and are situated below the stillwater flood surface to be inundated areas. Low-lying areas without a hydraulic connection to the flood source are identified during overlaying the stillwater flood surface over a digital elevation model (DEM) in order to identify disconnected areas that should not be considered as floodplains (i.e., Bathtub method without hydrological connectivity) (Yunus et al. 2016). The approach neglects the effects of terrain roughness and vegetation on the spread of floodwater flow (Ramirez et al. 2016). In addition, the duration of the flood event is not considered, and it is assumed that the flood propagation is only limited by topography. These limitations and assumptions are the reason that the bathtub model could overestimate flood extents (Mcleod et al. 2010; NOAA 2010; Bates et al. 2010). Regardless of the shortcomings of the bathtub method, the simplicity of the algorithm and low computational complexity of this model has made it a valuable method to create regional to large scale potential coastal inundation maps (e.g., Mokrech et al. 2014; Lloyd et al. 2016). The bathtub method is primarily based on topography, and the quality of DEM can significantly affect the inundation area (Van de Sande et al. 2012). In this study, we used 1/9 arc-second (~ 3-meter) DEM data.

The produced flood hazard maps (i.e., flood extent and depth) were subsequently used in the HAZUS flood loss estimation module to calculate physical damages, which were interpreted in direct dollar values of building replacement cost (i.e., the cost of replacement by an identical object) (Scawthorn et al. 2006a; FEMA, 2018). Consequently, monetary losses to buildings were estimated at the Census block scale for different SWL exceedances above MHHW (i.e., 0.3 m to 3 m with equidistant steps of 0.3 m). The losses were estimated based on the general building stock inventory data aggregated at the Census block scale in HAZUS Level 1 analysis (Scawthorn et al. 2006b). This approach provides an estimate of the direct losses to buildings and the immediate impact of building damages on the community such as business interruption and job losses are not incorporated.

The available datums in HAZUS-MH are NAVD88 and NGVD29. Thus, the reference datum for Key West tidal station was used to change the datum for SWL data from MHHW to NAVD88. The estimated damages from HAZUS were used to develop a loss function (i.e., losses versus SWL of h, $C_i(h)$) for each Census block (i) in the region, which accounts for spatial variability. It was assumed that losses value is linearly changed between consecutive SWLs.

3.2.3. Mixture Normal-GPD probability model

Historical adjusted SWL data from the Key West tidal station was used to estimate the annual exceedance probability of SWL of h under current and future conditions using a nonstationary Mixture Normal_GPD probability distribution (Ghanbari et al. 2019). The mixture model uses the

Normal distribution to characterize the non-extreme (i.e., bulk) component of the SWL data and the extreme component of the data (i.e., upper tail) is represented by the GPD. The nonstationarity of SWL data is incorporated by expressing the location parameters of the Normal and GP distributions as functions of SLR instead of time. Thus, the future risk of coastal flooding under alternative SLR levels can be evaluated regardless of projected time to certain sea-level conditions. Following Ghanbari et al. 2019, the mixture cumulative distribution function (F) of SWL (h) is defined as:

$$F(h|\mu,\sigma,u,\alpha,\xi,\phi) = \begin{cases} \dfrac{(1-\phi)}{1+erf\left(\dfrac{u-\mu}{\sigma\sqrt{2}}\right)}\left[1+erf\left(\dfrac{h-\mu}{\sigma\sqrt{2}}\right)\right] & h < u \\ (1-\phi)+\phi\left[1-\left(1+\xi\dfrac{h-u}{\alpha}\right)^{-\frac{1}{\xi}}\right] & h \geq u \end{cases} \tag{3.1}$$

where u, α and ξ denote the location (i.e., threshold), scale, and shape of the GPD. Variables μ and σ represent location and scale of the Normal distribution, ϕ denotes the probability of independent exceedances over threshold, and erf is the error function.

3.2.4. Coastal flood risk assessment

Flood risk emerges from the interaction of flood hazard probability, exposed values, and their vulnerability (Crichton 1999; Merz et al. 2010). A commonly used risk indicator for flood risk assessment is Average Annual Losses (AAL) (Kron 2005; Purvis et al. 2008). AAL can be estimated by integrating the area under a loss exceedance function, which is a function that presents the relationship between exceedance probability of SWL of h (here $p(h) = 1-F(h)$) and the value of losses that the level of water inflicts on property and assets (here $C_i(h)$) (Jonkman et al. 2008; Grossi et al. 2005). In this study, risks from coastal flooding were categorized into two types: (1) chronic risk from frequent non-extreme (i.e., minor) flooding events with multiple occurrences per year, which are largely driven by tidal fluctuations rather than storm surge, and (2) acute risk from infrequent extreme flood events with less than one event per year frequency that usually arise from hurricanes and extreme weather conditions. Annual losses as a function of the exceedance probability of the daily SWL (i.e., loss exceedance function) were estimated for each Census block as:

$$L_i(p) = n_y * C_i\big(F^{-1}(1-p)\big) \tag{3.2}$$

where n_y denotes the number of SWL observations per year, C_i represents the loss function corresponding to the i^{th} Census block, F^{-1} is the inverse cumulative distribution function of the SWL from Eq. 1, and p represents the daily SWL exceedance probability. Subsequently, acute AAL was estimated as follows:

$$\text{Acute } AAL = \sum_{i=1}^{k} \int_{0}^{\tau_1} L_i(p)\, dp \tag{3.3}$$

where $L_i(p)$ is loss exceedance function corresponding to the i^{th} Census block, k is the number of Census blocks in Miami-Dade County, and τ_1 denotes the upper bound of daily exceedance probability for estimation of acute AAL. τ_1 may be determined such that acute risk encompasses occasional extreme flooding events with an annual return period larger than 1-year.

Similarly, chronic AAL was estimated by:

$$\text{Chronic } AAL = \sum_{i=1}^{k} \int_{\tau_1}^{\tau_2} L_i(p)\, dp \tag{3.4}$$

where τ_2 represents the upper bound of daily exceedance probability in the estimation of chronic AAL. τ_2 may be determined such that the chronic damages from frequent minor flooding events are independent. Thus, τ_2 represents the inverse of the smallest expected length (i.e., number of days) between two consecutive minor flooding events that lead to independent damages (i.e., the smallest daily exceedance probability). For example, if damages that are at least 1 day or 5 days apart are assumed to be independent, τ_2 would be equal to 1 or 1/5 d^{-1}, respectively. Schematic representation of the relationship between losses and exceedance probability of SWL of h is shown in Figure 3.1.

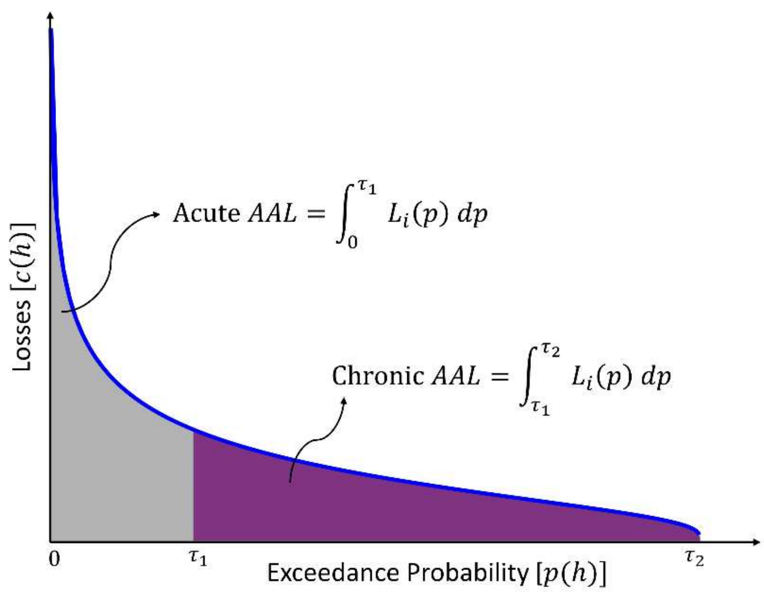

Figure 3.1. Schematic of the relationship between losses and exceedance probability of sea water level of h

3.2.5. Study region

The coastal flood risk assessment was limited to the eastern part of Miami-Dade County since the preliminary results using the bathtub method provided unrealistic flooding in response to SLR in western regions. It is possible that the western regions could experience flooding due to reduced drainage capacity when the existing extensive canal and pumping infrastructure system is compromised as sea level rises. However, the determination of the potential flooding in western portions of the county requires the application of a comprehensive hydrologic/hydraulic routing model, which also simulates the rising groundwater levels due to both rainfall and SLR. Such a modeling task was beyond the scope of this study. Moreover, coastal flooding induced by tidal or storm surge currents is likely to be concentrated in the coastal regions.

3.2.6. Projected SLR scenarios

The regional SLR projections for Key West tidal station from the report by Sweet et al. (2017) were used to perform an assessment of expected time to certain changes in MSL by 2100. The available projections include “Low”, “Intermediate-Low”, “Intermediate”, “Intermediate-High”, “High”, and “Extreme” SLR scenarios, which correspond to 0.3m, 0.5m, 1m, 1.5m, 2m, and 2.5m global SLR, respectively. While the “Intermediate Low” scenario has a 73% chance of being exceeded under Representative Concentration Pathway (RCP) 4.5 climate change scenario, the “Intermediate” and “Intermediate-High” scenarios have 17% and 1.3% chances of being exceeded under the RCP 8.5 climate change scenario, respectively (Kopp et al., 2014; Sweet et al., 2017). The chance of exceedance of more extreme scenarios (i.e., high or extreme scenario) is extremely low.

3.2.7. Adaptation of rising coastal flood risk

Coastal planners and decision makers should evaluate and implement various adaptation strategies to manage and reduce enhanced future flood risk due to uncertain SLR (Hinkel et al. 2013; Baxter 2013). All three elements of flood risk (i.e., flood hazard probability, exposed values, and their vulnerability) can be altered by different strategies (Baxter 2013). For example, technical engineering measures such as sea walls, forward pumps, flood barriers, and levees lower the chance of flooding and spatial zoning regulations limit the number of people and values at risk. Other measures such as elevating houses and wet or dry flood proofing (Baxter 2013) may reduce flood risks by lowering the vulnerability of buildings (Kreibich et al. 2005; Kreibich and Thieken 2009). Although the choice among these solutions requires diligent planning, deployment of any of these measures ultimately leads to an increase in the SWL at which a community begins to flood (i.e., increase in the flood threshold).

In this study, chronic and acute AAL were estimated under different SLR levels when hypothetical adaptation strategies (e.g., seawall, flood barriers, levee, and coastal retreat) were adopted to increase the level at which the region begins to flood (i.e., increase in the flood threshold). The flood adaptation was incorporated in the analysis by truncating the loss exceedance function at the exceedance probability of the new flood threshold (i.e., revised τ_2) and estimating the AAL as the area of the remaining part of the loss exceedance function. Chronic and acute AAL from coastal flooding events were calculated under continuous SLR levels (i.e., 0 to 60 cm) and increase in flood threshold (i.e., 0 to 90 cm) with equidistant steps of 3 cm.

3.3. Results and Discussion

The return period of future coastal flooding events will likely become shorter in Miami-Dade County if sea level continues to rise. Subsequently, both chronic and acute coastal flood risks could increase. However, under higher MSL conditions, the bathtub model applied here suggests that the chronic risk from frequent non-extreme flooding could surpass the acute risk from occasional extreme events. In addition, the minimum adaptation level that might be needed to maintain the current level of flood risk varies with SLR values. Due to the simplification of the physical processes in the determination of flood extent and depth, the results from this study should be used with care but they should be useful for screening-level assessments of damages due to future stresses such as SLR.

3.3.1. Determination of limits for the estimation of chronic and acute risks

The upper limit (τ_1) in the estimation of acute AAL is approximately 1/365 d^{-1}, since acute risk is defined as risks from infrequent extreme flood events with a frequency of less than one event per year. The precise estimation of expected time between independent damages (i.e., $1/\tau_2$) requires information about the relation between the building recovery time (e.g., number of days) and the functionality reached for a given damage level (i.e. building restoration functions) (Lin and Wang 2017). However, this information specific to the study region is rarely available. Thus, in the current study, in order to approximate the upper limit (τ_2), the sensitivity of chronic AAL to the lengths between independent damages (i.e., 1 to 90 days) was explored under three SLR levels (Figure 3.2).

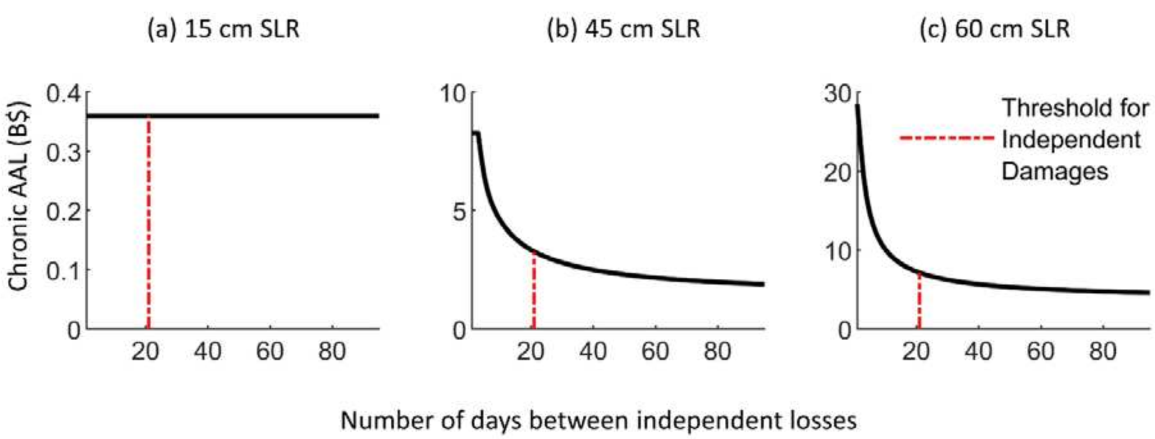

Figure 3.2. The empirical relationship between chronic AAL and the number of days between independent losses under (a) 15 cm SLR (b) 45 cm SLR and (c) 60 cm SLR

The results show that the number of days between independent losses does not affect chronic AAL under 15 cm SLR since the expected length between flood events would remain greater than 90 days. However, under higher MSL values (e.g., 45 cm and 60 cm SLR) the number of days between independent losses affects the estimated chronic AAL. Clearly, as the length of time between independent events decreases, the chronic AAL increases. However, the rate of change becomes less steep when the number of days is more than about 21. Thus, it was assumed that losses should be at least 21 days apart to be considered as independent. Furthermore, it may be assumed that buildings are protected and losses are negligible when SWL is lower than the flood threshold. Thus, τ_2 should be less than the daily exceedance probability of the flood threshold, which is 0.52 m above MHHW at the Key West station (Sweet et al. 2018). Hence, τ_2 was set as the minimum of 1/21 (0.048 d^{-1}) and the daily probability of exceedances over the flood threshold, which for instance is equal to 0.0005, 0.003, and 0.84 under current condition, 15 cm, and 60 cm SLR, respectively.

3.3.2. Current and future coastal flood frequency

Figure 3.3 (left panel) illustrates changes in the return periods of future coastal flooding at the Key West tidal station under four SLR values. The year when the indicated SLR values are anticipated to occur is presented in Table 3.1 under all regional SLR scenarios (Sweet et al. 2017). The future return periods of coastal flooding could decrease and even under the smallest indicated SLR level (15 cm), a considerable decrease in return periods might happen. For example, the 100-year flood will become a 5-year flood under 15 cm SLR, which may happen by 2035 or 2045 under the "Intermediate" or "Intermediate-Low" SLR Scenarios, respectively.

Table 3.1. The year when indicated SLR values are anticipated to occur under alternative regional SLR scenarios (The values are rounded to the nearest 5-year interval)

SLR Scenario	SLR value			
	15 cm	30 cm	45 cm	60 cm
Low	2050	2090	>2100	>2100
Intermediate-Low	2045	2070	>2100	>2100
Intermediate	2035	2050	2060	2075
Intermediate-High	2030	2040	2050	2060
High	2025	2035	2045	2055
Extreme	2020	2030	2040	2050

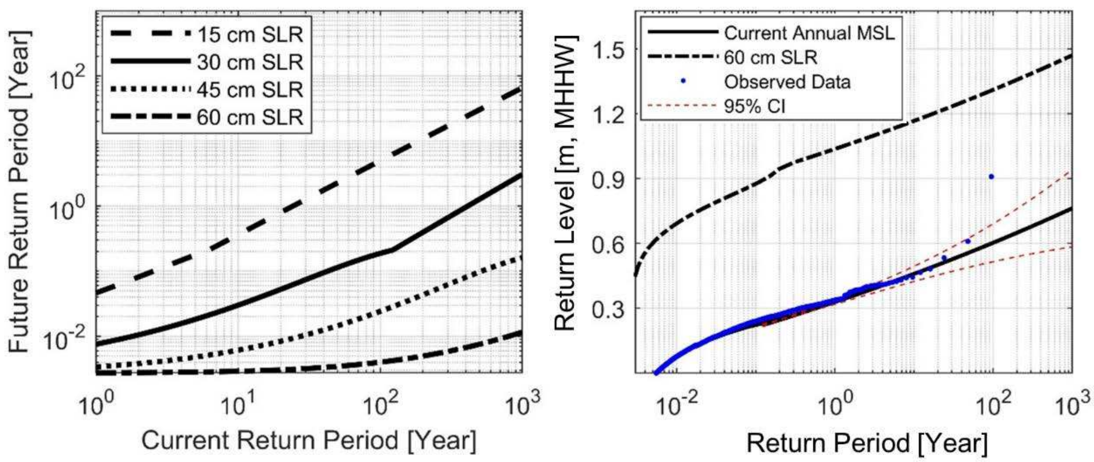

Figure 3.3. (Left) Current vs. future coastal flood return period at the Key West tide gauge (Right) Return level interval curves for the current situation and 60 cm SLR level along with the empirical return period return level intervals (dots)

This sensitive response to SLR can be attributed to small extreme sea-level variance at the Key West station (Church et al. 2006; Hunter et al. 2013). The empirical and simulated relationships between return periods and the corresponding flood heights are depicted in Figure 3.3 (right panel). The relationship between flood levels and corresponding annual return periods will change if sea levels continue to rise (Rahmstorf and Coumou 2011; Ray and Foster 2016).

3.3.3. Impacts of SLR on acute and chronic coastal flood risks

Without the implementation of adaptation strategies, based on the bathtub approach used here, the total AAL could increase to almost 12 billion dollars as a result of SLR (Figure 3.4). Under the current condition, acute extreme coastal flooding accounts for most of the expected annual losses. However, cumulative chronic AAL from frequent minor flood events could exceed the acute AAL from extreme events under future MSL conditions. With a 15 cm increase in MSL, chronic flooding events would account for almost 50% of total AAL. Under 30 cm SLR value the chronic and acute AAL could be approximately \$1.6 B and \$0.9 B, respectively.

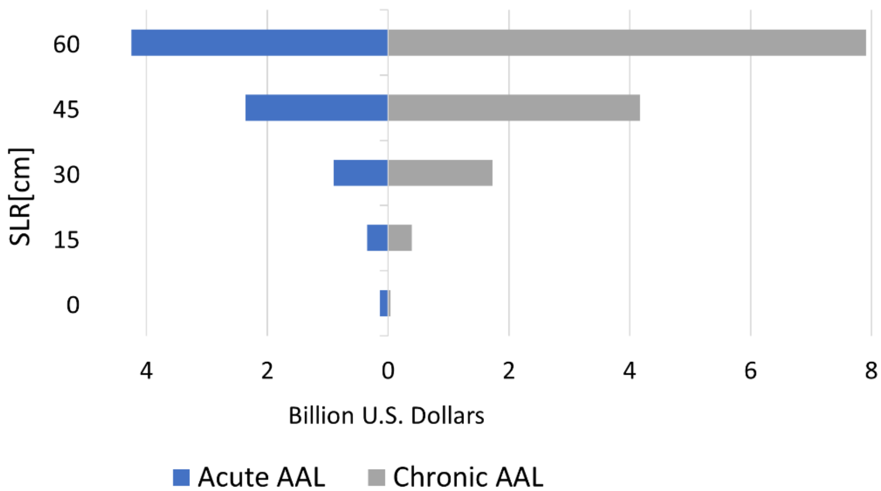

Figure 3.4. Chronic and acute *AAL* in Miami-Dade County

Chronic coastal flood risks in Miami-Dade County could be highly sensitive to even small shifts in sea-level due to low topography and densely populated coastal areas (Chakraborty et al. 2014; Genovese and Green 2015). Therefore, if sea level continues to rise, appropriate adaptation strategies might be needed to protect the region against cumulative losses from frequent non-extreme flooding events. The spatial distribution of chronic and acute *AAL* under current condition and 30 and 60cm SLR is presented in Figure 3.5. The City of Miami Beach has potentially the highest chronic and acute flood risks under 30 and 60 cm SLR. Especially the low-lying areas in the western part of the city are highly vulnerable to chronic risks from minor flooding induced by tidal fluctuations.

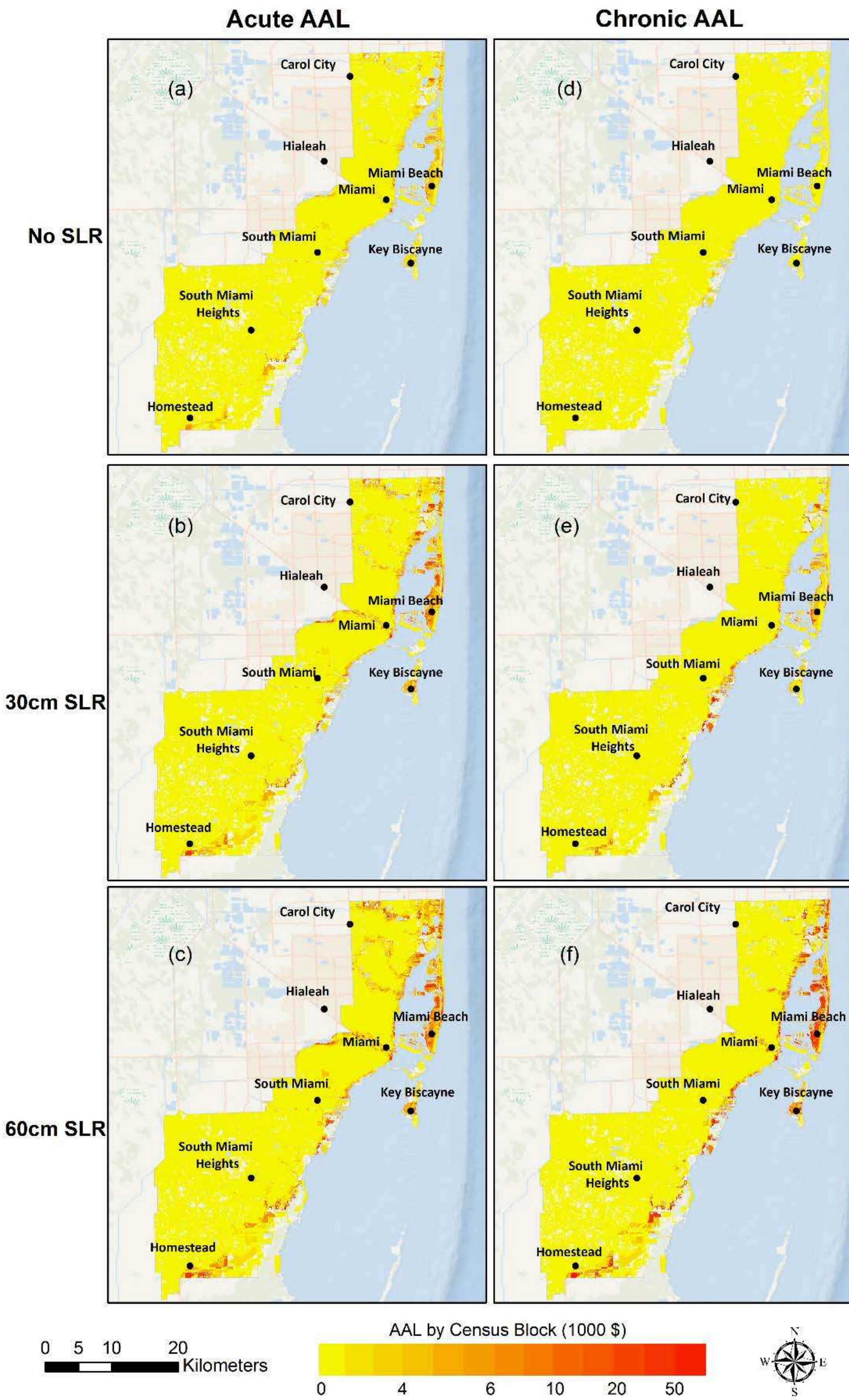

Figure 3.5. (a), (b), (c) Spatial distribution of acute *AAL* by Census Block under current condition, 30 cm SLR, and 60 cm SLR, respectively. (d), (e), (f) Spatial distribution of chronic *AAL* under current condition, 30 cm SLR, and 60 cm SLR, respectively.

3.3.4. Assessing the effects of flood adaptation strategies

The relationships between SLR and total AAL under different flood threshold levels could be used to specify the magnitude of SLR beyond which current adaptation plans may no longer be effective to meet policy targets (i.e., tipping point) (Kwadijk et al. 2010). The analysis can subsequently provide information to develop a sequence of adaptation measures over time to meet predefined targets under an uncertain future (e.g., Adaptation pathways) (Haasnoot et al. 2013; Zandvoort et al. 2017).

In this study, the current coastal flood risk ($ 170 M) is used as the acceptable AAL risk target (i.e., policy target) to maintain the current level of flood risk. Figure 3.6 illustrates the estimated total AAL versus SLR for four flood threshold levels. As sea-level rises, total AAL could exceed the target (the current flood threshold line relative to the dashed line). Thus, it could be necessary to change the adaptation strategy level to meet the target under higher MSL conditions. The analysis also suggests the expected time at which the new adaptation strategies are needed based on different SLR projections. For example, in the case of a 30 cm increase in flood threshold, the tipping point would be reached within approximately 30, 20 and 15 years (i.e., the year 2050, 2040, and 2035) under the Intermediate-low, Intermediate, and Intermediate-high SLR projections, respectively.

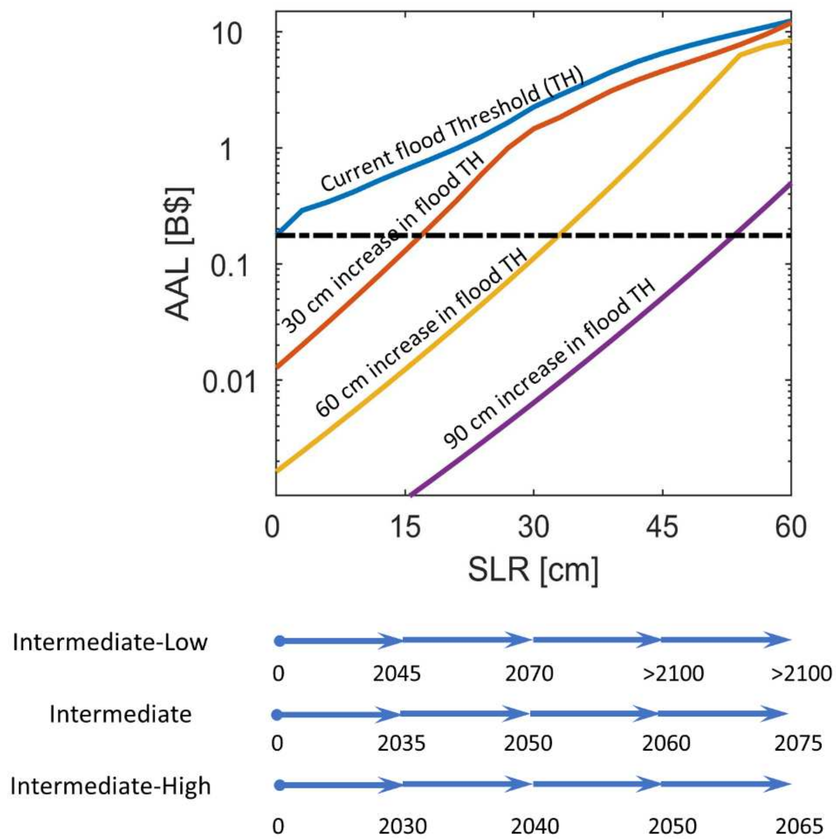

Figure 3.6. Total *AAL* under continuous SLR values and four levels of flood threshold and the year when indicated sea level rise values are anticipated to occur under Intermediate-Low and Intermediate and Intermediate-High sea level rise scenarios (The values are rounded to the nearest 5-year interval)

The potential impacts of different SLR values on chronic and acute *AAL* under varying flood threshold levels are illustrated in Figure 3.7. The *x*-axis represents the primary driving force (i.e., SLR), while the y-axis represents the adaptation strategy levels (i.e., increase in flood threshold). This analysis could be used to estimate minimum adaptation levels in terms of increases in the flood threshold to prevent increases in chronic, acute, and total *AAL* at varying SLR levels in order to maintain the current level of flood risk. The slope of isolines indicates that the least adaption level that would be needed to compensate the negative impacts of SLR varies by SLR. The least adaptation level that would be needed to keep the current flood risk at the same value is higher than the value of SLR itself. For example, an approximately 45 cm increase in flood threshold is needed to offset a 30 cm SLR. The vertical isolines in the middle panel illustrate the level of increase in flood threshold that might not be effective in decreasing acute AAL under different SLR values. For example, under 30 cm SLR, a 30 cm increase in flood threshold might not be effective to compensate the negative impact of SLR on acute AAL. However, they could be effective in decreasing chronic AAL.

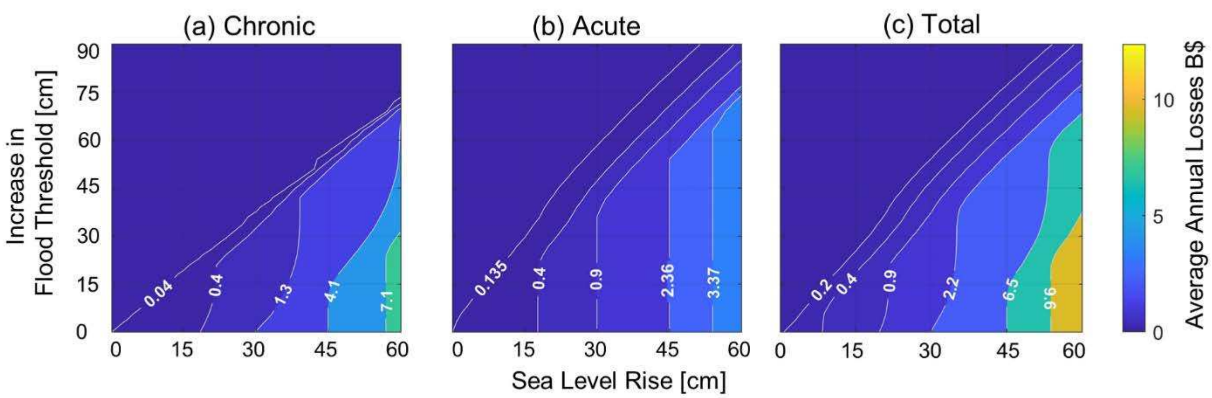

Figure 3.7. Illustration of the relationship between SLR and increases in flood threshold and (a) chronic AAL (b) acute AAL, and (c) total AAL

While quantification of losses using HAZUS analysis may provide reasonable first estimates for flood risk analysis, deploying a comprehensive hydrologic/hydraulic routing model could improve the flood hazard mapping. Moreover, management of surface waters in the region via the existing extensive canal and pumping infrastructure system were not considered in the current study, which likely leads to overestimation of flood risks. Furthermore, indirect losses such as traffic disruptions, business interruption, road closures, economic losses, and public inconvenience (Sweet and Park 2014; Moftakhari et al. 2018) were not included in the analysis and should be taken into account in future studies Risks from pluvial flooding and heavy precipitation may also increase due to alterations in groundwater (Groves et al. 2018) and weather conditions. Thus, the compounding effect of pluvial/fluvial and coastal flooding (Nadal et al. 2010; Karamouz et al. 2015; Moftakhari et al. 2017b) should also be considered in future work.

3.4. Conclusion

The potential chronic and acute impacts of SLR on coastal flooding were assessed in Miami-Dade County under nonstationary sea-level conditions by incorporating a nonstationary mixture Normal-Generalized Pareto distribution in a screening-level risk assessment framework. Flood inundation maps and corresponding monetary losses to buildings associated with different SWLs were estimated using HAZUS coastal flood hazard modeling and loss estimation tool. Under higher MSL conditions, the approach applied here suggests that the chronic risk from frequent minor flooding events may surpass the acute risk from extreme events. The possibility that chronic risk from frequent minor events may aggregate over time and turn into high-cost impacts could become a serious challenge for policymakers and politicians in Miami-Dade County. The coastal communities of Miami-Dade County should take steps toward adaptation strategies to reduce losses from minor repetitive events since their chronic impacts could pose considerable cumulative costs over time.

In order to identify the effect of different adaptation levels on future coastal flood risks, the chronic and acute AAL from coastal flooding were estimated under different plausible combinations of SLR and adaptation level values. The results specify how increases in the flood threshold could affect chronic and acute risks from minor and extreme flooding events under a continuous range of SLR values. The approach is less dependent on SLR projections than traditional top-down approaches that start from SLR scenarios. This approach also allows estimation of the minimum adaptation level to compensate the negative impacts of SLR in order to maintain the current level of chronic and acute flood risk. The results show that delayed response to chronic risks could result in costly losses that might have been avoided if appropriate adaptation strategies had been adopted in time.

CHAPTER 4.

CLIMATE CHANGE AND CHANGES IN COMPOUND COASTAL-RIVERINE FLOODING HAZARD ALONG THE U.S. COASTS

Highlights

The co-occurrence of coastal and riverine flooding leads to compound events with substantial impacts on human life, property, and infrastructure safety in low-lying coastal areas. Climate change could increase the level of compound flood hazard through higher extreme sea levels (SLs) and river flows. In this study, a bivariate flood hazard assessment method is proposed to estimate compound coastal-riverine frequency under current and future climate conditions. A copula-based approach is used to estimate the joint return period (JRP) of compound floods by incorporating sea level rise (SLR) and changes in extreme river flows into the marginal distributions of flood drivers. Specifically, the changes in JRP of compound major coastal-riverine flooding, defined based on flood impact thresholds, are explored by mid-century. Subsequently, the compound flood risk is assessed in terms of probability of occurrence of at least one compound major coastal-riverine flooding for a given design life. The proposed compound flood hazard assessment is conducted at 26 paired tidal-riverine stations along the Contiguous United States coast with long-term observed data and defined flood impact thresholds. We show that the northeast Atlantic and western part of the Gulf coasts are experiencing the highest compound major coastal-riverine flood probability under current conditions. However, future SLR scenarios show emerging high compound major flooding probability along the southeast Atlantic coast. The impact of changes in extreme river flows is found to be negligible in most of the locations except the southeast Atlantic coast. However, even in this region, its impact is considerably less than that of SLR.

4.1. Introduction

Coastal cities are exposed to multiple flood drivers such as extreme coastal high tide, storm surge, extreme precipitation, and river flow. The interaction among these flood drivers may cause a compound flood event (Moftakhari et al., 2017; Wahl et al., 2015) that could exacerbate flood impacts and cause huge social and economic losses (Hemmati et al. 2020; Zscheischler et al. 2018). In regions where the flood level is influenced by both extreme sea levels (SLs; either from tide or storm surge) and river flows, considering the co-occurrence of these flood drivers is important to predict the potential of high-impact compound flood events (Moftakhari et al., 2019).

Compound coastal-riverine flooding could happen as a result of two distinct mechanisms: 1) low-pressure systems passing through coasts have the potential to increase SLs above the coastal flood thresholds. The accompanying frontal systems lead to excessive precipitation, which can result in streamflows exceeding critical thresholds (Zheng et al., 2014; Feifei Zheng et al., 2013). When these flood drivers coincide in space and time compound flood events happen, which can amplify flood risk and severity in coastal low-lying areas. 2) river flow can be affected by high SLs due to backwater effects and impeding a free river flow to sea. Estuary regions with low elevation may be affected more by this mechanism (Ganguli and Merz 2019).

Several compound coastal-riverine flood events have been recorded in the past century in the U.S. Among the most severe of them, the coincidence of storm surge and excessive precipitation during Hurricane Harvey in August 2017 resulted in extensive flooding with over 80 fatalities and large economic costs in Houston (Van Oldenborgh et al. 2017). Hydrographs show that most rivers and bayous in Houston crested within a 24-hour period. Despite several recent studies on interaction between extreme SLs and river flows at local (Fang et al. 2020; Khanal et al. 2019; Moftakhari et al. 2017b; Orton et al. 2020), continental (Bevacqua et al. 2019a) and, global (Couasnon et al. 2020; Eilander et al. 2020; Ward et al. 2018) scale, a comprehensive assessment of impact of climate change on compound coastal-riverine flooding has not been explored along the coastal U.S. This research gap is important due to several reasons.

First, climate change is expected to increase the level of compound coastal-riverine flood hazard through higher extreme SLs and river flows. The global mean sea level (GMSL) has risen over the past decades and it is anticipated to continue to rise at increasing rates, globally and regionally (Le Cozannet et al. 2015; Howat et al. 2007; Rahmstorf 2017). The freeboard between high SLs and local flood thresholds will reduce as a result of sea level rise (SLR). Thus, coastal flood thresholds will be exceeded more frequently under higher GMSL (Kemp and Horton 2013; Vandenberg-Rodes et al. 2016; Vousdoukas et al. 2017). Considering SLR, the risks of compound flooding are likely to increase due to an increase in exceedances over coastal flood threshold (Ghanbari et al. 2019) and also impeding a free river flow to sea (Moftakhari et al. 2019). Thus, it is essential to consider future SLR projections in compound coastal-riverine flood hazard assessment.

Several studies based on modeling and observations show that climate change is also influencing extreme hydrological events regionally (Ahn and Palmer 2016; Peterson et al. 2008). For example, while some areas have experienced an increase in the frequency of heavy precipitation and extreme streamflow events (e.g., central U.S., Pryor et al. 2009; and eastern U.S., Groisman et al. 2001, 2005), some other regions have experienced prolonged droughts (e.g., Southwest U.S. , Cook et al. 2015; Heidari et al. 2020a; b). Such changes in hydrological conditions have an immediate impact on the risks of fluvial and pluvial flooding. With the increase of extreme streamflow frequencies, coastal regions threatened by SLR could experience exacerbation of consequence of compound flooding events. Therefore, consideration should be given to possible increase in co-occurrence of exceedances of high SLs or river flows above flood thresholds.

Under rapidly changing environments, nonstationarity in the future extreme does not necessarily depend on the historical series characteristics and the future may not follow the trend laid down in the past. Hence, incorporating the model-driven climate change projections in assessing compound flood hazard has now become more and more essential to obtain the future realizations of sea level and streamflow extremes. It is important to understand the effect of projected SLRs and river flows on compound flood hazards in coastal communities to better support coastal planners and policymakers for more informed adaptation and mitigation strategies.

Second, a comprehensive assessment of compound coastal-riverine flooding based on impact flood thresholds is lacking. The flooding impacts are dependent on the existing flood defenses, the extent of infrastructure vulnerabilities, adaptation strategies that are in place, and the social and economic status of the region (Hague et al. 2019). Previous global and national studies on compound coastal-riverine flooding explore annual exceedance probability without specific consideration of compound flood impacts in different locations. To explore high flood levels due to the concurrence of high SLs and river flows at a large scale, metrics should be based on consequences rather than just probability (Hague et al. 2020). In many situations, there is no exact correspondence between the extremeness of flood events based on return periods (i.e., probability of occurrences) and the impact they cause. Considering just probability, a comparison of flooding impacts over large areas is difficult to obtain. However, using flood impact thresholds facilitates comparison between different regions.

Impact flood thresholds are established for many tide gauges and river stations in the U.S. by the National Oceanic and Atmospheric Administration (NOAA)(Sweet et al. 2018) and National Water Information System (NWIS) World Wide Web site (NWS 2019), respectively, for forecasting purpose, securing public safety, and taking steps to increase preparedness level. Flood categories based on exceedances over impact flood thresholds describe the severity of flood impact. While minor flooding refers to events with minimal or no property damage, moderate flooding is accompanied with some inundation of structures and roads and has relatively considerable damages to private and commercial property. As flood level increases to major flood threshold, inundated area and infrastructure impact escalate significantly.

Now suppose that both coastal and riverine major flood thresholds are exceeded simultaneously or in close succession (hereinafter, compound major flooding). The flood extent, depth, and duration can be exacerbated, and consequently, the disruptive impact increases strongly. The joint occurrence of compound major flooding may elevate flood water levels to a critical point that devastate coastal communities through erosion and inundation of low-lying areas and might consequently have implications for flood protection policy. Thus, the information about the current and future frequency of simultaneous or near-simultaneous exceedances over both coastal and riverine flood thresholds should be considered in planning and designing in estuary regions especially the projects that are highly sensitive to flood impacts such as critical infrastructure.

In this study, we propose a bivariate flood hazard assessment framework, which aims to investigate the impacts of climate change including SLR and changes in extreme river flows on compound coastal-riverine flooding events defined by impact flood thresholds. Specifically, the objectives of the study are to 1) develop a nonstationary bivariate flood hazard assessment that accounts for the joint behaviors of extreme SLs and river flows; 2) project frequencies at which both major coastal and riverine flood thresholds will be exceeded simultaneously or in close succession by mid-century along the coastal CONUS with consideration of projected SLR and changes in extreme river flows; and 3) quantify the increase in compound flood risk in selected estuary regions by mid-century. Considering projections of SLR and streamflow in compound flood hazard assessment based on flood impact flood threshold may bring model-driven climate change signals into future flood risk predictions that can raise local awareness by allowing localization of compound flood risks and lead to an increase in resilience of coastal communities.

4.2. Materials and Methods

To capture the effects of climate change including SLR and changes in extreme river flows on compound coastal-riverine flood events and to better understand changes of compound flood risk in the estuary regions, we propose a bivariate flood hazard assessment framework focusing on extreme SLs and river flows. Projected SLR and streamflow are used to incorporate the potential impact of climate change in the analysis. The flood impact thresholds are used to define major coastal and major riverine flooding events. The study involves the following steps, which are described in later sections:

1) Selecting datasets of SLs and river flows along the coastal CONUS
2) Selecting pairs of extreme SLs and river flows for bivariate analysis
3) Quantifying joint return period (JRP) of extreme SLs and river flows using the selected pairs
4) Assessing JRP of floods exceeding both major coastal and riverine threshold (i.e., compound major flooding) under current and future conditions

5) Assessing changes in risk of failure due to compound major flooding over a 30-year design lifetime

4.2.1. Selecting datasets of SLs and river flows along the coastal CONUS

For the coastal component, we use the hourly observed sea level data from tidal stations. The data are available from the NOAA (http://tidesandcurrents.noaa.gov/) and composed of mean sea level, astronomical tide height, and non-tidal residual components. For the riverine component, we use daily streamflow provided by the U.S. Geological Survey (USGS) (waterdata.usgs.gov/nwis/rt). The paired NOAA-USGS stations are selected if a USGS station with at least 30 years of data and defined flood impact thresholds are found within 100 km of the NOAA tidal station. Figure 4.1 presents the 26 selected paired stations along with their watershed boundaries. The information about stations is provided in Table B1. Major coastal and riverine flood thresholds are obtained from Sweet et al. (2018) and the national weather service website (https://water.weather.gov/ahps/rss/alerts.php), respectively.

4.2.2. Selecting pairs of extreme values for compound coastal-riverine analysis

The bivariate model should be fitted with pairs of extreme SLs and river flows to prevent representation of extreme tail with bias. Different methods were used in literature for sampling pairs of extreme events from the full bivariate time series that the most common of them are threshold-excess, point process, and conditional methods (Zheng et al. 2014). Each method has its advantages and disadvantages. While the threshold-excess method offers approximately unbiased estimates for dependence parameters, the point process and the conditional method overestimate and underestimate the dependence strength, respectively. However, the threshold-excess method is unable to fully handle flood events that only one of the drivers is extreme (Zheng et al. 2014).

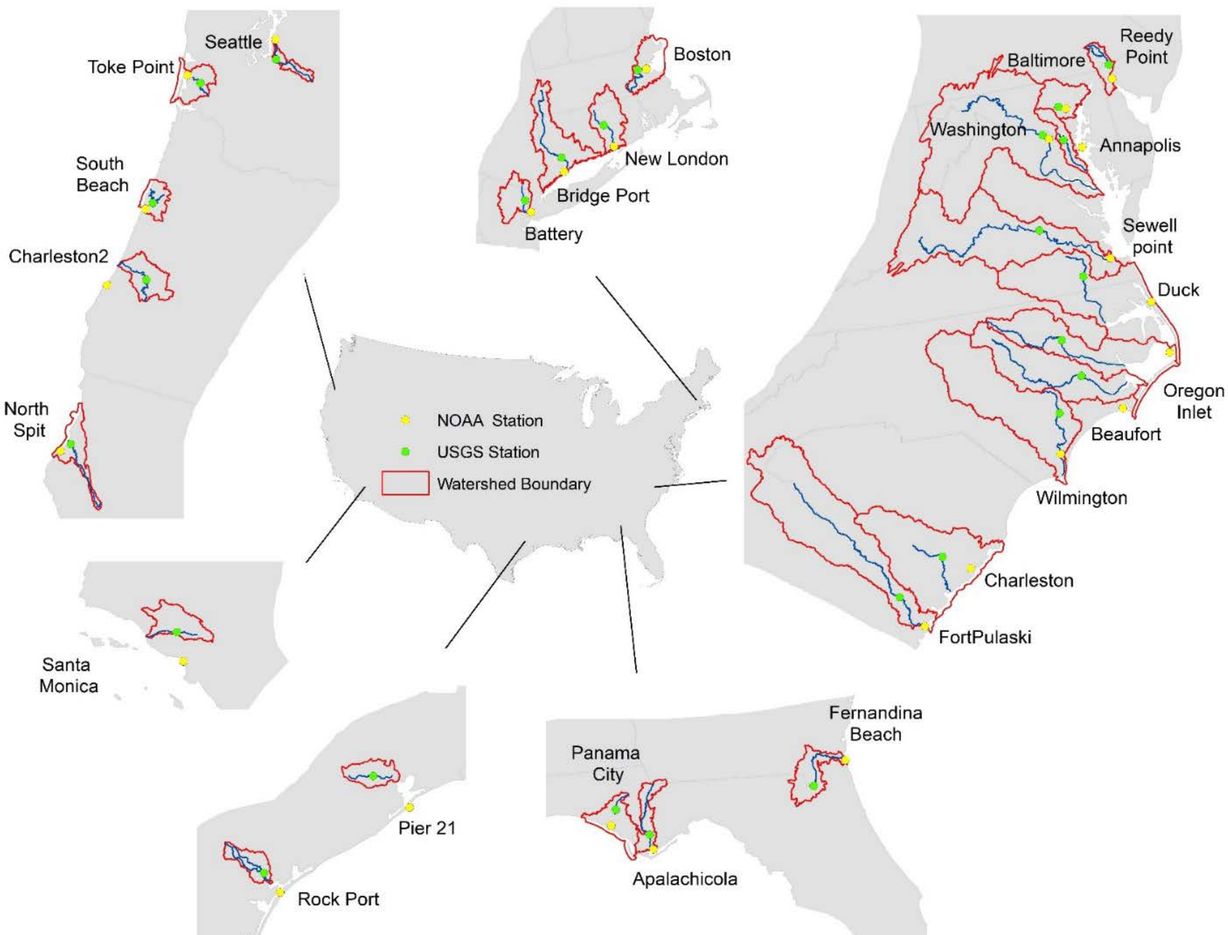

Figure 4.1. The location of tidal and riverine gauges

Both conditional method (Moftakhari et al., 2017; Wahl et al., 2015; Ward et al., 2018) and threshold-excess method (Bevacqua et al., 2019; Kew et al., 2013) were used in previous studies on estimation of the statistical dependence between coastal-riverine flood drivers. Here, the threshold-excess method is implemented to identify bivariate extreme events since our focus is on the compound flood events that both drivers are extreme.

For the coastal component, we use the variable threshold approach provided by Ghanbari et al. (2019), which is applied to the daily sea level observations to identify extreme sea level samples. The variable threshold is used to avoid exceedances over threshold occurring more frequently in future years that could violate the basic assumption of extreme value analysis (Coles 2001). The variable threshold is computed as the 97% quantile regression (Koenker and Hallock 2001; Kyselý et al. 2010) assuming linear dependence between daily mean sea level (explanatory variable) and daily maximum sea level (response variable). Using this approach, we consider SLR (i.e., changes in mean SL) as a covariate instead of time (Salas and Obeysekera 2014). Figure 4.2(b) shows how the variable threshold determines extreme SLs in Washington D.C. station (all the dots above the threshold). For some locations, we reduce the threshold using a 95% quantile regression to ensure that sufficient data are selected to support bivariate frequency analysis. We also assume that exceedances of sea level should be at least 3 days apart to be considered as independent (Runs Method, Coles, 2001) and take only the maximum of successive extremes.

For the riverine component, the daily river flow above the 97th quantile is considered as the extremes. The quantile regression method is used to determine the threshold by determining the relationship between time and daily river flow as is shown in Figure 4.2(a) for the Potomac River. 3-day window is used to ensure independent events. Then, pairs of extremes are selected when both sea level and river flow values exceed their defined thresholds within ±1 days from each other (Moftakhari et al., 2017). Green dots in Panel c illustrates the pairs of independent extreme sea level and river flow (H_{ext}, Q_{ext}).

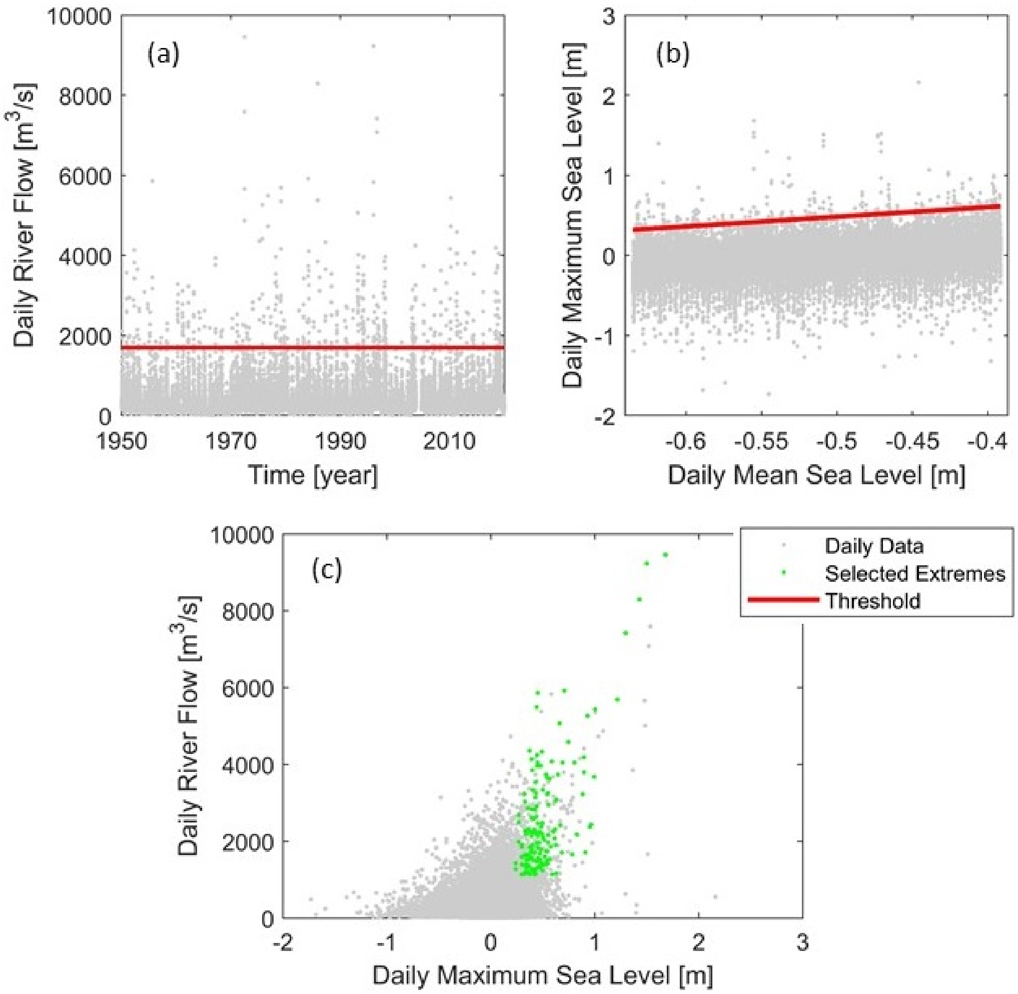

Figure 4.2. Threshold-excess method for identifying (a) Extreme river flows (b) Extreme sea levels; (c) Selected pairs of independent extreme sea level and river flow (H_{ext}, Q_{ext})

For the pairs of extreme sea level and river flow we estimate the parameters of generalized Pareto distribution (GPD) as the marginal distribution (since the threshold-excess method is used for selecting extremes) with cumulative distribution function as follow:

$$F_X\left(x|\theta_x^{\delta(t)}\right) = F_X\left(x|\xi,\alpha,u_{\delta(t)}\right) = \begin{cases} 1-\left(1+\xi\dfrac{x-u_{\delta(t)}}{\alpha}\right)^{-\frac{1}{\xi}} & if\ \xi \neq 0 \\ 1-\exp\left(-\dfrac{x-u_{\delta(t)}}{\alpha}\right) & if\ \xi = 0 \end{cases} \quad (4.1)$$

where $F_X\left(x|\theta_x^{\delta(t)}\right)$ is the GPD function with SLR (δ) or time (t) as a covariate. $u_{\delta(t)}$, α and ξ denote the location (i.e., variable threshold), scale, and shape parameters of GPD. u_δ equals to $\beta_1 \times \delta + u$ and in u_t equals to $\beta_1 \times t + u$, which β_1 denotes the slope coefficient of the quantile regression model and u is the current threshold of SLs or river flows. If no trend is found in extreme river flow data (97th quantile), the slope of threshold (β_1) would be equal to zero and consequently u_t would be constant and equal to u (i.e., no nonstationarity based on historical extreme river flows). However, the future can be nonstationary even though there is stationarity in the past observations (Mondal and Mujumdar 2016). This nonstationarity in the future is captured by incorporating the streamflow projections as discussed in the next sections.

The year 2020 is used as the reference year in the study and the 183rd day of the year 2020 (the middle day of the year) or the value of daily MSL corresponding to that day is used to calculate the current threshold value (i.e., current GPD location parameter (u)) for river flow and SL, respectively. Here, the nonstationarity is considered only in the first moment and the shape and scale parameters are treated as constants.

4.2.3. Quantifying *JRP* of extreme SLs and river flows using the selected pairs

The significance of statistical dependence between the paired data (H_{ext}, Q_{ext}) is assessed using Kendall's rank correlation coefficient (τ), which provides a nonparametric measure of association between extreme paired sea level and river flow (Sokal and Rohlf 2001).

The copula method is then used to build the joint distribution of pairs data with significant dependence. Copula functions have been widely applied in hydrological studies over the last decade to model the dependence structure of two (or more) random variables regardless of their marginal distributions (Bender et al. 2014; Jiang et al. 2015; Ming et al. 2015; Moftakhari et al. 2017b; Sadegh et al. 2018; Salvadori et al. 2007). According to Sklar's theorem (Sklar 1959), copulas describe and model the dependence structure between random variables (Salvadori and De Michele 2004). A bivariate distribution function F_{XY} of two random variables X and Y with marginal distributions $F_X(.)$ and $F_Y(.)$ can be written in the form:

$$F_{XY}(x, y) = C(F_X(x|\theta_x), F_Y(y|\theta_y)|\theta_c) \tag{4.2}$$

where F_{XY} is a joint distribution function with marginals F_X and F_Y, θ_x and θ_y are the marginal distribution parameters, $C(.,.)$ is a unique copula of the two continuous random variables X and Y with the parameters of θ_c.

If there is a significant dependence between paired data, the best copula fit among 26 copulas is selected for bivariate dependence analysis based on maximum likelihood, Akaike Information Criterion (AIC), and Bayesian Information Criterion (BIC) to describe the dependence structure between the paired data (Sadegh et al. 2017).

Unlike univariate analysis, hazard scenarios are not unique in bivariate analysis (Salvadori et al. 2011). Several definitions of hazard scenarios are available in the literature including *OR*, *AND*, Kendal, and survival Kendal (Salvadori et al. 2014; Salvadori and De Michele 2004). Each definition provides specific information and the aim of the study should be considered for choosing the proper definitions. In this study, we consider *AND* hazard scenario since we are interested to estimate the frequency of simultaneous or near-simultaneous exceedances over both coastal and riverine flood thresholds. Moreover, *AND* hazard scenario is proposed to estimate the JRP of extreme SLs and river flows for assessing compound coastal-riverine flooding risk in estuaries (Moftakhari et al., 2019). In case of interest in information about the probability of flooding due to exceedance over either coastal or riverine flood threshold or both *OR* hazard scenario should be used (Bender et al., 2016; Moftakhari et al., 2017; Ward et al., 2018). The Kendall and the Survival Kendall hazard scenarios do not have a direct physical/structural interpretation and they should be used for preliminary risk assessments (Salvadori et al., 2016).

If x^* and y^* are coastal and riverine flood thresholds, respectively, the joint exceedance probability based on *AND* hazard scenario refers to the probability of exceedances over x^* and y^* simultaneously or in close succession (Herweijer et al., 2008; Salvadori et al., 2011; Salvadori et al., 2016; Salvadori & De Michele, 2004; Salvadori et al., 2007) $[p(X > x^* \cap Y > y^*)]$ and defined as follow:

$$P_{AND} = 1 - F_X(x^*|\theta_x) - F_Y(y^*|\theta_y) + C(F_X(x^*|\theta_x), F_Y(y^*|\theta_y)|\theta_c) \tag{4.3}$$

Subsequently, the joint return period is defined as:

$$JRP = \frac{\lambda}{P_{AND}} \tag{4.4}$$

where λ is the average interarrival time between compound flood events occurrences.

Specifically, in this study, thresholds ($x^*$and y^*) are defined as major coastal and riverine flooding threshold (i.e., H_{Major}, Q_{Major}) since our focus is on JRP of compound major flooding.

4.2.4. Assessing *JRP* of compound major floodings under current and future conditions

Under a changing climate, the marginal distributions of high SLs or river flows or their dependence structure might be nonstationary. The nonstationarity of F_{XY} could be due to nonstationarity in (1) marginal distributions of variables (i.e., a change of univariate distribution parameters θ_x^t and θ_y^t), (2) the dependence structure of variables (i.e., a change of copula parameters θ_C^t), or (3) both(Salvadori et al. 2018). Here we incorporate nonstationarity into the marginal distributions of extreme SLs and river flows using projected SLR and river flows.

To incorporate nonstationarity into the marginal distribution of extreme SLs, first the new GPD threshold ($u_\delta = \beta_1 \times \delta + u$) is estimated under different SLR values (δ) and the frequency of major coastal flooding is recalculated using the new threshold (Ghanbari et al. 2019). Then the regional SLR projections provided by Sweet et al. (2017) are used to perform an assessment of expected time to certain SLR values. The available projections include Low, Intermediate-low, Intermediate, Intermediate-high, High, and Extreme SLR scenarios, which correspond to 0.3m, 0.5m, 1m, 1.5m, 2m, and 2.5m global SLR, respectively. For each of the six scenarios there is a low, medium and high sub-scenario, corresponding to the 17th, 50th, and 83rd percentile of the climate-related sea level projections consistent with the GMSL scenario. The value for medium sub-scenario is used in this study.

While Intermediate-Low and Intermediate scenarios have a 96% and 17% chance of being exceeded under Representative Concentration Pathway (RCP) 8.5 climate change scenario, respectively, Intermediate-high scenario has a chance of 1.3%. The chance of exceedance of High and extreme scenarios is too low (0.3% and 0.1%). Here, we consider the Intermediate-low, Intermediate scenarios as they are the most probable scenarios by mid-century.

To incorporate nonstationarity into the marginal distribution of extreme river flows, we use a ten-member ensemble streamflow projection derived from runoff simulated by Naz et al. (2016). The projected daily runoff is simulated by the Variable Infiltration Capacity (VIC) hydrologic model forced with ten dynamically downscaled Global Climate Models (GCMs) from the Coupled Model Intercomparison Project phase 5 (CMIP5) archive under the RCP 8.5 emission scenario. Each downscaled GCM consists of 40 years in the historic baseline (1966–2005) and near future (2011–2050) periods. The simulated VIC runoff is then routed using the Routing Application for Parallel Computation of Discharge (RAPID; David et al., 2011a, 2011b) routing model along the NHDPlus (McKay et al. 2012) river network. Although these ten sets of hydroclimate projections do not capture the overall uncertainty in the future, they can provide a best-available model-based projection of potential future streamflow conditions for the purpose of our study. Naz et al. (2016) provide a detailed description of the VIC model setup and evaluation. The use of RAPID routing model along with NHDPlus river network can be further referred to Tavakoly et al. (2017) and Forbes et al. (2019). Observed flow data are compared with simulated flow data using different statistical indices (Figure B2-1 to B2-26).

The quantile regression method, as described above is used to estimate the threshold for the projected near future river flows, which allows the estimation of trends at extreme quantiles of the river flow distribution (Koenker and Hallock 2001). We assume that the slope of the new threshold expresses the trend in the future extreme river flows. This is based on the idea that the variations in the future extremes (i.e., either upward or downward trend) can be expressed by the slope of an extreme quantile (Yu et al. 2003). Hence, the future changes in riverine flooding frequency (i.e., extreme river flows) are explored by incorporation of the new slope into the location parameter of GPD. The new slope (β_1^*) is then used as the slope of the variable threshold of historical river flows (β_1) to estimate the new threshold as $u_t = \beta_1^* \times t + u$ (i.e., location of GPD). Upward trend in extreme quantiles of river flows ($\beta_1^* > 0$) implying more riverine flooding.

4.2.5. Assessing changes in risk of failure over design lifetime

Return period alone does not account for planning horizon and is unable to characterize the likelihood of an event occurring during a project lifetime (Read and Vogel 2015). Risk of failure over a given design life is shown to provide a more suitable measure for risk assessment and communication (Serinaldi 2015). Here risk of failure is defined as the probability of observing at least one compound major flooding in a given design life (Salvadori et al., 2016; Serinaldi, 2015) and formulated to allow for changing exceeding probabilities over time. For a hypothetical structure, having design life n, the failure probability is a monotonically increasing function of t and is given by:

$$RF = 1 - \prod_{t=1}^{n} (F_X(x^*|\theta_x^t) + F_Y\big(y^*|\theta_y^t\big) - C\big[F_X(x^*|\theta_x^t), F_Y\big(y^*|\theta_y^t\big)\big]|\theta_C^t) \tag{4.5}$$

As already mentioned, in this study, x^* and y^* are major coastal and riverine flood thresholds, respectively, and RF indicates the risk of failure due to compound major flooding (hereinafter, RF_{Major}).

4.3. Results and Discussions

The proposed bivariate flood hazard framework to quantify compound flooding is based on exceedances above coastal and river flood thresholds with consideration of projected SLR and changes in extreme river flows. We demonstrate the applicability of the framework in assessing the frequency of compound major flooding (i.e., simultaneous or near-simultaneous exceedance of SLs and river flows above major flood thresholds) by mid-century along the Contiguous United

States (CONUS) coast. First, we investigate the dependence between the extreme SLs and river flows based on the observed dataset, utilizing data from the NOAA tidal station and the closest USGS river station. Then we estimate the JRP of compound major flooding in locations with significant dependence structure between high SLs and river flows under current and future conditions. We show that, under current conditions, the northeast Atlantic and Gulf coast regions are experiencing the highest compound major flood probability. However, future SLR scenarios show emerging high compound flooding probability along the southeast Atlantic coast. The impact of changes in extreme river flows is found to be negligible in most of the locations except the southeast Atlantic coast. However, even in this region, its impact is considerably less than that of SLR. It should be noted that here we focus on major flood thresholds; however, the framework is applicable to any flood threshold.

4.3.1. Spatial variability in dependence of extreme sea levels and river flows

The dependence between extreme pairs of high SLs and river flows is assessed using Kendall's rank correlation coefficient. The dependence behavior patterns are almost similar to those found by previous studies (Ward et al. 2018; Couasnon et al. 2020), although the method for selecting pairs of extreme events are not the same. For the northeast Atlantic coast, we find significant dependence at all stations. Concurrent extreme SLs and river flows along the northeast Atlantic coast can be associated with the combination of storm surge and heavy precipitation due to the passage of extratropical cyclone and nor'easter (i.e., macro-scale extratropical), which are usually accompanied by very heavy rain or snow that can cause compound flooding. For the southeast Atlantic coast, significant dependence was found for most of the stations except two stations (Oregon Inlet and Fort Pulaski). In this region, tropical cyclones produce high SLs and intense precipitation. However, other mechanisms also lead to high river flows such as convective storms (Berghuijs et al. 2016). For the Gulf coast, we find statistical dependence for the western part, however, no significant dependence is found for the eastern part. High SLs in this region typically occur during hurricane seasons when the flow of the western part is also at its highest. However, the maximum flow for the east part of the Gulf is late winter and early spring (Berghuijs et al. 2016). For the Pacific coast, we find significant dependence at most locations except Santa Monica and Seattle stations. This is attributed to relatively high variability in tide levels compared to small storm surges variability in these two stations. Kendall's rank correlation coefficient (τ) are presented in Table B2 along with the p-values.

4.3.2. The *JRP* of compound major flooding under current conditions

The current JRP between co-occurrence of high SLs and river flows is estimated for all the studied locations using the proposed bivariate flood hazard assessment method. Figure 4.3 illustrates the results for Potomac River Estuary, Washington D.C. as an example and the same information for the rest of the studied estuary locations is presented in Figures B3-1 to B3-26. The figure shows that, if we consider only the coastal component, the return period of major coastal flooding (i.e., exceedances above major coastal flood threshold (H_{Major})) is approximately 20 years (Panel c). If we consider only the riverine component, the return period of major riverine flooding (i.e., exceedances above riverine flood threshold (Q_{Major})) is estimated to be approximately 50 years (Panel a). Now the question is: what is the frequency of compound extremes such as major coastal-riverine flooding? Using *AND* hazard scenario, exceedance above both major coastal and riverine flood threshold (H_{Major}, Q_{Major}), appears to be a 180-year extreme compound event, which is indicated by a red square in panel b. In other words, (H_{Major}, Q_{Major}) with the JRP of 180 years has marginal univariate return periods equal to 20 and

50 years. The comparison between fitted marginal distributions and empirical distribution along with Q-Q plots are provided in Figures B1-1 to B1-26.

It should be highlighted that the estimated JRP is based on the _AND_ hazard scenario and presents the frequency of compound flood events when both coastal and riverine flood thresholds are exceeded simultaneously or in close succession. In the case when the frequency of exceedance over either coastal or riverine flood threshold or both is of interest, the JRP should be estimated based on the _OR_ hazard scenario.

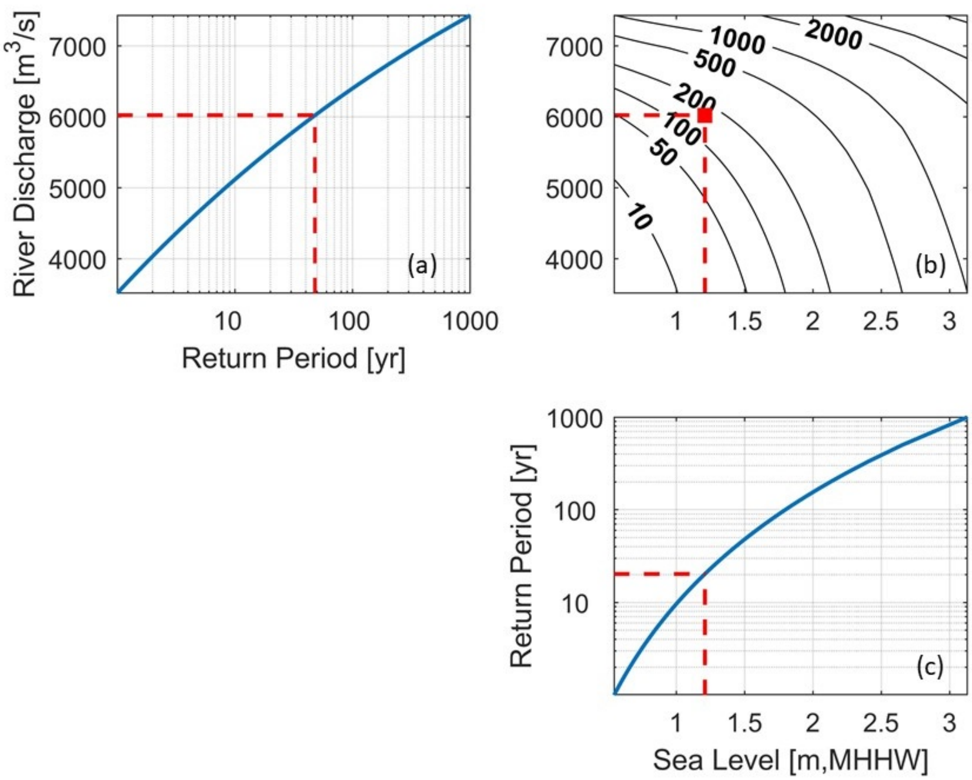

Figure 4.3. Marginal distribution based on generalized Pareto Distribution (GPD) for (a) extreme river flows, (c) extreme sea levels; (b) joint return period of extreme paired data based on the selected copula. The dashed red line shows the major flood threshold and corresponding univariate return period in panel (a) and (c). The red square in panel (b) shows the JRP of compound major flooding under current conditions.

Figure 4.4 presents the relationship between the return period of major coastal and major riverine flooding based on univariate analysis and the corresponding JRP for all the studied locations, which is shown by the size of the circles. The figure shows how major coastal and riverine flood thresholds are exceeded with different return periods in different coastal regions and how the associated return period deviates from a 100-year event. This highlights the necessity for using impact flood thresholds to compare compound flooding impacts over large areas. It should be noted that most of the locations in the Pacific coasts are not historically exposed to major flooding. Thus, the major coastal flood return period in these locations are shown by larger than a 1000-year event. Also, the JRP of locations with no significant dependence between SLR and river flows, which are marked by an asterisk (*), are present as larger than a 1000-year event.

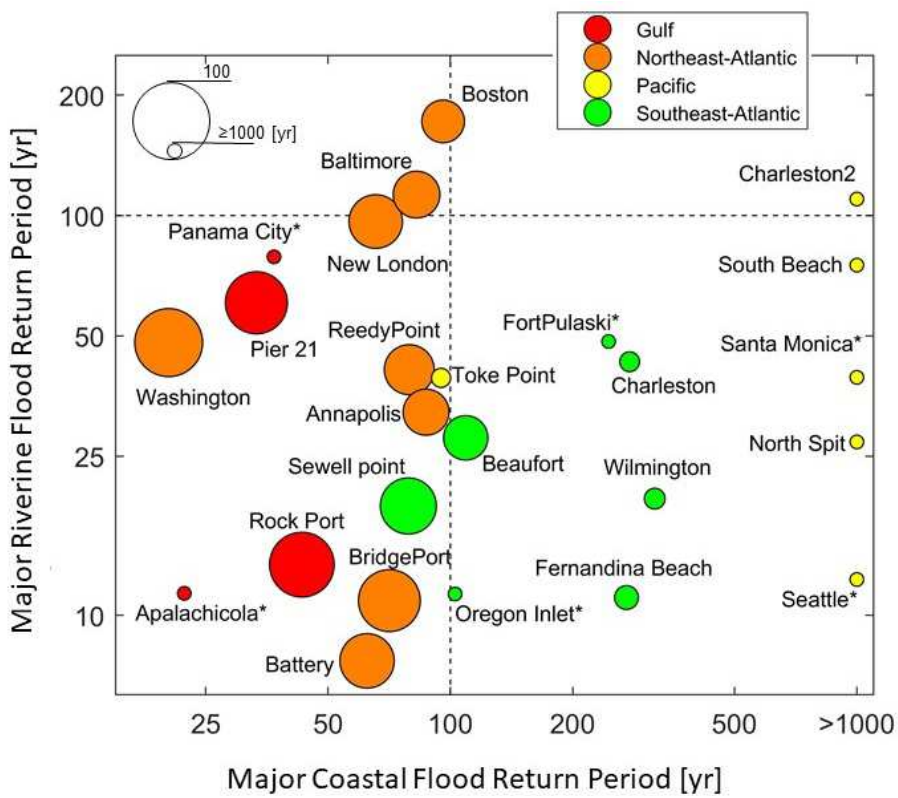

Figure 4.4. The relationship between the return period of major coastal and riverine flooding based on univariate analysis and the corresponding joint return period (JRP) based on bivariate analysis. The locations with no significant dependence are marked by an asterisk (*). The JRP is shown by the size of the circles.

4.3.3. The JRP of compound major flooding under future conditions

With SLR the likelihood of exceedances of high SLs above coastal flood thresholds will increase (Ghanbari et al. 2020). Changes in extreme river flows might also increase the likelihood of exceedances of high river flow above riverine flood thresholds (Groisman et al. 2001). Consequently, in a warming climate the frequency of compound major flooding could increase (i.e., shorter JRP). Thus, a further question is, to what extend SLR and changes in extreme river flows could affect the frequency of compound major flooding?

Frequencies at which SLs and river flows are projected to exceed the major flood thresholds simultaneously or in close succession are estimated in terms of the JRP for all the selected locations. Figure 4.5, illustrates the changes in JRP by 2050 in Potomac River Estuary, Washington D.C. as an example. The results show almost 15% and 25% decrease in JRP by 2050 under Intermediate-low and Intermediate SLR scenarios, respectively. The impact of changes in extreme flows in addition to the Intermediate SLR scenario is illustrated by the dashed pink line (multi-model ensemble) and gray lines (single GCM). Previous research has demonstrated that multi-model ensemble forecasts perform better than any single GCM.

The frequency of compound major flood events might slightly increase when the nonstationarity of extreme streamflow is considered. However, the impact of SLR is much greater. The same information for the rest of the selected studied locations is presented in Figure B4-1 to B4-26.

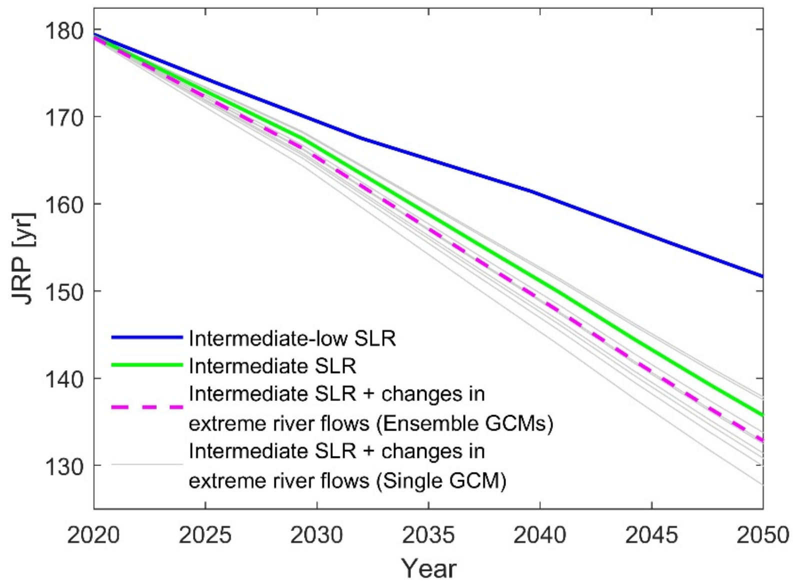

Figure 4.5. The changes in the joint return period (JRP) of compound major flooding by mid-century in Potomac River Estuary, Washington D.C.

Figure 4.6 shows the JRP along the coastal CONUS under the current condition (middle panel) and by mid-century under Intermediate-low SLR scenario (panel a), Intermediate SLR scenario (panel b), and Intermediate SLR with changes in extreme river flows (Panel c). The frequencies of compound major flooding are anticipated to change as a result of climate change, however, changes in their frequencies are not the same across regions. Thus, frequency amplification of compound major flooding is also calculated as the ratio of current JRP to future JRP to assess the changes in the frequency of compound major flooding across different coastal regions, which is illustrated by changes in color.

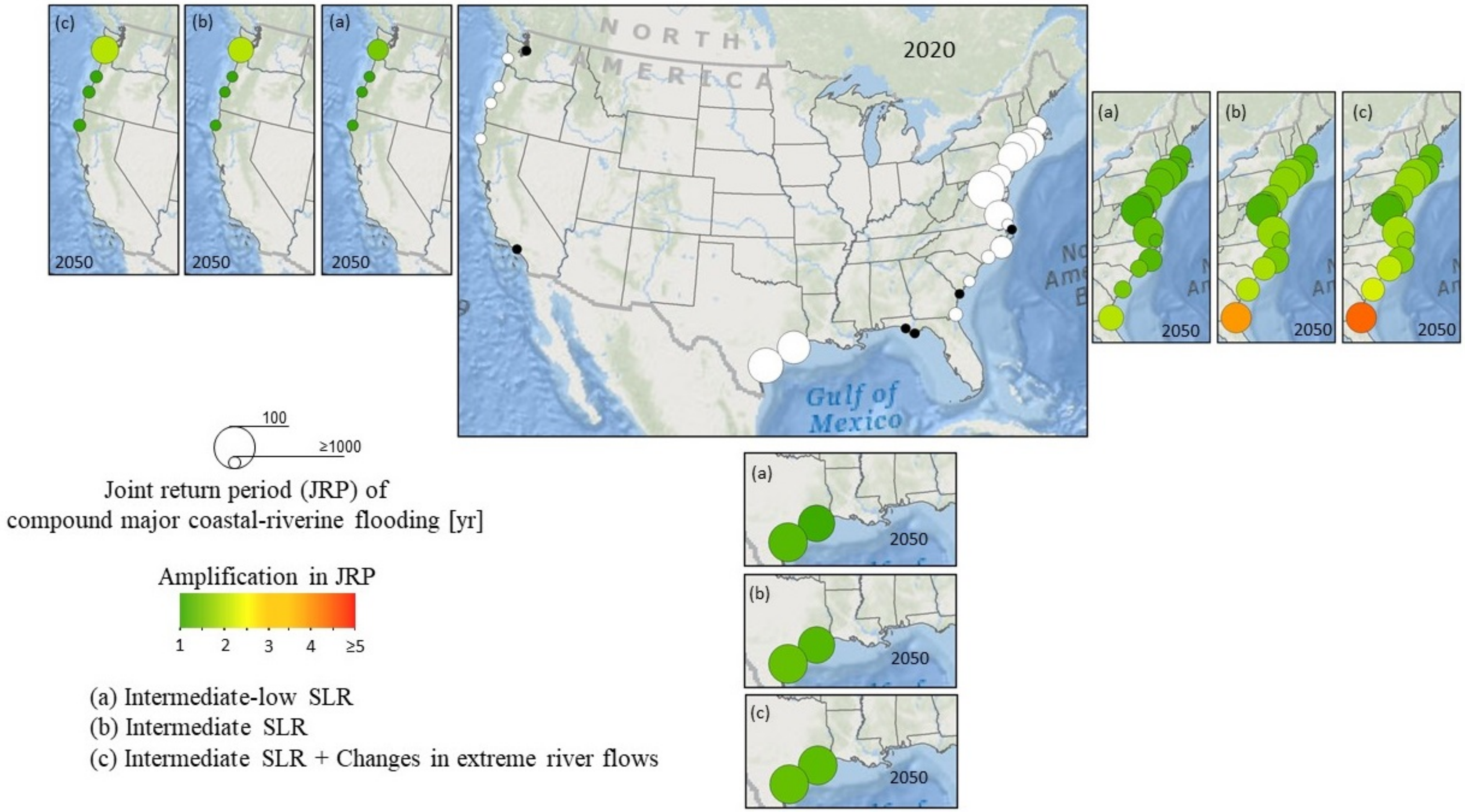

Figure 4.6. The joint return period of compound major flooding (middle panel) under current condition, (a) with consideration of Intermediate-low SLR scenario (2050), (b) with consideration of Intermediate-low SLR scenario (2050), (c) with consideration of Intermediate-low SLR scenario and river flow change. Black circles denote locations with no significant dependence.

Under the current condition, the northeast Atlantic and west Gulf coast regions are experiencing the highest compound flood major probability. However, the future SLR scenarios show emerging high compound major flooding probability along the southeast Atlantic coasts. Under the Intermediate SLR scenario, by 2050, the southeast Atlantic coast could experience the amplification of up to 5 times and all the locations tend to be exposed to major coastal riverine flooding with a return period of 200-400 years. For the pacific coast, despite the significant dependence between high SLs and river flows (Table B2), JRP of compound major flooding is infinite since the major coastal flood threshold has not yet been exceeded in the majority of Pacific coast locations. However, as sea level continues to rise, the region may experience compound major flooding by the end of century.

While SLR exacerbates compound major flooding along the coastal CONUS, the impact of river flow change is spatially diverse. The impact of river flow change is found to be negligible in most of the locations except in southeast Atlantic coasts where future JRP is found to be impacted by changes in extreme streamflow flows as well. However, its impact is considerably less than that of SLR, highlighting the important impact of SLR on future frequency of compound flooding events.

4.3.4. The risk of failure over a design lifetime (2020-2050)

The risk of failure due to compound major flooding (RF_{Major}) over a 30-year design life (2020-2050) is calculated for all selected locations. Figure 4.7 illustrates the behavior of RF_{Major} in Washington D.C. and Wilmington as an example. The same information for the rest of the selected estuary locations is presented in Figure B4-1 to B4-26.

This plot compares RF_{Major} without consideration of SLR (dashed black line) versus that with consideration of the two most probable SLR projections by the mid-century. Even without consideration of SLR the RF_{Major} would increase as service time of hydrologic infrastructure increases(Xu et al. 2019). For example, in Washington D.C., the RF_{Major} is equal to 0.5% (i.e., 180-year event as estimated in the previous section) in the first year, increases to 6% and 18% when the service time is 10 and 30 years, respectively, according to Intermediate SLR scenario. This highlights the point that return period is not explicitly tied to a planning horizon and may not be representative of the time to the next flood event (Read and Vogel 2015).

Moreover, in general, the risk of failure assuming stationarity is smaller than the ones considering any of the SLR scenarios. For example, based on the current conditions, the RF_{Major} in Wilmington after 30 years of design life is expected to be 3%. Now if we consider the Intermediate-low SLR scenario, the failure probability increases to 5%. The situation becomes worse under the Intermediate SLR scenario ($RF_{Major} = 6\%$).

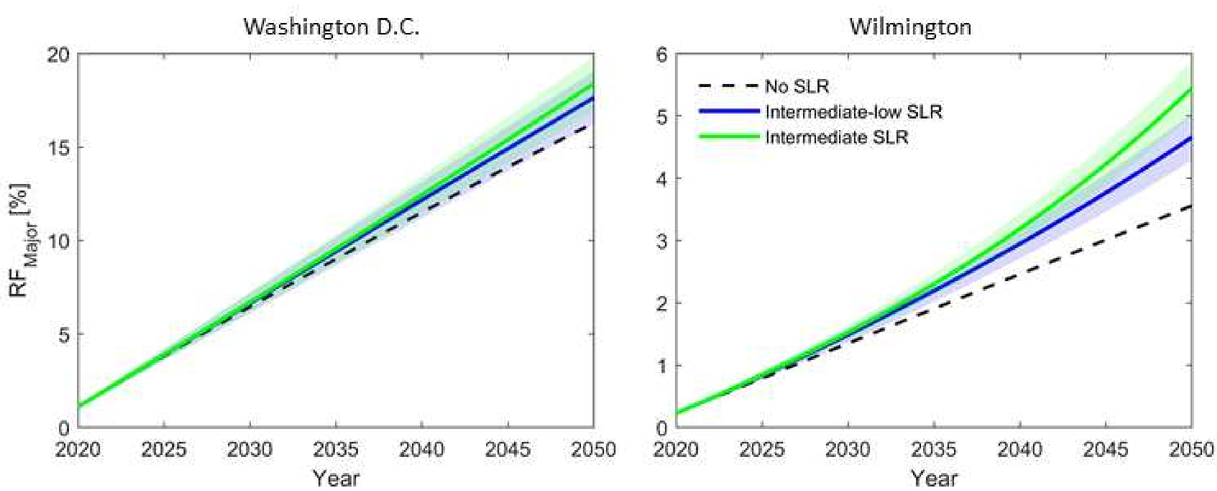

Figure 4.7. Bivariate risk of failure due to compound major flooding (RF_{Major}) over a design life of 30 years (2020-2050). The dashed black line shows the estimated RF_{Major} computed according to current climate conditions. RF_{Major} for the Intermediate-low and Intermediate SLR scenarios are shown with a blue and green line, respectively. The highlighted boundaries show low and high SLR sub-scenario, corresponding to the 17th and 83rd percentile.

Figure 4.8 illustrates the RF_{Major} after 30 years of design life (2050) for eight major cities close to estuaries with high dependence structure between extreme SLs and river flows. The figure suggests that under future SLR scenarios the RF_{Major} will increase in all the selected locations. However, the changes in RF_{Major} are regionally different. The highest increase in RF_{Major} is found for the locations along the southeast Atlantic coast. The coastal cities along the southeast Atlantic coast are expected to be exposed to double risk of compound major flooding by midcentury under the Intermediate SLR scenario. These findings highlight the potential for compound major flooding to produce destructive impacts more frequently if sea levels continue to rise.

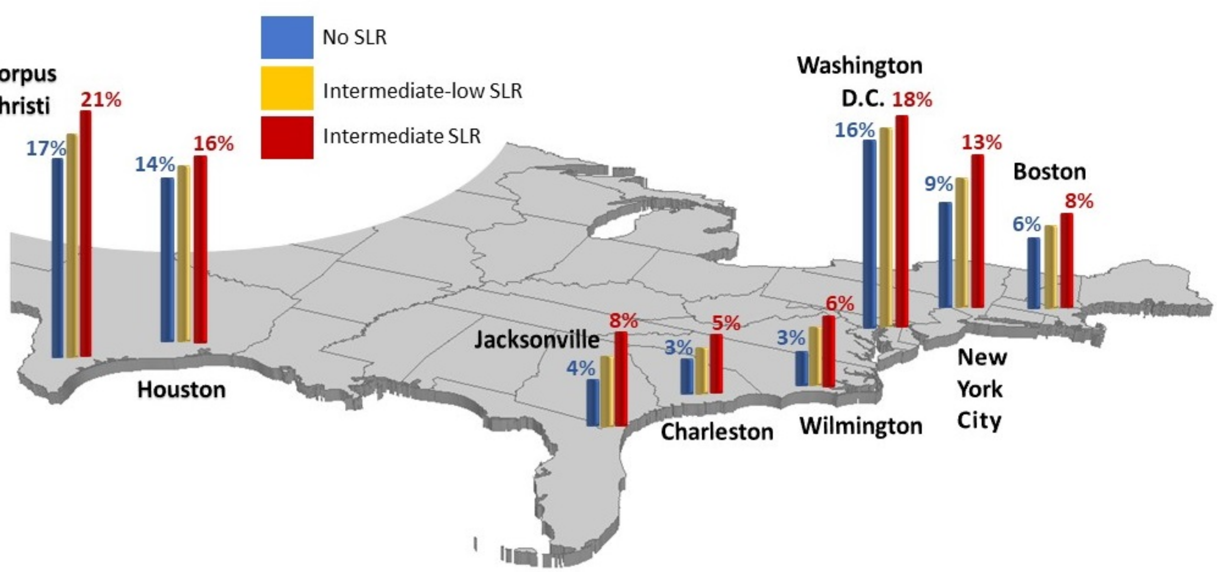

Figure 4.8. Risk of failure due to compound major flooding $\left(RF_{Major}\right)$ after 30 years of design life (2020-2050)

It should be noted that the calculations do not consider nonstationarity in the dependency between high SLs and river flows. Lack of such consideration likely produces underestimation in projected JRP and is worthy to be considered in future studies. Although it was shown that in some cases incorporating nonstationarity in the marginal distribution parameters is substantially more important than incorporating nonstationarity in the copula parameter (i.e., the dependence structure (Bender et al. 2014)), future work could improve on this by incorporating future changes in dependence structure between variables.

4.4.Conclusion

The interaction between high SLs and river flows determines the flood level in estuaries. Knowledge about the joint return period of high SLs and river flows is essential to understand the risk of flooding in these regions. Climate change could alter the statistical characteristic of these flood drivers, leading to increase in frequency of compound coastal-riverine flooding. Thus, a statistically robust analysis of compound coastal-riverine flooding requires incorporation of future projections of climate change. This study proposes a bivariate flood hazard assessment framework that accounts for compound coastal-riverine flooding with consideration of the impact of SLR and changes in extreme river flows. In particular, projected SLR and streamflow are incorporated in the marginal distribution of high SLs and river flows, respectively, as drivers of compound coastal-riverine flooding.

We focus on major coastal and riverine flood thresholds and project how often these two impact flood thresholds will be exceeded simultaneously or in close succession by mid-century along the coastal CONUS. Bivariate flood analysis based on impact thresholds under current and future conditions can raise local awareness by allowing localization and personalization of flood risks. Identifying current and future hotspots of compound major coastal-riverine flooding is highly relevant information for flood risk management in estuary regions. In locations with dependence between high SLs and river flows a storm could cause inundation not only above the coastal major flood threshold but also above the riverine major flood threshold, leading to extreme flood level.

The results show regional differences in JRP of compound major flooding under current climate conditions. The northeast Atlantic and western part of the Gulf coasts are experiencing the highest compound major flood frequency. Projected JRPs according to the Intermediate-low and Intermediate SLR scenarios show a high frequency of compound major flooding along the southeast Atlantic coast. The impact of changes in extreme river flows is found to be negligible in most of the locations except the southeast Atlantic coast. However, even in this region SLR is the dominant reason for increasing the frequency of compound major flooding.

Our results highlight that the increased risk of co-occurrence of major coastal and riverine flooding under future climate conditions cannot be neglected in a robust risk assessment. More major coastal-riverine flooding can be expected due to the impacts of climate change, especially SLR, which should be considered as a basis for a range of future adaptation responses in estuary regions.

CHAPTER 5.

GREEN STORMWATER INFRASTRUCTURE IN NEW YORK CITY: COMPLEMENTARY OR SUBSTITUTIVE?

Highlights

Urban and compound flooding poses serious threats to many cities around the world. Climate change could increase the level of urban and compound flood hazard through higher extreme precipitation and sea level rise (SLR). To offset future flood risks in urban cities like New York City (NYC), implementation of effective and viable stormwater management strategies is essential. In this study, we assess four stormwater intervention scenarios including gray (i.e., conventional centralized conveyance systems and water treatment plants) and green (i.e., decentralized infiltration measures) infrastructure, to examine whether green systems' effects on flood control and combined sewer outflow (CSO) reduction are complementary or substitutive. A citywide Hydrologic and Hydraulic model was used to evaluate the effects of interventions on flood control, combined sewer outflow (CSO) mitigation, and potential co-benefits. The results revealed that although the effect of green interventions on flood control was substantial, they cannot substitute traditional gray interventions, particularly given their inability to deal with extreme rainfalls and compound flooding. On the other hand, gray systems appear to be most effective in mitigating CSOs. The results revealed that in developed and urbanized cities, green and gray systems should not be considered as competing but rather as complementary and mutually reinforcing. Sustainable stormwater management approaches should consider strategies that implement both systems in combination to provide complementary effects on flood and CSO reduction and other co-benefits. Also, adding cloudburst systems in different locations could substantially reduce flood hazard during extreme storm events.

5.1. Introduction

Urban flooding from extreme precipitation poses public safety risks and substantial threat to human life and property across the world (Jha et al. 2012). In coastal urban areas like New York City (NYC), these threats can further compound by the co-occurrence of high sea level (SL) either from tide or storm surge events (Smith and Rodriguez 2017). The co-occurrence of high precipitation runoff and high sea level may cause compound flooding events, like that caused by Superstorm Sandy in 2012, which can result in substantial damages and fatalities (Moftakhari et al. 2017b; Wahl et al. 2015a; Ward et al. 2018).

Climate change is increasing the risk of urban and compound flooding due to increasing frequency and intensity of extreme precipitation events (Rahmstorf and Coumou 2011), sea level rise (SLR) (Rahmstorf 2007; Sweet et al. 2017; Ghanbari et al. 2019), and increasing frequency and magnitude of surge events and tides (Rahmstorf and Coumou 2011; Bevacqua et al. 2019; Ganguli et al. 2020; Hallegatte et al. 2013). Considering the increased risk of flooding, the complex network of stormwater conveyance systems is increasingly overwhelmed, leading to flooding and water quality degradation. Water systems in NYC comprise a complex network of natural and built infrastructure that is increasingly vulnerable to flooding and water quality degradation (Rosenzweig et al. 2007). Pressures on the city water systems are on the rise due to the increased frequency of extreme precipitation events, SLR, and land-use change (Karamouz et al. 2015; Yohe and Leichenko 2010).

Stormwater interventions play a critical role in enhancing the resilience of urban cities by protecting them from flooding and water quality impacts, particularly when considering the impacts of climate change (Roy et al. 2008). Stormwater interventions include gray infrastructure (i.e., centralized conveyance systems), green infrastructure (i.e., distributed infiltration systems), and hybrid systems that can be designed and deployed individually or in combination as a part of a comprehensive strategy (Zhang et al. 2017).

Gray infrastructure, such as pipelines, large-scale storages, and treatment plants historically served society's needs for water security, public sanitation, and flood protection. However, over time, this system causes negative environmental impacts to downstream receiving environments and exacerbates the pressure from climate change, and subsequently erodes the resilience of cities (Bell et al. 2019). Over recent decades, green infrastructure systems have emerged as a promising flood risk management alternative or complementary to gray infrastructure (Ferguson et al. 2013; Vogel et al. 2015). Green stormwater management infrastructure treats stormwater as a resource to be infiltrated, stored, and/ or re-used at the site instead of dealing with runoff as waste (Li et al. 2019; Moore et al. 2016; Zhang et al. 2017). The main goal of green practices is to achieve a reduction in runoff volume and peak using decentralized stormwater control measures and subsequently reducing runoff on gray stormwater systems, while increasing infiltration, groundwater recharge, and water quality enhancement (Ahiablame et al. 2012).

While green and gray stormwater infrastructure is often referred as either this-or-that choice (Jayasooriya and Ng 2014; Li et al. 2019), there is another opportunity to incorporate their complementary functionality and to obtain the best of what both green and gray systems can offer for flood hazard control, combined sewer outflow (CSO) reduction and other co-benefits (Sanders and Grant 2020). More recently attention has also been paid to the integrated use of green and gray infrastructure (Tavakol-Davani et al. 2016; Hu et al. 2019). In order for an ultra-urban city like NYC to better prepare for future stormwater issues, it is important to implement and deploy effective and viable stormwater management strategies to improve the reliability and resiliency of stormwater systems across the city. A prerequisite for this is to identify, model, and assess different green and gray intervention options, individually or in combination, to find the most beneficial and effective intervention scenarios for offsetting flood impacts (Rosenzweig et al. 2011; Meney and Pantelic 2020).

The main goal of this study is to examine the effect of green systems, as a complementary and substitutive stormwater management intervention, on flood impacts in NYC. Specifically, the objectives of the study are to (1) evaluate the effectiveness of different green and gray stormwater intervention measures, individually or in combination, on flood hazard and CSO reduction under current and future climate; (2) quantify potential co-benefits of green practices at varying implementation levels; (3) assess the intervention scenarios using a multi-criteria evaluation approach. Control of urban flooding through the most effective and efficient stormwater interventions reduces flood-induced damages and water quality impacts and subsequently enhances the safety and resilience of communities.

5.2. Methodology

Four stormwater intervention scenarios including prevailing and currently funded green and gray stormwater interventions, planned green and gray stormwater interventions for the City by 2050, and additional gray interventions to manage volume targets were assessed using a citywide hydraulic and hydrology (H&H) model under five current and future storm scenarios. The combination of intervention strategies and storm behaviors provides insight into how different types and levels of interventions influence the performance of interventions.

5.2.1. Hydraulic and hydrologic (H&H) model

A citywide H&H model, which had been developed as part of the NYC Stormwater Resiliency study was used to model and evaluate intervention scenarios. InfoWorks Integrated Catchment Model (ICM) was used to present both the overland runoff (i.e., 2D hydrologic model) and underground sewer system components (i.e., 1D hydraulic model) of the NYC stormwater system. The 2D elements simulate generation and movement of surface water from various land covers along the terrain into the 1D collection and conveyance elements.

To develop the model, stormwater conveyance components were extracted from the existing Department of Environmental Protection (DEP) InfoWorks 1D sewer models. Several additional City data sources including high-resolution digital elevation model data (DEM) from the most recent 2018 LiDAR surveys to represent the terrain and create the 2D model, land use data from the NYC Parks' Department to represent pervious surfaces, parameters for surface roughness, and infiltration processes, and the location of surrounding water bodies were used in the model.

The H&H model was separated into 13 sewershed models as follows: 26thWard, Bowery Bay, Coney Island-Owls Head, Hunts Point, Jamaica, Newtown Creek, North River, Oakwood Beach, Port Richmond, Red Hook, Rockaway, Tallman Island, and Wards Island. The resolution of the model was a triangular mesh network with minimum areas of 250 ft^2 and maximum areas of 1000 ft^2.

5.2.2. Storm scenarios

Several different storm types such as tropical cyclones, extratropical and convective storms can cause precipitation over NYC. Convective storms, during the warm season, have temporal scales of minutes to hours and spatial scales ranging from miles to over all of NYC (Colle et al. 2012; Lombardo and Colle 2010). The rain rates in convective storms can exceed 2 inches per hour (Smith and Rodriguez 2017). During the late summer and fall, tropical cyclones can move northward along the east coast and cause an extensive region of heavy precipitation (5-15 inches) over a 12- to 24-hour period that extends hundreds of miles ahead of the storm, such as that during Tropical Storm Floyd in 1999 (Colle 2003). Cool-season extratropical storms can also produce large areas of heavy rain over several hours. The coincidence of storm surge with the precipitation from these cyclones may lead to compound flooding.

Given these multiple storm types, requisite to a coherent flood risk assessment is utilizing scenarios spanning a wide range of rain intensity, storm duration, tide level, and storm surge layered with climate change effects. Thus, five storm scenarios were created to cover the wide range of NYC rain and coastal sea level parameters. Each storm scenario includes both a rainfall time series and spatially varying sea water level time series for local tidal waterways. These scenarios cover a mixture of current and future rainfall and tide scenarios, compound (extreme precipitation and surge) scenarios, and common and extreme scenarios. Climate change was represented for the midcentury with the high-end estimates (90^{th} percentile) of future changes in sea level and rain intensity.

Extreme Value Analysis (Coles 2001) was used to determine current relationships between rainfall return periods, durations, and intensities under the current climate. Results from DeGaetano and Castellano (2017) were used to determine these return period relationships for a future climate (i.e., the year 2050). Storm surge depth was assigned to a certain storm scenario based on results from analyzing the joint probability that rainfall and storm surge events occur simultaneously (Salvadori et al. 2007, 2016b). SLR, for future scenarios, was determined based on high-end (90th percentile) projections of the 2050s, based on results from the New York City Panel on Climate Change, NPCC (Horton et al. 2015), which is 30 inches above a baseline at 2000-2004.

Table 5.1. Characteristics of the storm scenarios used in the H&H model

Scenario	Intensity (in/hr)	Depth (in)	Duration (hours)	Current Return Period (years)	Future Return Period (years)	Present or Future Climate	SLR (feet)	Surge (feet)
SC1	1	1	1	< 1	< 1	Present day rainfall	-	-
SC2	1.77	1.77	1	5	< 5	Present day rainfall	-	-
SC3	1.77	1.77	1	5	< 5	Present day rainfall and surge	-	1.3
SC4	0.85	2.55	3	5	<5	Present day rainfall	-	-
SC5	0.38	9.12	24	>50	50	2050s SLR and rainfall	2.3	-

All storm scenarios incorporated time-varying tides, one scenario incorporated a surge, and one scenario incorporated SLR imposed on top of the tide. The offshore water level data, which represents the combination of tide, surge, and SLR, was determined from the New York Harbor Observing and Prediction System (NYHOPS; e.g., Georgas and Blumberg 2009; Orton et al. 2016). Rain durations vary from 1 to 24-hour events, with intensity varying and peaking over periods as short as 5 minutes, capturing the range of rain characteristics from common convective downpours to hurricane events. For detailed information about the creation of the storm scenarios refer to Appendix C, Section C1.

Table 5.1. shows the characteristics of the storm scenarios. SC1 is currently used by the NYC Emergency Management (NYCEM) and is the least severe storm modeled for the study. SC2 represents a short duration and high intensity event. SC3 repeats SC2 to include surge at a 90th percentile based on statistical analysis of the joint occurrence of extreme rain and surge. SC4 is

used to evaluate the DEP site retention standard. SC5 is a future event that models future 50-year event factoring in SLR. In summary, the scenarios show how rain intensity increase (SC2), a combination of rain intensity increase and surge (SC3), rain duration increase (SC4), and combination of rain duration increase and SLR (SC5) will worsen flooding and consequently affect the effectiveness of interventions.

5.2.3. Stormwater interventions

Stormwater intervention strategies consist of gray, green, and hybrid infrastructure that may be used individually or in combination to mitigate flood hazard, reduce CSO and provide other and co-benefits.

5.2.3.1. Gray infrastructure system

Gray systems include conveyance pipes, large centralized storage basins (i.e., tanks, vaults, tunnels), pump stations, weirs, and treatment facilities. An extensive network of centralized gray infrastructure systems underpins stormwater and flood control in NYC. The long-term control plans (LTCPs) provide recommendations for improvements of gray systems by identifying the appropriate CSO controls necessary to achieve water-body specific water quality standards for enhanced performance and readiness for future weather and sea level conditions (DEP 2019).

Subsurface storage tanks and tunnels are designed to increase the storage capacity of combined sewer systems. Storage tunnels were represented in the H&H model by modifying existing nodes along the stormwater system to represent the added underground storage capacity. Additional storage prevents water from ponding on the surface and reduces flooding.

Storage within pipe systems can be used as a strategy to add storage capacity within the gray infrastructure when extreme flooding occurs. This is because sewer pipes are designed and installed with a minimum freeboard to ensure that overflow does not occur at peak flow. Therefore, placing a weir or other elevation regulating structure can allow water to back up within the pipes into the unutilized storage space. This strategy was modeled in the H&H model by adding weir links to the system to control the depth of water within the system and fully utilize pipe capacity.

Pumping stations are implemented in low-lying areas of cities near bodies of water that are threatened by flooding due to heavy precipitation, SLR, and other pressures, particularly in locations where terrain restricts the ability to move water by gravity. Pumping can also be used to increase the flow rate of water moving through the sewer system, causing less water to back up onto the surface. Pumps were represented in the H&H model using pumping elements in the model that control release rates.

5.2.3.2. Green infrastructure system

Green infrastructure systems, such as rain gardens, sand filters, green roofs, and permeable pavement are implemented as distributed systems and are widely used for flood mitigation, water quality control, and improved ecological, social and economic co-benefits in cities. Green interventions consist of infrastructure implemented across catchments to manage rainfall where it falls and are typically designed to manage small drainage areas such as public right-of-way, stretches of roadways, parking lots, and private lots. These systems are considered nature-based solutions with environmental and social co-benefits since they facilitate natural hydrologic and biogeochemical cycles in cities and densely developed urban regions (Benedict and McMahon 2002). In this study flood reduction benefits from the city-led planned and constructed green infrastructure assets, from green infrastructure constructed as part of new/redevelopment, and from green infrastructure projected from potential stormwater regulation changes were evaluated. The information for each green intervention used in this study is provided in Appendix C, Section C2.

To model the already constructed green infrastructure intervention with the actual known location in the H&H model, a node with the storage capacity of the infrastructure is added to the 2D model to receive water from the 2D surface. The node was connected to an artificial outfall using a conduit link that was 1 inch in diameter, 1,000 ft long, at a slope of 0.5 percent to activate it within the H&H model. The connection significantly restricts flow, creating a near static volume within the node. These were the tested conduit parameters that allowed for the smallest flow rates without causing instability within the H&H model.

To model the planned green interventions, which their exact spatial locations were not yet determined, nodes were added to the H&H model in a distributed fashion adding one node for each 100 ft by 100 ft cell across the subcatchment. All nodes within each sewershed or subcatchment were then given a storage volume commensurate with the total planned storage capacity for each sewershed or subcatchment. These nodes were linked with an artificial outlet node via a 1-inch diameter 1,000 ft long pipe to allow the elements to function properly within the H&H model, in the same manner as previously described.

5.2.3.3. Cloudburst system

Cloudburst systems are promoted to manage stormwater in response to events referred to as "cloudburst" with extremely high amounts of rain over a short period of time (Ramboll 2017). Cloudburst management is a safe-to-fail approach where certain areas are allowed to flood without causing harm to people or property. By identifying areas that could be allowed to be flooded, the City could increase the available storage within the system to manage prevailing extreme events, while also increasing the resiliency of the system to changes in climate.

Cloudburst system was used as an intervention in this study and modeled in the H&H model by manually adding nodes using a 25 ft by 25 ft grid within an area that would be managed by cloudburst, with a design volume obtained from procedures outlined in the 2017 NYC DEP Cloudburst Studies Report (Ramboll 2017). The nodes were allowed to interact with the 2D mesh elements capturing water from the surface and storing within the node. The total volume managed was determined based on the type of cloudburst management being pursued and was evenly distributed to all nodes. All cloudburst nodes were connected to a collection point which was tied into the existing sewer system at the nearest point using a 0.5 inch diameter pipe which provided a stable model but still allowed the storage provided by cloudburst to be used.

5.2.3.4. Stormwater intervention scenarios

Four intervention scenarios were developed to examine the effects of centralized grey infrastructure, distributed green infrastructure, and combinations thereof to assess the complementary and substitutive effects of interventions under different storm scenarios. The scenarios include prevailing and currently funded green and gray stormwater interventions, planned green and gray stormwater interventions for the City by 2050, additional interventions to manage volume targets, and changes to private on-site detention requirements. The citywide H&H model was used to simulate flooding under these four intervention scenarios using the five storm scenarios.

Most interventions were modeled as nodes within the H&H model with a calculated volume that interacts with the 2-D mesh allowing water to fill the node until the node is at capacity after which it will continue to flow within the 2-D mesh until entering the 1-D storm sewer system. The stormwater intervention scenarios are incremental to the preceding scenarios and are as follows:

IS0: Baseline Conditions

The baseline scenario represents the prevailing NYC combined sewer and separate storm sewer collection and conveyance systems.

IS1: Current and Planned Distributed Green Infrastructure to 2035

IS1 represents constructed and imminent green infrastructure planned for implementation through 2035. The Intervention includes green infrastructure in both combined and separate storm sewers and includes both City-funded green infrastructure and green infrastructure implemented as a result of stormwater regulations. The storage volume of each added node was computed based on the constructed and planned green infrastructure dataset obtained from NYC DEP.

IS2: 2040 Long Term Control Plan Infrastructure

IS2 evaluates how the LTCP affects flooding in NYC and includes the distributed interventions from IS1 as well as additional gray infrastructure. Additional infrastructure elements were found by comparing the infrastructure in the current H&H model with the baseline LTCP models received from the City. These baseline models included infrastructure improvements meant to reduce CSO. The additional gray infrastructure elements in the baseline LTCP model include storage nodes scattered throughout the model, occasional tunnels or pipes for holding large quantities of water, additional/modified pump curves to provide additional pumping, or in some cases a change of the pipe network configuration.

IS3: Planned distributed Green infrastructure to 2050 and cloudburst systems

IS3 represents the additional green infrastructure throughout the city that would be required by proposed updates to the onsite water management rules for both combined and separate sewers. Currently, DEP is evaluating stormwater regulations that would require 1.5 inches of stormwater retention on sites that disturb 20,000 ft^2 or more of soil. IS3 investigates how reducing the threshold to 15,000 ft^2 would influence stormwater runoff and flooding. This expansion of the rule is estimated to add approximately 142 MG of distributed storage. Additionally, the scenario incorporates cloudburst management strategies in Bowery Bay and Jamaica Bay sewersheds. At the Bowery Bay location, 53,000 ft^3 of capacity was added to the system, and at the Jamaica Bay location, 38,400 ft^3 was added.

IS4: Additional Gray Infrastructure Scenario

IS4 evaluates how additional gray infrastructure impacts flooding. The additional infrastructure improvements such as pumps, tunnels, and conduits were identified from the recommended LTCP models and were added into the H&H model in addition to the interventions from IS1, IS2, and IS3. New infrastructure elements were identified similarly to IS2.

Overall, IS1 and IS3 contain distributed green infrastructure and provide approximately 190 and 142 MG capacity, respectively. IS2 and IS4 encompass centralized gray systems and provide approximately 121 and 68 MG capacity. Consequently, the total additional capacity obtained by IS1 through IS4 is approximately 190, 311, 453, and 521 MG. More detailed information about each intervention scenario is provided in Appendix C, section C3.

5.2.4. Assessment of intervention scenarios

The Intervention scenarios were added to the H&H model to generate 5 ft by 5 ft gridded maximum flood depth raster for five storm scenarios. The total volume of flooding greater than 4 inches and total area exposed to depth greater than 4 inches were calculated for primary evaluation of intervention scenarios. The total volume of flooding was calculated by multiplying the depth of flooding by the area of a raster cell size. The 4-inch threshold is selected from a definition of nuisance flooding considering hydrology, transportation, public health risk, and safety impacts

(Moftakhari et al. 2018). The effect of interventions on CSO volumes was also evaluated in comparison to the baseline scenario. The accumulated volumes of CSO were calculated for each outfall and were aggregated.

Many of the interventions, particularly distributed green systems, provide other benefits besides flood or CSO reduction. Co-benefits including carbon sequestration, reduction of heat adsorption leading to urban heat island effects (UHIE), reduced wastewater treatment costs, stormwater jobs, and air quality improvements were also quantified using equations provided through the NYC Green Infrastructure Co-benefit Calculator. The estimates are based on the surface area or volume of each practice that was implemented. More detailed information about the calculation of co-benefits is provided in Appendix C, section C4.

5.3.Results and Discussions

The effects of four stormwater management intervention scenarios on urban flood control in terms of flood depth, volume, and extent, and also CSO volume were assessed in NYC under five storm scenarios. Green infrastructure systems were found to be the most effective in controlling smaller storms in terms of percent reduction in flood volume and extent. However, the system was estimated to provide marginal benefits in capturing flood volumes for extreme precipitation events at which the capacity of the systems is fully utilized. Cloudburst management was by far the most effective strategy for controlling flooding from extreme storm events. Moreover, gray infrastructure systems appear to be most effective in mitigating CSOs.

5.3.1. Flood control assessment

5.3.1.1. Urban water balance

The effect of intervention scenarios was evaluated on water balance for storm SC4, which is used to evaluate the DEP site retention standard. Urban water fluxes estimated by the H&H model were divided into six categories including (1) Normal Boundaries, which refers to the water outflow from the surface of the 2D mesh; (2) Infiltration, which refers to water infiltrated or lost due to interventions; (3) CSOs, which refers to water outflow through combined sewer overflows; (4) WRRFs, which refers to water treated by the wastewater pollution control plants; (5) Additional 1D, which refers to water remaining in the 1D system at the end of the model simulation; and (6) 2D Remaining, which refers to water remaining on the 2D system at the end of the model simulation.

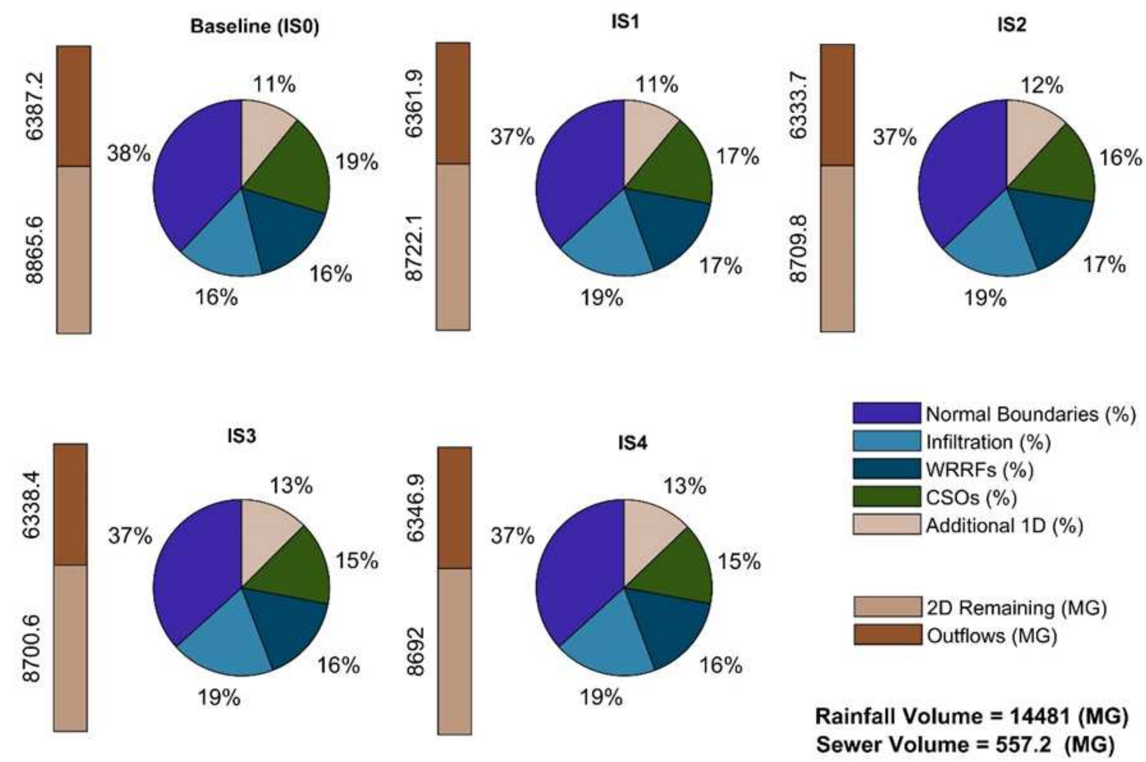

Figure 5.1. Urban water balance for storm SC4 under baseline condition and four intervention scenarios.

Figure 5.1 illustrates these urban water balance components under the baseline condition and four intervention scenarios. The bar graph shows the distribution between 2D remaining volume and outflows depicted in the pie charts.

Overall, the urban water balance was slightly altered by the intervention scenarios investigated in this study. This can be attributed to the small capacity of added interventions compared with the inflow rainfall and sewage volumes for storm scenario SC4 (1.3%, 2.1%, 3%, and 3.5% of the total inflow volume for storm SC4 for IS1 through IS4, respectively)

IS1 contained a large number of retention-based practices, which resulted in a 3% increase in infiltration compared to the baseline scenario. The increase in infiltration was achieved in conjunction with a 2% reduction of CSO volume. IS2 contained detention-based practices in addition to interventions in IS1. The additional interventions provided a 1% increase in water detained (i.e., Additional 1D) and a 1% reduction of CSO volume. Although the added storage capacity was merely 1% of the combined inflow rainfall and sewer volumes, Infiltration was increased by approximately 3% and CSO volume was reduced by 4%.

As it can be seen urban water balance is influenced by the implementation of both green and gray infrastructure systems. However, increased infiltration primarily resulted from implementation of green infrastructure systems.

5.3.1.2.Green and gray stormwater interventions

The gridded citywide maximum flood volumes were used to analyze changes in flood volume and extent for all interventions and storm scenarios. To evaluate the effects of each unique intervention scenario across various storms, the citywide maximum flood volume maps were compared to the baseline scenario to compute the difference in volume and extent for each storm scenario.

Flood volume reduction was improved from approximately 1% to 6% between the storm and intervention scenarios (Figure 5.2). IS1 and IS3 provided the greatest changes to the estimated flood volume. This observation may be explained by the larger capture area of distributed green systems compared with the centralized gray components, although gray systems may affect large changes for only a small area. The complementary benefit of additional gray practices (i.e., IS2) on flood volume is evident for longer storms (i.e., SC4 and SC5).

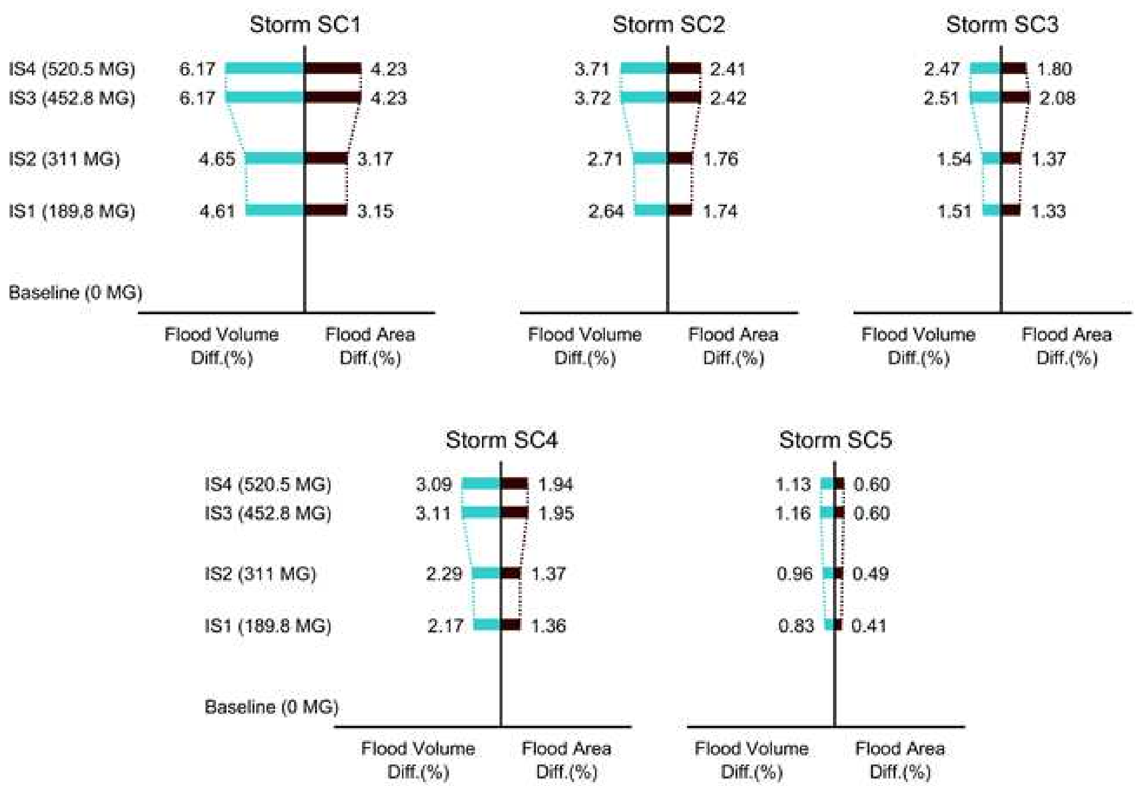

Figure 5.2. The effects of interventions on maximum flood volume and flood extent (The number in parentheses is the total additional capacity obtained by each intervention scenario)

Figure 5.2 also indicates that the change in flood extent that corresponded to a maximum flood depth greater than four inches was limited to only up to 4% of the baseline scenario. Changes for storm SC1 were the greatest in terms of percent change from baseline. Changes to flood extent for storm SC2, SC3, and SC4 varied between approximately 1% to 2.5% across the four intervention scenarios. The lowest change in flood extent was computed for storm SC5. Overall, these results indicate that changes in flood extent are not commensurate with changes in flood volume. This also suggests that maximum flood depths were changed by a small portion across large areas and not by a large portion in small areas.

On the basis of the above results, we can conclude that the effects of an intervention on maximum flood depth, volume, and extent depend on the capacity of the intervention, the intensity of rainfall, and the timing of the peak intensity of the rainfall. These factors collectively contributed to three situations that influenced the effectiveness of any given intervention based on its available volume capacity:

1. The existing capacity of the intervention was fully used when the peak intensity of rainfall occurred. In this situation, the capacity of the system was optimally used to minimize maximum flood depth, volume, and extent.
2. The intervention did not receive enough runoff volume to fully utilize its capacity because the storm and/or the upgradient contributing area were small. Under these circumstances, the capacity of the system is underutilized. This situation was most often observed for storm SC1 and SC2, which represented smaller events.
3. The capacity of the intervention was too small for runoff volume because the storm and/or the upgradient contributing area were too large, and thus, the intervention capacity was full before the peak rainfall intensity occurred, limiting the effectiveness of the intervention to

mitigate part of the storm that most likely produces the maximum flood depth. Although the full capacity of the system is utilized in this situation, the available storage in the system is not optimally used to manage the maximum flood depth. Also, interventions appeared less effective in mitigating maximum flood depth and volume of long storms for which peak intensity occurred hours after the storm began. In the case of storm SC5, it was observed that many of the added intervention nodes filled up before the peak intensity occurred.

Overall, the interventions added in IS1 and IS3 including decentralized green infrastructure outperformed gray centralized interventions added in IS2 and IS4 for flood control, especially during smaller storms. The modeling results indicate that the proximity of decentralized stormwater infrastructure to runoff sources is a key factor in their capacity to control flood volume and depths compared to centralized interventions.

However, flood control benefits of gray systems vary by sewershed and storm scenarios. For example, the additional 39.25 MG storage in IS2 in Hunts Point is estimated to reduce flood volume at maximum depth by approximately 0.5 percent for storm SC5. Conversely, the 12.65 MG of additional storage in IS2 in the Bowery Bay sewershed is estimated to reduce flood volume only by only 0.01 percent for the same storm scenario. This can be attributed to the larger volume of storage in Hunts Point provides the adequate capacity to reduce flood volume at peak runoff, whereas in Bowery Bay the interventions reach full capacity prior to the occurrence of peak runoff. On the other hand, the 23.6 MG additional centralized interventions in IS4 provide substantial reduction of CSO volume (2.4%) for storm SC5 in the Bowery Bay sewershed.

It should be noted that lack of complete representation of stormwater and sewer elements in the 1D component of the H&H model could influence the assessment of the flood impacts of interventions. Without including all of the pipes and inlets of the 1D system, higher runoff volumes remain overland than actually would be observed on site. Thus, the effects of increased capacity and conveyance improvements provided by additional interventions in scenario IS2 and IS4 may have been underestimated.

5.3.1.3.Cloudburst Management

Since cloudburst systems were implemented only in two locations, their effects were evaluated at a sewershed scale. Based on the flood depth maps and by investigating the response of the intervention nodes representing the cloudburst interventions, cloudburst management shows great promise for mitigating flooding from larger events.

While the percent capacity used at Bowery Bay for storm SC1 through SC5 were 59.5%, 86.6%, 86.6%, 98.0%, and 100%, The percent capacity used at Jamaica Bay were 55.3%, 76.2%, 70.1%, 93.8%, and 100%, respectively. During storm SC1, SC2, and SC3 the capacity of the interventions was not completely used. Thus, the use of cloudburst management for smaller storms may not be justified. However, cloudburst management was estimated to effectively improve flooding from storm SC4 (2.55 inches of rainfall). At both locations, storm SC4 produced stormwater volumes close to the full capacity of IS3 and the additional cloudburst capacity while maintaining adequate capacity for managing peak runoff conditions. Implementation of the cloudburst management system for storm SC4 was estimated to eliminate flooding in the area downgradient of the intervention.

However, cloudburst management interventions resulted in no improvement to the maximum flood depth extent for storm SC5 because the full capacity of the system was reached prior to peak stormwater runoff. These results demonstrate that 9.1 inches of rainfall generate too much runoff that would even exceed the capacity of cloudburst management systems. Clearly, adding cloudburst management in more locations could substantially reduce flood volume, maximum depth, and extent throughout the city sewersheds.

Overall, the analysis revealed that cloudburst management is a highly effective intervention strategy for flood control under extreme precipitation events. However, more investigations are needed to understand the optimal level of and strategies for cloudburst implementation to effectively mitigate extreme flooding from compounding effects of heavy precipitation and SLR as represented in storm SC5.

5.3.2. Co-benefits assessment

Co-benefits including CSO reduction, carbon sequestration, reduction of heat adsorption leading to urban heat island effects (UHIE), reduced wastewater treatment costs, stormwater jobs, and air quality improvements were also calculated.

5.3.2.1 Combined sewer overflows

Substantial percentage reductions of CSO volumes were estimated to range between 2% to 40% of baseline depending on storm and intervention scenarios. Figure 5.3 shows the effects of interventions on CSO volume reduced from baseline for the five storm scenarios.

CSOs were mostly influenced by gray interventions in IS2 and IS4 especially for storms with shorter duration since the interventions were not overwhelmed and their capacity can be fully utilized. It should be noted that since IS4 contains specific infrastructure improvements, CSO improvements were typically observed at the targeted outfall. A negligible percentage reduction in CSOs observed for SC3. This can be attributed to the negative compounding effect of storm surge that leads to submerging of outfalls and preventing water to drain.

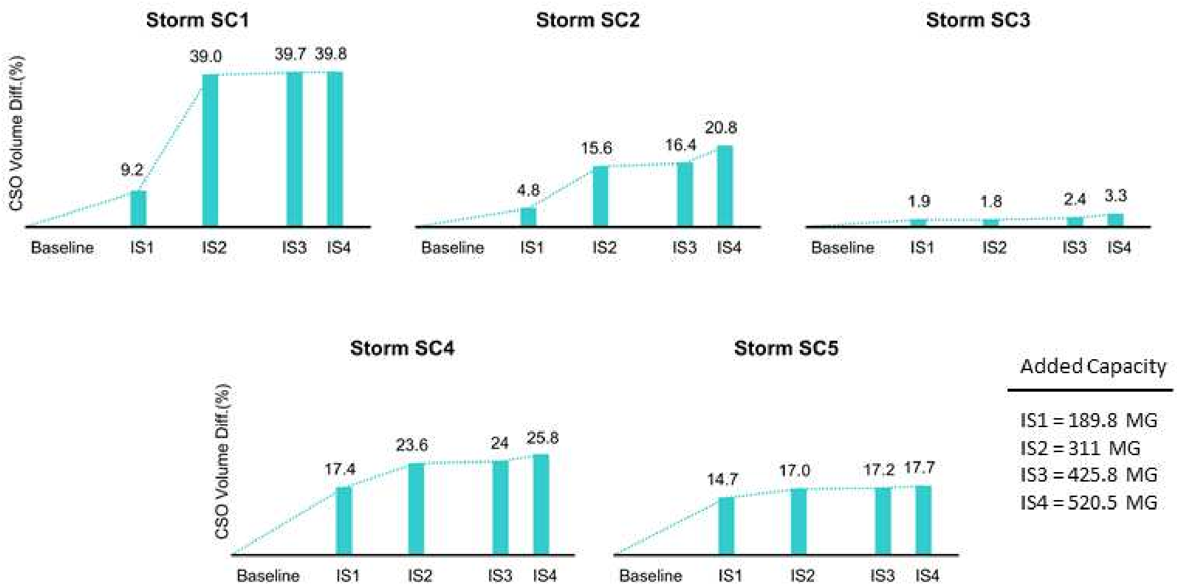

Figure 5.3. The effects of interventions on CSO volume reduction

5.3.2.2. Additional co-Benefits

Co-benefits of interventions are largely dependent on the type of intervention that is being used. According to the NYC Co-benefits calculator, the calculation of most co-benefits is dependent on the volume managed by each intervention. However, some benefits, such as UHIE, and carbon sequestration, are estimated by the surface area of the intervention type.

In order to calculate co-benefits, the total volume managed for each sewershed was partitioned into seven types of green infrastructure consistent with the options available in the NYC green infrastructure co-benefits calculator. These systems include blue roofs, green roofs, porous asphalt, porous concrete, rain gardens, rainwater harvesting, and subsurface detention. The amount of each type of intervention to be placed into each sewershed was estimated based on the general volumes expected to be managed. Then, an extensive review of the NYC green infrastructure design criteria was conducted to obtain a ratio of volume managed to surface area of various systems. The detailed procedure for calculation of unit volume ratios for different intervention technologies is provided in Appendix C, section C4.1.

Added surface area of each intervention type for IS1 and IS3 was estimated and the estimated volumes and surface areas for IS1 and IS3 were used in the NYC Green Infrastructure Calculator to compute co-benefits for the intervention scenarios. For more detailed information about the co-benefit analysis refer to Appendix C, section C4.2.

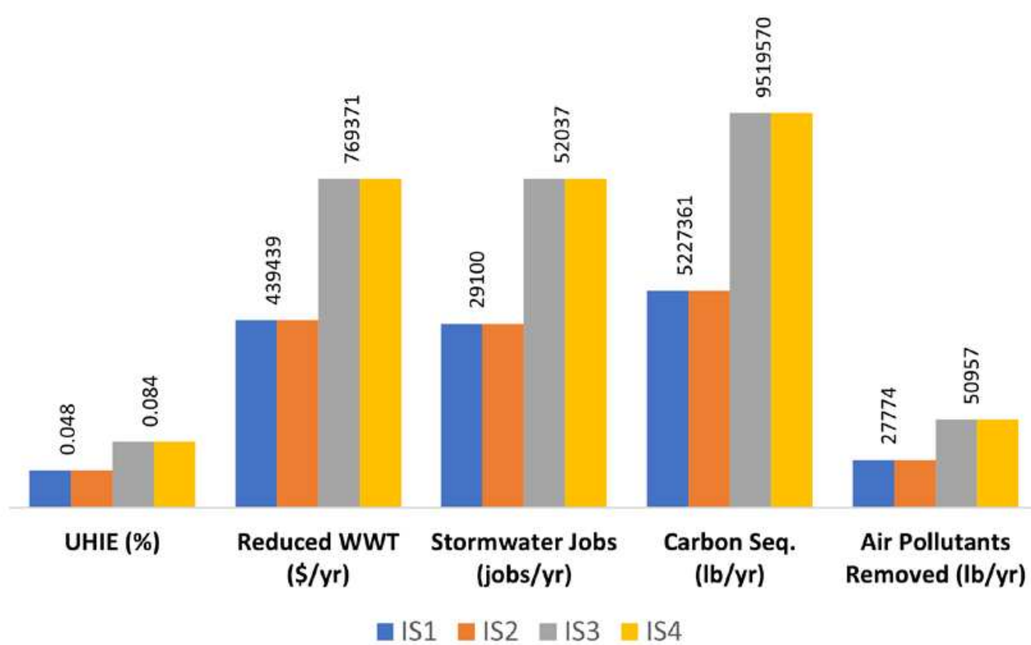

Figure 5.4. Total co-benefits from the NYC Green Infrastructure Benefit Calculator for each intervention scenario

Figure 5.4 shows the resulting co-benefits for each intervention scenario. IS1 and IS3 provided the largest co-benefits as these scenarios contain additional decentralized green interventions. IS2 and IS4 encompass additional gray systems, which do not provide significant co-benefits. Many of the co-benefits calculated vary with the type of the implemented infrastructure. For example, Rain gardens and green roofs both provide carbon sequestration, stormwater jobs, and air quality benefits. Management strategies can reduce or improve the co-benefits a specific practice provides. These decisions include plant selection, amount of plant diversity and cover as well as overall maintenance strategies for ensuring the practice continues to function (Li 2015; Young and McPherson 2013).

5.3.3. Multi-criteria assessment

A multi-criteria assessment of the intervention scenarios is illustrated in Figure 5.5. The value of "0" and the value of "1" reflect the values for IS0 and IS4, respectively. The capital, operation, and maintenance costs of grey and green infrastructure systems depend on their design specifications. Since these considerations were available for the planned and recommended interventions, the planned storage volumes were used as a surrogate for these costs. Thus, the total volume of additional storage to be achieved by improvement of the green and gray infrastructure systems is summarized for each intervention scenario.

For smaller storms, the additional gray infrastructure volume added in IS2 and IS4 was not effective in flood volume reduction. However, the effects of this additional storage on CSO volume reduction were substantial. Also, for longer storms, this additional gray capacity had a slightly positive effect on lowering flood volume (Sanders and Grant 2020). Overall, the multicriteria assessment indicates the complementary benefits of additional decentralized green infrastructure systems for flood and CSO mitigation.

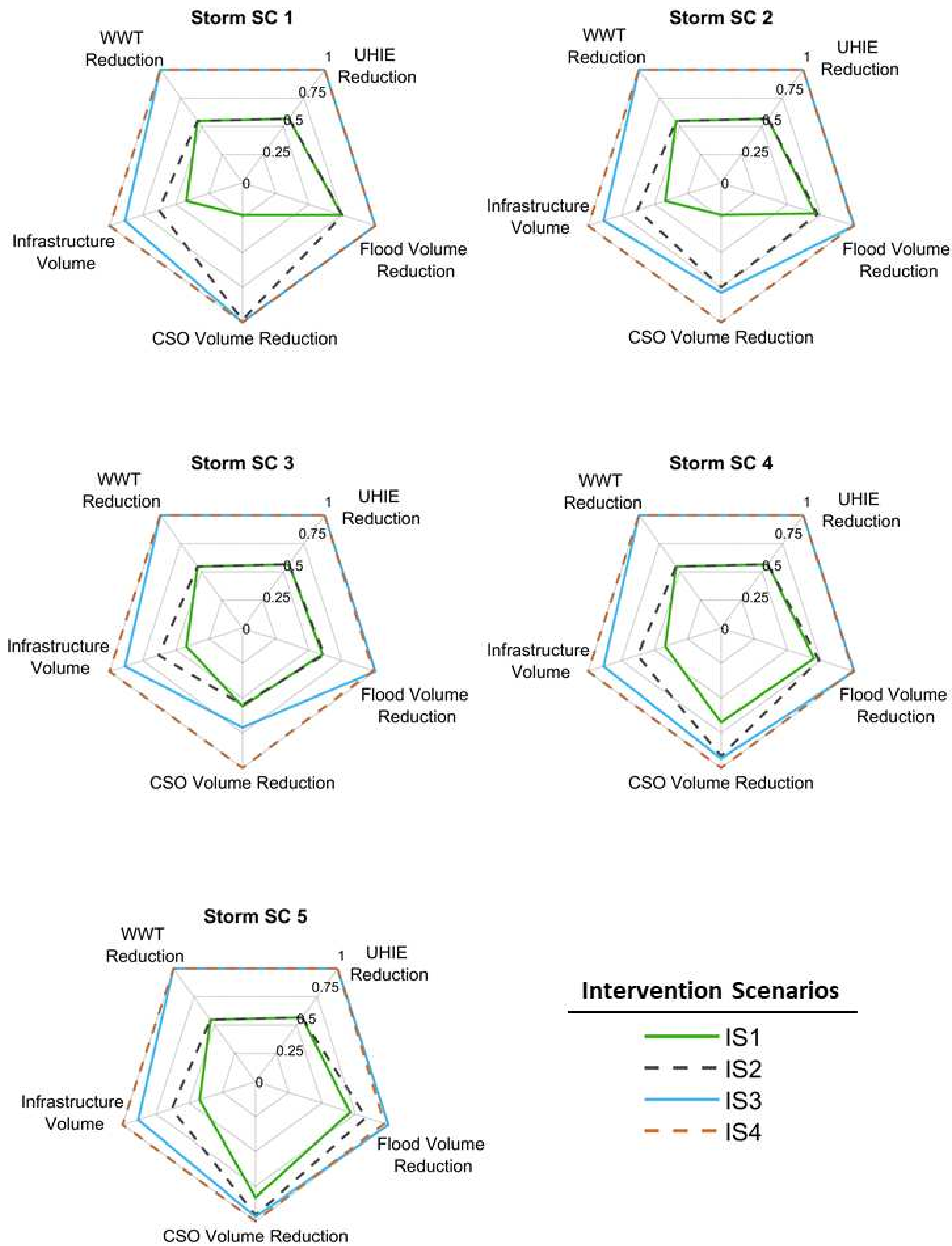

Figure 5.5. A multi-criteria assessment of the intervention scenarios

5.4. Conclusion

With the increased frequency of extreme precipitation and SLR, the prevailing stormwater conveyance network in NYC is increasingly overwhelmed, leading to flooding and water quality degradation. Recent storms demonstrate that NYC's stormwater conveyance system faces increasing risks from the impact of climate change that must be addressed through implementation of further stormwater management interventions.

Four scenarios comprising interventions from the baseline LTCP, distributed green interventions required by prevailing and planned onsite water management regulations, and other recommended LTCP interventions were assessed using a citywide H&H model under current and future storm scenarios. Storm scenarios were created so that span a wide range of intensity and duration, as well as compound rain plus storm surge scenarios, and climate change effects. The suite of interventions and storm scenarios provide insight on ways to improve climate resiliency in the City.

Distributed green practices were found significantly effective in reducing flood hazard during nonextreme storm events. On the other hand, gray infrastructure systems were found to be necessary to mitigate flood hazard during more extreme storm events and also compound flooding. Also, they appear to be most effective in mitigating CSOs. Overall the results suggest that in urbanized and developed cities green and gray stormwater management practices should be considered complementary and mutually reinforcing. Decentralized green stormwater management strategies should be implemented as complementary systems to centralized gray measures. Flood and CSO reduction and other co-benefits, can be gained from integration of green and gray infrastructure.

One of the intervention scenarios also incorporated a cloudburst management system in two locations, which was found a highly effective strategy for flood control under extreme precipitation events. The results indicated that diligent design and implementation of cloudburst systems could completely eliminate downstream flooding even for large storm exceeding 2 inches. Adding cloudburst management in more locations could substantially reduce flood volume, maximum depth, and extent throughout the city sewersheds.

All the interventions seem to have less effect on flood hazard and especially CSO reduction for the compound rain plus storm surge scenario. This indicated that compounding effects of extreme precipitation and storm surge can cause more water quality degradation and expose a much greater amount of assets at risk of flooding unless further stormwater management interventions compensate the risks.

CHAPTER 6.

SUMMARY AND FUTURE RESEARCH DIRECTION

6.1. Summary and closing remarks

Coastal cities are more vulnerable to flood hazard since they are exposed to multiple flood drivers including high tide and storm surge, extreme precipitation, and high river flows. Climate change impacts could exacerbate the existing vulnerabilities by changing the statistical behavior of flood drivers. This dissertation was an attempt to compensate the negative impacts of climate change in coastal cities through a better understanding and estimation of flood hazard and risk under future climate conditions and adaptation options.

To achieve this goal, two nonstationary flood risk assessment frameworks were developed, which facilitate univariate and bivariate flood risk analysis under future climate conditions. First, a nonstationary mixture probability distribution was developed in order to simultaneously characterize minor and extreme coastal flood events under future sea level conditions. The reason for utilizing a mixture probability model was insufficiency of common extreme value distributions in characterization of future frequency of minor flood events under future sea level rise (SLR). Using the idea of extreme value mixture model, a Generalized Parero distribution (GPD) for the data in the tail of the sea level distribution was mixed with a Normal distribution for the data in the bulk of the sea level distribution to derive a single-spliced distribution that coherently characterizes probability density of the entire range of sea level data.

The application of the proposed mixture probability model along the Contiguous United States (CONUS) coast shows a significant increase in frequency of both minor and major flood events under future sea level conditions. However, the frequency amplification of minor and major flooding varies by coastal regions. The Gulf and northeast Atlantic coastal regions should expect the highest minor flood frequency amplification. On the contrary, Pacific coast regions followed by regions within the southeast Atlantic coast are likely to be exposed to higher frequency amplification in major flooding. The study suggests that while effective adaptation strategies should give more priority to measures reducing unprecedented major flood risk in the Pacific and Southeast Atlantic regions, they must account for increasing frequency of repetitive minor flooding in the Gulf and northeast Atlantic coasts.

Three Regional SLR projections (Sweet et al. 2017) including “Intermediate-Low”, “Intermediate”, “Intermediate-High” scenarios were used to perform a decadal assessment of expected time to certain changes in mean sea levels. The projections correspond to 0.5m, 1m, 1.5m global SLR, respectively. While the “Intermediate Low” scenario has a 73% chance of being exceeded under Representative Concentration Pathway (RCP) 4.5 climate change scenario, the “Intermediate” and “Intermediate-High” scenarios have 17% and 1.3% chances of being exceeded under the RCP 8.5 climate change scenario, respectively (Kopp et al., 2014; Sweet et al., 2017). Antarctic ice sheet instability could transition to more extreme scenarios (i.e., Intermediate-High, High, and Extreme) later in the century. However, those outcomes are less likely to occur. The regional projections are relative sea levels, which include both ocean-level change and vertical land motion projections. Important factors such as shifts in oceanographic factors, vertical land movement (subsidence or uplift), and changes in the Earth’s gravitational field and rotation were considered in the regional projection of relative SLR (Sweet et al. 2017). The results show that by the end of the century, under the “Intermediate” SLR scenario, major flooding is anticipated to occur with return period less than a year throughout the coastal CONUS.

The proposed mixture model was incorporated in the risk assessment framework in order to assess future acute and chronic coastal flood risk under different SLR and adaptation levels in Miami-Dade County, which encompasses one of the highest value of assets exposed to coastal flooding. The HAZUS-MH coastal flood hazard modeling and loss estimation tool was used to develop flood inundation maps and corresponding monetary losses to buildings associated with different sea water levels. Under current sea level conditions, coastal flood risks were found to be predominantly from exposure to acute extreme events. However, as sea level rises, chronic risks from repetitive nonextreme flooding may exceed those from extreme floods.

The possibility that chronic losses from repetitive nonextreme flooding will aggregate over time into high-cost losses is a big challenge for decision makers and coastal planners. As sea level rises, chronic losses from repetitive nonextreme flooding have the potential to become cumulative losses when their frequency increases. Responding too late to these cumulative losses can result in significant costs. Estimation of chronic and acute flood risk under combinations of different SLR values and adaptation levels provides insight on ways to improve understanding about when these cumulative losses will be aggregated to significant cumulative losses and how different levels of adaptation could compensate the negative impact of SLR. The approach allows estimating the minimum adaptation level needed to offset the negative impacts of SLR to maintain the current level of flood risk. In Miami-Dade County, the least adaptation level that would be needed to keep the current flood risk at the same value was found to be higher than the value of SLR itself.

In addition to storm surge and tidal flooding events, coastal cities are exposed to urban and riverine flooding. The concurrence of these flood events could exacerbate flood impacts, which may become more exacerbated under future climate conditions. Thus, in the next step, a bivariate flood hazard assessment framework was developed that accounts for compound coastal-riverine flooding with consideration of the impact of SLR and hydrologic changes including changes in extreme river flows. The compound flood hazard assessment framework was applied in 26 paired tidal-riverine stations along the CONUS coast with long-term observed data and defined flood impact thresholds. Definition of compound flooding based on exceedances above flood impact thresholds can allow localization and personalization of flood risks that help to explore and compare compound flood risk at a large scale.

Estimation of the joint return period of compound major coastal-riverine flooding by midcentury under current and future climate conditions showed regional differences. While the northeast Atlantic and western part of the Gulf coasts are experiencing the highest compound major flood frequency, locations along the southeast Atlantic coasts are exposed to fewer compound major flood events. The majority of the stations along the Pacific coast are exposed to no risk from compound major coastal-riverine flooding. However, Projected joint return periods according to the Intermediate-low and Intermediate SLR scenarios showed a significant amplification in the frequency of compound major flooding along the southeast Atlantic coast. The impact of changes in extreme river flows on compound major coastal-riverine flood events was found to be negligible except for the locations along the southeast Atlantic coast. However, even in this region, its impact is considerably less than that of SLR. In general, the results revealed that although the frequency of compound major coastal-riverine flooding under current climate conditions is low, climate change impact, especially SLR, may lead to more frequent compound events in the future, which cannot be ignored for future adaptation responses in estuary regions. The increasing flood risk must be addressed through implementation of flood adaptation and intervention measures.

In the final step, different green (i.e., distributed infiltration systems) and gray (i.e., centralized conveyance systems) stormwater infrastructure, alone or in combination, were assessed in New York City (NYC) using a citywide hydraulic and hydrologic model under current and future storm scenarios. Four intervention scenarios were proposed which include interventions based on baseline and other recommended Long Term Control Plan, distributed green interventions required by prevailing and planned onsite water management regulations, and Cloudburst systems. Five storm scenarios were used so that cover a mixture of current and future rainfall and tide scenarios, compound (extreme precipitation and surge) scenarios, and common and extreme scenarios.

Distributed green measures were found significantly effective in reducing flood hazard in terms of flood volume during nonextreme storm events. On the other hand, gray infrastructure systems were found to be necessary to mitigate flood hazard during more extreme storm events and compound flooding. Also, they appeared to be most effective in mitigating combined sewer outflows (CSOs). Overall the results suggest that in urbanized and developed cities green and gray stormwater management practices should not be considered as competing but rather as complementary and mutually reinforcing. Green systems provide complementary effects on flooding impacts and cannot substitute gray systems. Flood and CSO reduction and other co-benefits can be gained from integration of green and gray infrastructure. Moreover, the results indicated that diligent design and implementation of cloudburst systems could reduce flood hazards during extreme storm events.

In general, this dissertation enhances the capacity for more resilient coastal management under uncertain future climate through a better understanding of future flood hazards and risks in coastal regions and evaluation of different adaptation levels. The developed univariate and bivariate flood risk assessment framework incorporates the model-driven climate change projections in assessing flood hazards and risks in coastal regions that help to better support coastal planners and policymakers for more informed adaptation and mitigation strategies under uncertain climate conditions.

6.2. Future research directions

Throughout the study period, several directions for future research were identified to better quantify future flood hazards and risks and to provide better guidance for adaptation strategies. The recommended areas of future research are outlined below:

1. Considering changes in storminess can improve estimation and prediction of extreme coastal flood events. Allowing for changes in storminess should be based on reliable high resolution forcing from global climate models. Although previous studies showed that sea level rise has more immediate threat for the increase coastal flood frequency than possible changes in storm variability, this does not imply that changes in storm severity have a negligible impact on the return period of extreme events and worthy to be considered in future studies.
2. Estimated chronic and acute average annual losses can be improved in several ways. First, two-dimensional (2D) hydrodynamic modeling can be used to provide more accurate and detailed flood extent and depth. Second, loss estimation accuracy can be enhanced with more detailed information about the terrain and the located building inventory and depth-damage curves. Level-2 and Level-3 analysis in HAZUS-MH allows users to utilize more detailed and updated building inventory information and modified depth-damage curves to develop a more accurate hazard assessment. The accuracy of loss estimation through

HAZUS-MH will be enhanced with specific and updated data and a higher level of analysis.

3. In order to estimate future compound coastal-riverine flood frequency, considering variations in the dependency between extreme sea levels and river flows are also important and could improve analysis accuracy. The current analysis considered nonstationarity in the marginal distributions of flood drivers. However, future study is recommended to also assess changes in dependency between flood drivers under different climate conditions.
4. More accurate assessment of green and gray stormwater management systems in New York City can be gained through improving representation of distributed green stormwater and cloudburst systems at sufficiently finer resolution in space to adequately represent their responses to storm events. Also, lack of complete representation of stormwater and sewer elements in the 1 dimensional (1D) component of the H&H model could influence the assessment of the flood impacts of green and gray interventions. Including all of the pipes and inlets of the 1D system could provide more realistic estimates of the effect of interventions on flood control and CSO reduction.

REFERENCES

Aerts, J. C. J. H., Botzen, W. J. W., Emanuel, K., Lin, N., and Moel, H. De. (2014). “Evaluating Flood Resilience Strategies for Coastal Megacities.” *Science*, 344(6183), 473–475.

Aerts, J. C. J. H., Botzen, W. J. W., de Moel, H., and Bowman, M. (2013). “Cost estimates for flood resilience and protection strategies in New York City.” *Annals of the New York Academy of Sciences*, 1294(1), 1–104.

Ahiablame, L. M., Engel, B. A., and Chaubey, I. (2012). “Effectiveness of low impact development practices: Literature review and suggestions for future research.” *Water, Air, and Soil Pollution*, 223(7), 4253–4273.

Ahn, K. H., and Palmer, R. N. (2016). “Trend and variability in observed hydrological extremes in the United States.” *Journal of Hydrologic Engineering*, 21(2), 1–10.

Arns, A., Dangendorf, S., Jensen, J., Talke, S., and Bender, J. (2017). “Sea-level rise induced amplification of coastal protection design heights.” *Nature Publishing Group*, Nature Publishing Group, 7(40171), 1–9.

Bates, P. D., Horritt, M. S., and Fewtrell, T. J. (2010). “A simple inertial formulation of the shallow water equations for efficient two-dimensional flood inundation modelling.” *Journal of Hydrology*, Elsevier B.V., 387(1–2), 33–45.

Baxter, J. (2013). “Mitigation Ideas : A Resource for Reducing Risk to Natural Hazards.” *US Department of Homeland Security. FEMA*, (January).

Behrens, C. N., Lopes, H. F., and Gamerman, D. (2004). “Bayesian analysis of extreme events with threshold estimation.” *Statistical Modelling*, 4(3), 227–244.

Bell, C. D., Spahr, K., Grubert, E., Stokes-Draut, J., Gallo, E., McCray, J. E., and Hogue, T. S. (2019). “Decision Making on the Gray-Green Stormwater Infrastructure Continuum.” *Journal of Sustainable Water in the Built Environment*, 5(1), 04018016.

Bender, J., Wahl, T., and Jensen, J. (2014). “Multivariate design in the presence of non-stationarity.” *Journal of Hydrology*, Elsevier B.V., 514, 123–130.

Bender, J., Wahl, T., Müller, A., and Jensen, J. (2016). “A multivariate design framework for river confluences.” *Hydrological Sciences Journal*, Taylor & Francis, 61(3), 471–482.

Benedict, M. A., and McMahon, E. T. (2002). “Green Infrastructure: Smart Conservation for the 21st Century.” *Renewable Resources Journal*, 12–18.

Berghuijs, W. R., Woods, R. A., Hutton, C. J., and Sivapalan, M. (2016). “Dominant flood generating mechanisms across the United States.” *Geophysical Research Letters*, 43(9), 4382–4390.

Bevacqua, E., Maraun, D., Vousdoukas, M. I., Voukouvalas, E., Vrac, M., Mentaschi, L., and Widmann, M. (2019a). “Higher probability of compound flooding from precipitation and storm surge in Europe under anthropogenic climate change.” *Science Advances*, 5(9).

Bevacqua, E., Maraun, D., Vousdoukas, M. I., Vrac, M., Mentaschi, L., and Widmann, M. (2019b). “Higher probability of compound flooding from precipitation and storm surge in Europe under anthropogenic climate change.” *Science Advances*, 5(September).

Boettle, M., Rybski, D., and Kropp, J. P. (2013). “How changing sea level extremes and protection measures alter coastal flood damages." *Water Resources Research*, 49(3), 1199–1210.

Buchanan, M. K., Oppenheimer, M., and Kopp, R. E. (2017). "Amplification of flood frequencies with local sea level rise and emerging flood regimes." *Environmental Research Letters*, 12(6).

Castellano, C. M., and Degaetano, A. T. (2017). "Downscaled Projections of Extreme Rainfall in New York State Technical Document Cornell University Ithaca , NY." 1–25.

Chakraborty, J., Collins, T. W., Montgomery, M. C., and Grineski, S. E. (2014). "Social and Spatial Inequities in Exposure to Flood Risk in Miami, Florida." *Natural Hazards Review*, 15(3), 04014006.

Church, J. a., Clark, P. U., Cazenave, a., Gregory, J. M., Jevrejeva, S., Levermann, a., Merrifield, M. a., Milne, G. a., Nerem, R. ., Nunn, P. D., Payne, a. J., Pfeffer, W. T., Stammer, D., and Unnikrishnan, a. S. (2013). "Sea level change." *Climate Change 2013: The Physical Science Basis. Contribution of Working Group I to the Fifth Assessment Report of the Intergovernmental Panel on Climate Change*, 1137–1216.

Church, J. A., Hunter, J. R., McInnes, K. L., and White, N. J. (2006). "Sea-level rise around the Australian coastline and the changing frequency of extreme sea-level events." *Australian Meteorological Magazine*, 55, 253–260.

Climate Central. (2016). "Surging Seas: Risk Finder." <https://riskfinder.climatecentral.org/>.

Coles, S. (2001). *An Introduction to Statistical Modeling of Extreme Values*.

Colle, B. A. (2003). "Numerical simulations of the extratropical transition of Floyd (1999): Structural evolution and responsible mechanisms for the heavy rainfall over the Northeast United States." *Monthly Weather Review*, 131(12), 2905–2926.

Colle, B. A., Lombardo, K. A., Tongue, J. S., Goodman, W., and Vaz, N. (2012). "Tornadoes in the New York metropolitan region: Climatology and multiscale analysis of two events." *Weather and Forecasting*, 27(6), 1326–1348.

Cook, B. I., Ault, T. R., and Smerdon, J. E. (2015). "Unprecedented 21st century drought risk in the American Southwest and Central Plains." *Science Advances*, 1(1), 1–8.

Couasnon, A., Eilander, D., Muis, S., Veldkamp, T. I. E., Haigh, I. D., Wahl, T., Winsemius, H. C., and Ward, P. J. (2020). "Measuring compound flood potential from river discharge and storm surge extremes at the global scale." *Natural Hazards and Earth System Sciences*, 20(2), 489–504.

Le Cozannet, G., Rohmer, J., Cazenave, A., Idier, D., van de Wal, R., de Winter, R., Pedreros, R., Balouin, Y., Vinchon, C., and Oliveros, C. (2015). "Evaluating uncertainties of future marine flooding occurrence as sea-level rises." *Environmental Modelling and Software*, 73, 44–56.

Crichton, D. (1999). "The risk triangle." *Natural Disaster Management,, Tudor Rose, London*, 102–103.

Dahl, K. A., Fitzpatrick, M. F., and Spanger-Siegfried, E. (2017). "Sea level rise drives increased tidal flooding frequency at tide gauges along the U.S. East and Gulf Coasts: Projections for 2030 and 2045." *PLoS ONE*, (G. J.-P. Schumann, ed.), Public Library of Science, 12(2), e0170949.

Dangendorf, S., Marcos, M., Wöppelmann, G., Conrad, C. P., Frederikse, T., and Riva, R. (2017). "Reassessment of 20th century global mean sea level rise." *Proc Natl Acad Sci USA*, 114(23), 1–6.

David, C. H., Habets, F., Maidment, D. R., and Yang, Z. L. (2011a). “RAPID applied to the SIM-France model.” *Hydrological Processes*, 25(22), 3412–3425.

David, C. H., Maidment, D. R., Niu, G. Y., Yang, Z. L., Habets, F., and Eijkhout, V. (2011b). “River network routing on the NHDPlus dataset.” *Journal of Hydrometeorology*, 12(5), 913–934.

DeGaetano, A. T., and Castellano, C. M. (2017). “Future projections of extreme precipitation intensity-duration-frequency curves for climate adaptation planning in New York State.” *Climate Services*, The Authors, 5, 23–35.

Department of Environmental Protection. (2019). “Citywide Long-Term Control Plan- DEP, City of New York.” <https://www1.nyc.gov/site/dep/water/citywide-long-term-control-plan.page>.

Dessai, S., and Hulme, M. (2007). “Assessing the robustness of adaptation decisions to climate change uncertainties: A case study on water resources management in the East of England.” *Global Environmental Change*, 17(1), 59–72.

Devlin, A. T., Jay, D. A., Talke, S. A., Zaron, E. D., Pan, J., and Lin, H. (2017). “Coupling of sea level and tidal range changes , with implications for future water levels.” *Scientific Reports*, Springer US, 7(17021).

Eilander, D., Couasnon, A., Ikeuchi, H., Muis, S., Yamazaki, D., Winsemius, H. C., and Ward, P. J. (2020). “The effect of surge on riverine flood hazard and impact in deltas globally.” *Environmental Research Letters*.

Ezer, T., and Atkinson, L. P. (2014). “Accelerated flooding along the U.S. East Coast: On the impact of sea-level rise, tides, storms, the Gulf Stream, and the North Atlantic Oscillations." *Earth's Future*, 2(8), 362–382.

Ezer, T., Atkinson, L. P., Corlett, W. B., and Blanco, J. L. (2013). "Gulf Stream's induced sea level rise and variability along the U.S. mid-Atlantic coast." *Journal of Geophysical Research: Oceans*, 118(2), 685–697.

Fang, J., Wahl, T., Fang, J., Sun, X., Kong, F., and Liu, M. (2020). "Compound flood potential from storm surge and heavy precipitation in coastal China." *Hydrology and Earth System Sciences*, (July), 1–24.

FEMA. (2018). "Hazus Flood Model User Guidance." *Federal Emergency Management Agency*, (August), 1–263.

Ferguson, B. C., Brown, R. R., Frantzeskaki, N., de Haan, F. J., and Deletic, A. (2013). "The enabling institutional context for integrated water management: Lessons from Melbourne." *Water Research*, Elsevier Ltd, 47(20), 7300–7314.

Forbes, W. L., Mao, J., Ricciuto, D. M., Kao, S. C., Shi, X., Tavakoly, A. A., Jin, M., Guo, W., Zhao, T., Wang, Y., Thornton, P. E., and Hoffman, F. M. (2019). "Streamflow in the Columbia River Basin: Quantifying Changes Over the Period 1951-2008 and Determining the Drivers of Those Changes." *Water Resources Research*, 55(8), 6640–6652.

Ganguli, P., and Merz, B. (2019). "Extreme Coastal Water Levels Exacerbate Fluvial Flood Hazards in Northwestern Europe." *Scientific Reports*, Springer US, 9(1), 1–14.

Ganguli, P., Paprotny, D., Hasan, M., Güntner, A., and Merz, B. (2020). "Projected Changes in Compound Flood Hazard From Riverine and Coastal Floods in Northwestern Europe."

Earth's Future, 8(11).

Genovese, E., and Green, C. (2015). "Assessment of storm surge damage to coastal settlements in Southeast Florida." *Journal of Risk Research*, 18(4), 407–427.

Genovese, E., Hallegatte, S., and Dumas, P. (2011). "Damage Assessment from Storm Surge to Coastal Cities: Lessons from the Miami Area." *Advancing Geoinformation Science for a Changing World 1*, 21–43.

Georgas, N., and Blumberg, A. (2009). "Establishing Confidence in Marine Forecast Systems: The Design and Skill Assessment of the New York Harbor Observation and Prediction System, Version 3 (NYHOPS v3)." *Estuarine and Coastal Modeling*.

Ghanbari, M., Arabi, M., and Obeysekera, J. (2020). "Chronic and Acute Coastal Flood Risks to Assets and Communities in Southeast Florida." *Journal ofWater Resources Plan- ning and Management*, 146(7).

Ghanbari, M., Arabi, M., Obeysekera, J., and Sweet, W. (2019). "A Coherent Statistical Model for Coastal Flood Frequency Analysis Under Nonstationary Sea Level Conditions." *Earth's Future*, John Wiley and Sons Inc, 7(2), 162–177.

Groisman, P. Y., Knight, R. W., Easterling, D. R., Karl, T. R., Hegerl, G. C., and Razuvaev, V. N. (2005). "Trends in intense precipitation in the climate record." *Journal of Climate*, 18(9).

Groisman, P. Y., Knight, R. W., and Karl, T. R. (2001). "Heavy precipitation and high streamflow in the contiguous United States: Trends in the twentieth century." *Bulletin of the American Meteorological Society*, 82(2), 219–246.

Grossi, P., Solutions, R. M., and Kunreuther, H. (2005). "Catastrophe Modeling: A New Approach to Managing Risk.” *Springer Science, Business Media Inc., New York,* 25(March).

Groves, D. G., and Lempert, R. J. (2007). “A new analytic method for finding policy-relevant scenarios.” *Global Environmental Change*, 17(1), 73–85.

Groves, D., Knopman, D., Berg, N., Bond, C., Syme, J., and Lempert, R. (2018). “Adapting Land Use and Water Management Plans to a Changing Climate in Miami-Dade and Broward Counties, Florida.” *Santa Monica, CA: RAND Corporation, 2018.*

Haasnoot, M., Kwakkel, J. H., Walker, W. E., and ter Maat, J. (2013). “Dynamic adaptive policy pathways: A method for crafting robust decisions for a deeply uncertain world.” *Global Environmental Change*, Elsevier Ltd, 23(2), 485–498.

Hague, B. S., McGregor, S., Murphy, B. F., Reef, R., and Jones, D. A. (2020). “Sea-Level Rise Driving Increasingly Predictable Coastal Inundation in Sydney, Australia.” *Earth’s Future*, 0–3.

Hague, B. S., Murphy, B. F., Jones, D. A., and Taylor, A. J. (2019). “Developing impact-based thresholds for coastal inundation from tide gauge observations.” *Journal of Southern Hemisphere Earth Systems Science*, 69(1), 252.

Haigh, I. D., Wahl, T., Rohling, E. J., Price, R. M., Pattiaratchi, C. B., Calafat, F. M., and Dangendorf, S. (2014). “Timescales for detecting a significant acceleration in sea level rise.” *Nature Communications*, 5, 1–11.

Hall, J. A., Gille, S., Obeysekera, J., Sweet, W., Knuuti, K., and Marburger, J. (2016). “Regional Sea Level Scenarios for Coastal Risk Management: Managing the Uncertainty of Future Sea Level Change and Extreme Water Levels for Department of Defense Coastal Sites

Worldwide.” (April), 224pp.

Hallegatte, S., Green, C., Nicholls, R. J., and Corfee-Morlot, J. (2013). “Future flood losses in major coastal cities.” *Nature Climate Change*, 3.

Hallegatte, S., Ranger, N., Mestre, O., Dumas, P., Corfee-Morlot, J., Herweijer, C., and Wood, R. M. (2011). “Assessing climate change impacts, sea level rise and storm surge risk in port cities: A case study on Copenhagen.” *Climatic Change*, 104(1), 113–137.

Hallegatte, S., Shah, A., Lempert, R., Brown, C., and Gill, S. (2012). “Investment Decision Making Under Deep Uncertainty Application to Climate Change.” *The World Bank.*

Hanson, S., Nicholls, R., Ranger, N., Hallegatte, S., Corfee-Morlot, J., Herweijer, C., and Chateau, J. (2011). “A global ranking of port cities with high exposure to climate extremes.” *Climatic Change*, 104(1), 89–111.

Heidari, H., Arabi, M., Ghanbari, M., and Warziniack, T. (2020a). “A Probabilistic Approach for Characterization of Sub-Annual Socioeconomic Drought Intensity- Duration-Frequency (IDF) Relationships in a Changing Environment.” *Water (Switzerland)*, 12(5).

Heidari, H., Arabi, M., Warziniack, T., and and Shih-Chieh Kao. (2020b). “Assessing Shifts in Regional Hydroclimatic Conditions of U.S. River Basins in Response to Climate Change over the 21st Century.” *Earth’s Future*, 8(10).

Hemmati, M., Ellingwood, B. R., and Mahmoud, H. N. (2020). “The Role of Urban Growth in Resilience of Communities Under Flood Risk.” *Earth’s Future*, 8(3).

Herweijer, C., Nicholls, R. J., Hanson, S., Patmore, N., Hallegatte, S., Corfee-Morlot, J., Chateau, J., and Muir-Wood, R. (2008). “How do our coastal cities fare under rising flood risk?”

Catastrophe Risk Management, Kluwer Academic-Plenum-Human Sciences Press.

Hinkel, J., Lincke, D., Vafeidis, A. T., Perrette, M., Nicholls, R. J., Tol, R. S. J., Marzeion, B., Fettweis, X., Ionescu, C., and Levermann, A. (2014). “Coastal flood damage and adaptation costs under 21st century sea-level rise.” *Proceedings of the National Academy of Sciences*, 111(9), 3292–3297.

Hinkel, J., van Vuuren, D. P., Nicholls, R. J., and Klein, R. J. T. (2013). “The effects of adaptation and mitigation on coastal flood impacts during the 21st century. An application of the DIVA and IMAGE models.” *Climatic Change*, 117(4), 783–794.

Hino, M., Belanger, S. T., Field, C. B., Davies, A. R., and Mach, K. J. (2019). “High-tide flooding disrupts local economic activity.” *Science Advances*, 5(2), eaau2736.

Horton, R., Little, C., Gornitz, V., Bader, D., and Oppenheimer, M. (2015). “New york city panel on climate change 2015 report chapter 2: Sea level rise and coastal storms.” *Annals of the New York Academy of Sciences*, 1336(1), 36–44.

Howat, I. M., Joughin, I., and Scambos, T. A. (2007). “Rapid Changes in Ice Discharge from.” *Science*, 315(5818), 1559–1561.

Hu, M., Zhang, X., Li, Y., Yang, H., and Tanaka, K. (2019). “Flood mitigation performance of low impact development technologies under different storms for retrofitting an urbanized area.” *Journal of Cleaner Production*, 222, 373–380.

Hunter, J. (2012). “A simple technique for estimating an allowance for uncertain sea-level rise.” *Climatic Change*, 113(2), 239–252.

Hunter, J. R., Church, J. A., White, N. J., and Zhang, X. (2013). “Towards a global regionally varying allowance for sea-level rise." *Ocean Engineering*, Elsevier, 71, 17–27.

IPCC. (2014). "Climate Change 2014: Synthesis Report." *Contribution of Working Groups I, II and III to the Fifth Assessment Report of the Intergovernmental Panel on Climate Change. In: Core Writing Team, Pachauri RK, Meyer LA (eds) IPCC, Geneva, Switzerland, 151 p.*, 1–112.

Jacobs, J. M., Cattaneo, L. R., Sweet, W., and Mansfield, T. (2018). "Recent and Future Outlooks for Nuisance Flooding Impacts on Roadways on the US East Coast." *Transportation Research Record*.

Jayasooriya, V. M., and Ng, A. W. M. (2014). "Tools for modeling of stormwater management and economics of green infrastructure practices: A review." *Water, Air, and Soil Pollution*, 225(8).

Jha, A. K., Bloch, R., and Lamond, J. (2012). *A Guide to Integrated Urban Flood Risk Management for the 21st Century*.

Jiang, C., Xiong, L., Xu, C. Y., and Guo, S. (2015). "Bivariate frequency analysis of nonstationary low-flow series based on the time-varying copula." *Hydrological Processes*, 29(6), 1521–1534.

Jonkman, S. N., Vrijling, J. K., and Vrouwenvelder, A. C. W. M. (2008). "Methods for the estimation of loss of life due to floods: a literature review and a proposal for a new method." *Natural Hazards*, 46(3), 353–389.

Karamouz, M., Asce, F., Taheri, M., Khalili, P., and Chen, X. (2019). "Building Infrastructure Resilience in Coastal Flood Risk Management." 145(4), 1–18.

Karamouz, M., Zahmatkesh, Z., Goharian, E., and Nazif, S. (2015). “Combined impact of inland and coastal floods: Mapping knowledge base for development of planning strategies.” *Journal of Water Resources Planning and Management*, 141(8), 1–16.

Kemp, A. C., Hill, T. D., Vane, C. H., Cahill, N., Orton, P. M., Talke, S. A., Parnell, A. C., Sanborn, K., and Hartig, E. K. (2017). “Relative sea-level trends in New York City during the past 1500 years.” *Holocene*, 27(8), 1169–1186.

Kemp, A. C., and Horton, B. P. (2013). “Contribution of relative sea-level rise to historical hurricane flooding in New York City.” *Journal of Quaternary Science*, 28(6), 537–541.

Kew, S. F., Selten, F. M., Lenderink, G., and Hazeleger, W. (2013). “The simultaneous occurrence of surge and discharge extremes for the Rhine delta.” *Natural Hazards and Earth System Sciences*, 13(8), 2017–2029.

Khanal, S., Ridder, N., de Vries, H., Terink, W., and van den Hurk, B. (2019). “Storm Surge and Extreme River Discharge: A Compound Event Analysis Using Ensemble Impact Modeling.” *Frontiers in Earth Science*, 7(September), 1–15.

Klima, K., Lin, N., Emanuel, K., Morgan, M. G., and Grossmann, I. (2012). “Hurricane modification and adaptation in Miami-Dade County, Florida.” *Environmental Science and Technology*, 46(2), 636–642.

Knighton, J., Steinschneider, S., and Walter, M. T. (2017). “A Vulnerability-Based, Bottom-up Assessment of Future Riverine Flood Risk Using a Modified Peaks-Over-Threshold Approach and a Physically Based Hydrologic Model.” *Water Resources Research*, 53(12), 10043–10064.

Koenker, R., and Hallock, K. F. (2001). “Quantile Regression.” *Journal of Economic Perspectives*, 15(4), 143–156.

Konikow, L. F. (2011). “Contribution of global groundwater depletion since 1900 to sea-level rise.” *Geophysical Research Letters*, 38(17).

Kopp, R. E., Horton, R. M., Little, C. M., Mitrovica, J. X., Oppenheimer, M., Rasmussen, D. J., Strauss, B. H., and Tebaldi, C. (2014). “Probabilistic 21st and 22nd century sea-level projections at a global network of tide-gauge sites.” *Earth’s Future*, 2(8), 383–406.

Kreibich, H., and Thieken, A. H. (2009). “Coping with floods in the city of Dresden, Germany.” *Natural Hazards*, 51(3), 423–436.

Kreibich, H., Thieken, A. H., Petrow, T., Müller, M., and Merz, B. (2005). “Flood loss reduction of private households due to building precautionary measures – lessons learned from the Elbe flood in August 2002.” *Natural Hazards and Earth System Science*, 5(1), 117–126.

Kron, W. (2005). “Flood risk = hazard • values • vulnerability.” *Water International*, 30(1), 58–68.

Kruel, S. (2016). “The Impacts of Sea-Level Rise on Tidal Flooding in Boston, Massachusetts.” *Journal of Coastal Research*, 322(6), 1302–1309.

Kulp, S., and Strauss, B. H. (2017). “Rapid escalation of coastal flood exposure in US municipalities from sea level rise.” *Climatic Change*, Climatic Change, 142(3–4), 477–489.

Kwadijk, J. C. J., Haasnoot, M., Mulder, J. P. M., Hoogvliet, M. M. C., Jeuken, A. B. M., van der Krogt, R. A. A., van Oostrom, N. G. C., Schelfhout, H. A., van Velzen, E. H., van Waveren, H., and de Wit, M. J. M. (2010). “Using adaptation tipping points to prepare for climate change and sea level rise: A case study in the Netherlands." *Wiley Interdisciplinary Reviews: Climate Change*, 1(5), 729–740.

Kwakkel, J. H., Haasnoot, M., and Walker, W. E. (2015). "Developing dynamic adaptive policy pathways: a computer-assisted approach for developing adaptive strategies for a deeply uncertain world." *Climatic Change*, 132(3), 373–386.

Kyselý, J., Picek, J., and Beranová, R. (2010). "Estimating extremes in climate change simulations using the peaks-over-threshold method with a non-stationary threshold." *Global and Planetary Change*, 72(1–2), 55–68.

Lempert, R. J., Groves, D. G., Popper, S. W., and Bankes, S. C. (2006). "A General, Analytic Method for Generating Robust Strategies and Narrative Scenarios." *Management Science*, 52(4), 514–528.

Li, C., Peng, C., Chiang, P. C., Cai, Y., Wang, X., and Yang, Z. (2019). "Mechanisms and applications of green infrastructure practices for stormwater control: A review." *Journal of Hydrology*, Elsevier, 568(November 2018), 626–637.

Li, H. (2015). "Green Infrastructure for Highway Stormwater Management: Field Investigation for Future Design, Maintenance, and Management Needs." *Journal of Infrastructure Systems*, 21(4), 05015001.

Lian, J. J., Xu, K., and Ma, C. (2013). "Joint impact of rainfall and tidal level on flood risk in a coastal city with a complex river network: A case study of Fuzhou City, China." *Hydrology and Earth System Sciences*, 17(2), 679–689.

Lin, N., Emanuel, K., Oppenheimer, M., and Vanmarcke, E. (2012). "Physically based assessment of hurricane surge threat under climate change." *Nature Climate Change*, Nature Publishing Group, 2(6), 462–467.

Lin, P., and Wang, N. (2017). "Stochastic post-disaster functionality recovery of community building portfolios I: Modeling." *Structural Safety*, Elsevier Ltd, 69, 96–105.

Link, L., and Galloway, G. (2019). "Ellicott City & Vulnerability to UNMITIGATED DISASTER." *The Military Engineer*, 111(722), 56–59.

Liu, C., Ikeda, K., Rasmussen, R., Barlage, M., Newman, A. J., Prein, A. F., Chen, F., Chen, L., Clark, M., Dai, A., Dudhia, J., Eidhammer, T., Gochis, D., Gutmann, E., Kurkute, S., Li, Y., Thompson, G., and Yates, D. (2017). "Continental-scale convection-permitting modeling of the current and future climate of North America." *Climate Dynamics*, Springer Berlin Heidelberg, 49(1–2), 71–95.

Lloyd, S. J., Kovats, R. S., Chalabi, Z., Brown, S., and Nicholls, R. J. (2016). "Modelling the influences of climate change-associated sea-level rise and socioeconomic development on future storm surge mortality." *Climatic Change*, 134(3), 441–455.

Lombardo, K. A., and Colle, B. A. (2010). "The spatial and temporal distribution of organized convective structures over the Northeast and their ambient conditions." *Monthly Weather Review*, 138(12), 4456–4474.

MacDonald, A., Scarrott, C. J., Lee, D., Darlow, B., Reale, M., and Russell, G. (2011). "A flexible extreme value mixture model." *Computational Statistics and Data Analysis*, Elsevier B.V., 55(6), 2137–2157.

McInnes, K. L., White, C. J., Haigh, I. D., Hemer, M. A., Hoeke, R. K., Holbrook, N. J., Kiem, A.

S., Oliver, E. C. J., Ranasinghe, R., Walsh, K. J. E., Westra, S., and Cox, R. (2016). "Natural hazards in Australia: sea level and coastal extremes." *Climatic Change*, Climatic Change, 139(1), 69–83.

McKay, L., Bondelid, T., Dewald, T., Johnston, C., Moore, R., and Rea, A. (2012). *NHD Plus Version 2 : User Guide*.

Mcleod, E., Poulter, B., Hinkel, J., Reyes, E., and Salm, R. (2010). "Sea-level rise impact models and environmental conservation: A review of models and their applications." *Ocean & Coastal Management*, Elsevier Ltd, 53(9), 507–517.

Méndez, F. J., Menéndez, M., Luceño, A., and Losada, I. J. (2006). "Estimation of the long-term variability of extreme significant wave height using a time-dependent Peak Over Threshold (POT) model." *Journal of Geophysical Research*, 111(7), 1–13.

Menéndez, M., Méndez, F. J., Losada, I. J., and Graham, N. E. (2008). "Variability of extreme wave heights in the northeast Pacific Ocean based on buoy measurements." *Geophysical Research Letters*, 35(22), 1–6.

Menéndez, M., and Woodworth, P. L. (2010). "Changes in extreme high water levels based on a quasi-global tide-gauge data set." *Journal of Geophysical Research: Oceans*, 115(10), 1–15.

Meney, K. A., and Pantelic, L. (2020). "Decentralized Water and Wastewater Systems for Resilient Societies: A Shift Towards a Green Infrastructure-Based Alternate Economy." *The Palgrave Handbook of Climate Resilient Societies*, 1–29.

Merz, B., Kreibich, H., Schwarze, R., and Thieken, A. (2010). "Review article 'assessment of economic flood damage.'" *Natural Hazards and Earth System Science*, 10(8), 1697–1724.

Ming, X., Xu, W., Li, Y., Du, J., Liu, B., and Shi, P. (2015). “Quantitative multi-hazard risk assessment with vulnerability surface and hazard joint return period.” *Stochastic Environmental Research and Risk Assessment*, 29(1), 35–44.

Moftakhari, H. R., Aghakouchak, A., Sanders, B. F., Allaire, M., and Matthew, R. A. (2018). “What Is Nuisance Flooding? Defining and Monitoring an Emerging Challenge.” *Water Resources Research*, 1–10.

Moftakhari, H. R., AghaKouchak, A., Sanders, B. F., Feldman, D. L., Sweet, W., Matthew, R. A., and Luke, A. (2015). “Increased nuisance flooding due to sea-level rise: past and future.” *Geophysical Research Letters*, 42, 9846–9852.

Moftakhari, H. R., AghaKouchak, A., Sanders, B. F., and Matthew, R. A. (2017a). “Cumulative hazard: The case of nuisance flooding.” *Earth’s Future*, 5(2), 214–223.

Moftakhari, H. R., Salvadori, G., AghaKouchak, A., Sanders, B. F., and Matthew, R. A. (2017b). “Compounding effects of sea level rise and fluvial flooding.” *Proceedings of the National Academy of Sciences*, 114(37), 9785–9790.

Moftakhari, H., Schubert, J. E., AghaKouchak, A., Matthew, R. A., and Sanders, B. F. (2019). “Linking statistical and hydrodynamic modeling for compound flood hazard assessment in tidal channels and estuaries.” *Advances in Water Resources*, Elsevier Ltd, 128(April), 28–38.

Mokrech, M., Kebede, A. S., Nicholls, R. J., Wimmer, F., and Feyen, L. (2014). “An integrated approach for assessing flood impacts due to future climate and socio-economic conditions and the scope of adaptation in Europe.” *Climatic Change*, 128(3–4), 245–260.

Mondal, A., and Mujumdar, P. P. (2016). “Detection of change in flood return levels under global warming." *Journal of Hydrologic Engineering*, 21(8), 1–12.

Moore, T. L., Gulliver, J. S., Stack, L., and Simpson, M. H. (2016). "Stormwater management and climate change: vulnerability and capacity for adaptation in urban and suburban contexts." *Climatic Change*, Climatic Change, 138(3–4), 491–504.

Mudersbach, C., and Jensen, J. (2010). "Nonstationary extreme value analysis of annual maximum water levels for designing coastal structures on the German North Sea coastline." *Journal of Flood Risk Management*, 3(1), 52–62.

Nadal, N. C., Zapata, R. E., Pagán, I., López, R., and Agudelo, J. (2010). "Building damage due to riverine and coastal floods." *Journal of Water Resources Planning and Management*, 136(3), 327–336.

"National Weather Service Manual 10-950." (2019). *Operations and Services Hydrologic Services Program, NWSPD 10-9 "Definitions and General Terminology." http://www.nws.noaa.gov/direc-tives/sym/pd01009050curr.pdf*.

Naz, B. S., Kao, S. C., Ashfaq, M., Rastogi, D., Mei, R., and Bowling, L. C. (2016). "Regional hydrologic response to climate change in the conterminous United States using high-resolution hydroclimate simulations." *Global and Planetary Change*, Elsevier B.V., 143, 100–117.

NCDC. (2016). *No Title* □□□□ □□□□□□□ □□□□□□ □□□□□□.

Nicholls, R., and Cazenave, A. (2010). "Sea-Level Rise and Its Impact on Coastal Zones." *Science*, 328(August).

Nicholls, R. J., and Tol, R. S. J. (2006). "Impacts and responses to sea-level rise: A global analysis of the SRES scenarios over the twenty-first century." *Philosophical Transactions of the Royal Society A: Mathematical, Physical and Engineering Sciences*, 364(1841), 1073–1095.

Nicholls, R. J., Wong, P. P., Burkett, V. R., Codignotto, J. O., Hay, J. E., McLean, R. F., Ragoonaden, S., and S. Ragoonaden and C.D. Woodroffe. (2007). "Coastal systems and low-lying areas." *Parry OFC ML, Palutikof JP, van der Linden PJ, Hanson CE (eds) Climate change:*, (20), 315–356.

Niroomandi, A., Ma, G., Ye, X., Lou, S., and Xue, P. (2018). "Extreme value analysis of wave climate in Chesapeake Bay." *Ocean Engineering*, Elsevier Ltd, 159(November 2017), 22–36.

NOAA. (2014). "National Weather Service Instruction 10-320. Surf Zone Forecast & Coastal/Lakeshore Hazard Services."

Noto, L. V., and La Loggia, G. (2009). "Use of L-moments approach for regional flood frequency analysis in Sicily, Italy." *Water Resources Management*, 23(11), 2207–2229.

NWS. (2014). *United States Flood Loss Report - Water Year 2014*.

Obeysekera, J., Park, J., Irizarry-Ortiz, M., Barnes, J., and Trimble, P. (2013). "Probabilistic Projection of Mean Sea Level and Coastal Extremes." *Journal of Waterway, Port, Coastal, and Ocean Engineering*, 139(2), 135–141.

Van Oldenborgh, G. J., Van Der Wiel, K., Sebastian, A., Singh, R., Arrighi, J., Otto, F., Haustein, K., Li, S., Vecchi, G., and Cullen, H. (2017). "Attribution of extreme rainfall from Hurricane Harvey, August 2017." *Environmental Research Letters*, 12(12).

Orton, P. M., Conticello, F. R., Cioffi, F., Hall, T. M., Georgas, N., Lall, U., Blumberg, A. F., and MacManus, K. (2020). "Flood hazard assessment from storm tides, rain and sea level rise for a tidal river estuary." *Natural Hazards*, Springer Netherlands, 102(2), 729–757.

Orton, P. M., Hall, T. M., Talke, S. A., Blumberg, A. F., Georgas, N., Vinogradov, S., and 1Davidson. (2016). "A validated tropical-extratropical flood hazard assessment for New York Harbor." *Journal of Geophysical Research: Oceans*, 121, 8904–8929.

Pawlowicz, R., Pawlowicz, R., Beardsley, R. C., Beardsley, R., Lentz, S., and Lentz, S. (2002). "Classical tidal harmonic analysis including error estimates." *in MATLAB using T TIDE. Computers & Geosciences*, 28(8), 929–937.

Peterson, T. C., Zhang, X., Brunet-India, M., and Vázquez-Aguirre, J. L. (2008). "Changes in North American extremes derived from daily weather data." *Journal of Geophysical Research Atmospheres*, 113.

Protection, N. E. (2018). *NYC GREEN INFRASTRUCTURE 2018 Annual Report*.

Pryor S. C., Howea J.A., and Kunkelb, K. E. (2009). "How spatially coherent and statistically robust are temporal changes in extreme precipitation in the contiguous USA?" *International Journal of Climatology*, 29(3), 31–45.

Purvis, M. J., Bates, P. D., and Hayes, C. M. (2008). "A probabilistic methodology to estimate future coastal flood risk due to sea level rise." *Coastal Engineering*, Elsevier B.V., 55(12), 1062–1073.

Rahmstorf, S. (2007). "A Semi-Empirical Approach to Projecting Future Sea-Level Rise." *Science*, 315(January), 368–370.

Rahmstorf, S. (2017). "Rising hazard of storm-surge flooding." *Proceedings of the National Academy of Sciences*, 114(45), 11806–11808.

Rahmstorf, S., and Coumou, D. (2011). “Increase of extreme events in a warming world.” *Proceedings of the National Academy of Sciences*, 108, 17905–17909.

Ramboll. (2017). “Cloudburst Resiliency Planning Study.” *Department of Climate Adaption and Green Infrastructure / Rambøll Water*.

Ramirez, J. A., Lichter, M., Coulthard, T. J., and Skinner, C. (2016). “Hyper-resolution mapping of regional storm surge and tide flooding: comparison of static and dynamic models.” *Natural Hazards*, Springer Netherlands, 82(1), 571–590.

Ray, R. D., and Foster, G. (2016). “Future nuisance flooding at Boston caused by astronomical tides alone.” *Earth’s Future*, 4(12), 578–587.

Read, L. K., and Vogel, R. M. (2015). “Hazard function analysis for flood planning under nonstationarity.” *Water Resources Research*.

Rosenzweig, C., Major, D. C., Demong, K., Stanton, C., Horton, R., and Stults, M. (2007). “Managing climate change risks in New York City’s water system: Assessment and adaptation planning.” *Mitigation and Adaptation Strategies for Global Change*, 12(8), 1391–1409.

Rosenzweig, C., Solecki, W. D., Blake, R., Bowman, M., Faris, C., Gornitz, V., Horton, R., Jacob, K., LeBlanc, A., Leichenko, R., Linkin, M., Major, D., O’Grady, M., Patrick, L., Sussman, E., Yohe, G., and Zimmerman, R. (2011). “Developing coastal adaptation to climate change in the New York City infrastructure-shed: Process, approach, tools, and strategies.” *Climatic Change*, 106(1), 93–127.

Roth, M., Buishand, T. A., Jongbloed, G., Klein Tank, A. M. G., and Van Zanten, J. H. (2012). “A regional peaks-over-threshold model in a nonstationary climate." *Water Resources Research*, 48(11).

Roy, A. H., Wenger, S. J., Fletcher, T. D., Walsh, C. J., Ladson, A. R., Shuster, W. D., Thurston, H. W., and Brown, R. R. (2008). "Impediments and solutions to sustainable, watershed-scale urban stormwater management: Lessons from Australia and the United States." *Environmental Management*, 42(2), 344–359.

Sadegh, M., Moftakhari, H., Gupta, H. V., Ragno, E., Mazdiyasni, O., Sanders, B., Matthew, R., and AghaKouchak, A. (2018). "Multihazard Scenarios for Analysis of Compound Extreme Events." *Geophysical Research Letters*, 45(11), 5470–5480.

Sadegh, M., Ragno1, E., and AghaKouchak, A. (2017). "Multivariate Copula Analysis Toolbox (MvCAT): Describing dependence and underlying uncertainty using a Bayesian framework." *Water Resources Research*, 53, 1–44.

Salas, J. D., and Obeysekera, J. (2014). "Revisiting the Concepts of Return Period and Risk for Nonstationary Hydrologic Extreme Events." *Journal of Hydrologic Engineering*, 19(3), 554–568.

Salas, J. D., Obeysekera, J., and Vogel, R. M. (2018). "Techniques for assessing water infrastructure for nonstationary extreme events: a review." *Hydrological Sciences Journal*, Taylor & Francis, 63(3), 325–352.

Salvadori, G., Durante, F., Michele, C. De, and Bernardi, M. (2018). "Hazard assessment under multivariate distributional change-points: Guidelines and a flood case study." *Water (Switzerland)*, 10(6), 1–15.

Salvadori, G., Durante, F., Michele, C. De, Bernardi, M., and Petrella, L. (2016a). “A multivariate copula-based framework for dealing with hazard scenarios and failure probabilities.” *Water Resources Research*, 52, 3701–3721.

Salvadori, G., Durante, F., Michele, C. De, Bernardi4, M., and Petrella5, L. (2016b). “A multivariate copula-based framework for dealing with hazard scenarios and failure probabilities.” *Water Resources Research*, 52, 3701–3721.

Salvadori, G., and De Michele, C. (2004). “Frequency analysis via copulas: Theoretical aspects and applications to hydrological events.” *Water Resources Research*, 40(12), 1–17.

Salvadori, G., De Michele, C., and Durante, F. (2011). “On the return period and design in a multivariate framework.” *Hydrology and Earth System Sciences*, 15(11), 3293–3305.

Salvadori, G., Michele, C. De, Kottegoda, N. T., and Rosso, R. (2007). *Extremes in Nature: An Approach Using Copulas (Water Science and Technology Library)*.

Salvadori, G., Tomasicchio, G. R., and D’Alessandro, F. (2014). “Practical guidelines for multivariate analysis and design in coastal and off-shore engineering.” *Coastal Engineering*, 88, 1–14.

Van de Sande, B., Lansen, J., and Hoyng, C. (2012). “Sensitivity of coastal flood risk assessments to digital elevation models.” *Water (Switzerland)*, 4(3), 568–579.

Sanders, B. F., and Grant, S. B. (2020). “Re-envisioning stormwater infrastructure for ultrahazardous flooding.” *WIREs Water*, 7(2), 1–13.

Scawthorn, C., Flores, P., Blais, N., Seligson, H., Tate, E., Chang, S., Mifflin, E., Thomas, W., Murphy, J., Jones, C., and Lawrence, M. (2006a). “HAZUS-MH Flood Loss Estimation

Methodology. I: Overview and Flood Hazard Characterization." *Natural Hazards Review*, 7(2), 60–71.

Scawthorn, C., Flores, P., Blais, N., Seligson, H., Tate, E., Chang, S., Mifflin, E., Thomas, W., Murphy, J., Jones, C., and Lawrence, M. (2006b). "HAZUS-MH Flood Loss Estimation Methodology. II. Damage and Loss Assessment." *Natural Hazards Review*, 7(2), 72–81.

Serinaldi, F. (2015). "Dismissing return periods!" *Stochastic Environmental Research and Risk Assessment*, Springer Berlin Heidelberg, 29(4), 1179–1189.

Shepard, C. C., Agostini, V. N., Gilmer, B., Allen, T., Stone, J., Brooks, W., and Beck, M. W. (2012). "Assessing future risk: Quantifying the effects of sea level rise on storm surge risk for the southern shores of Long Island, New York." *Natural Hazards*, 60(2), 727–745.

Sklar, A. (1959). "Fonctions de répartition à dimensions et leurs marges." *Publications de l'Institut Statistique de l'Université de Paris*, (8), 229–231.

Smith, B., and Rodriguez, S. (2017). "Spatial analysis of high-resolution radar rainfall and citizen-reported flash flood data in ultra-urban New York City." *Water (Switzerland)*, 9(10), 1–17.

Sokal, R. R., and Rohlf, F. J. (2001). "Biometry. 3th edn W.H. Freemanand Co., New York."

Spanger-Siegfried, E., Dahl, K., Caldas, A., Udvardy, S., Cleetus, R., Worth, P., and Hammer, N. H. (2017). *When Rising Seas Hit Home Hard Choices Ahead for Hundreds of US Coastal Communities*.

Stephens, S. A., Bell, R. G., and Lawrence, J. (2018). "Developing signals to trigger adaptation to sea-level rise." *Environmental Research Letters*, IOP Publishing, 13(10).

Sweet, W. V., Dusek, G., Obeysekera, J., and Marra, J. J. (2018). "Patterns and projections of high tide flooding along the u.s. coastline using a common impact threshold." *NOAA Tech. Rep. NOS CO-OPS 44p.*, (February).

Sweet, W. V., Kopp, R. E., Weaver, C. P., Obeyskera, J., Horton, R. M., Thieler, E. R., and Zervas, C. (2017). "Global and Regional Sea Level Rise Scenarios for the United States." *NOAA Technical Report NOS CO-OPS 083*, (January).

Sweet, W. V., and Park, J. (2014). "From the extreme to the mean: Acceleration and tipping points of coastal inundation from sea level rise." *Earth's Future*, 2(12), 579–600.

Sweet, W. V., Park, J., Marra, J., Zervas, C., and Gill, S. (2014). "Sea Level Rise and Nuisance Flood Frequency Changes around the United States." *NOAA Technical Report NOS CO-OPS 073*, (June), 58.

Tavakol-Davani, H., Burian, S. J., Devkota, J., and Apul, D. (2016). "Performance and Cost-Based Comparison of Green and Gray Infrastructure to Control Combined Sewer Overflows." *Journal of Sustainable Water in the Built Environment*, 2(2).

Tavakoly, A. A., Snow, A. D., David, C. H., Follum, M. L., Maidment, D. R., and Yang, Z. L. (2017). "Continental-Scale River Flow Modeling of the Mississippi River Basin Using High-Resolution NHDPlus Dataset." *Journal of the American Water Resources Association*, 53(2), 258–279.

Tebaldi, C., Strauss, B. H., and Zervas, C. E. (2012). "Modelling sea level rise impacts on storm surges along US coasts." *Environmental Research Letters*, 7(1).

Tompkins, F., and DeConcini, C. (2014). "Sea-Level Rise and Its Impact on Miami-Dade County." *World Resources Institute Fact Sheet*, 1–8.

Vandenberg-Rodes, A., H. R. Moftakhari, A. A., B. Shahbaba, B. F. Sanders, A., and Matthew, R. A. (2016). “Projecting nuisance flooding in a warming climate using generalized linear models and Gaussian processes.” *Journal of Geophysical Research : Oceans*, 121, 1–15.

Vogel, J. R., Moore, T. L., Coffman, R. R., Rodie, S. N., Hutchinson, S. L., McDonough, K. R., McLemore, A. J., and McMaine, J. T. (2015). “Critical Review of Technical Questions Facing Low Impact Development and Green Infrastructure: A Perspective from the Great Plains.” *Water Environment Research*, 87(9), 849–862.

Vousdoukas, M. I., Mentaschi, L., Feyen, L., and Voukouvalas, E. (2017). “Extreme sea levels on the rise along Europe’s coasts.” *Earth’s Future*, 1–20.

Wahl. (2017). “Sea-level rise and storm surges , relationship status : complicated!” *Environmental Research Letters*, 12(11), 111001.

Wahl, T., Jain, S., Bender, J., Meyers, S. D., and Luther, M. E. (2015a). “Increasing risk of compound flooding from storm surge and rainfall for major US cities.” *Nature Climate Change*, 5(12), 1093–1097.

Wahl, T., Jain, S., Bender, J., Meyers, S. D., Luther, M. E., and Perrette, M. (2015b). “S : Increasing risk of compound flooding from storm surge and rainfall for major US cities.” *Nature Climate Change*, 5(12), 1093–1097.

Walker, W. E., Haasnoot, M., and Kwakkel, J. H. (2013). “Adapt or perish: A review of planning approaches for adaptation under deep uncertainty.” *Sustainability*, 5(3), 955–979.

Walsh, J., Wuebbles, D., Hayhoe, K., and et al. (2014). “Our Changing Climate.” *Climate Change Impacts in the United States: The Third National Climate Assessment, J. M. Melillo, Terese*

(T.C.) Richmond, and G. W. Yohe, Eds., U.S. Global Change Research Program.

Ward, P. J., Couasnon, A., Eilander, D., DHaigh, I., Hendry, A., Muis, S., Veldkamp, T. I. E., Winsemius, H. C., and Wahl, T. (2018). “Dependence between high sea-level and high river discharge increases flood hazard in global deltas and estuaries.” *Environmental Research Letters*, 13(084012).

Wdowinski, S., Bray, R., Kirtman, B. P., and Wu, Z. (2016). “Increasing flooding hazard in coastal communities due to rising sea level: Case study of Miami Beach, Florida.” *Ocean and Coastal Management*, Elsevier Ltd, 126, 1–8.

Wolf, J., and Woolf, D. K. (2006). “Waves and climate change in the north-east Atlantic.” *Geophysical Research Letters*, 33(6), 2–5.

Woodworth, P. L., and Blackman, D. L. (2004). “Evidence for systematic changes in extreme high waters since the mid-1970s.” *Journal of Climate*, 17(6), 1190–1197.

Xu, H., Xu, K., Lian, J., and Ma, C. (2019). “Compound effects of rainfall and storm tides on coastal flooding risk.” *Stochastic Environmental Research and Risk Assessment*, Springer Berlin Heidelberg, 33(7), 1249–1261.

Xu, S., and Huang, W. (2008). “Frequency analysis for predicting 1% annual maximum water levels along Florida coast, US.” *Hydrological Processes*, 22, 4507–4518.

Yamamoto, Y. (2006). “Measures to Mitigate Urban Heat Islands.” *Environmental and Energy research Unit. Quaterly Review*, 18, 65–83.

Yohe, G., and Leichenko, R. (2010). “Chapter 2: Adopting a risk-based approach: Ch 2. Adopting a risk-based approach.” *Annals of the New York Academy of Sciences*, 1196(1), 29–40.

Young, R. F., and McPherson, E. G. (2013). “Governing metropolitan green infrastructure in the United States.” *Landscape and Urban Planning*, Elsevier B.V., 109(1), 67–75.

Yu, K., Lu, Z., and Stander, J. (2003). “Quantile regression: applications and current research areas.” *Journal of the Royal Statistical Society: Series D (The Statistician)*, 52(3), 331–350.

Yunus, A. P., Avtar, R., Kraines, S., Yamamuro, M., Lindberg, F., and Grimmond, C. S. B. (2016). “Uncertainties in tidally adjusted estimates of sea level rise flooding (bathtub model) for the greater London.” *Remote Sensing*, 8(5).

Zahmatkesh, Z., Burian, S. J., Karamouz, M., Tavakol-Davani, H., and Goharian, E. (2015). “Low-impact development practices to mitigate climate change effects on urban stormwater runoff: Case study of New York City.” *Journal of Irrigation and Drainage Engineering*, 141(1), 1–13.

Zandvoort, M., Campos, I. S., Vizinho, A., Penha-Lopes, G., Lorencová, E. K., van der Brugge, R., van der Vlist, M. J., van den Brink, A., and Jeuken, A. B. M. (2017). “Adaptation pathways in planning for uncertain climate change: Applications in Portugal, the Czech Republic and the Netherlands.” *Environmental Science and Policy*, 78, 18–26.

Zhang, D., Gersberg, R. M., Ng, W. J., and Tan, S. K. (2017). “Conventional and decentralized urban stormwater management: A comparison through case studies of Singapore and Berlin, Germanyfile:///C:/Users/mahshid7.ETS00803/Downloads.” *Urban Water Journal*, 14(2), 113–124.

Zheng, F., Westra, S., Leonard, M., and Sisson, S. a. (2014). “Modeling dependence between extreme rainfall and storm surge to estimate coastal flooding risk.” *Water Resources Research*, 50, 2050–2071.

Zheng, F., Westra, S., and Sisson, S. A. (2013). “Quantifying the dependence between extreme rainfall and storm surge in the coastal zone.” *Journal of Hydrology*, Elsevier B.V., 505, 172–187.

Zscheischler, J., Westra, S., Van Den Hurk, B. J. J. M., Seneviratne, S. I., Ward, P. J., Pitman, A., Aghakouchak, A., Bresch, D. N., Leonard, M., Wahl, T., and Zhang, X. (2018). “Future climate risk from compound events.” *Nature Climate Change*, Springer US, 8(6), 469–477.

APPENDIX A

SUPPORTING INFORMATION FOR CHAPTER 2: A COHERENT STATISTICAL MODEL FOR COASTAL FLOOD FREQUENCY ANALYSIS UNDER NONSTATTIONARY SEA LEVEL

Figure A1 illustrates the schematic Mixture Normal-Generalized Pareto Distribution (GPD) nonstationary model under the present and future condition (e.g., 2 ft increase in MSL). The changes in location parameter of Normal and GP distribution are express as a function of changes in mean sea level(δ). β_1 denotes the slope coefficients of the Quantile Regression model.

Figures A2 to **Figures A69** provided detailed analysis information for each station as follows:

(Panel A) Present Daily mean sea level (DMSL) calculated using linear function (blue line) fitted to the daily sea levels (i.e. Daily time series of mean of hourly observed water levels)

(Panel B) Present estimated variable threshold (red line) using Quantile Regression method. Daily maximum sea level is response variable and daily mean sea level is independent variable. Green dots presents independent excesses which are estimated using declustering Run Method and are at least 3 days apart. β_1 and β_0 denote the slope and intercept coefficients of the Quantile Regression model.

(Panel C) Present empirical cumulative distribution function (blue line) and Mixture Normal-GPD cumulative distribution function (red dashed line) along with GPD threshold (black dash-dotted line).

(Panel D) Present return level interval (x_N) curves using mixture model for current situation (pink line) and 2ft sea level rise scenario (blue line) along with the return level interval using empirical CDF (Black dots). the 95% confidence intervals for GPD component are estimated via the delta method (Coles 2001) as follows:

$$Var(_{x_N}) \approx \nabla {x_N}^T V \nabla x_N$$

$$V = \begin{bmatrix} \varphi(1-\varphi)/n & 0 & 0 \\ 0 & v_{1,1} & v_{1,2} \\ 0 & v_{2,1} & v_{2,2} \end{bmatrix}$$

$$\nabla {x_N}^T = [\alpha N^\xi \varphi^{\xi-1}, \xi^{-1}\{(N\varphi)^\xi - 1\}, -\alpha\xi^{-2}\{(N\varphi)^\xi - 1\} + \alpha\xi^{-1}(N\varphi)^\xi \log(N\varphi)]$$

where α and ξ and Φ are estimated scale and shape parameters of the GPD distribution. φ denotes the probability of independent exceedances over threshold. $v_{i,j}$ denotes the (i,j) term of the variance-covariance matrix of α and ξ. n is total number of observations (Coles 2001).

(Panel E) Present current return period versus future return period under 0.5ft (blue line), 1ft (green line) and 2ft (red line) sea level rise levels.

Table B1 presents Summary of mixture model parameters. α and ξ denote the scale and shape of the GPD distribution along with confidence interval (CI) in parentheses. φ denotes the probability of independent exceedances over threshold. μ and σ represent mean and standard deviation of the Normal distribution.

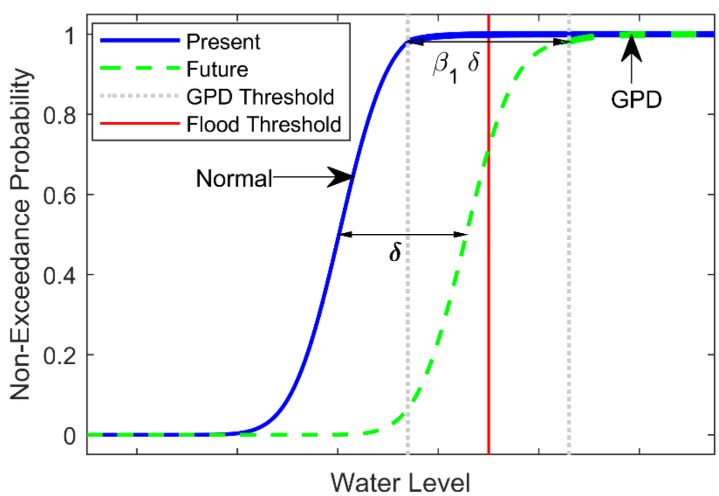

Figure A1. Schematic of the nonstationary Mixture Normal-GPD probability model

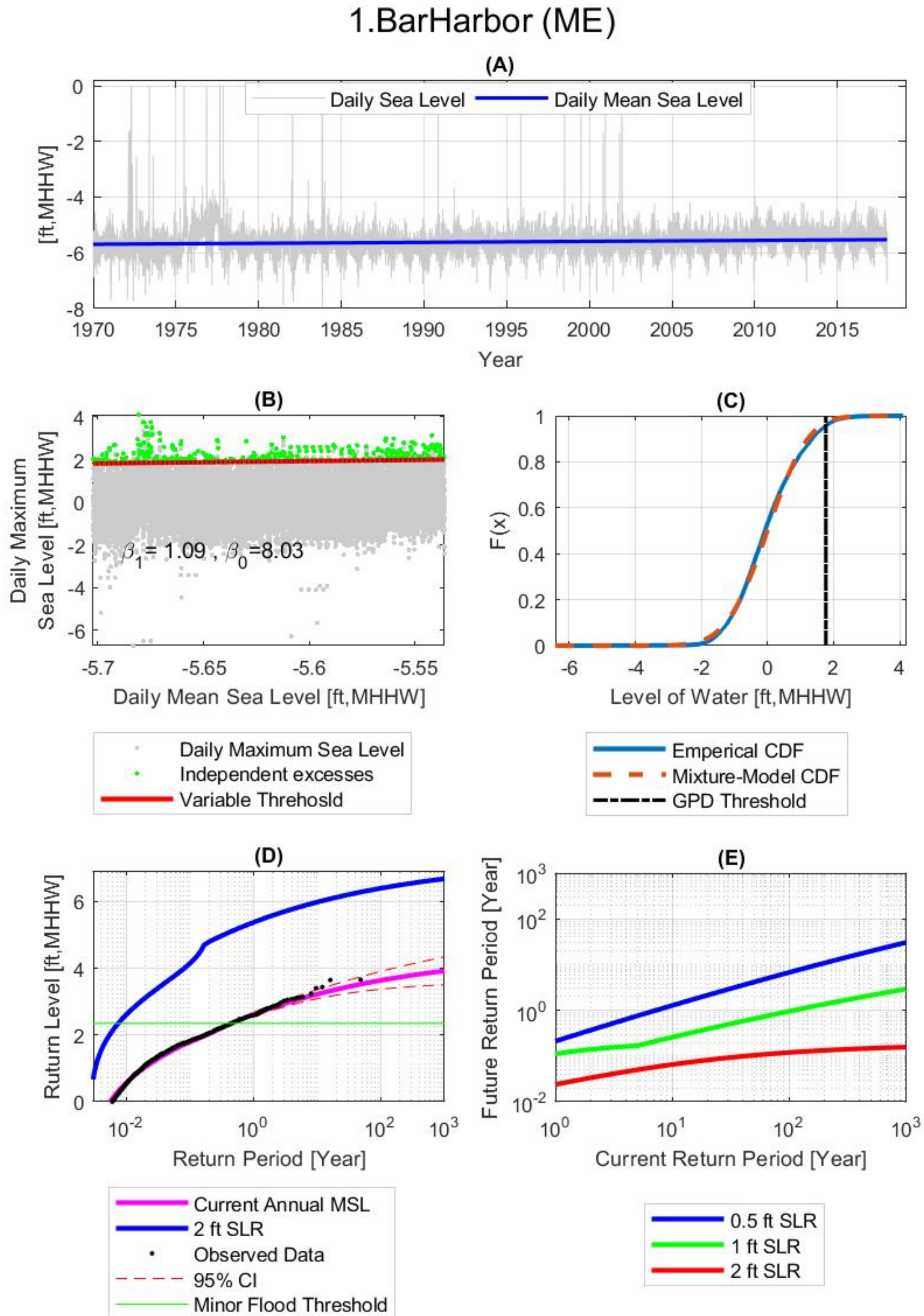

Figure A2. BarHorbor (ME) station

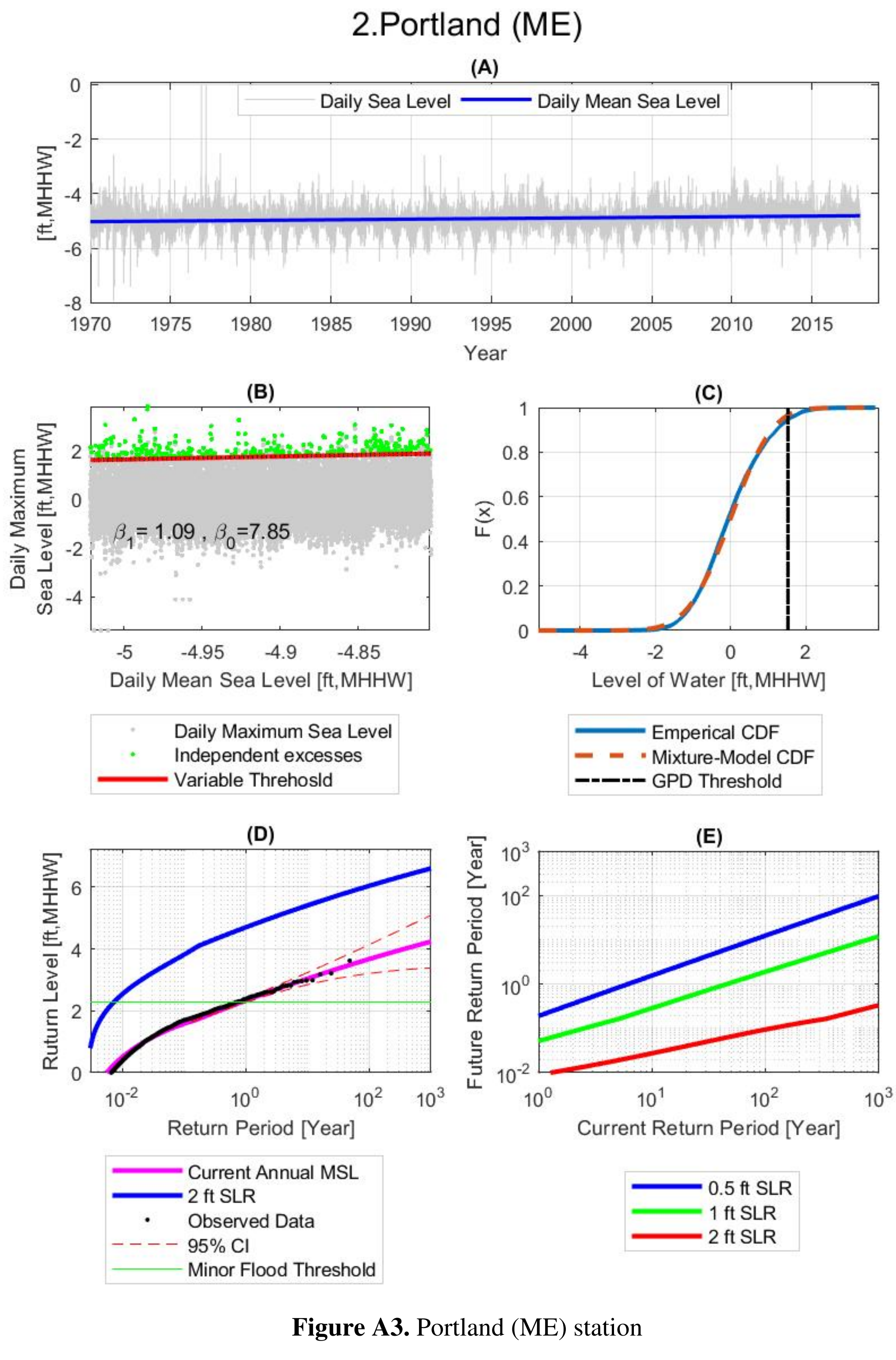

Figure A3. Portland (ME) station

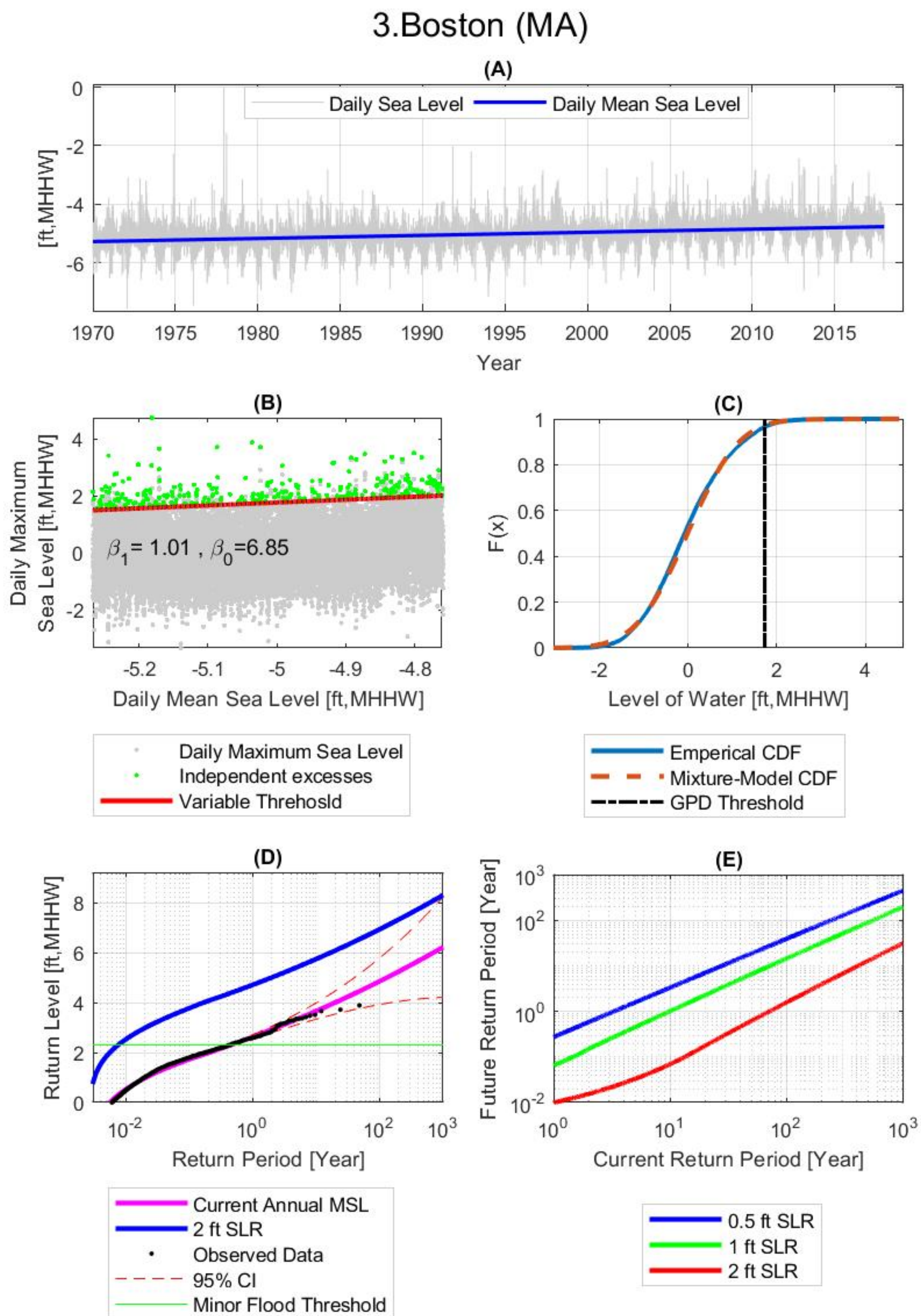

Figure A4. Boston (MA) station

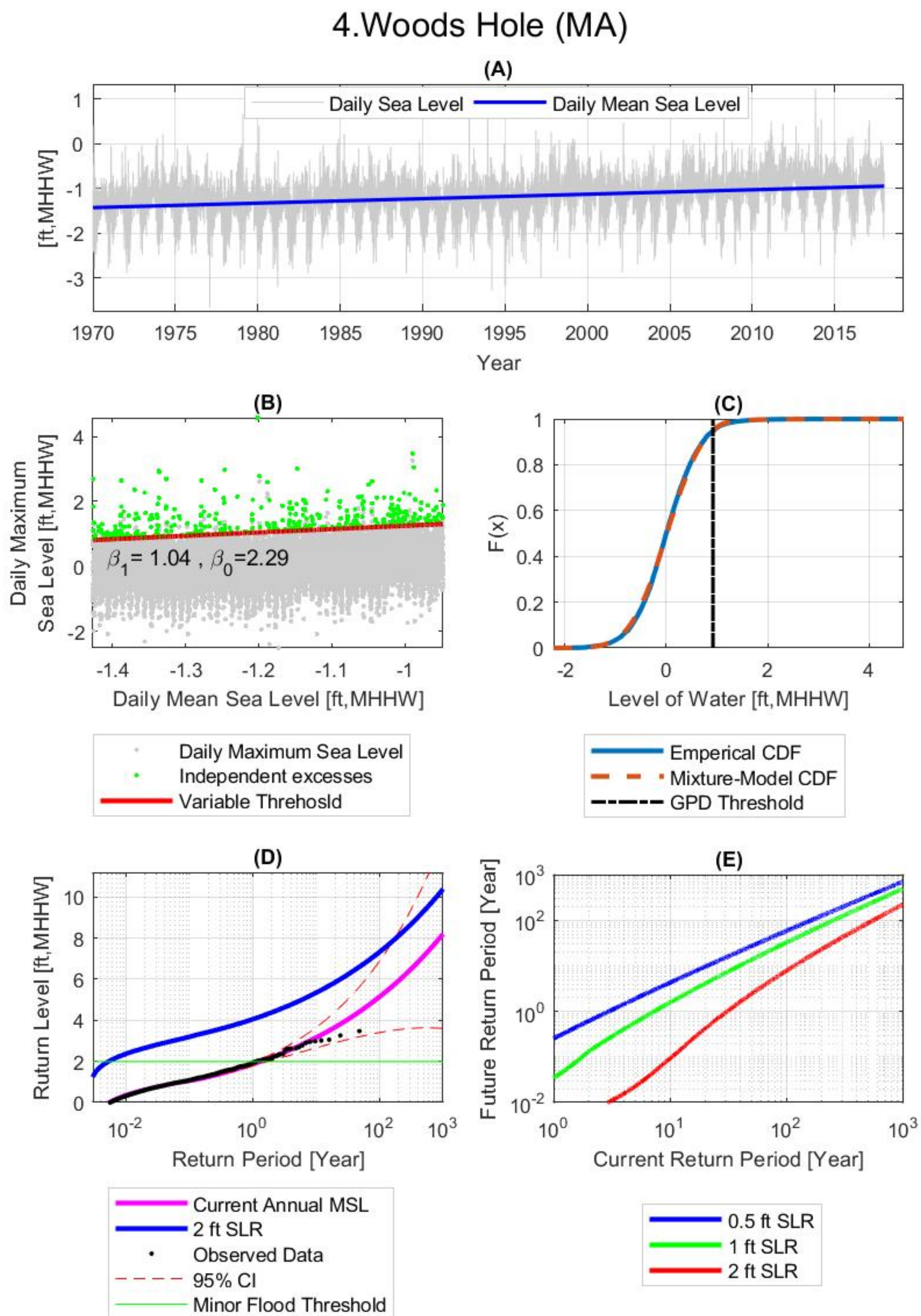

Figure A5. Woods Hole (MA) station

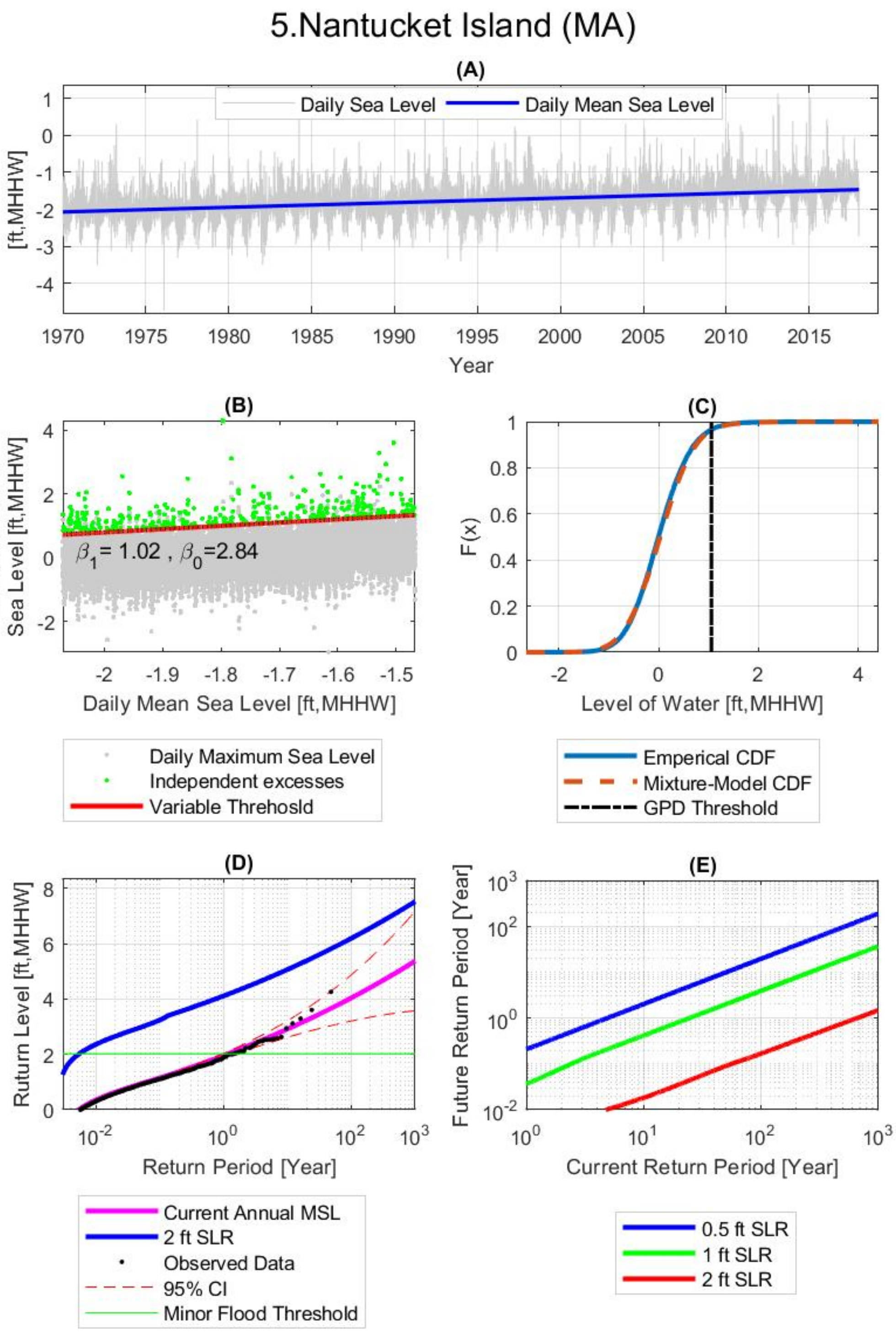

Figure A6. Nantucket Island (MA) station

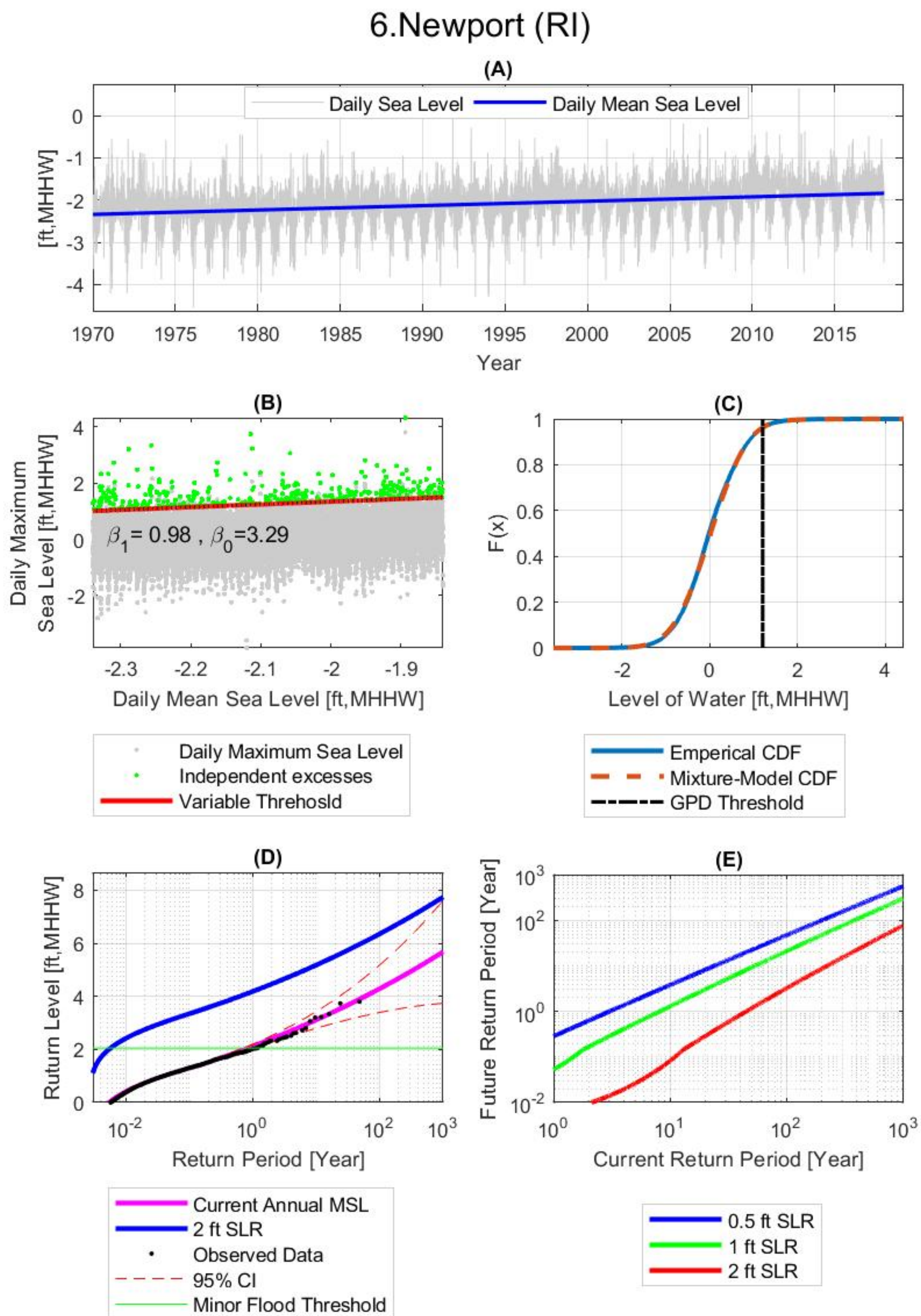

Figure A7. Newport (RI) station

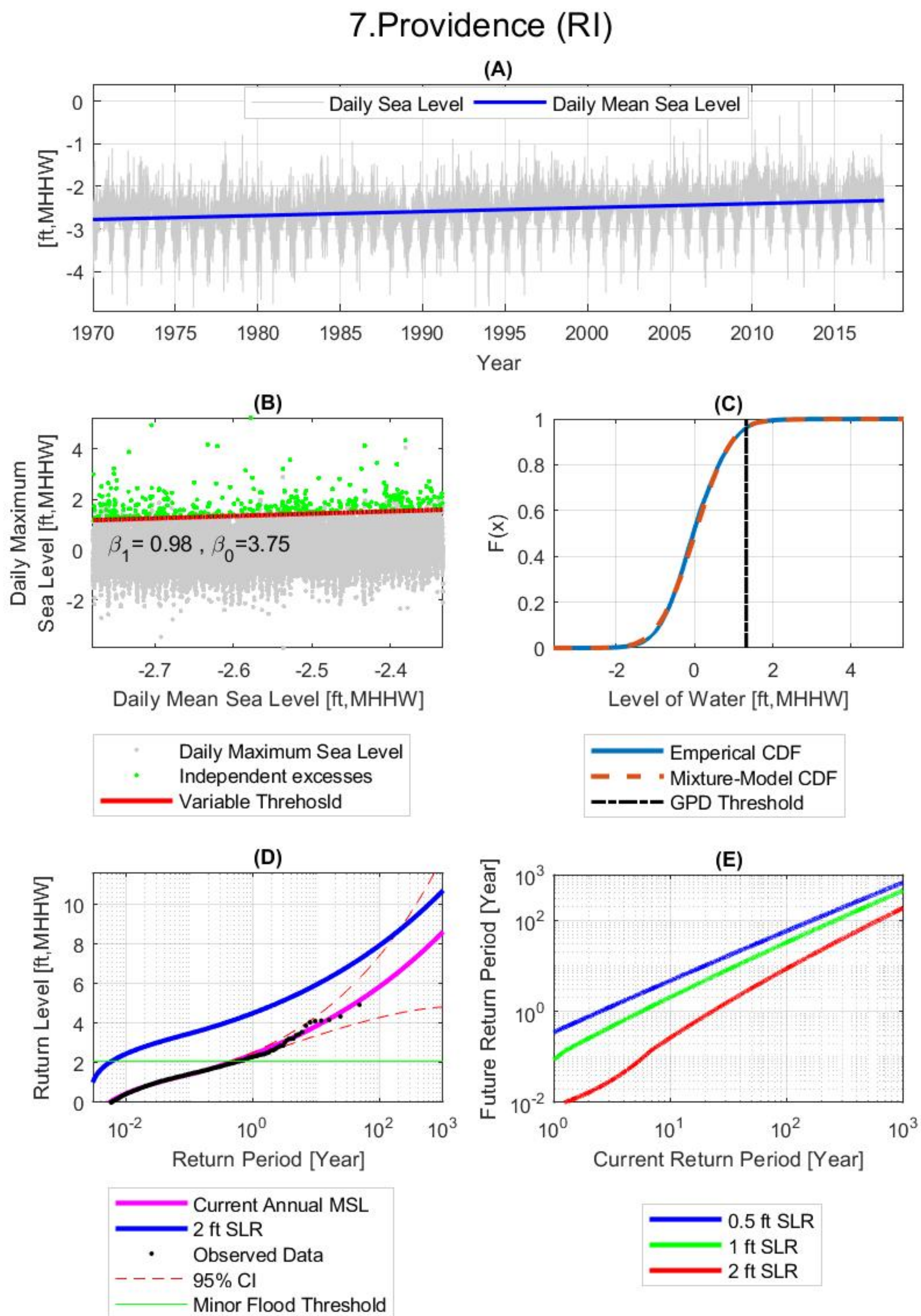

Figure A8. Providence (RI) station

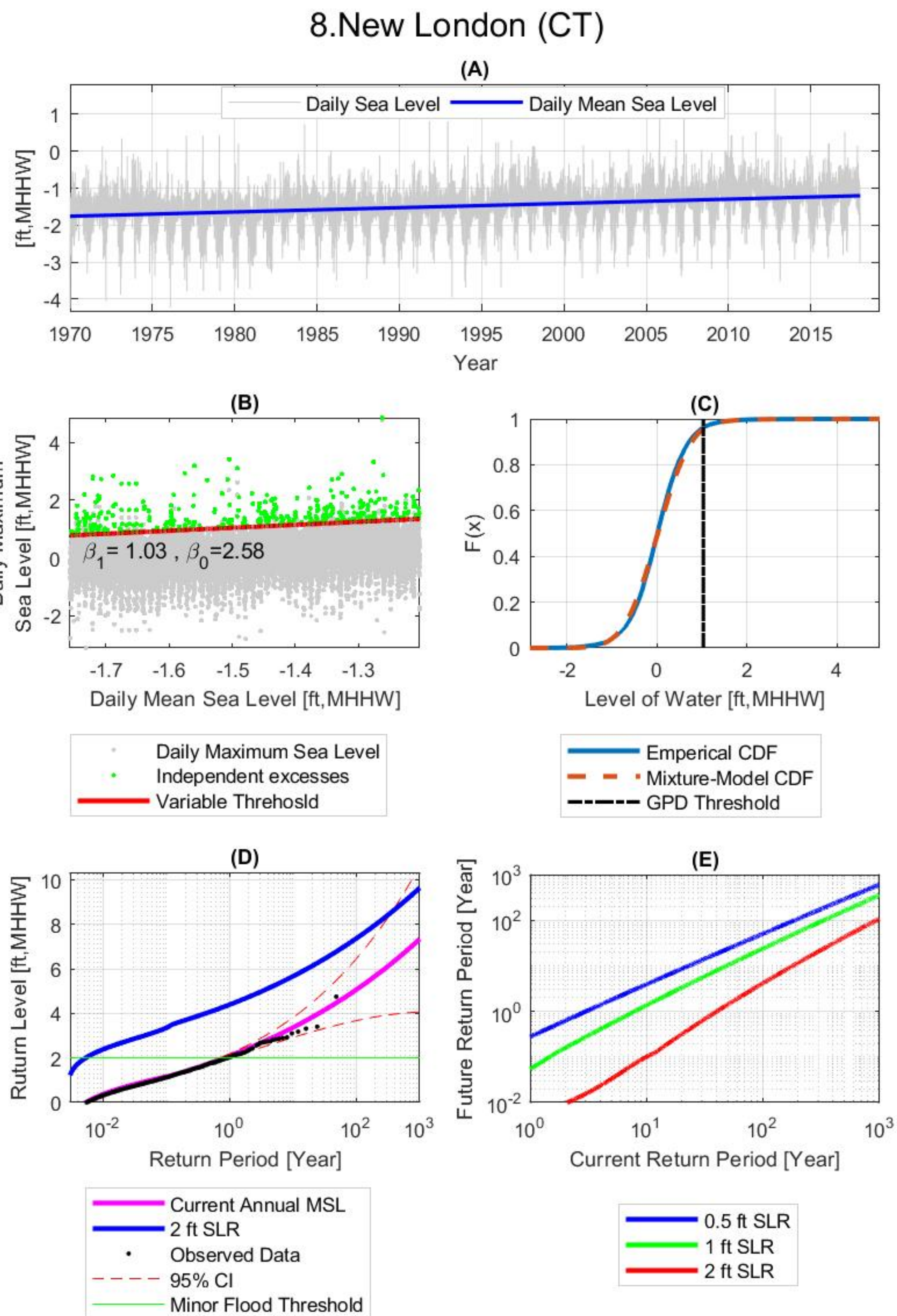

Figure A9. New London (CT) station

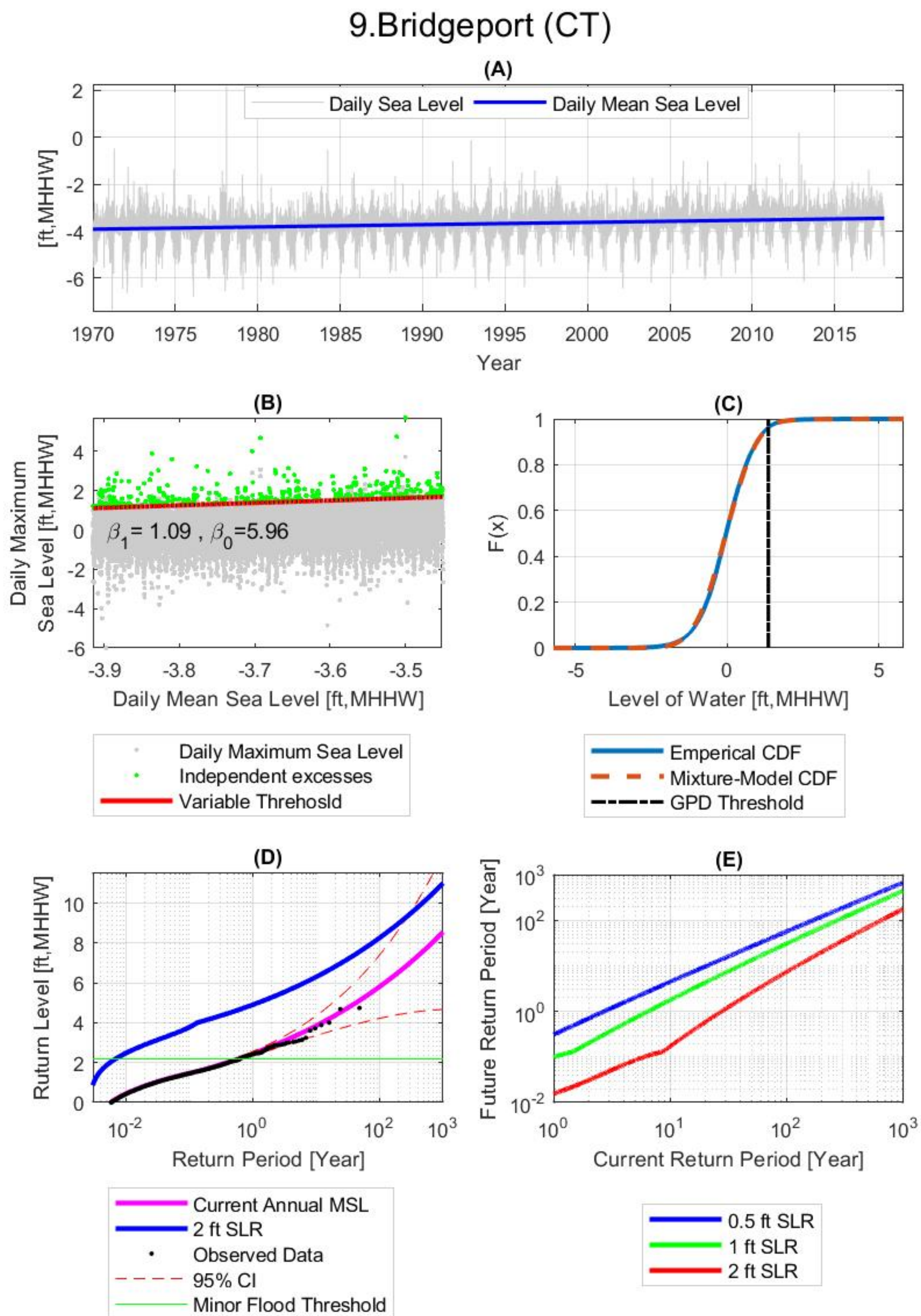

Figure A10. Bridgeport (CT) station

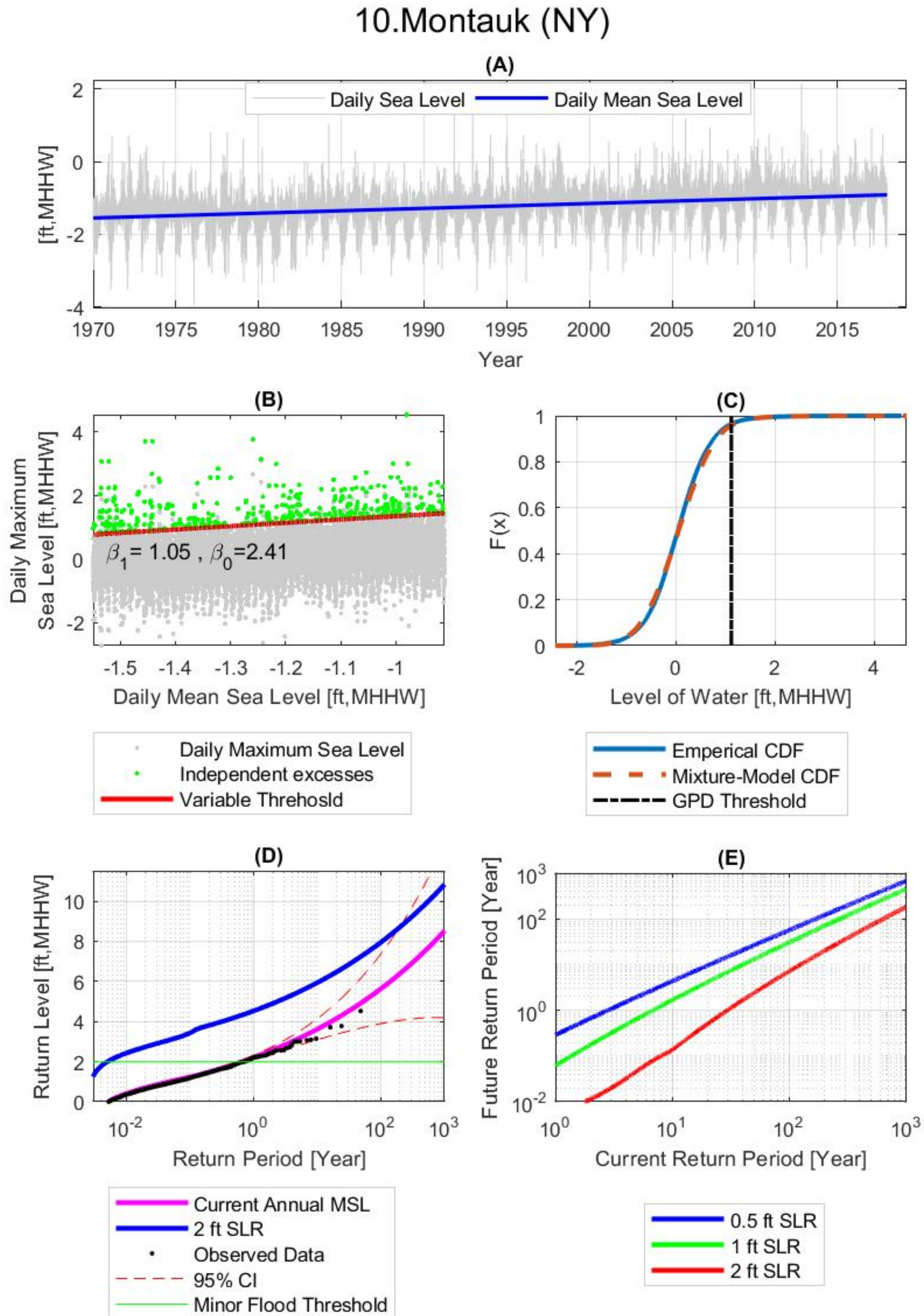

Figure A11. Montauk (NY) station

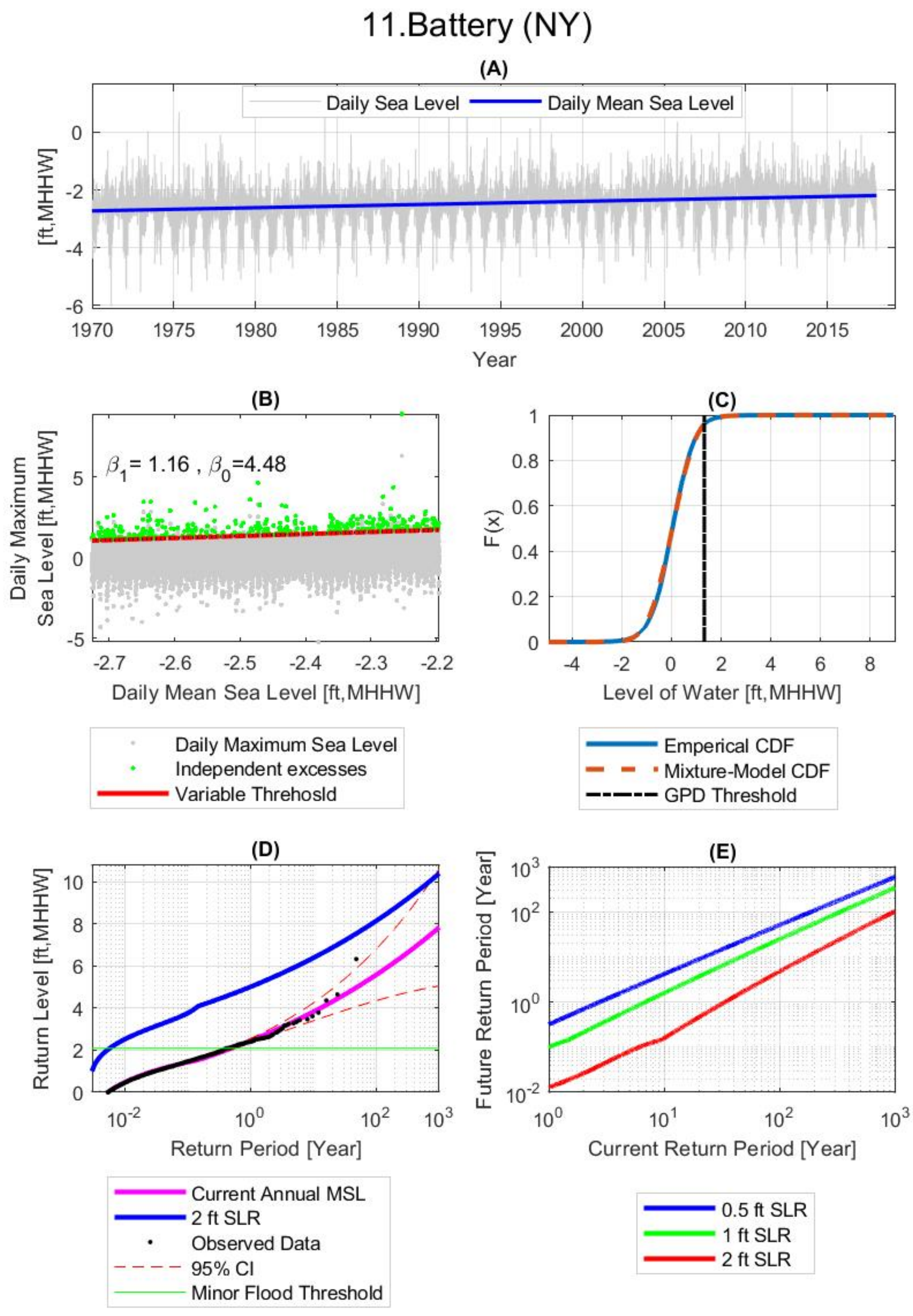

Figure A12. Battery (NY) station

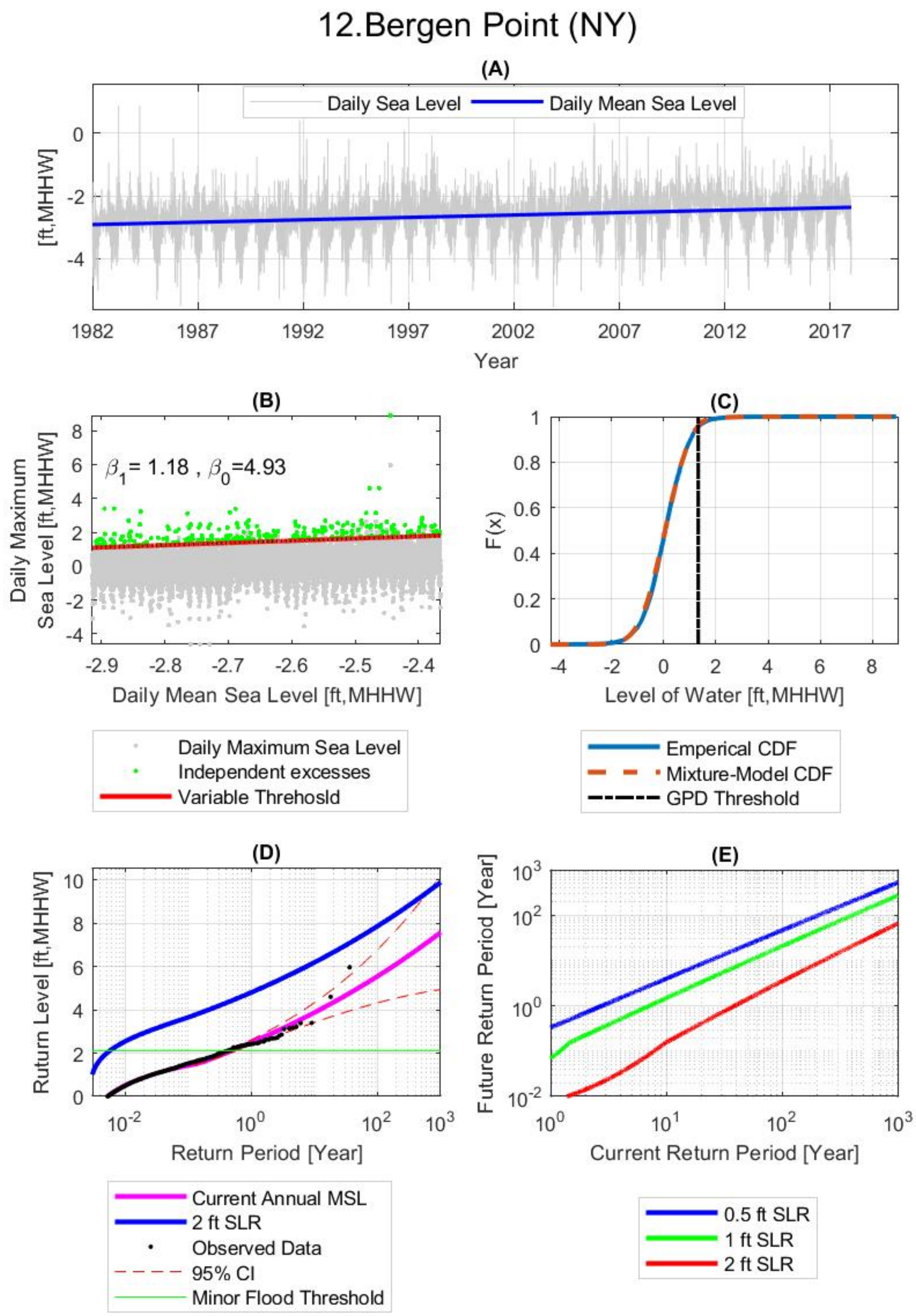

Figure A13. Bergen Point (NY) station

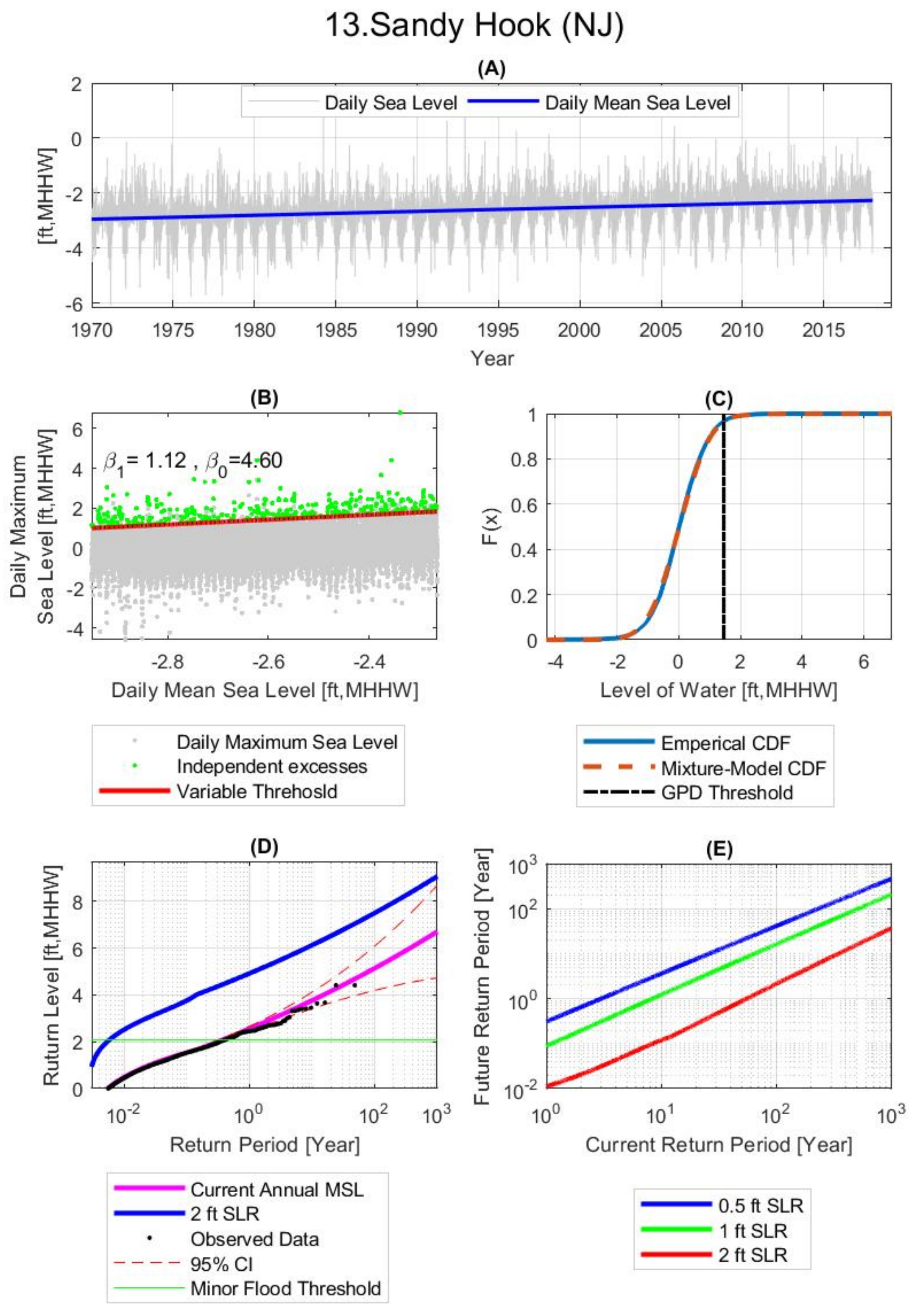

Figure A14. Sandy Hook (NJ) station

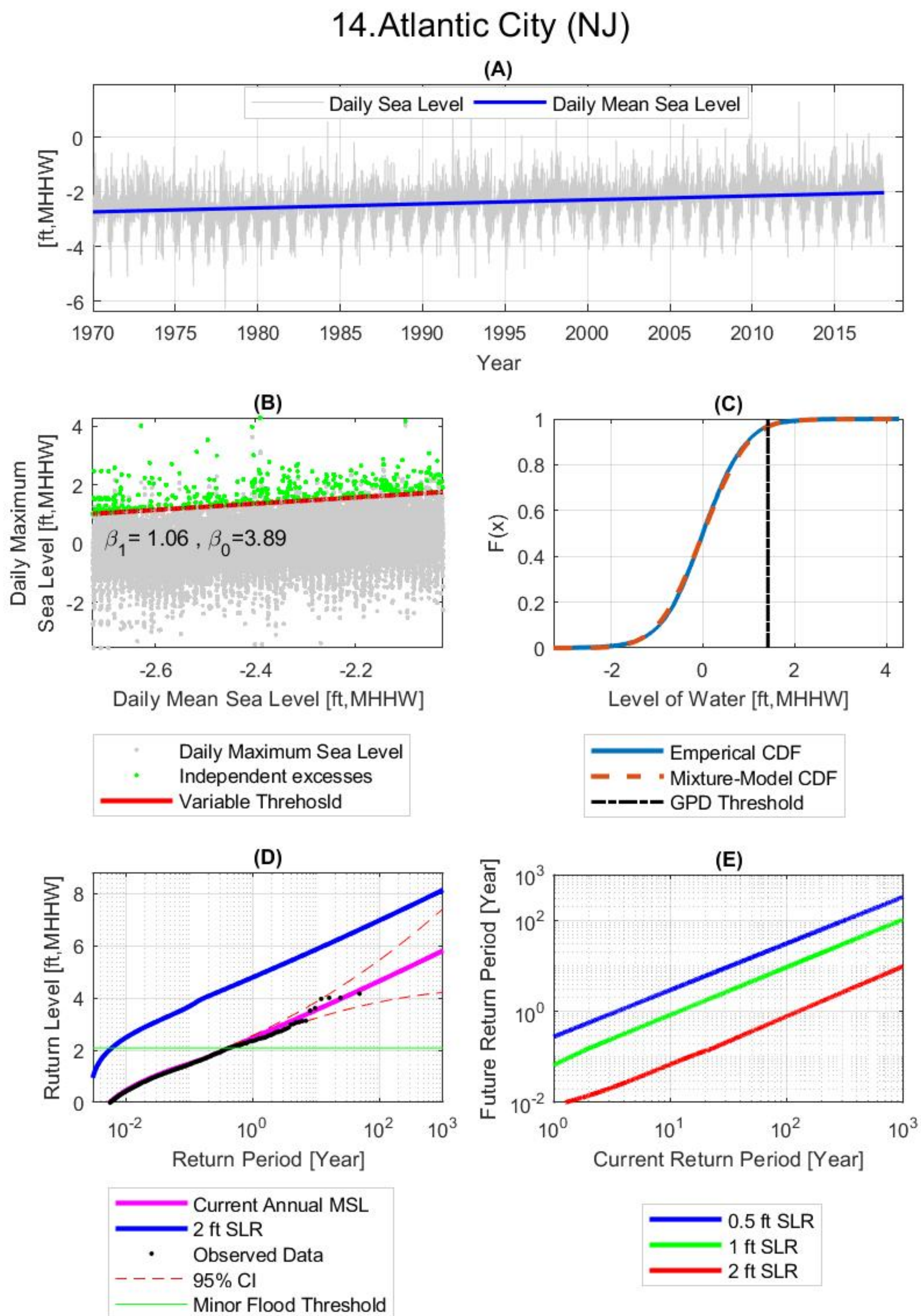

Figure A15. Atlantic City (NJ) station

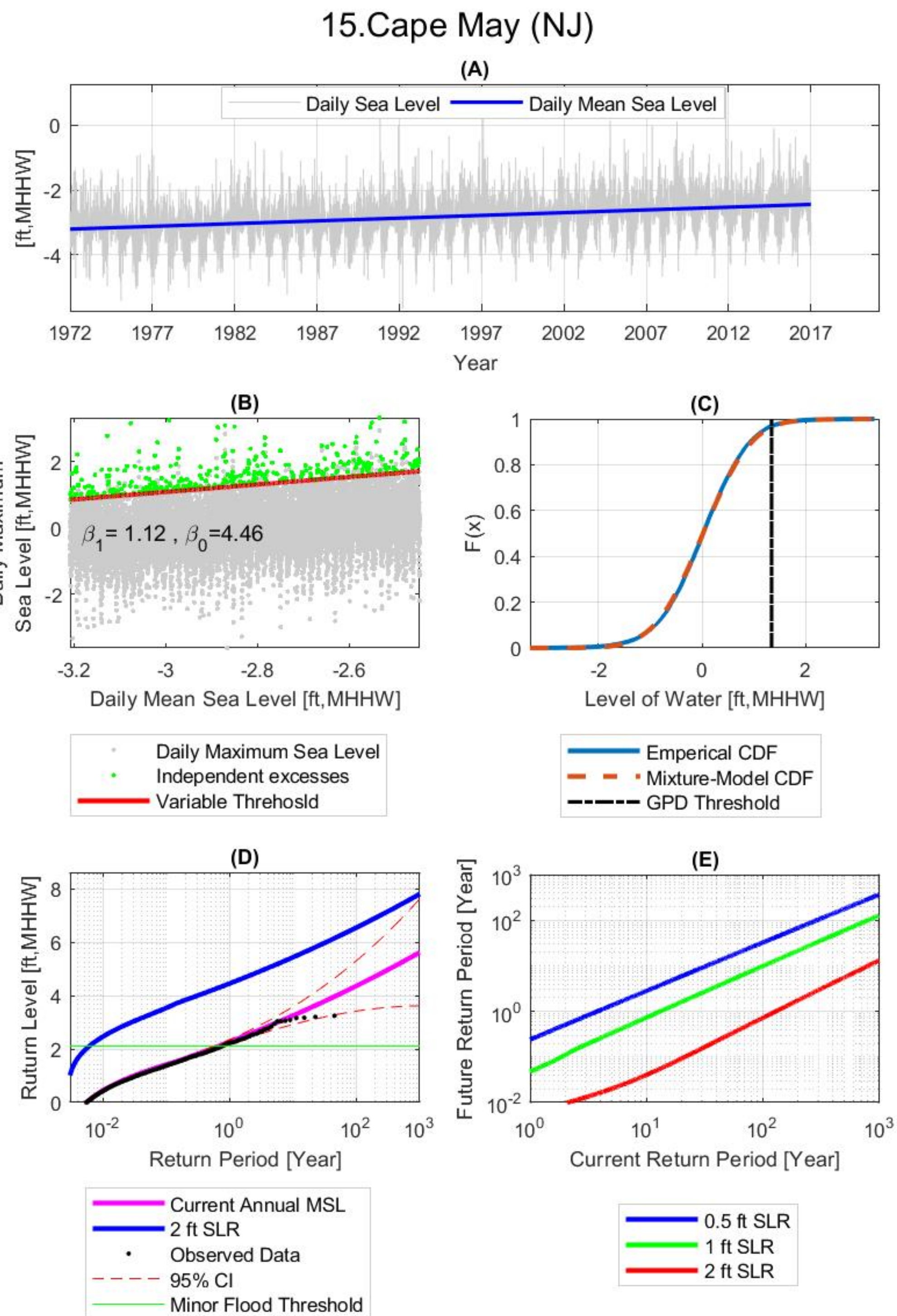

Figure A16. Cape May (NJ) station

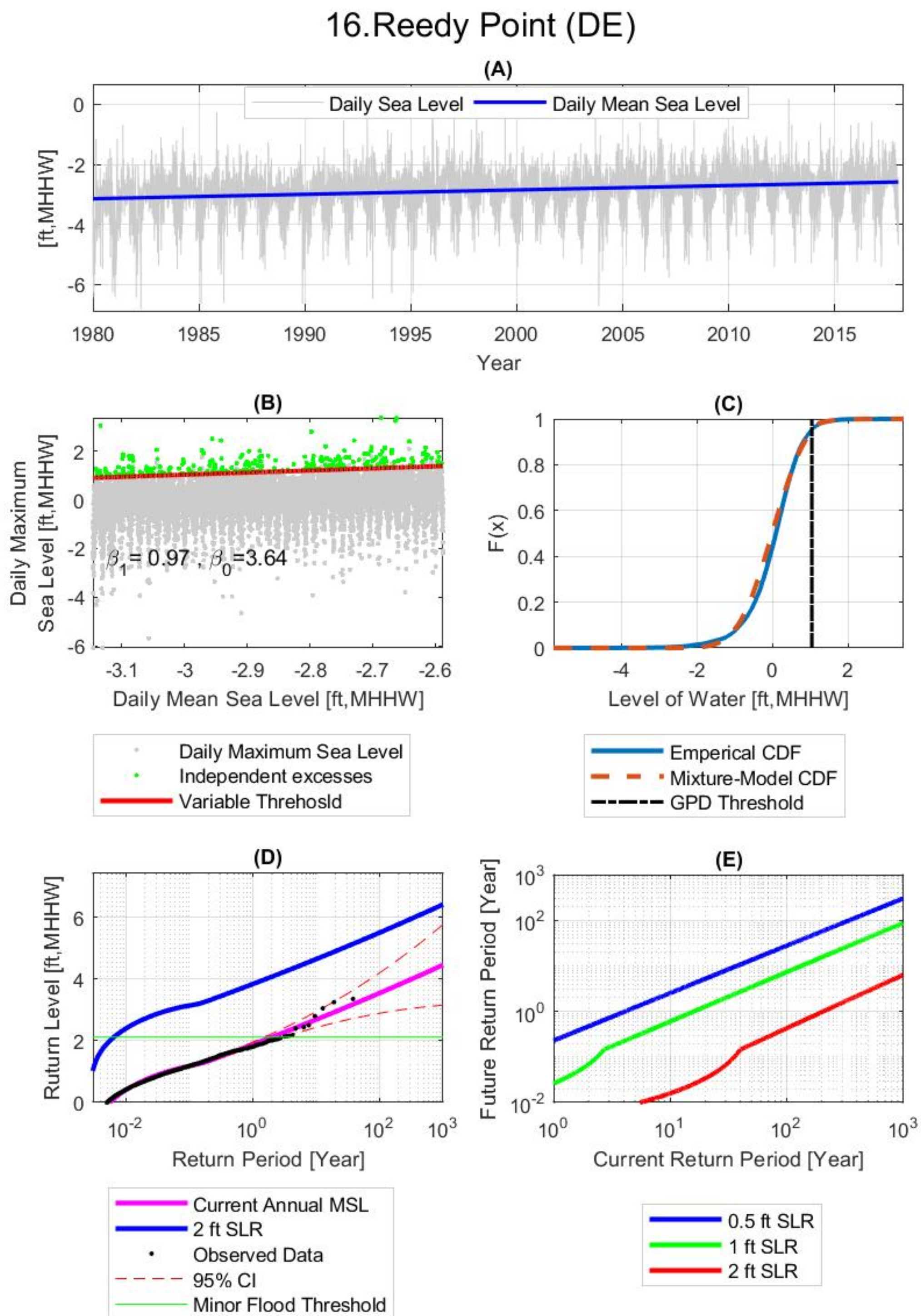

Figure A17. Reedy Point (DE) station

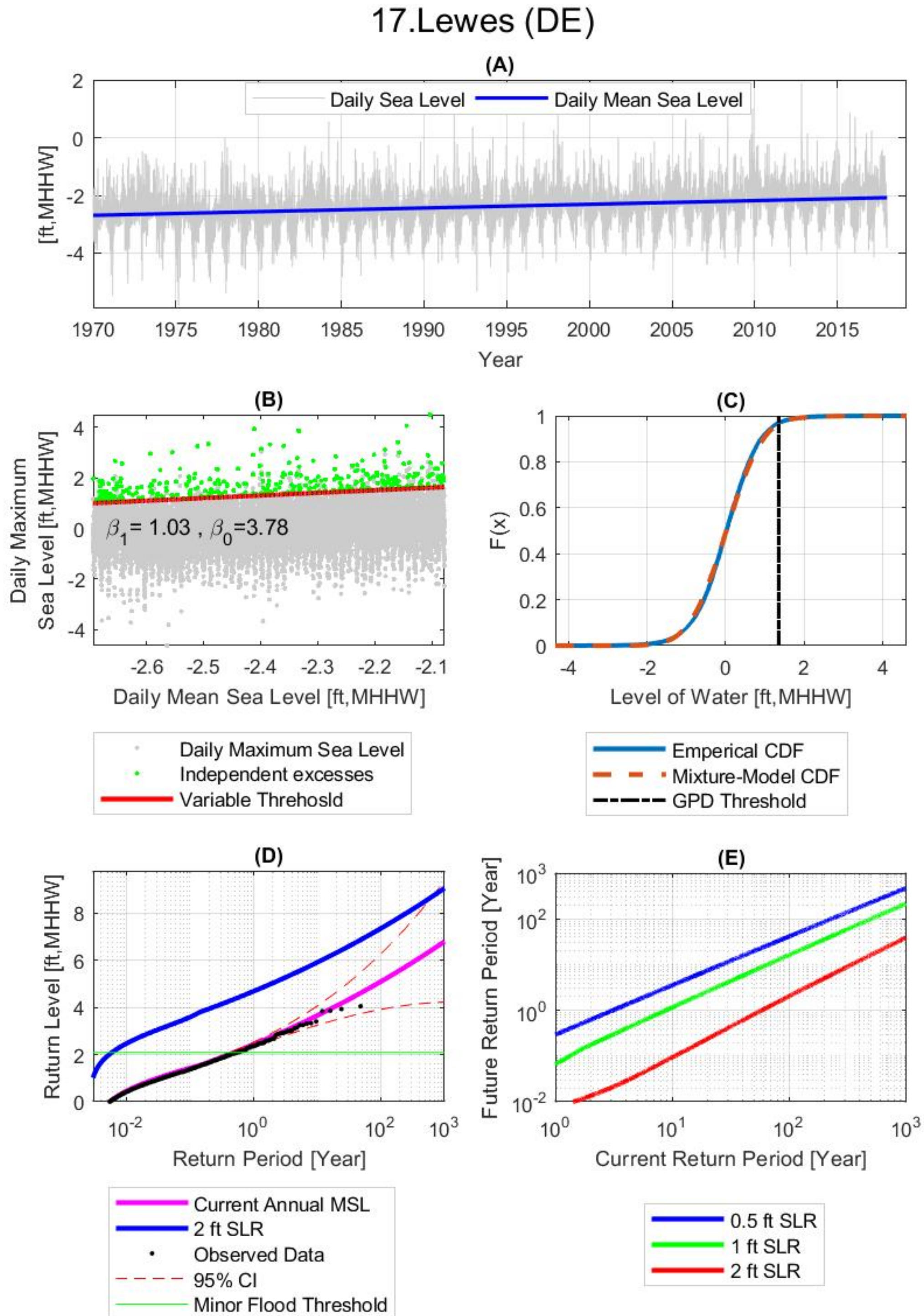

Figure A18. Lewes (DE) station

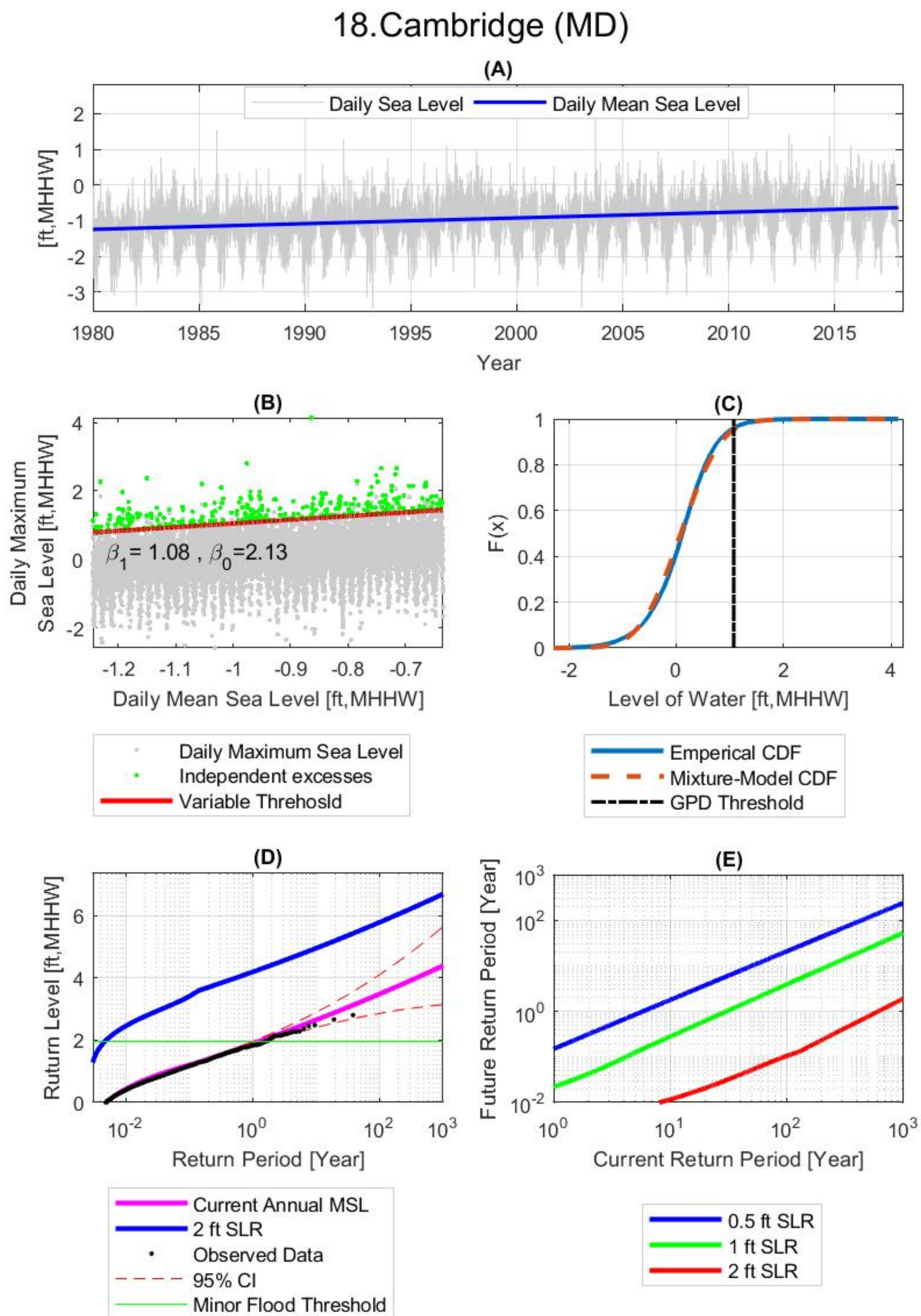

Figure A19. Cambridge (MD) station

19.Tochester Beach (MD)

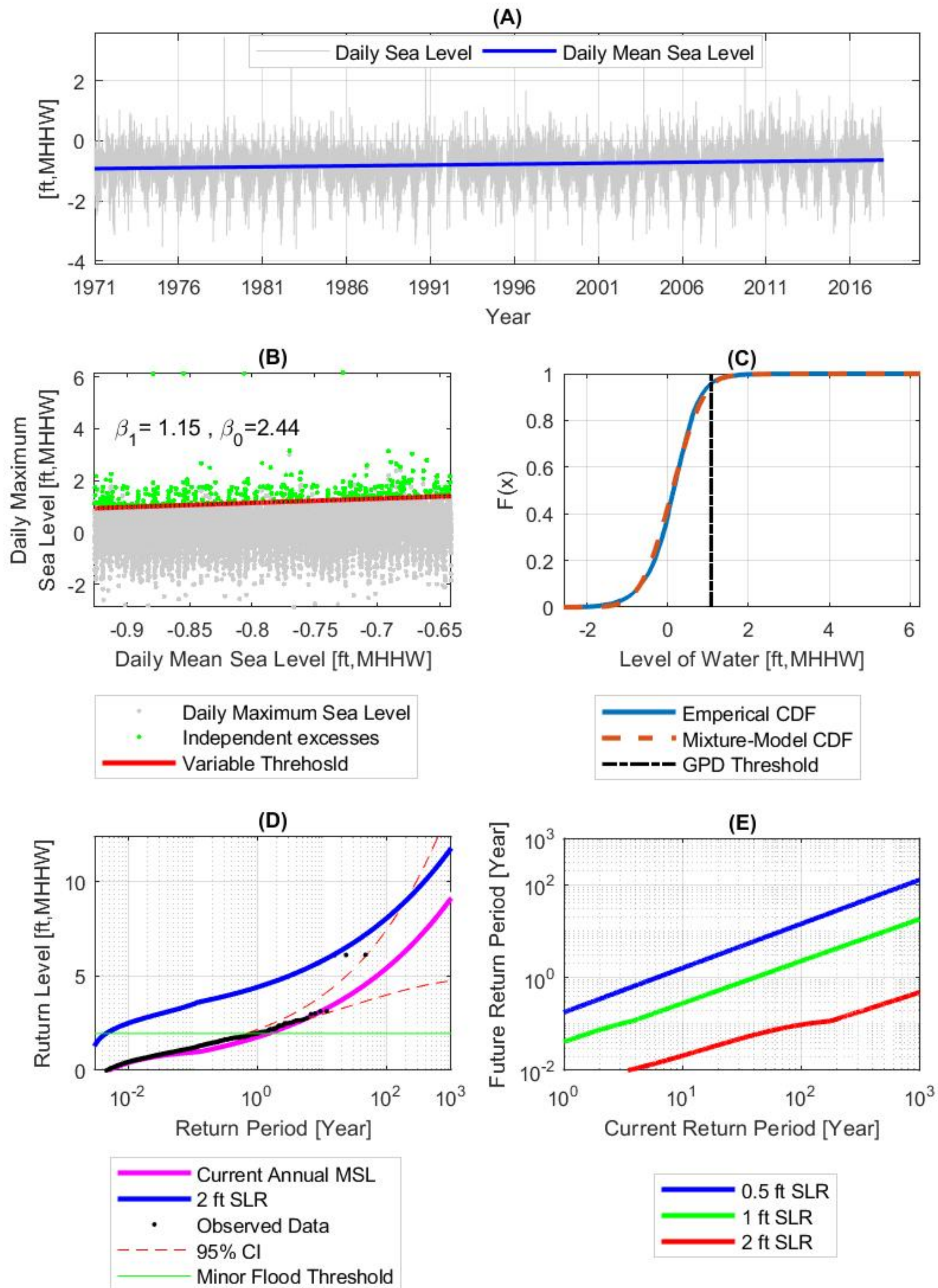

Figure A20. Tochester Beach (MD) station

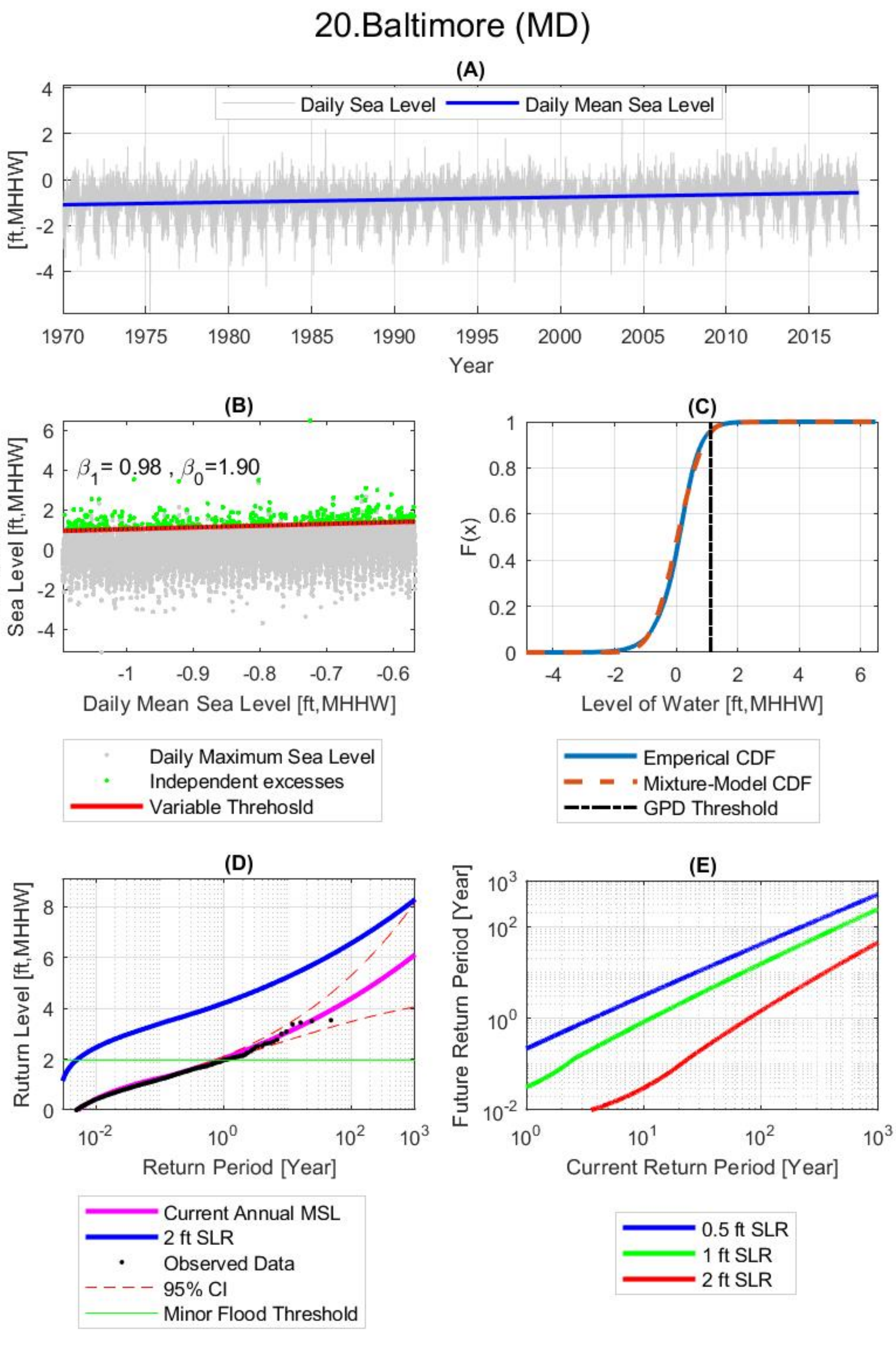

Figure A21. Baltimore (MD) station

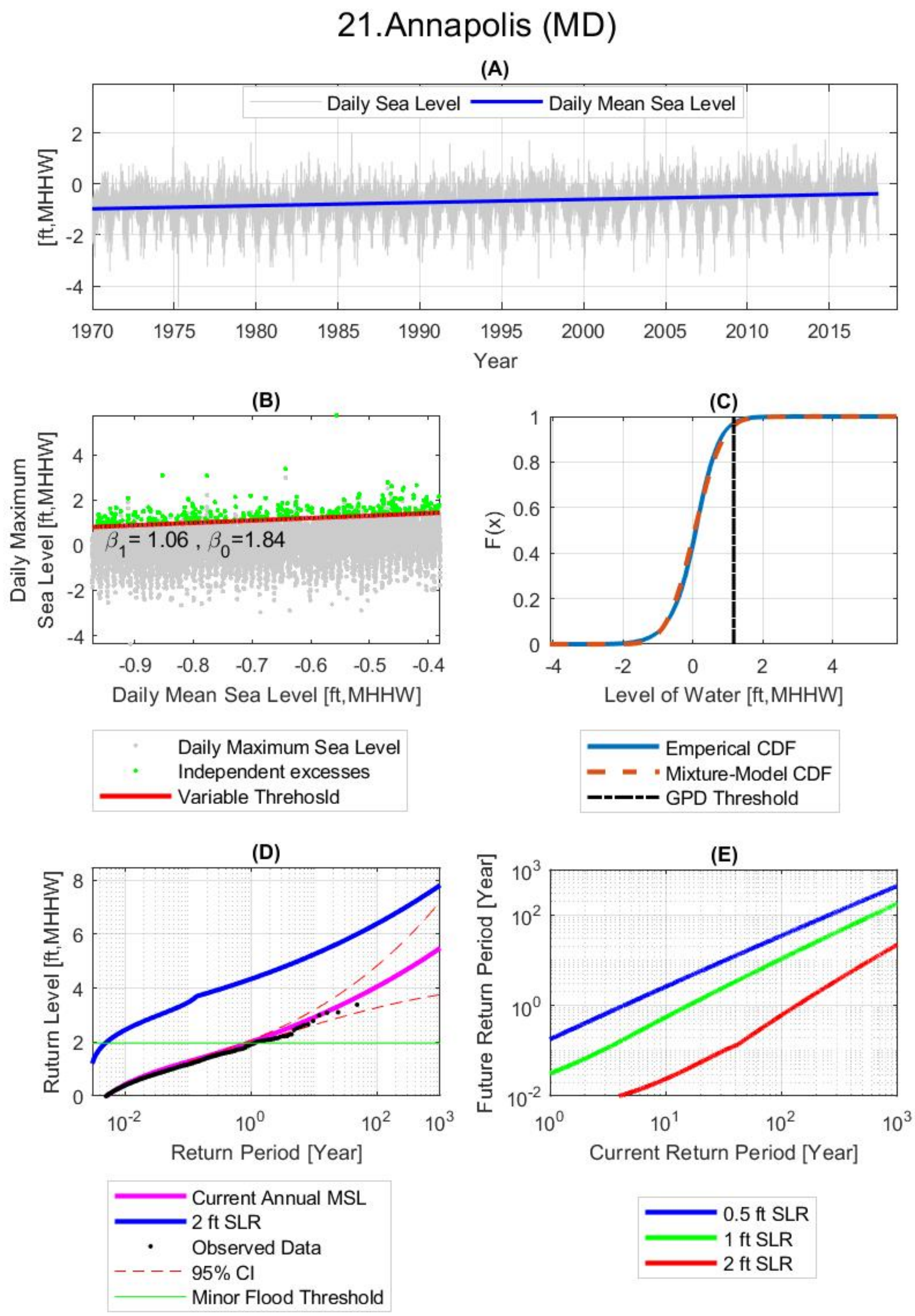

Figure A22. Annapolis (MD) station

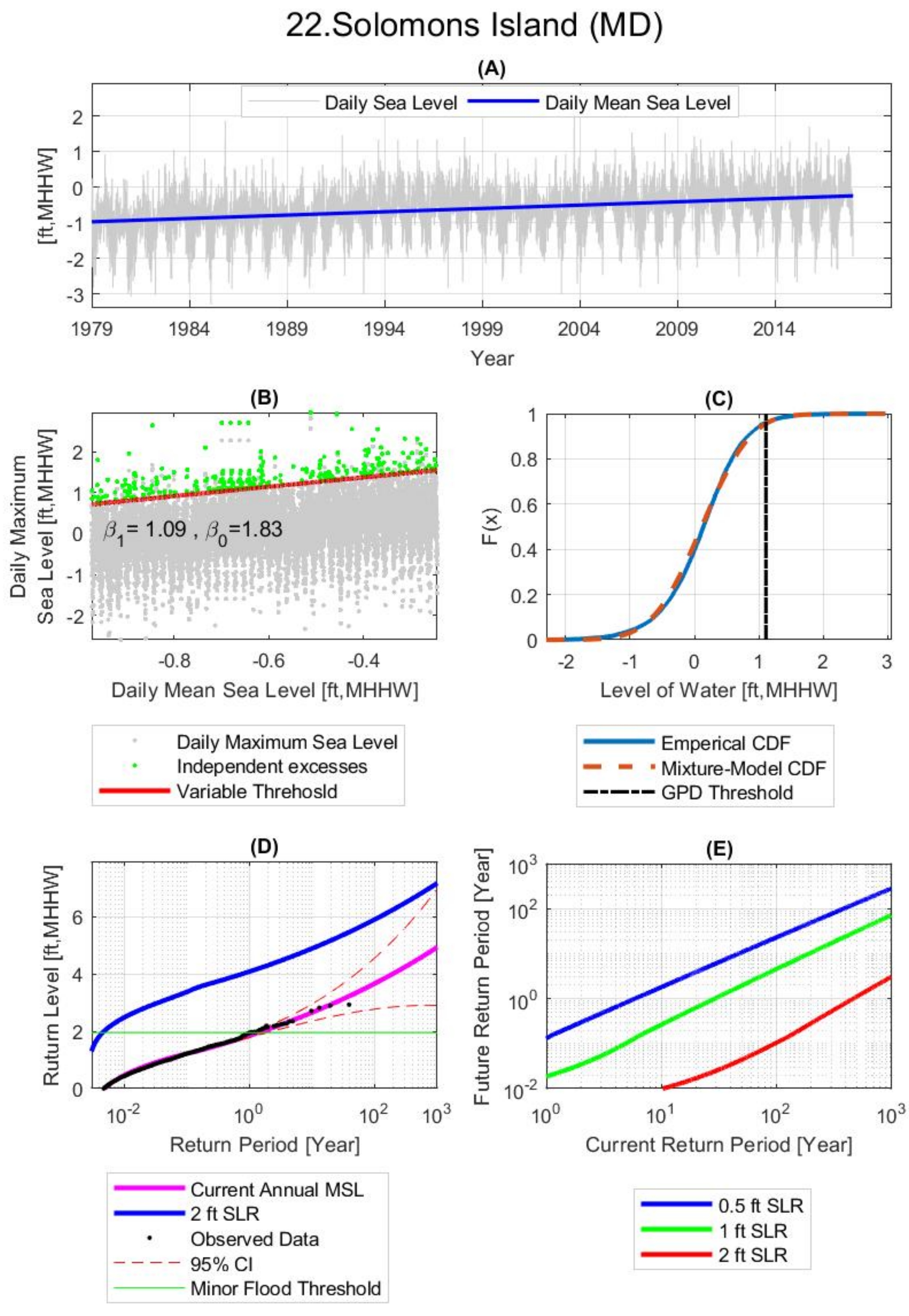

Figure A23. Solomons Island (MD) station

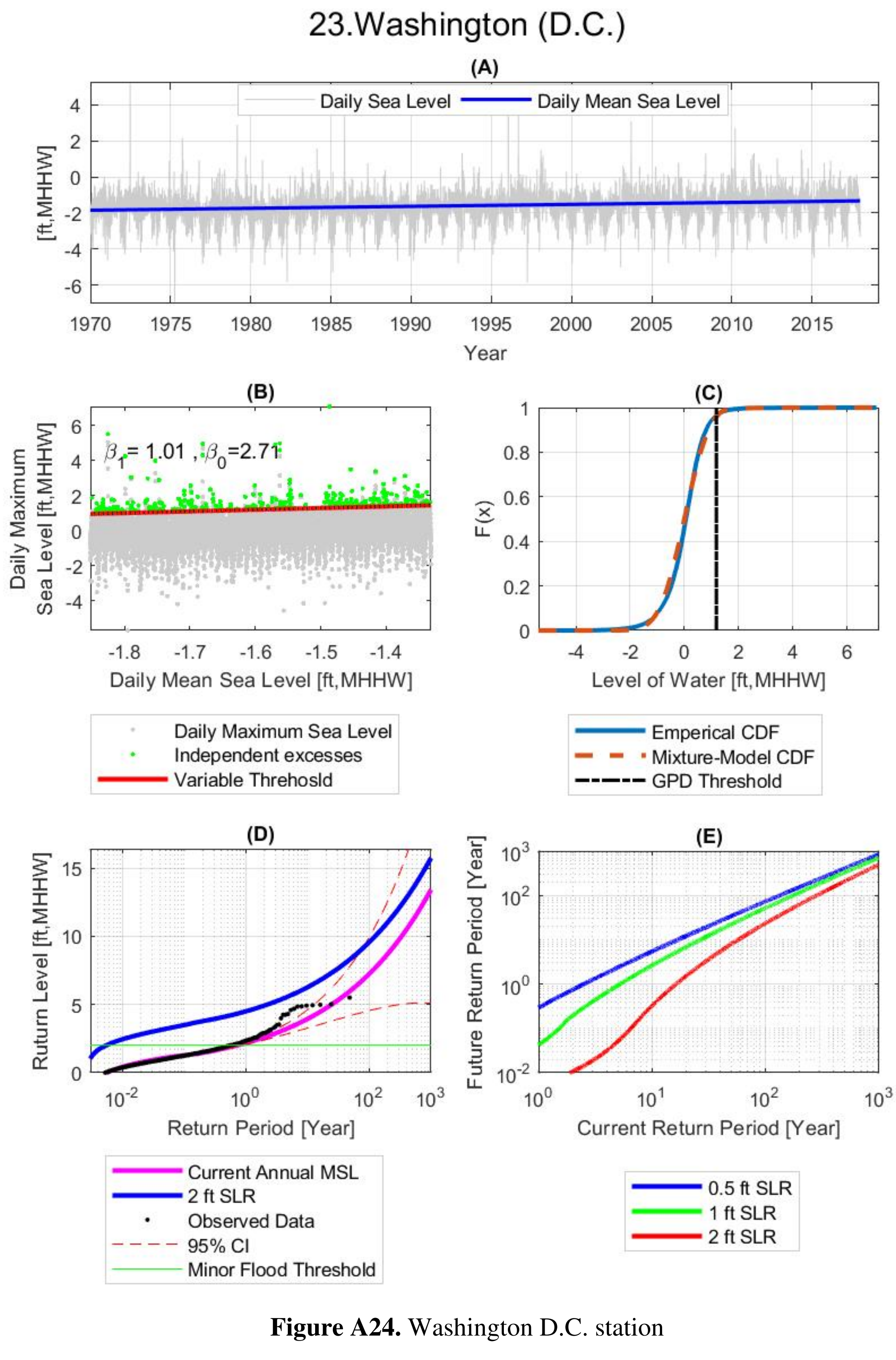

Figure A24. Washington D.C. station

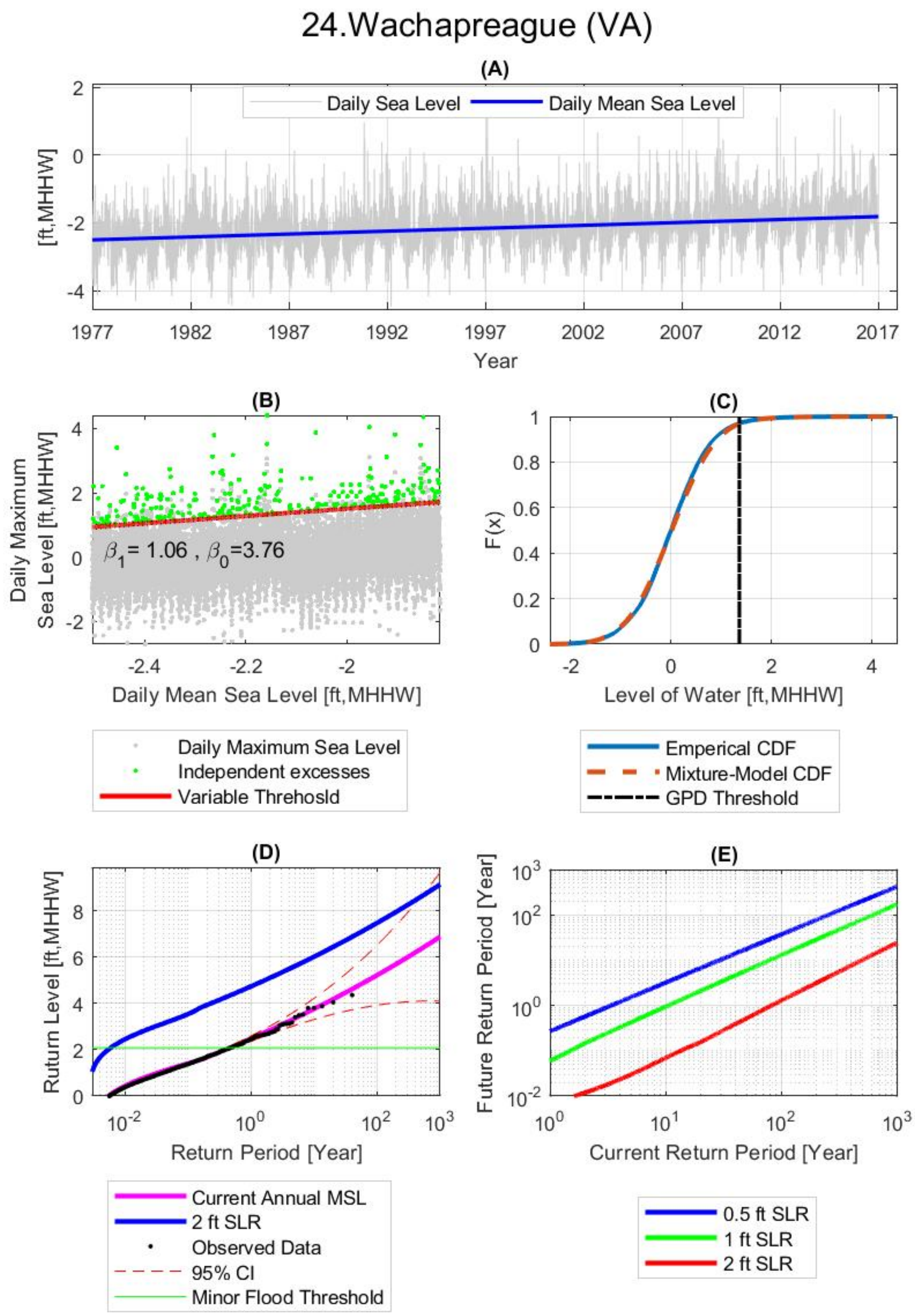

Figure A25. Wachapreague (VA) station

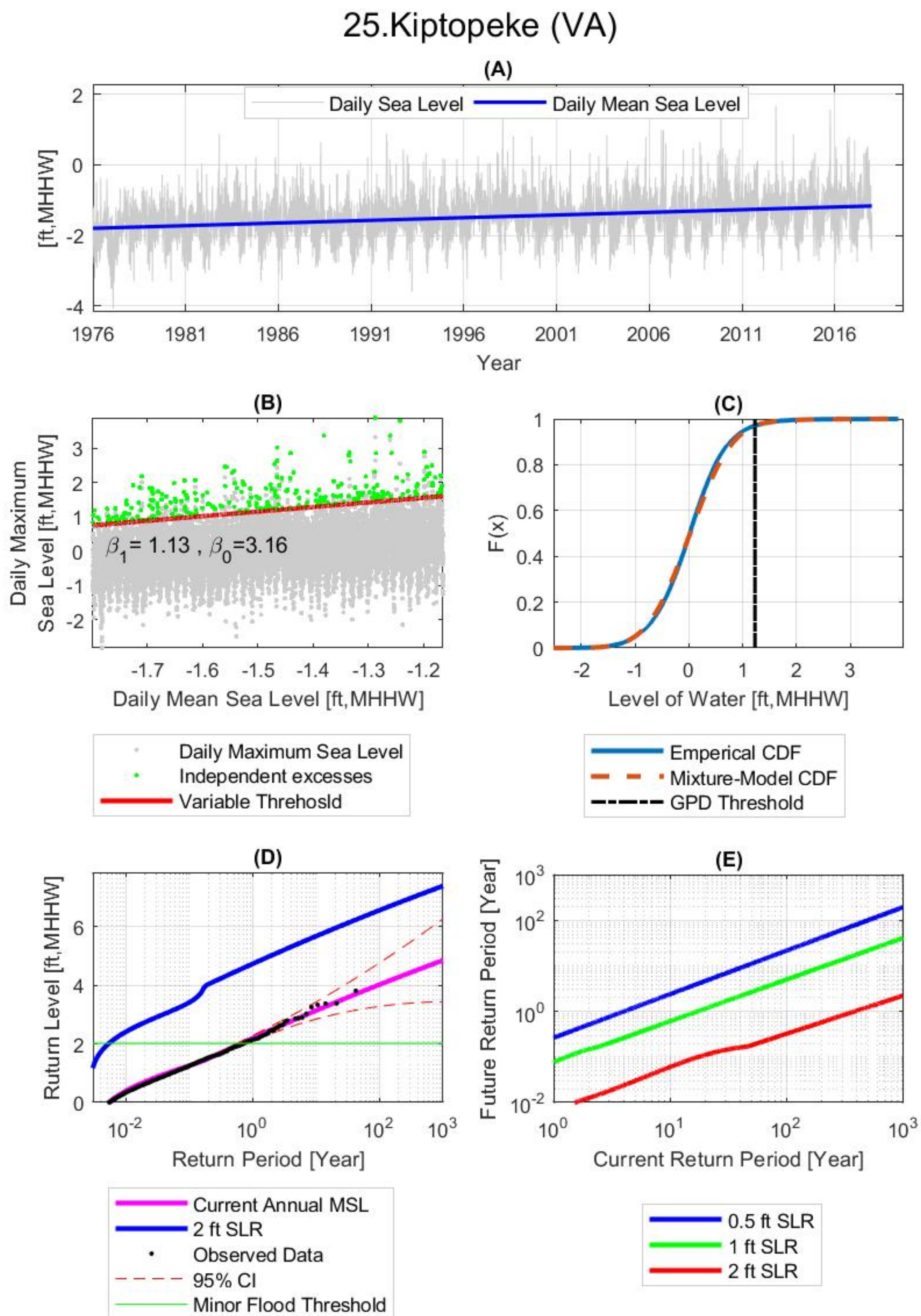

Figure A26. Kiptopeke (VA) station

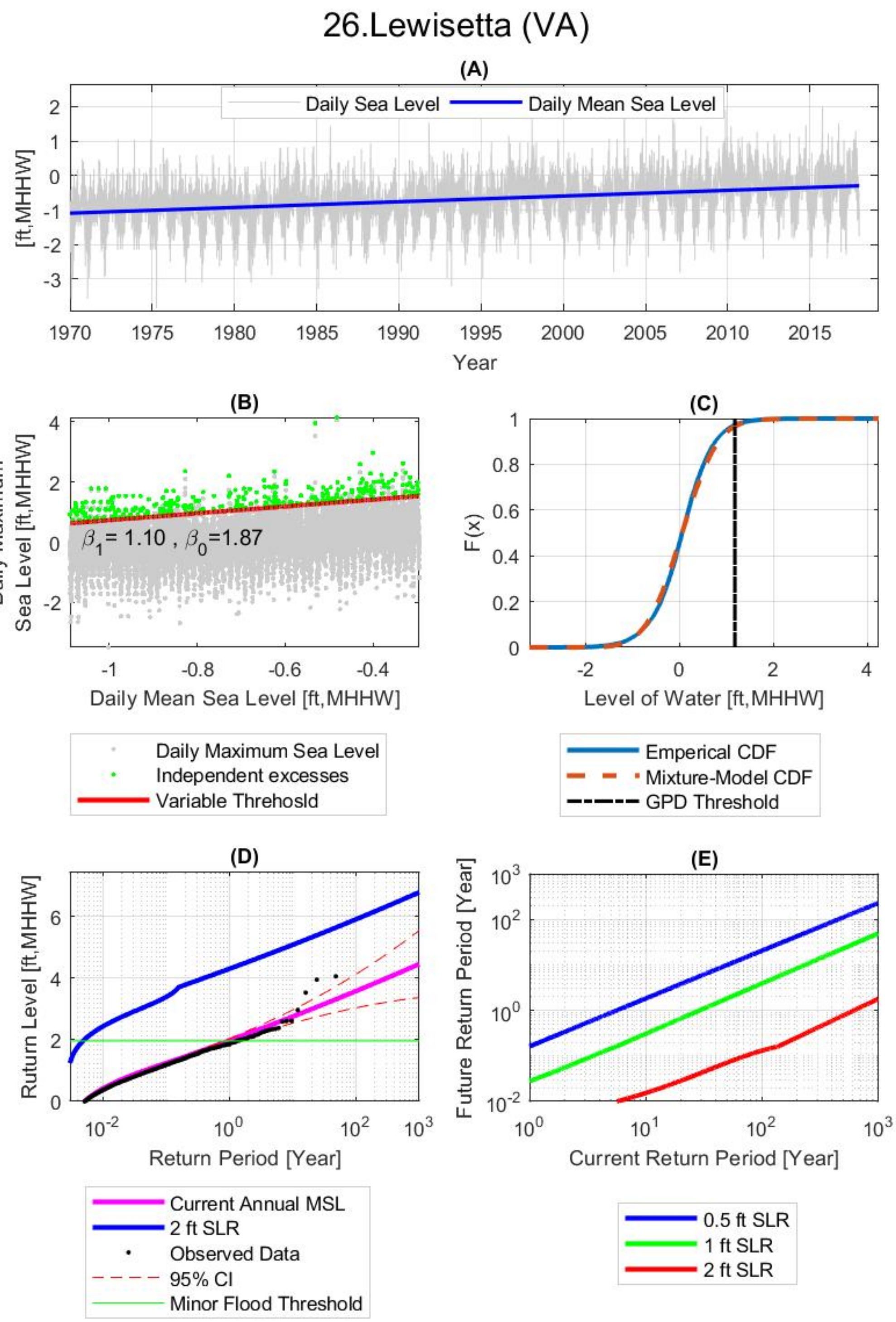

Figure A27. Lewisetta (VA) station

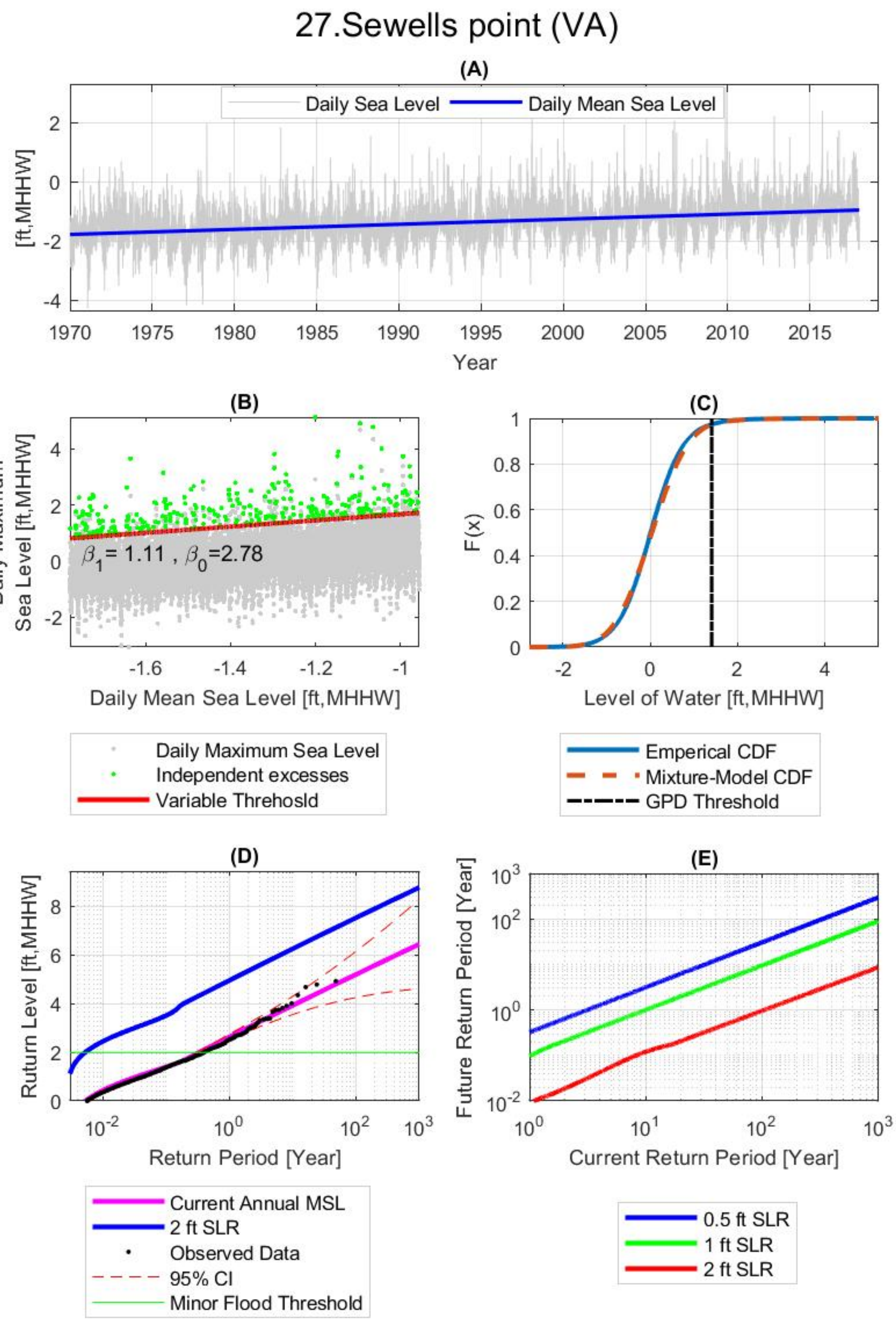

Figure A28. Sewells point (VA) station

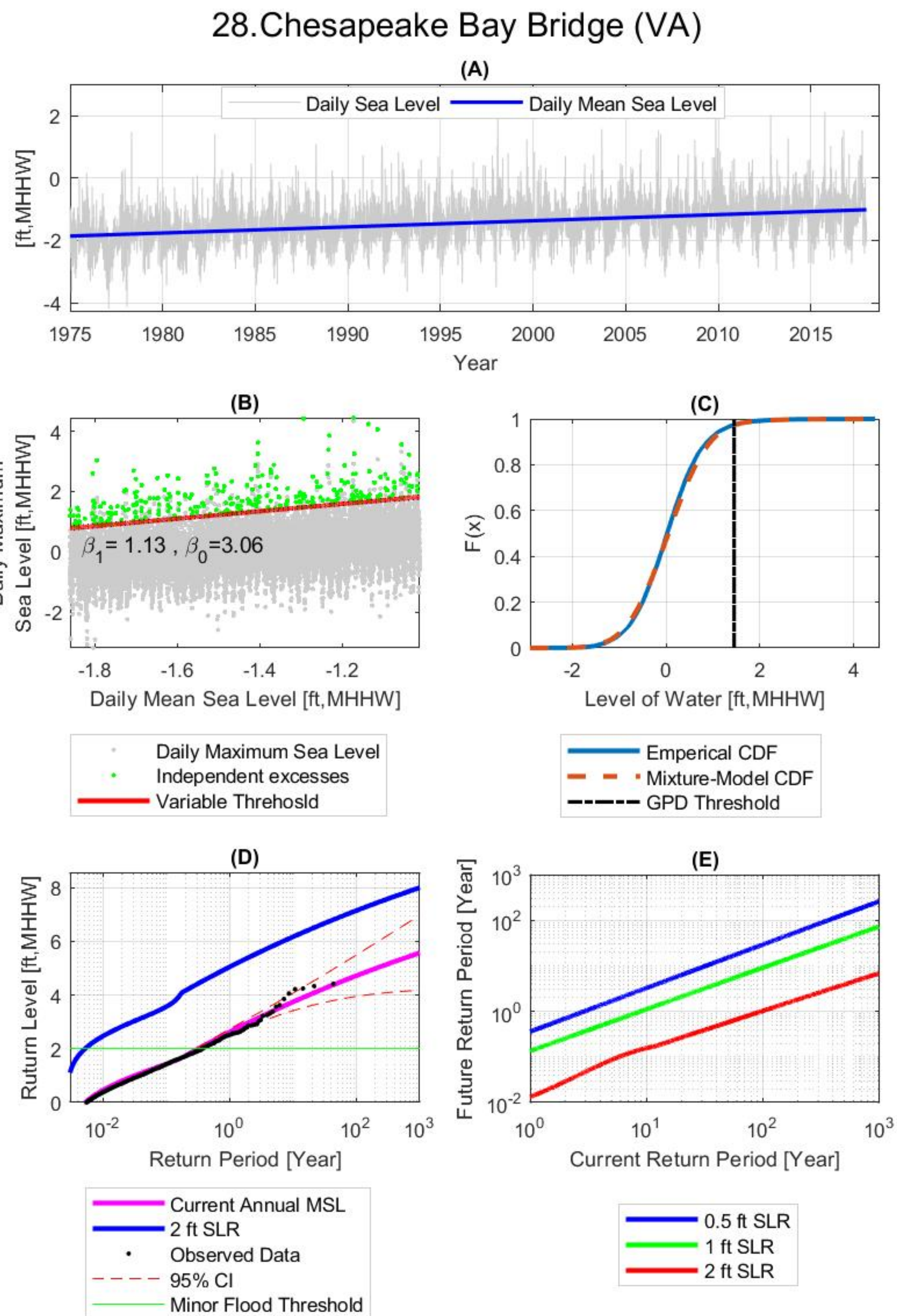

Figure A29. Chesapeake Bay Bridge (VA) station

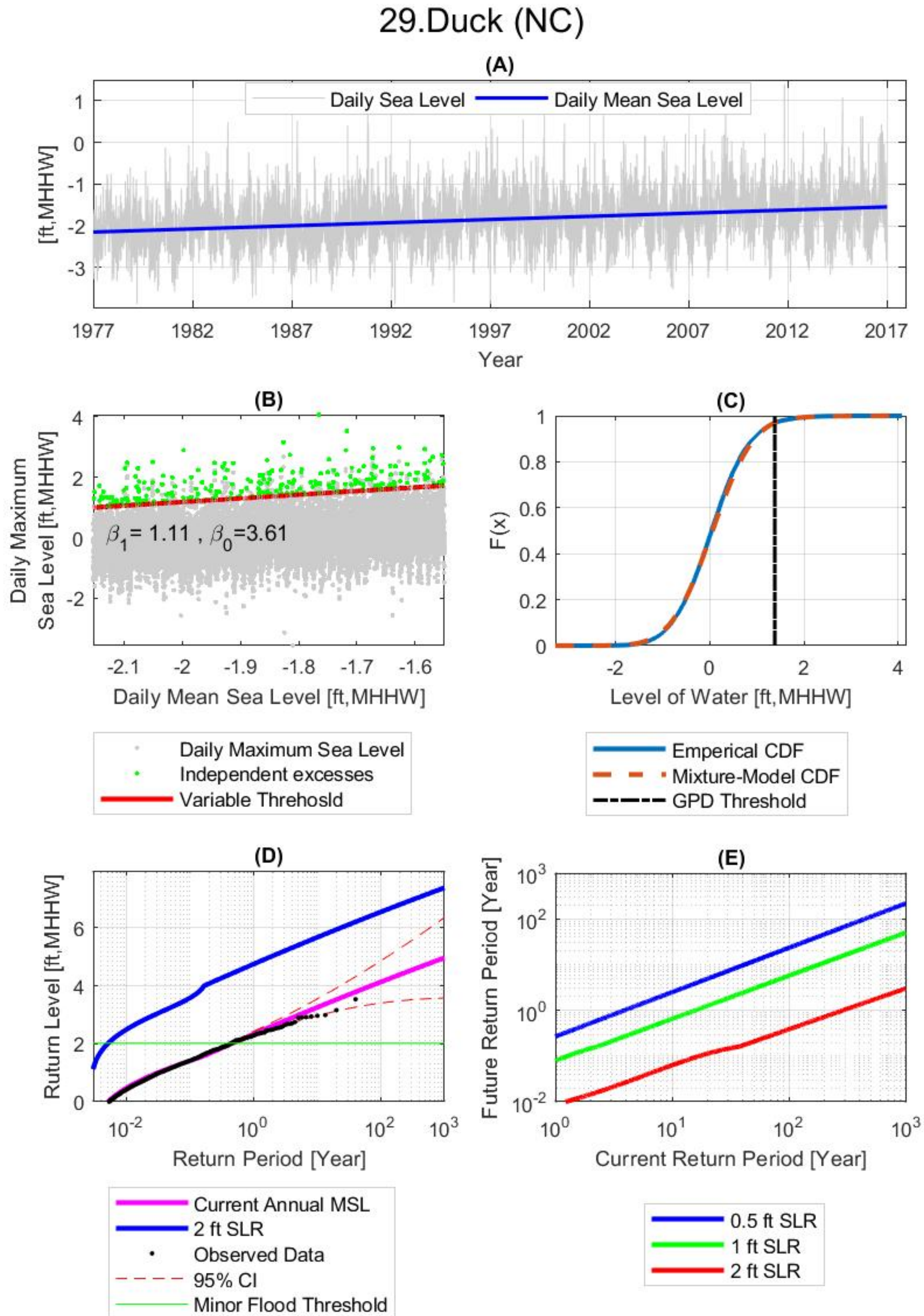

Figure A30. Duck (NC) station

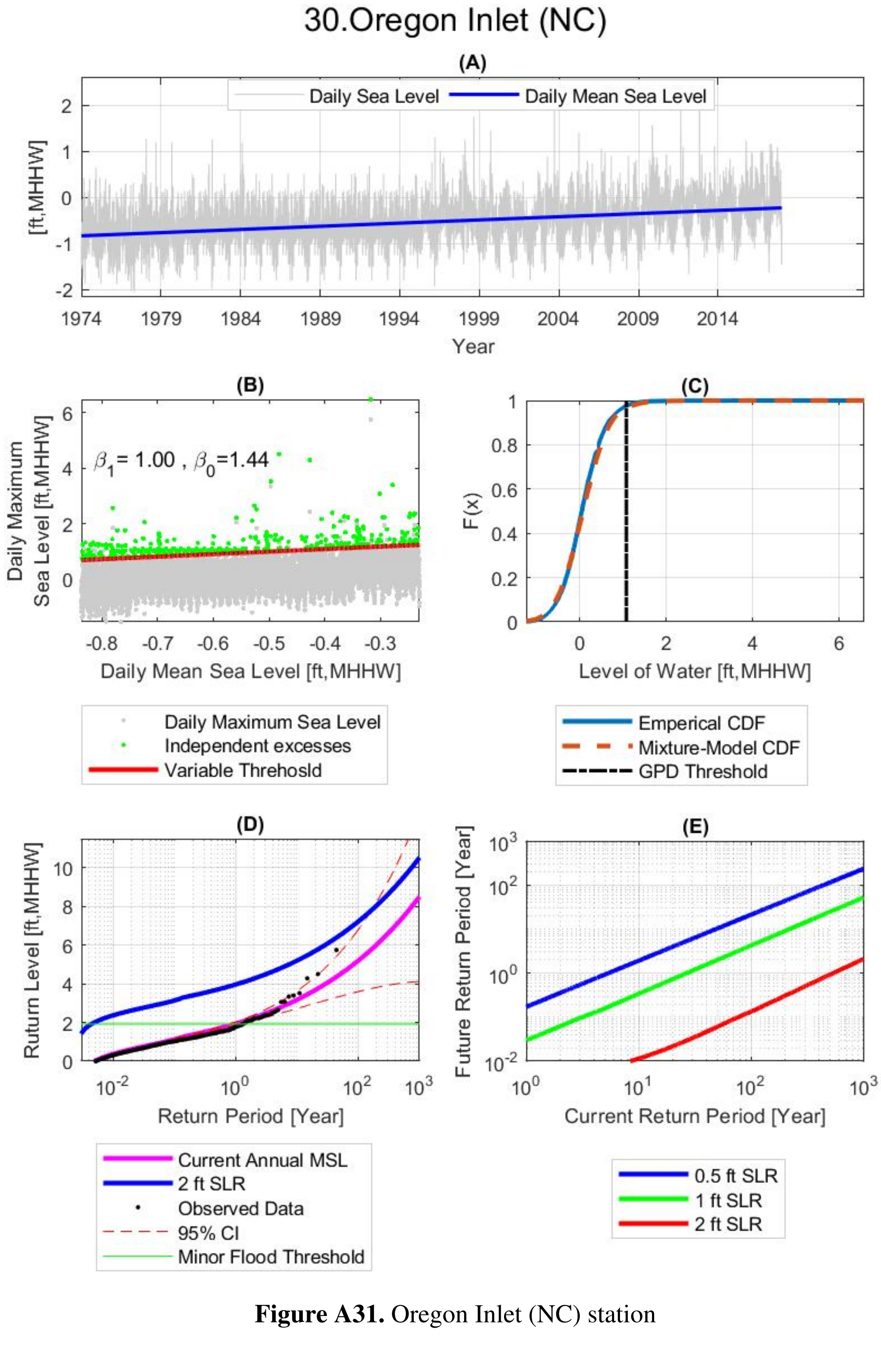

Figure A31. Oregon Inlet (NC) station

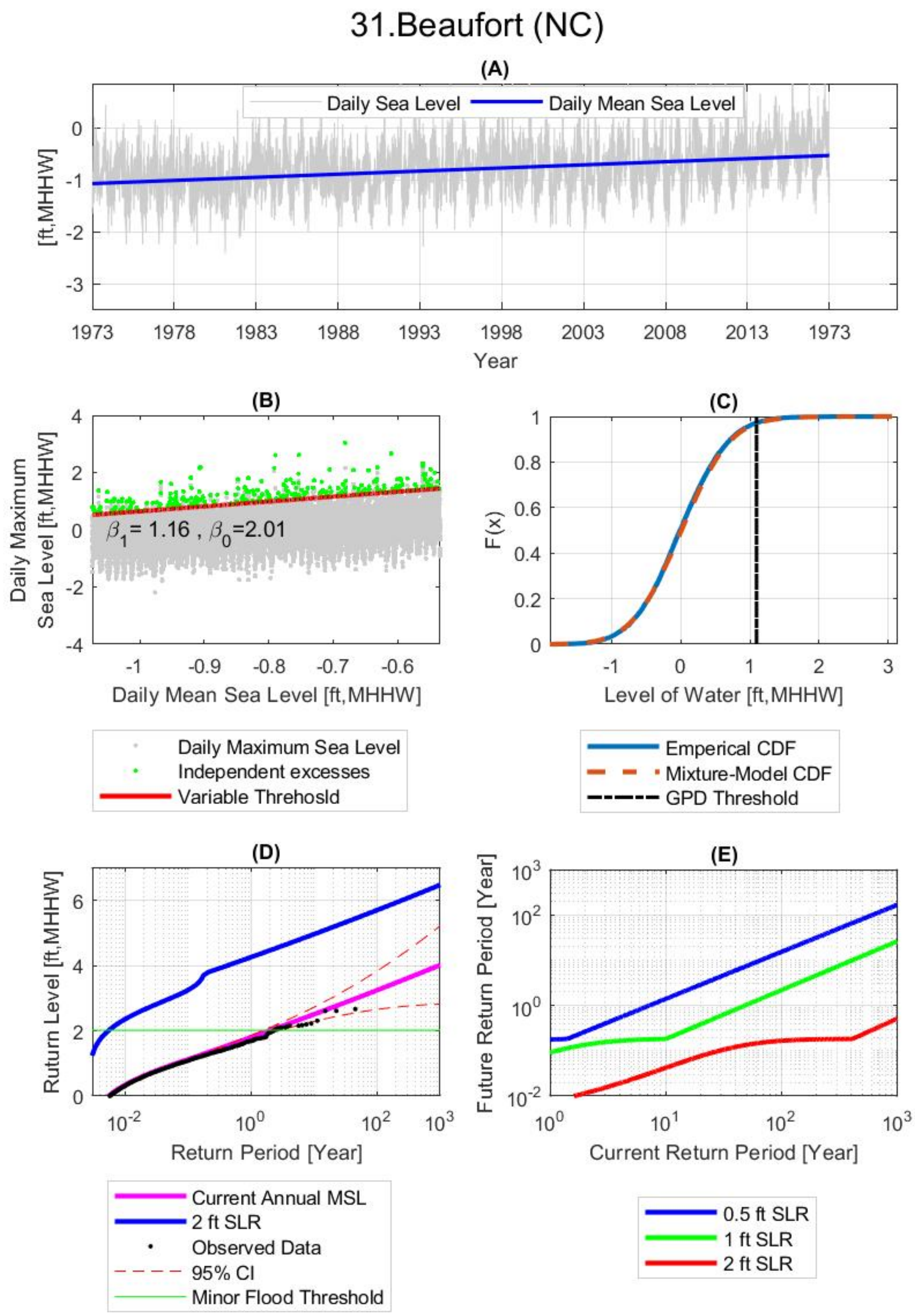

Figure A32. Beaufort (NC) station

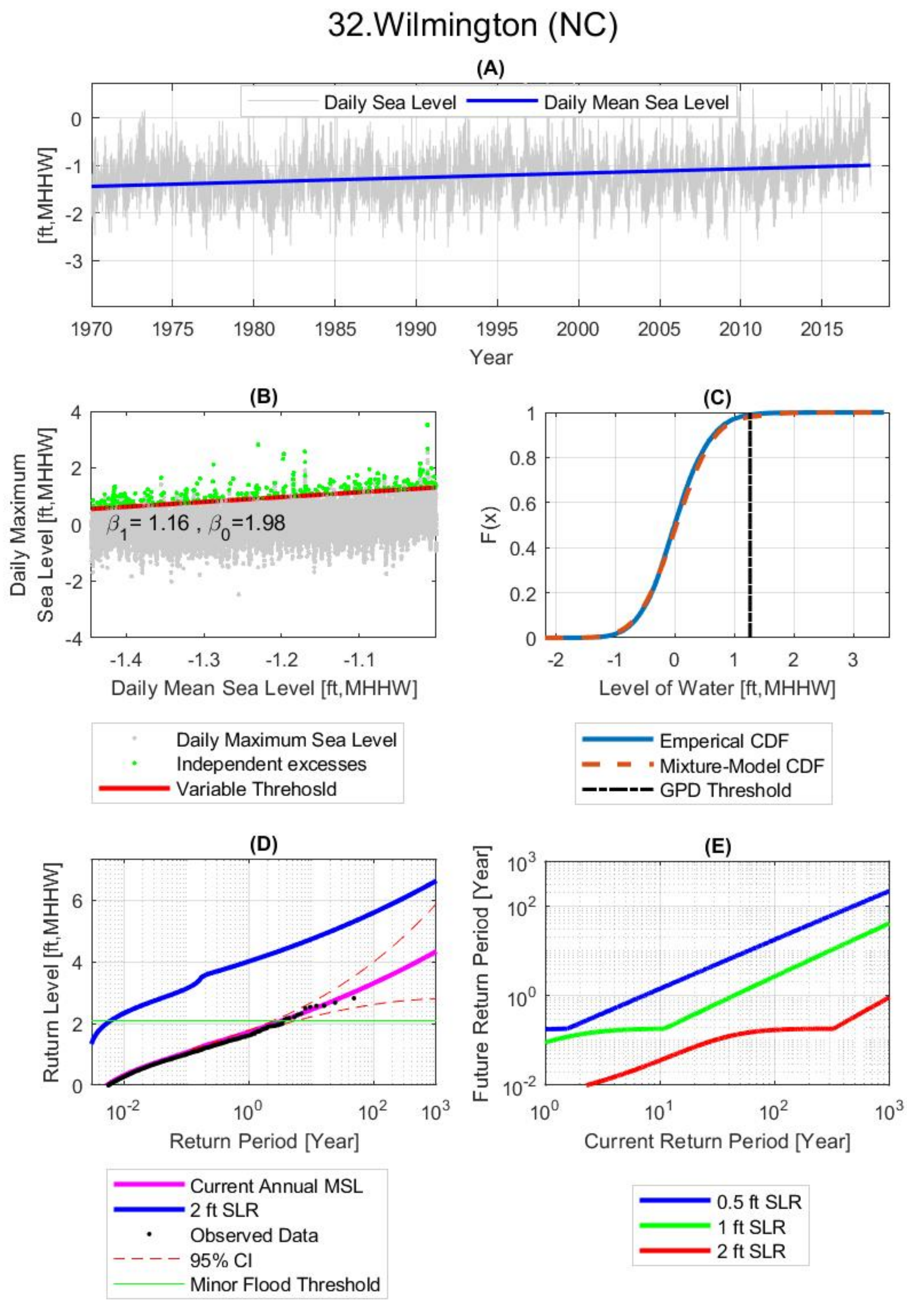

Figure A33. Wilmington (NC) station

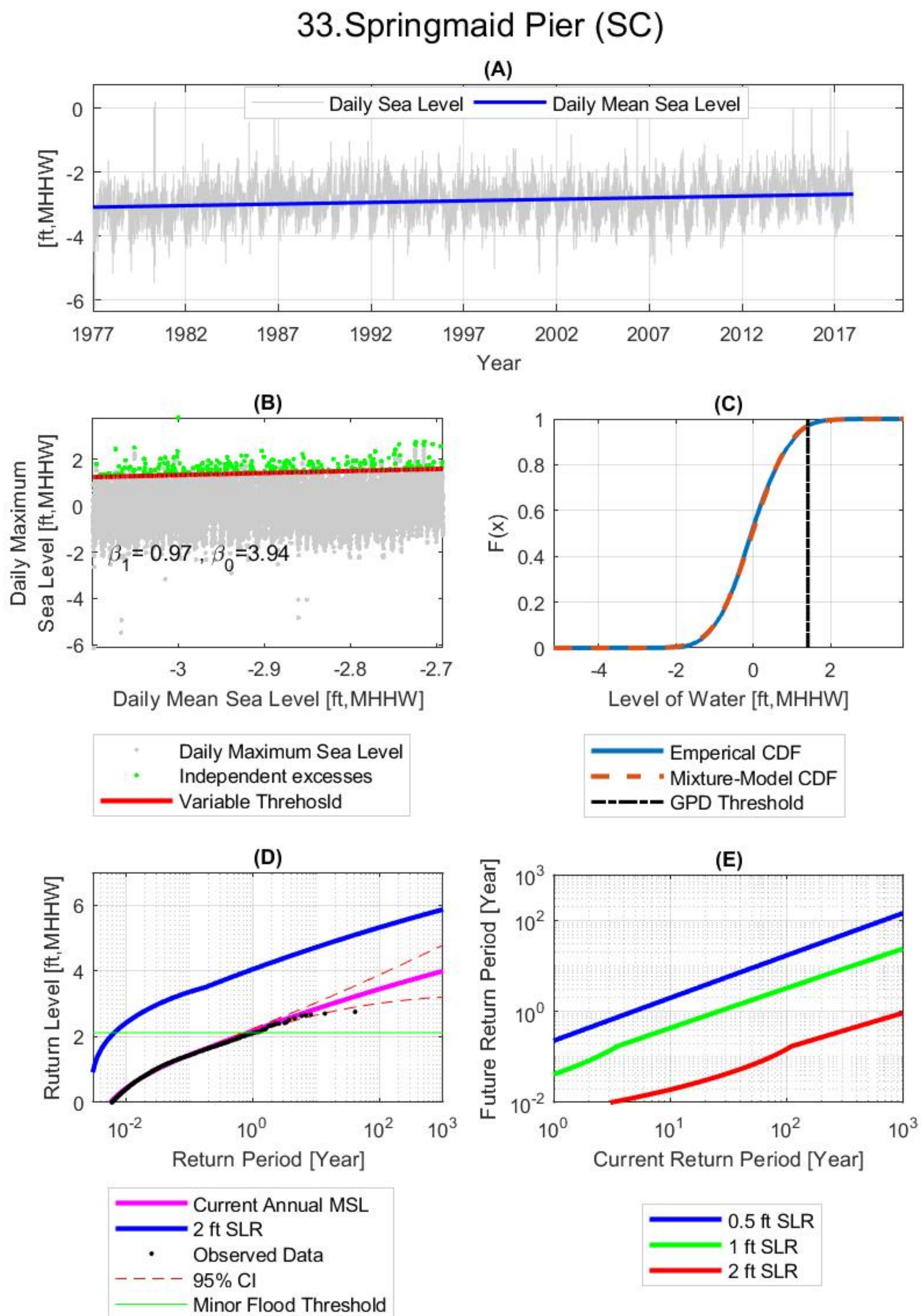

Figure A34. Springmaid Pier (SC) station

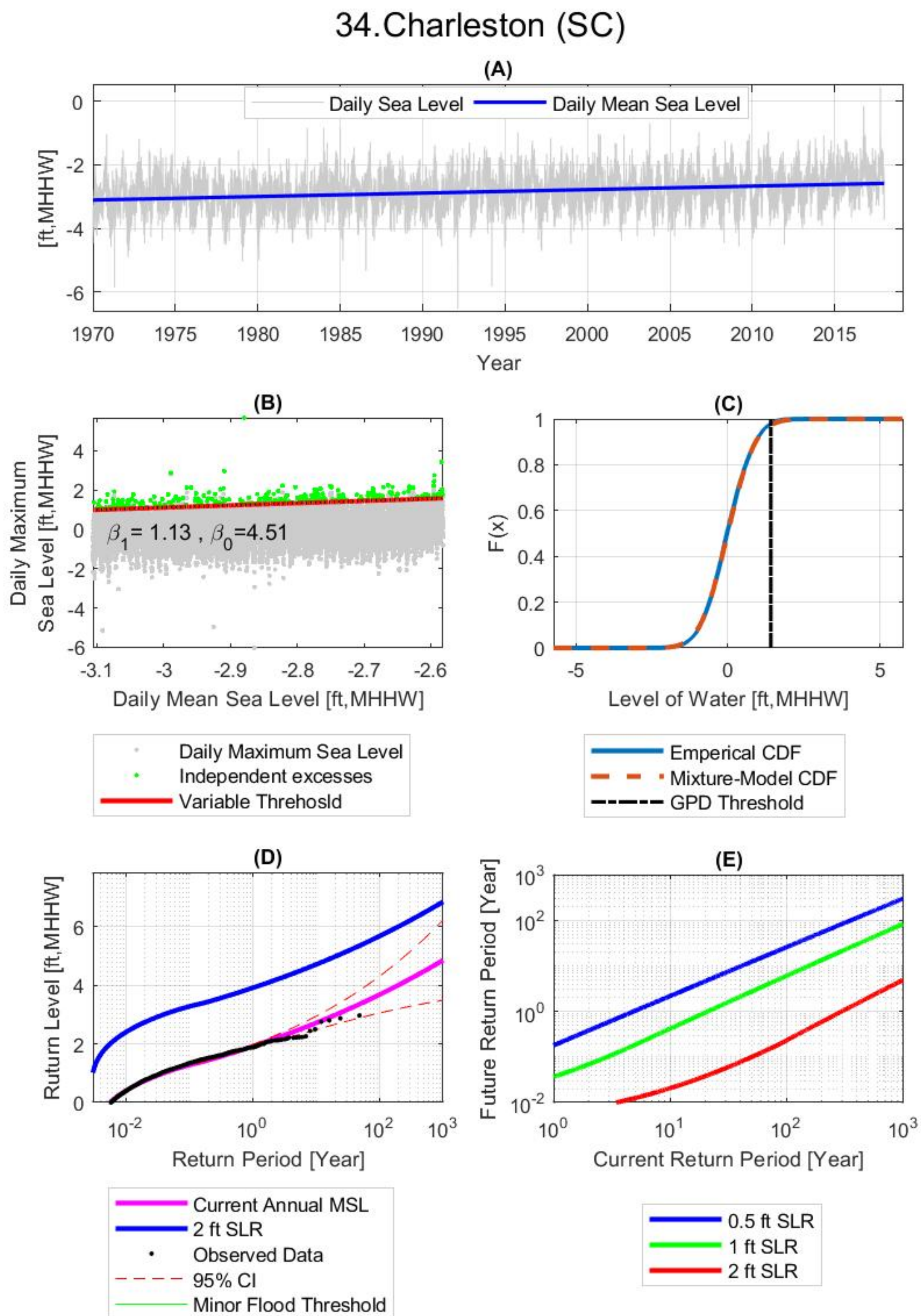

Figure A35. Charleston (SC) station

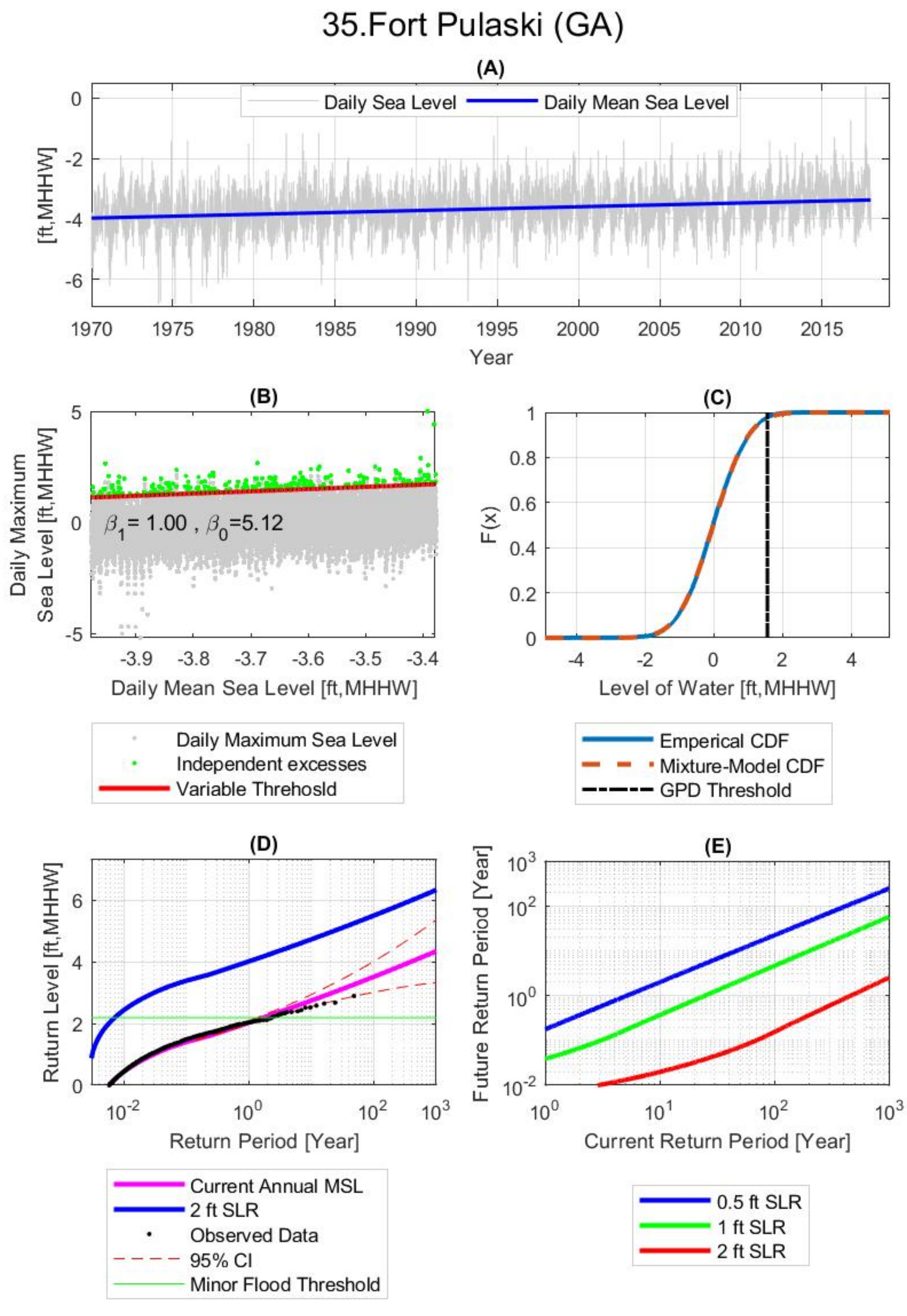

Figure A36. Fort Pulaski (GA) station

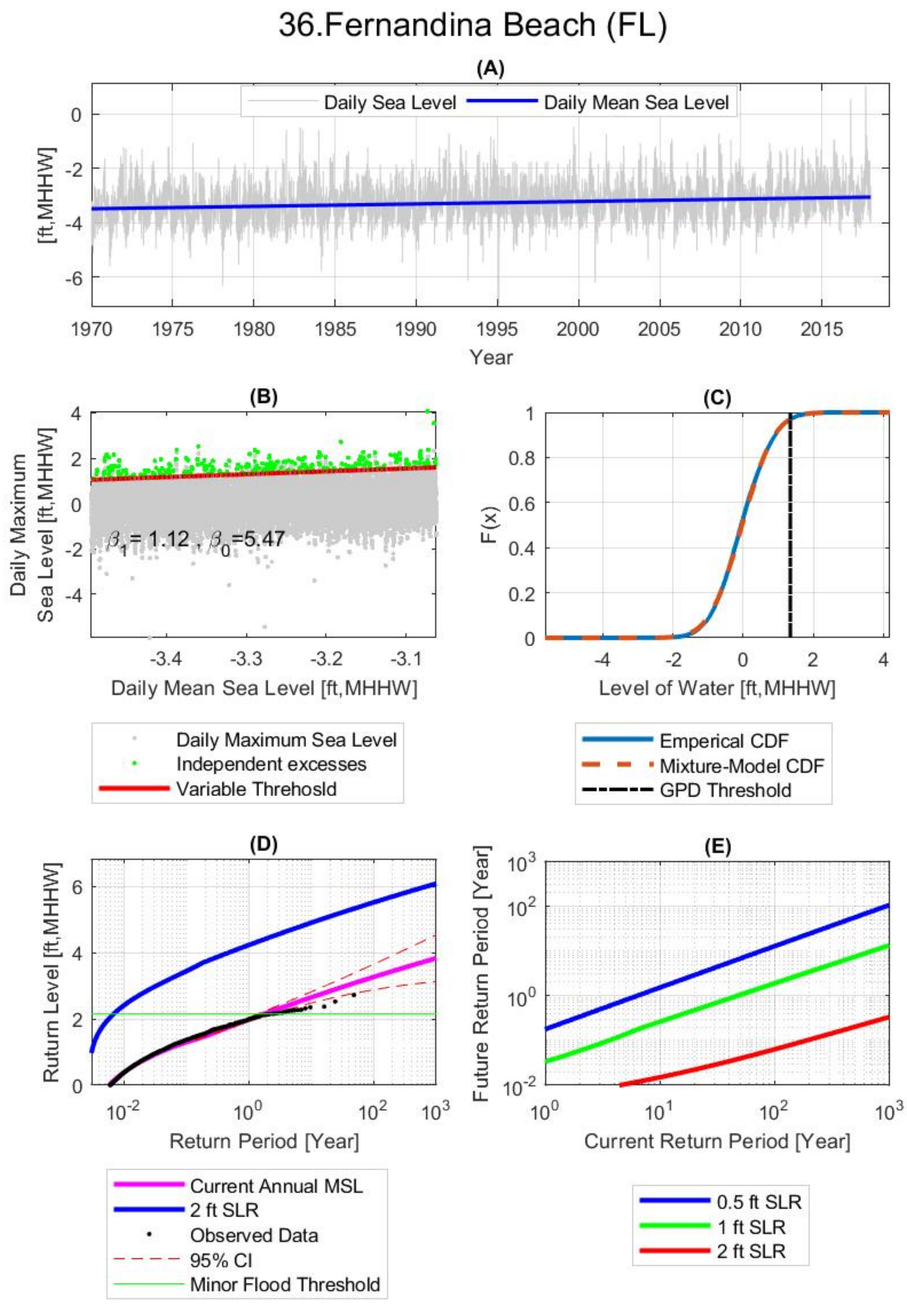

Figure A37. Fernandina Beach (FL) station

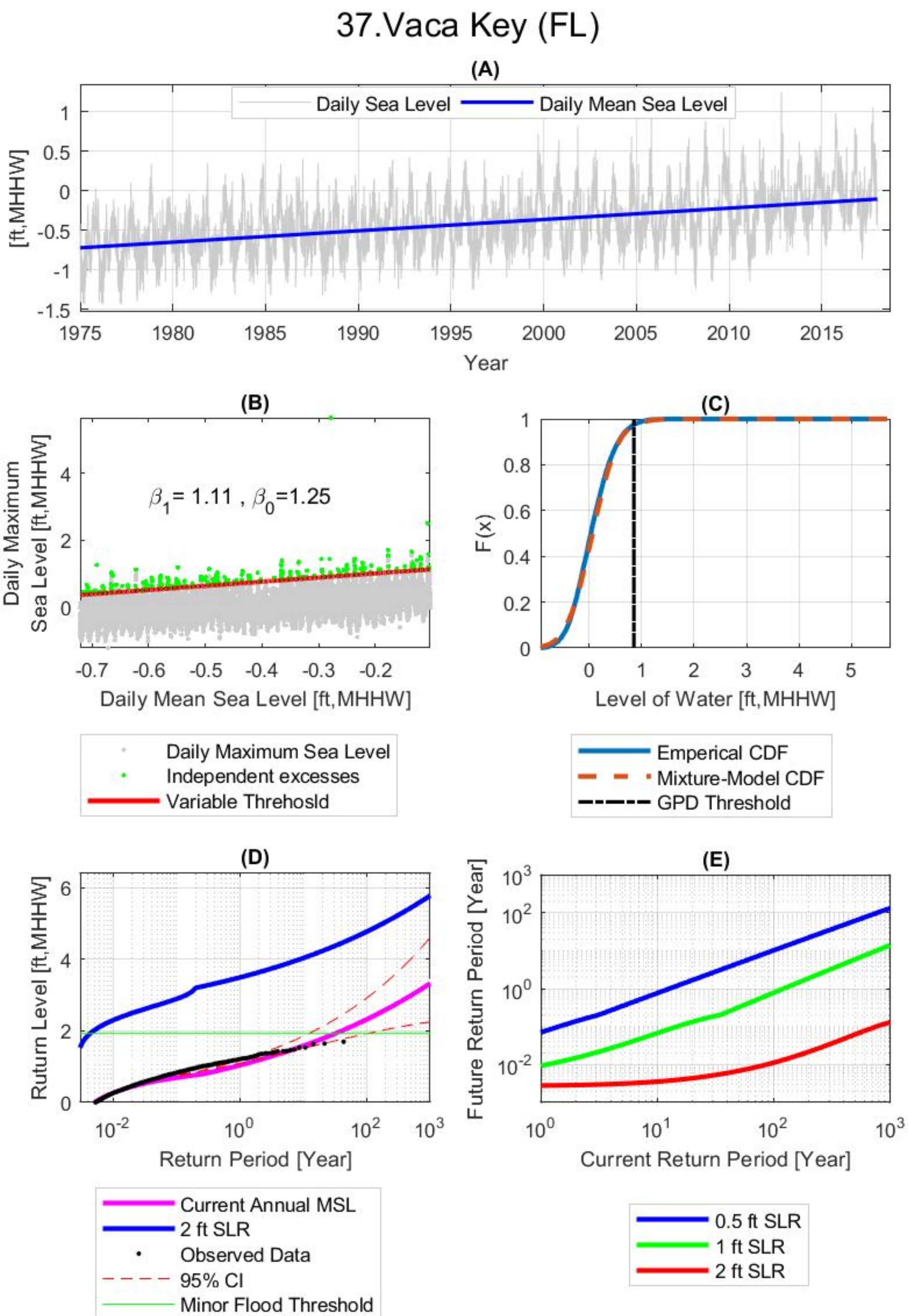

Figure A38. Vaca Key (FL) station

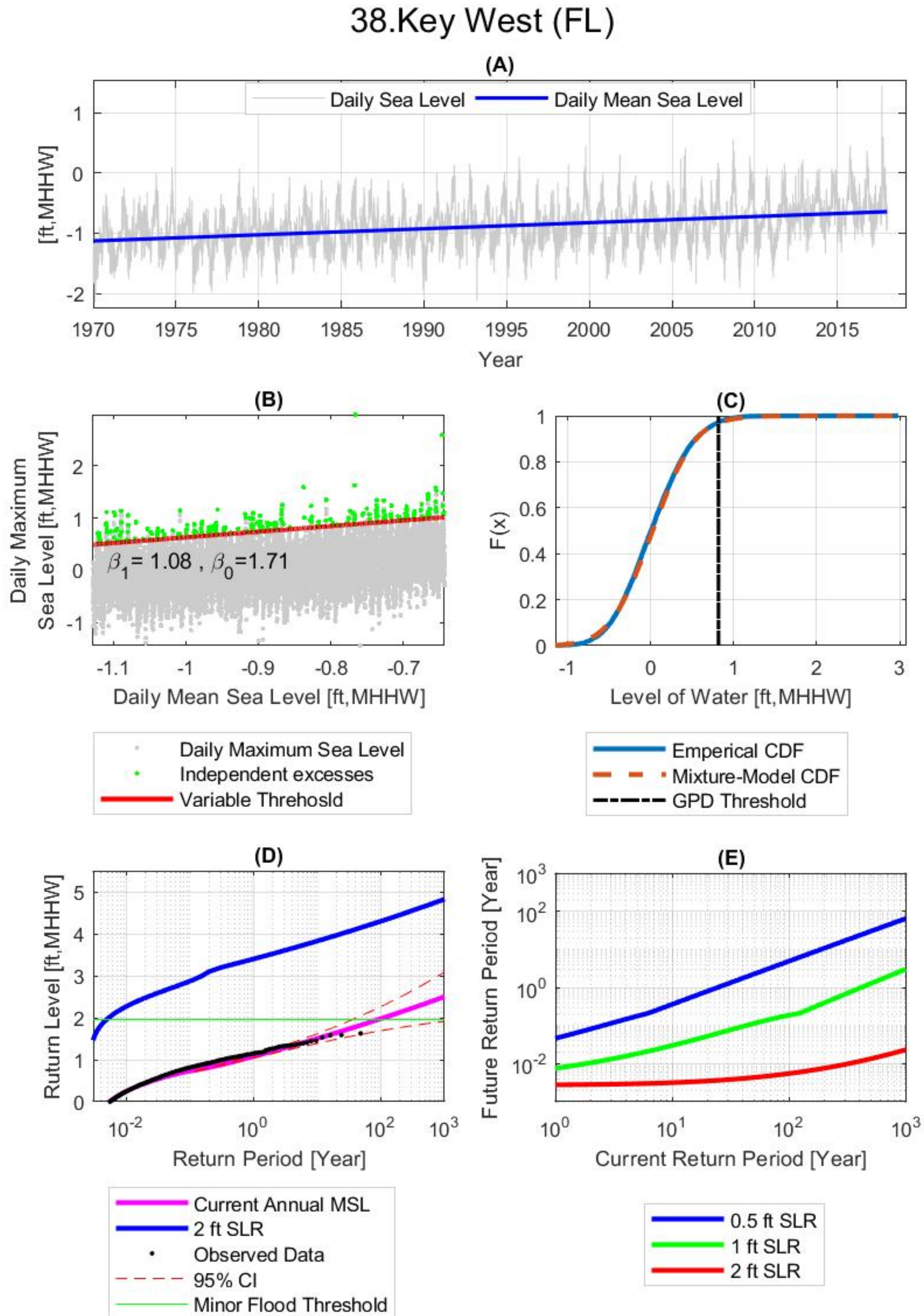

Figure A39. Key West (FL) station

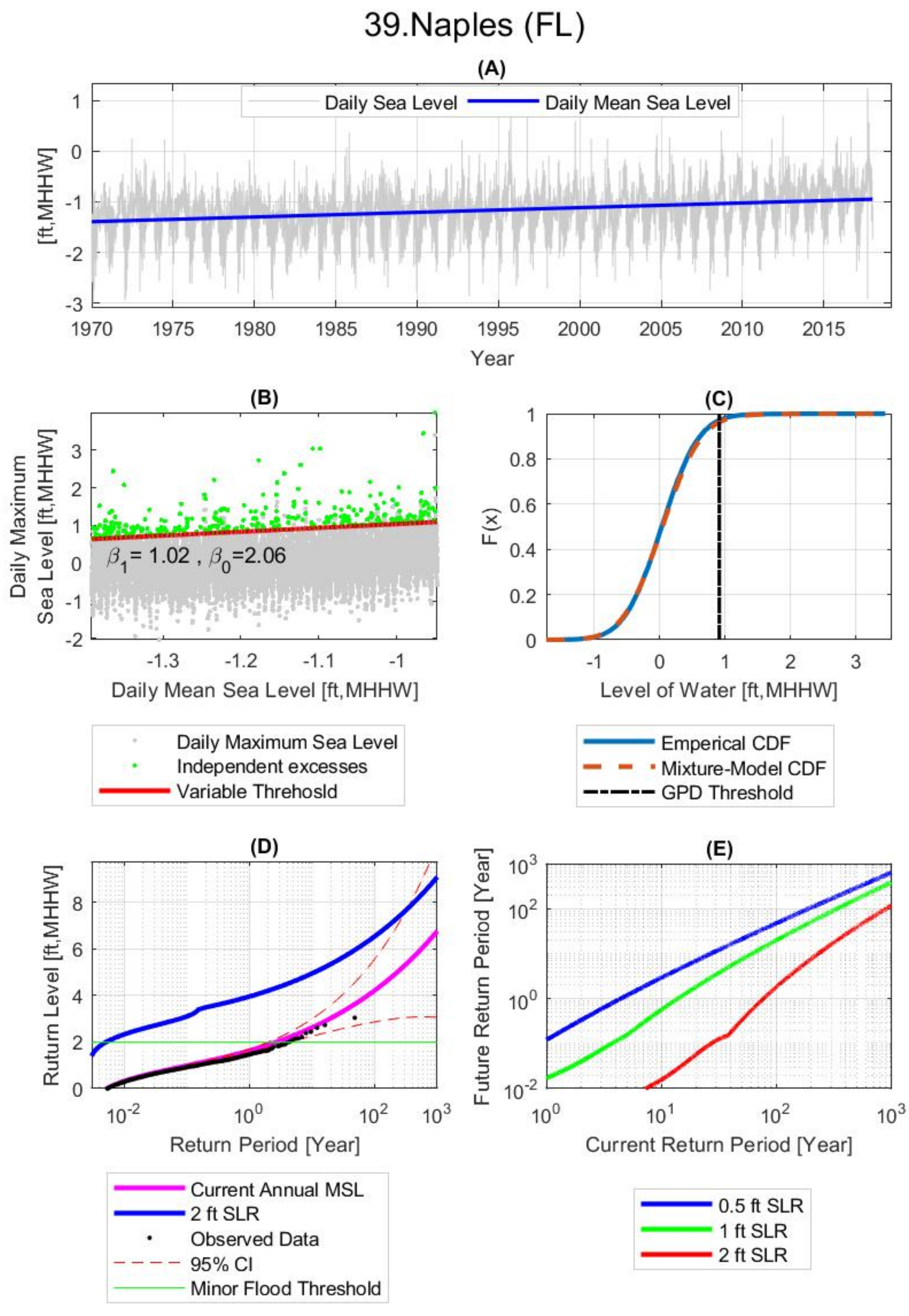

Figure A40. Naples (FL) station

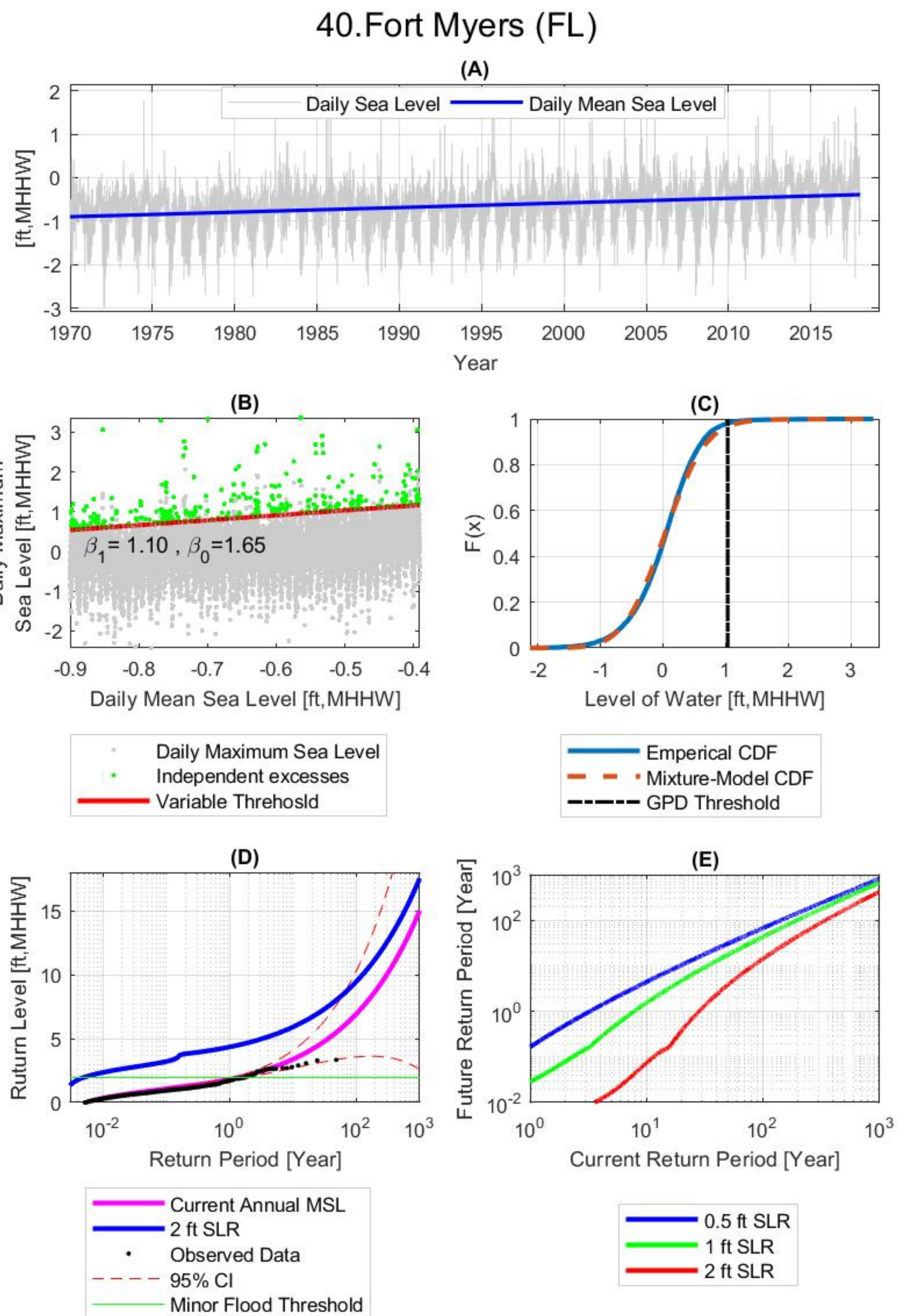

Figure A41. Fort Myers (FL) station

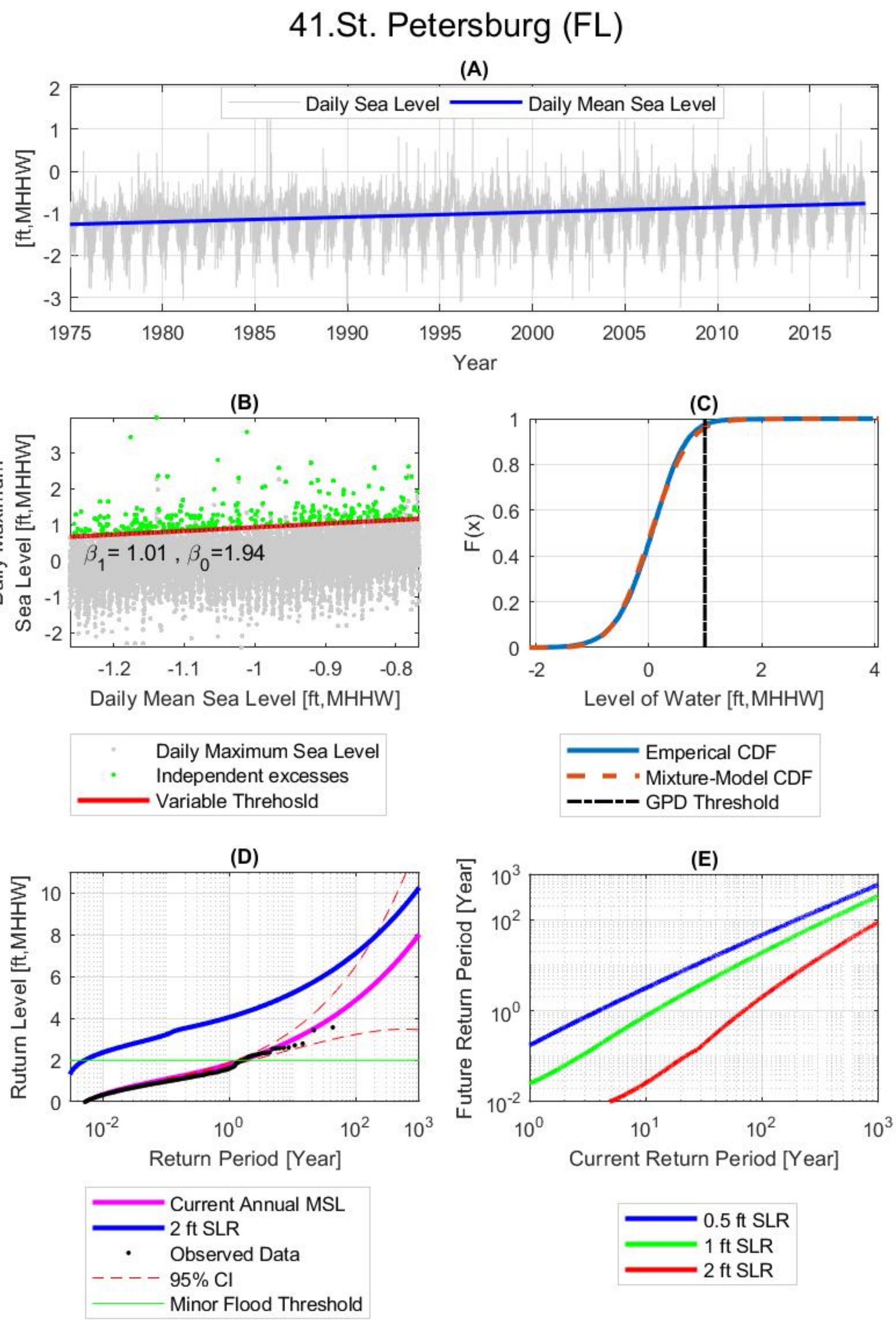

Figure A42. St. Petersburg (FL) station

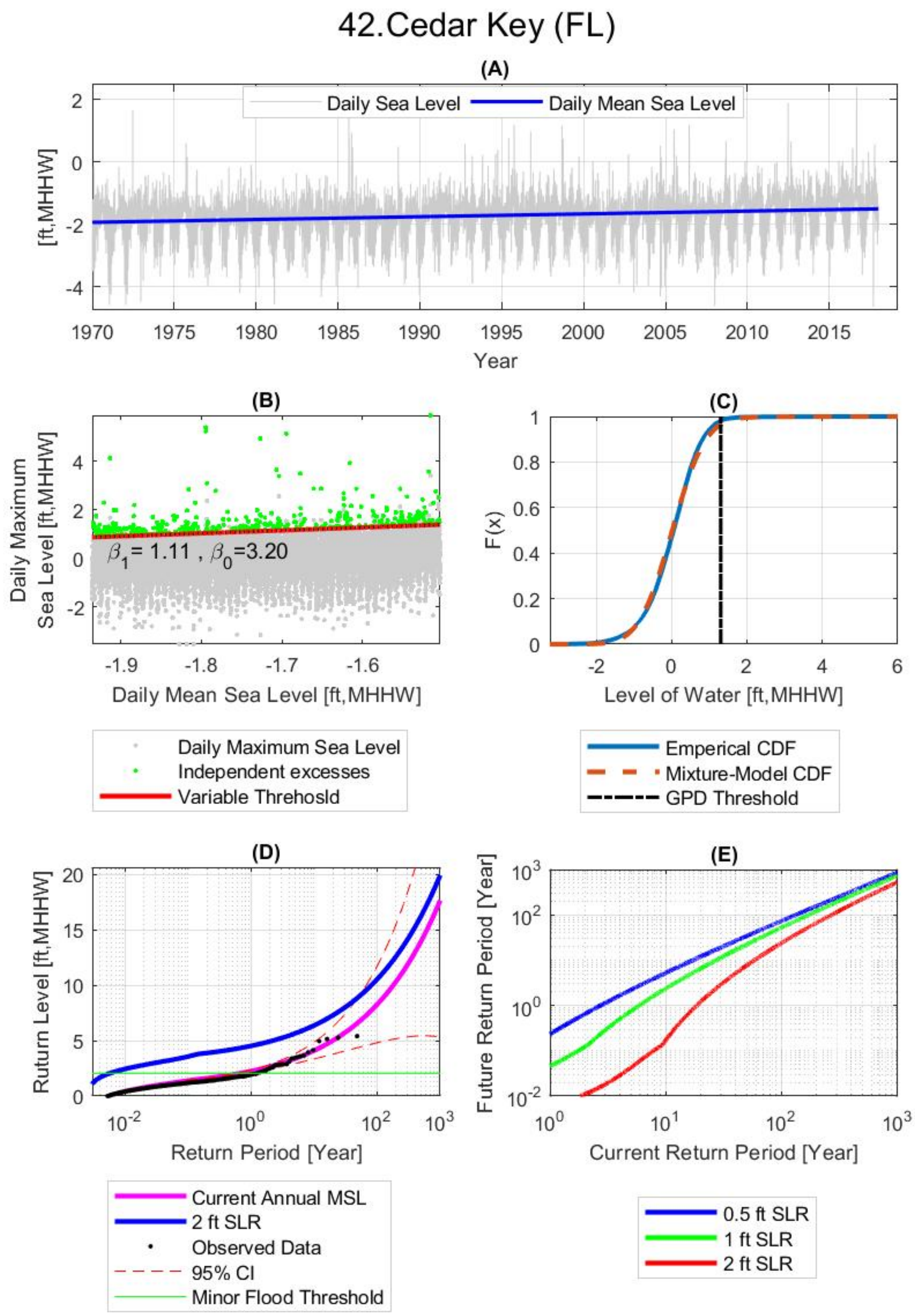

Figure A43. Cedar Key (FL) station

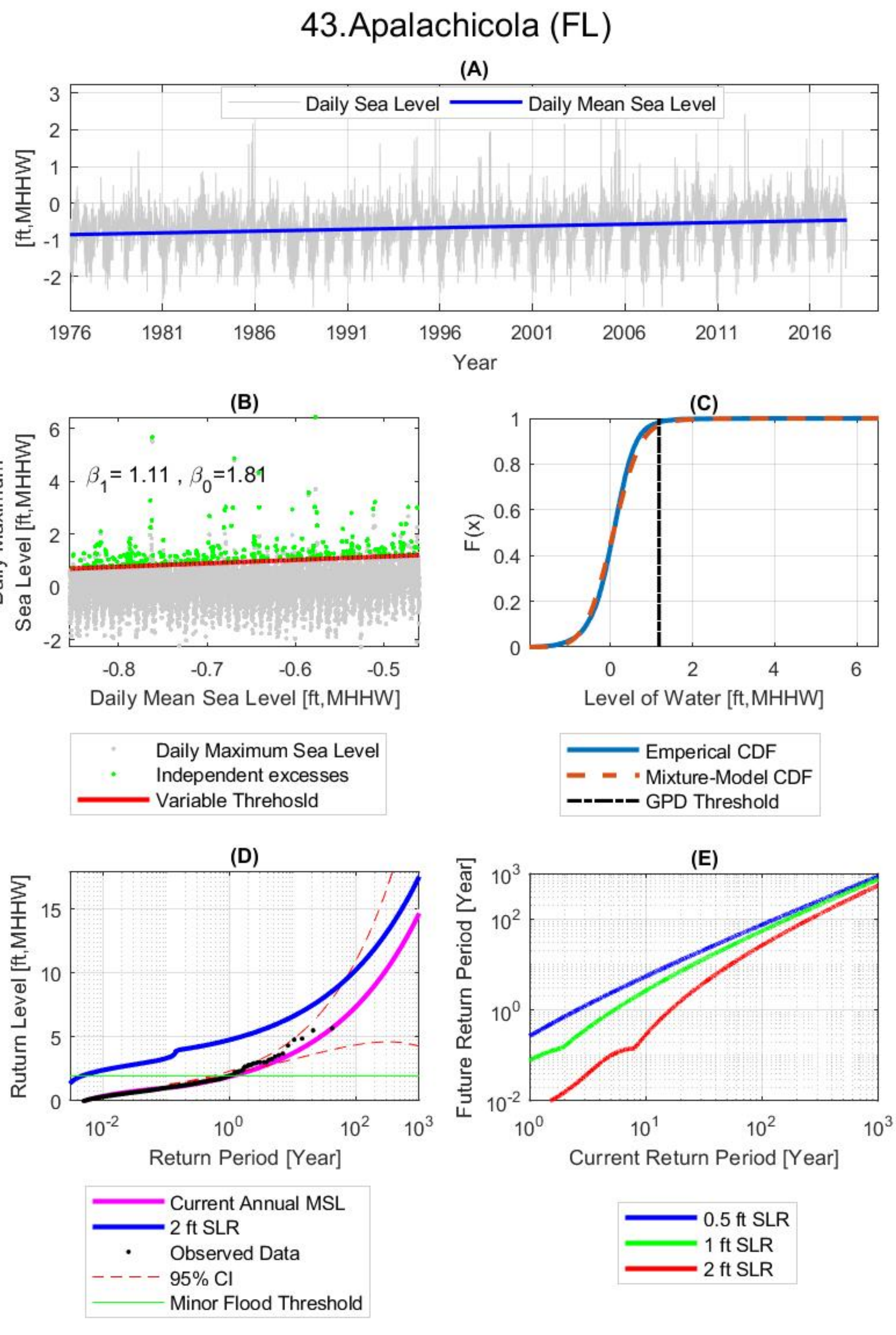

Figure A44. Apalachicola (FL) station

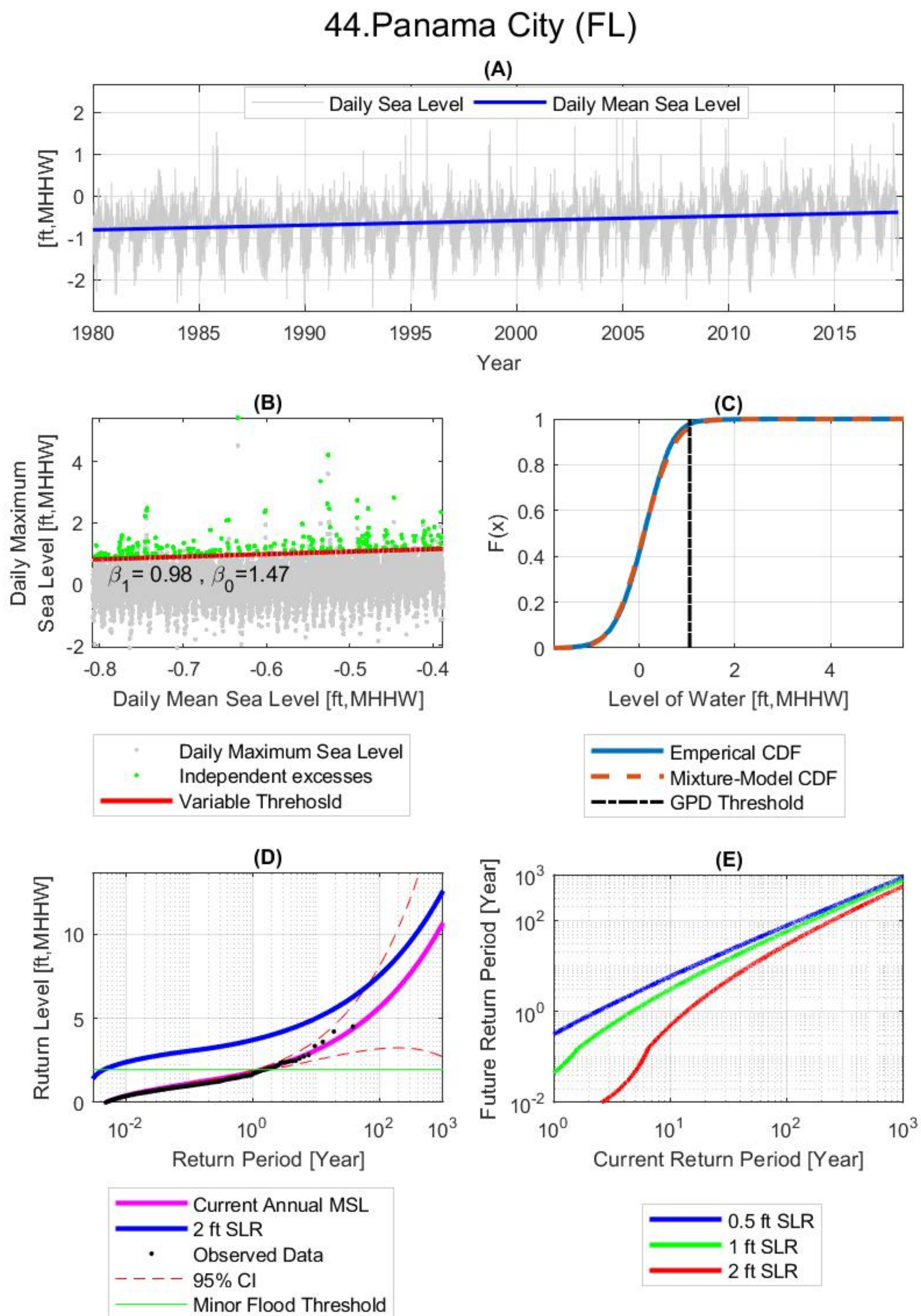

Figure A45. Panama City (FL) station

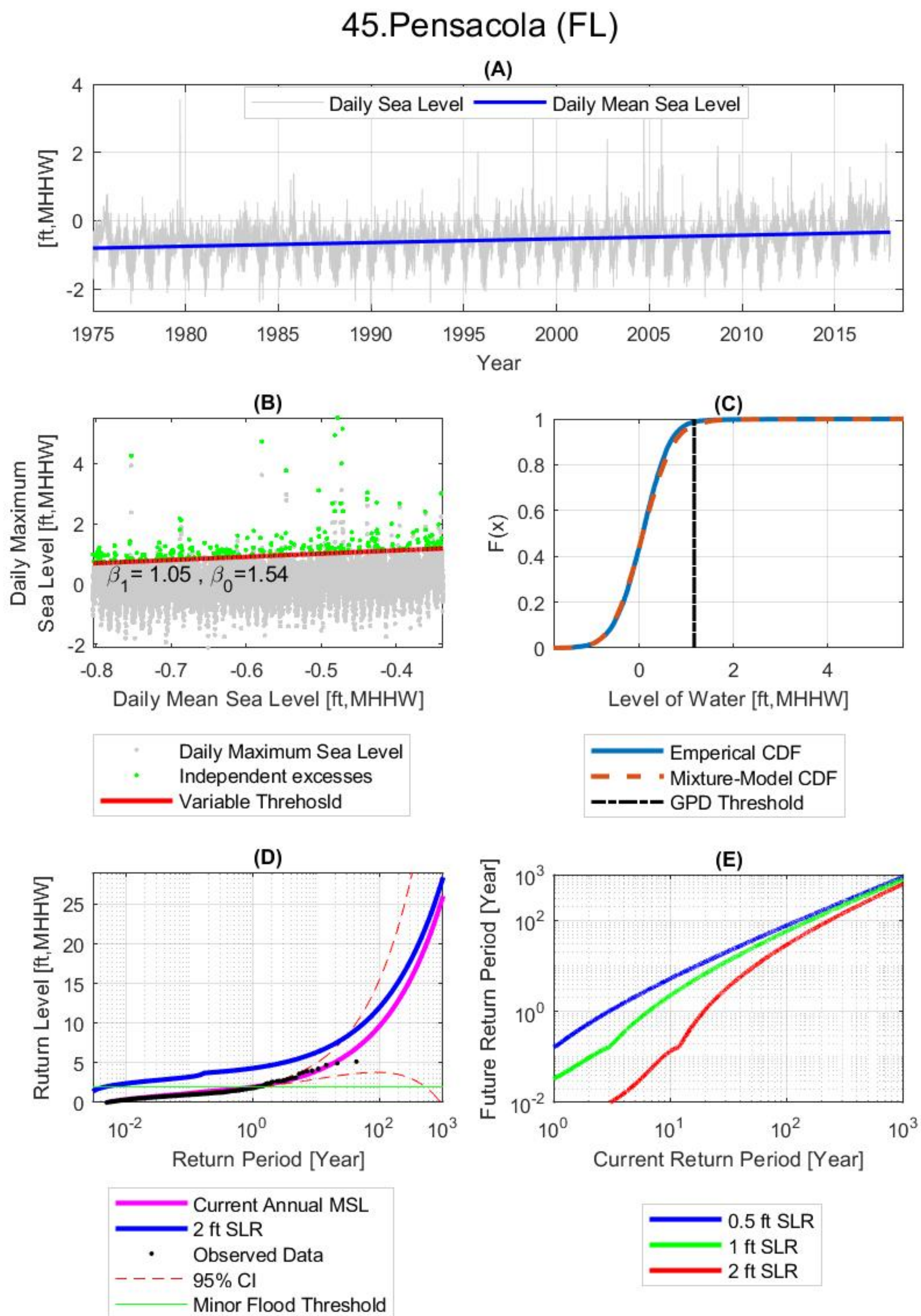

Figure A46. Pensacola (FL) station

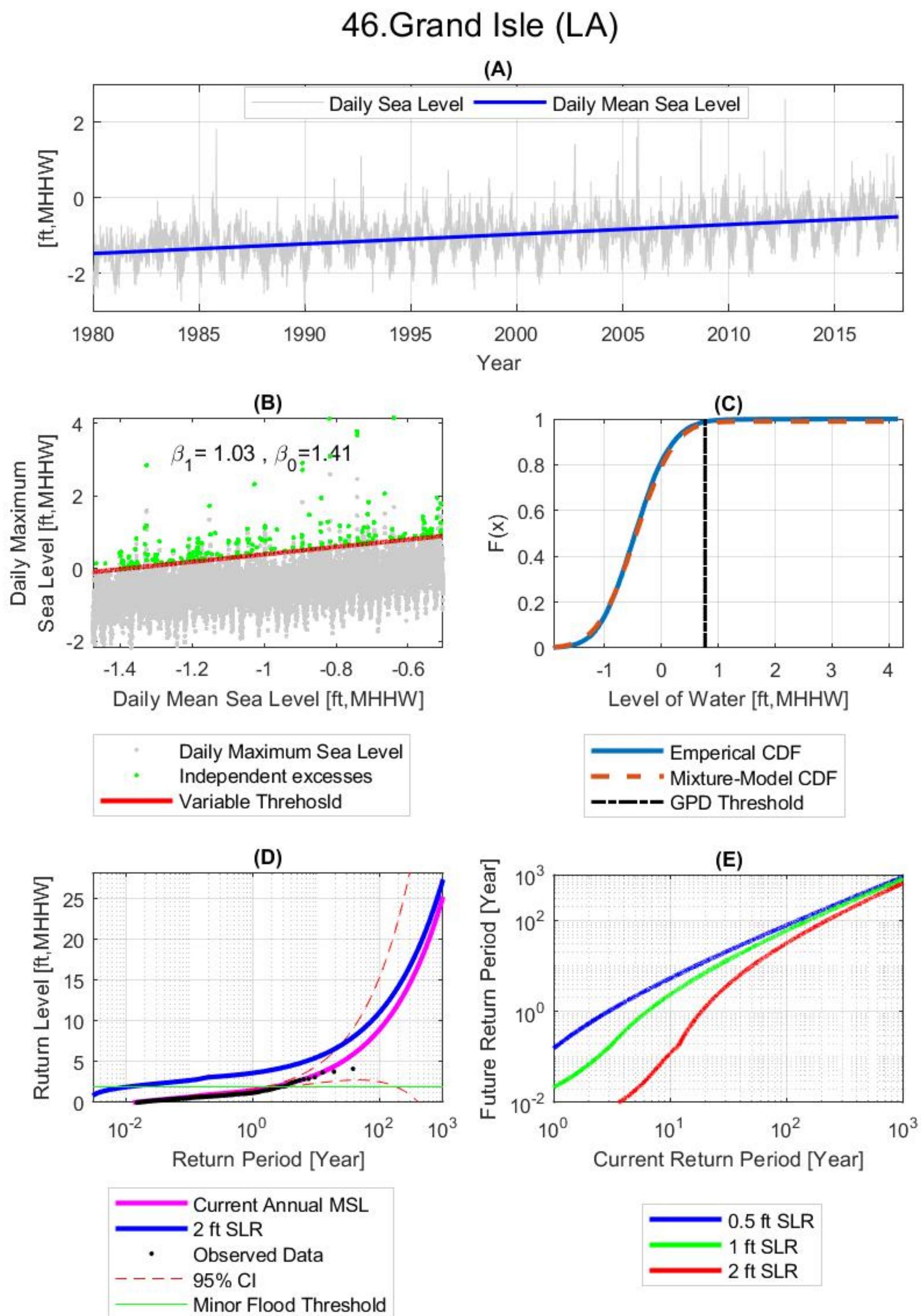

Figure A47. Grand Isle (LA) station

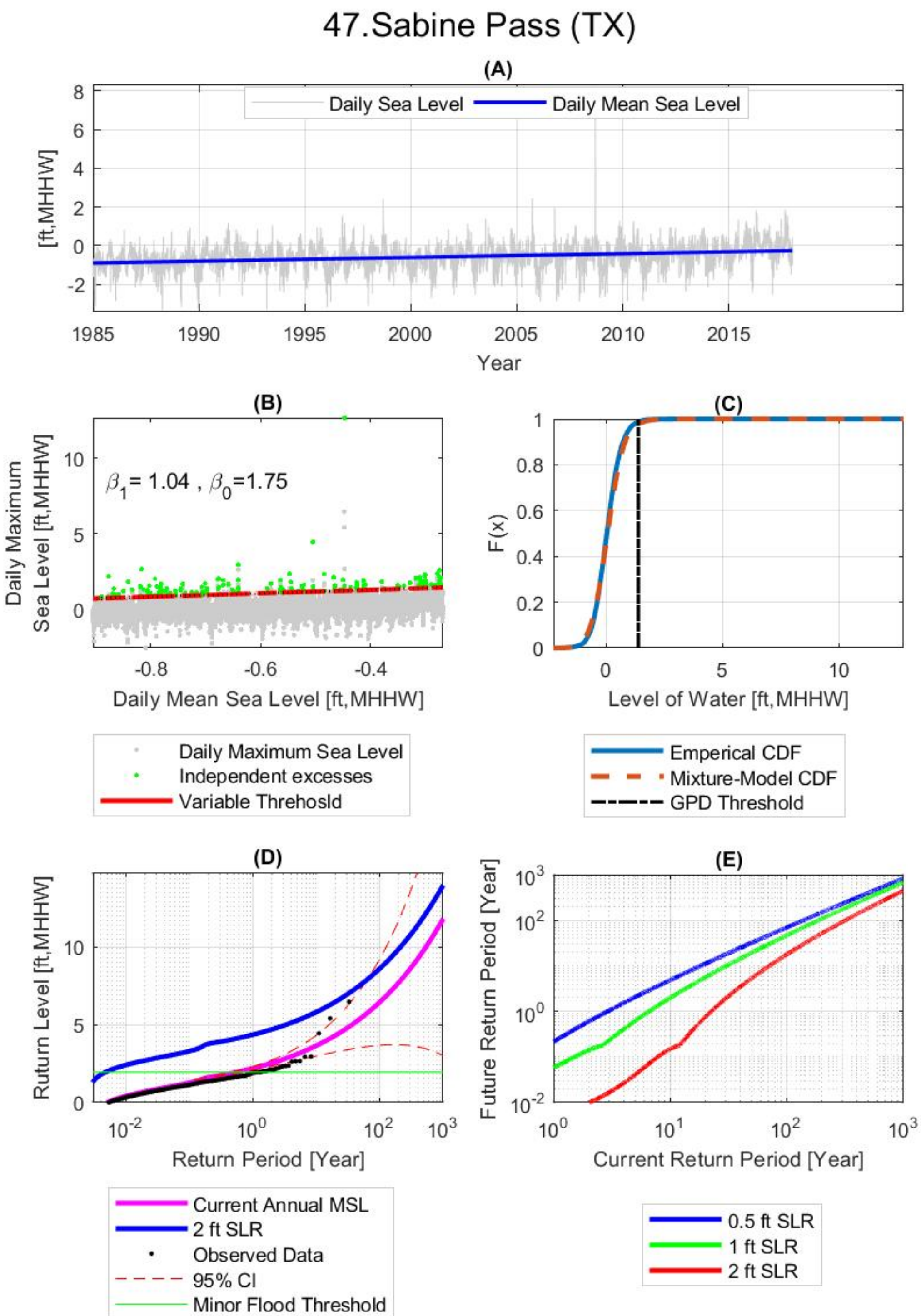

Figure A48. Sabine Pass (TX) station

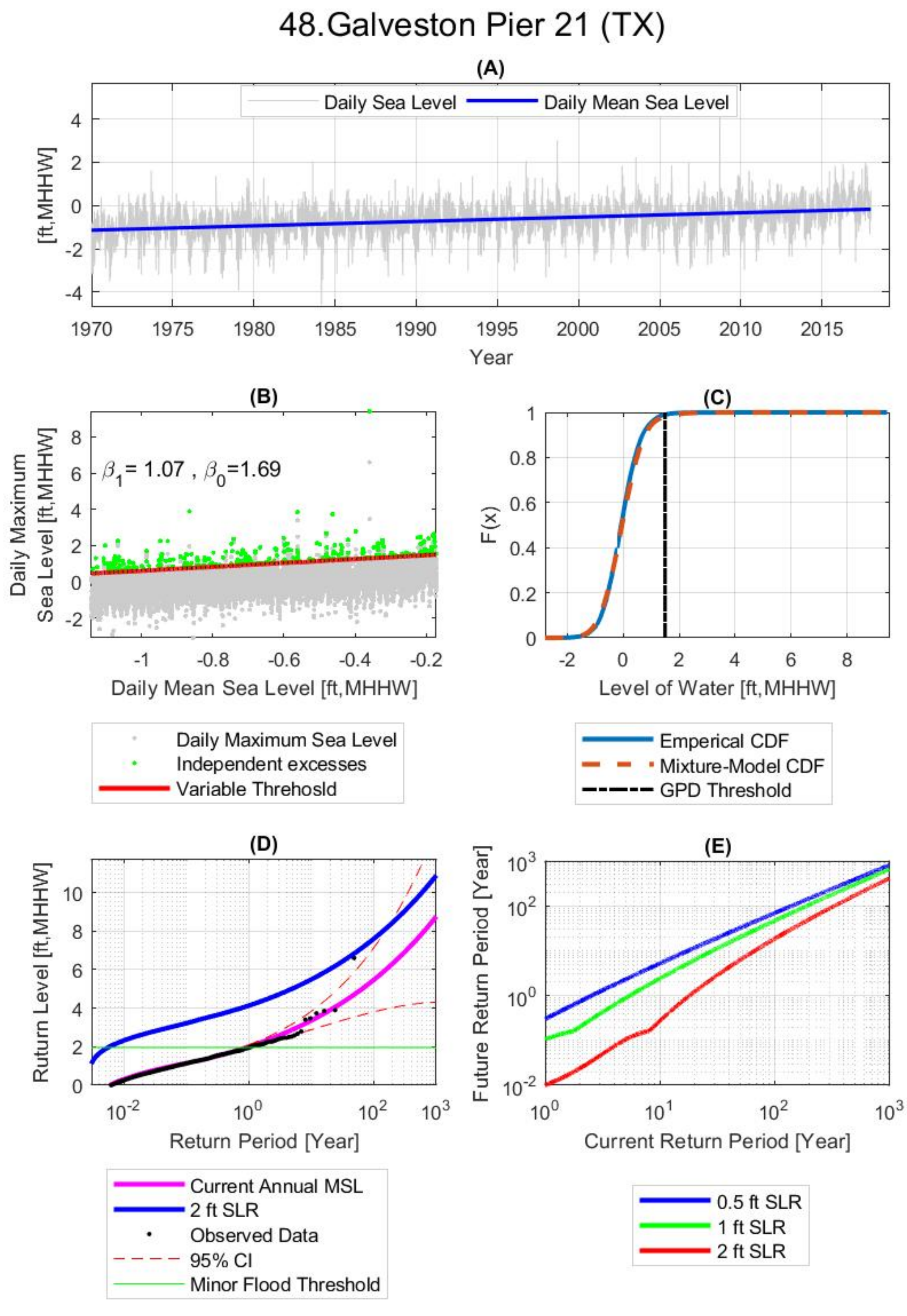

Figure A49. Galveston Pier 21 (TX) station

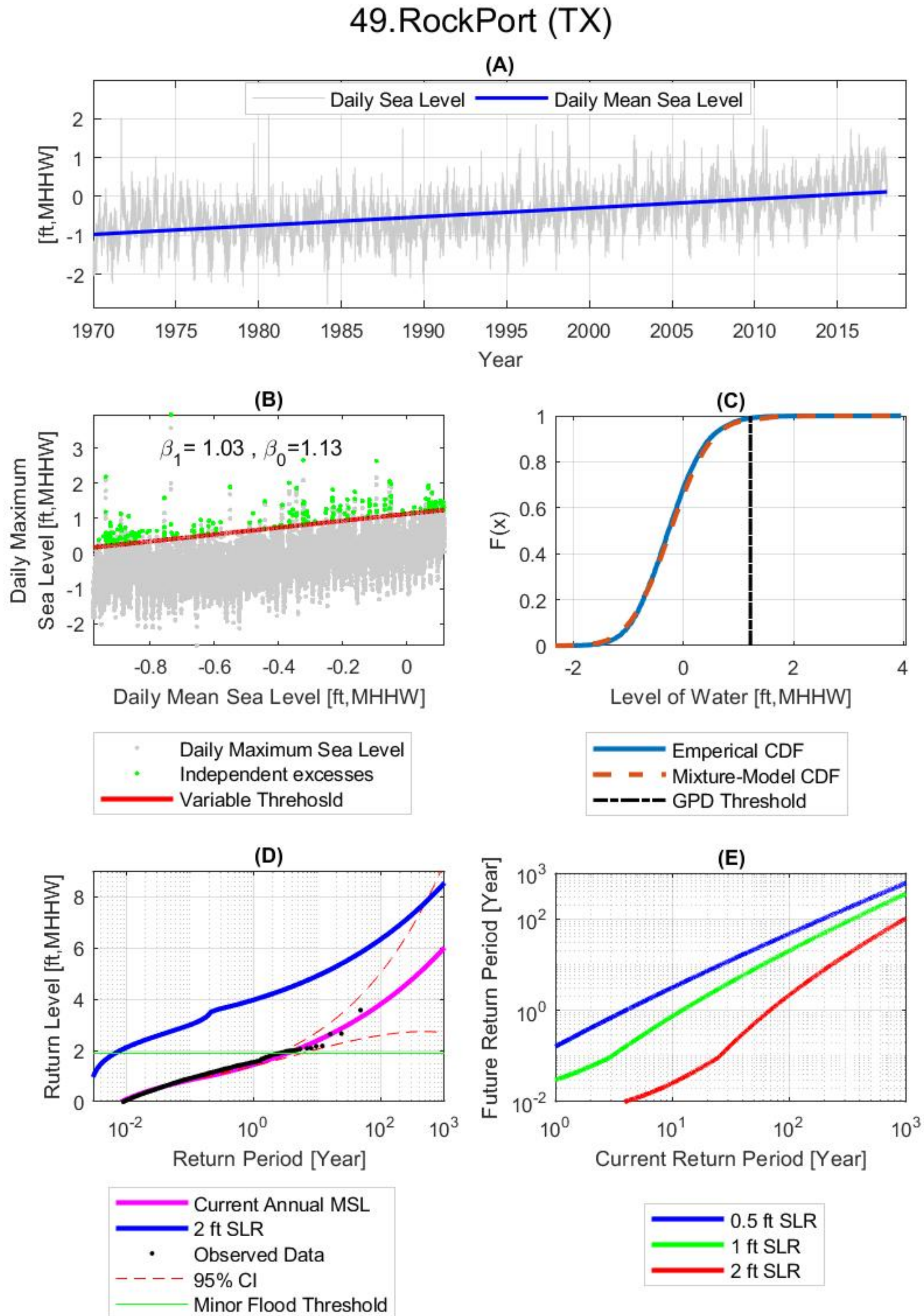

Figure A50. RockPort (TX) station

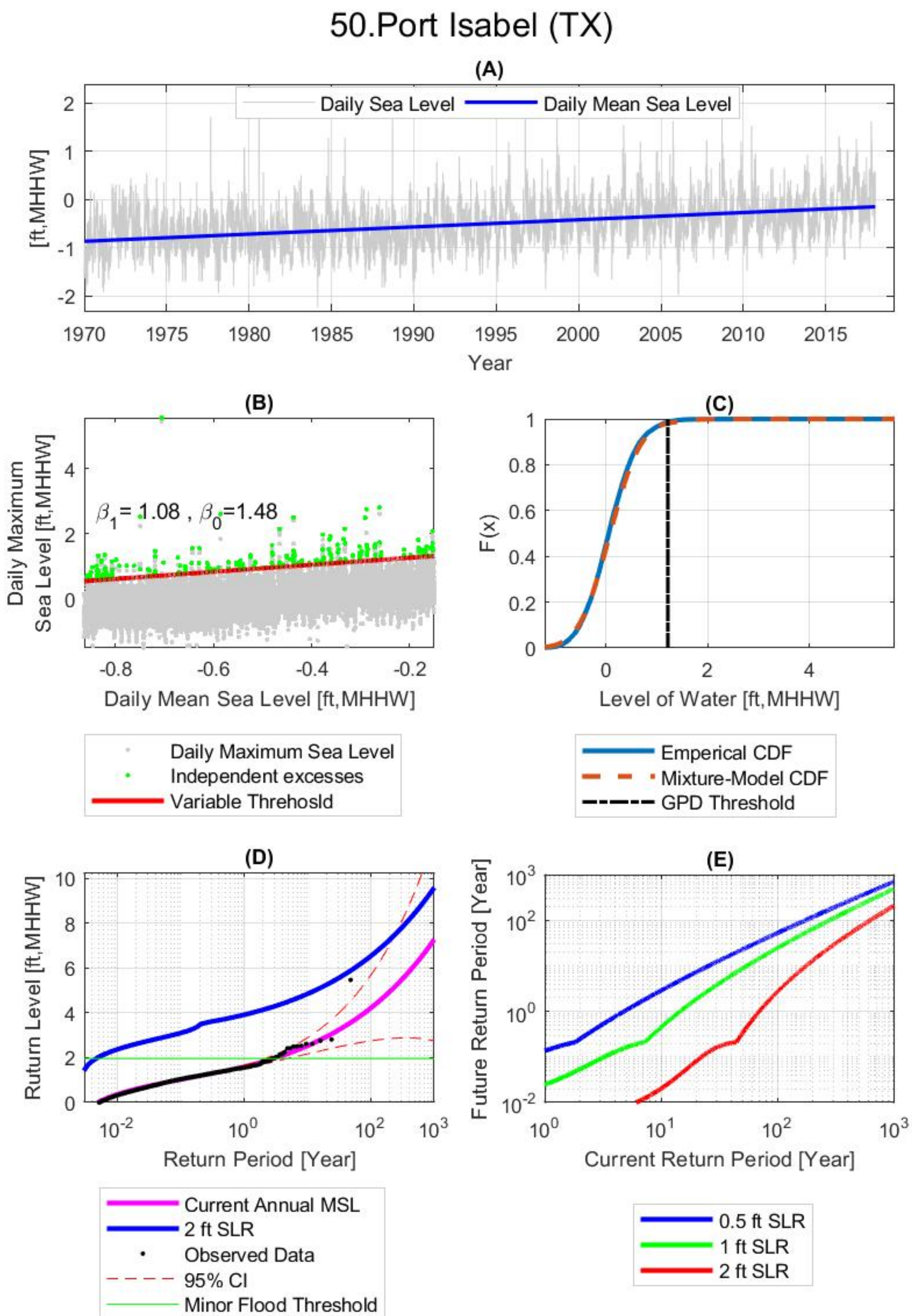

Figure A51. Port Isabel (TX) station

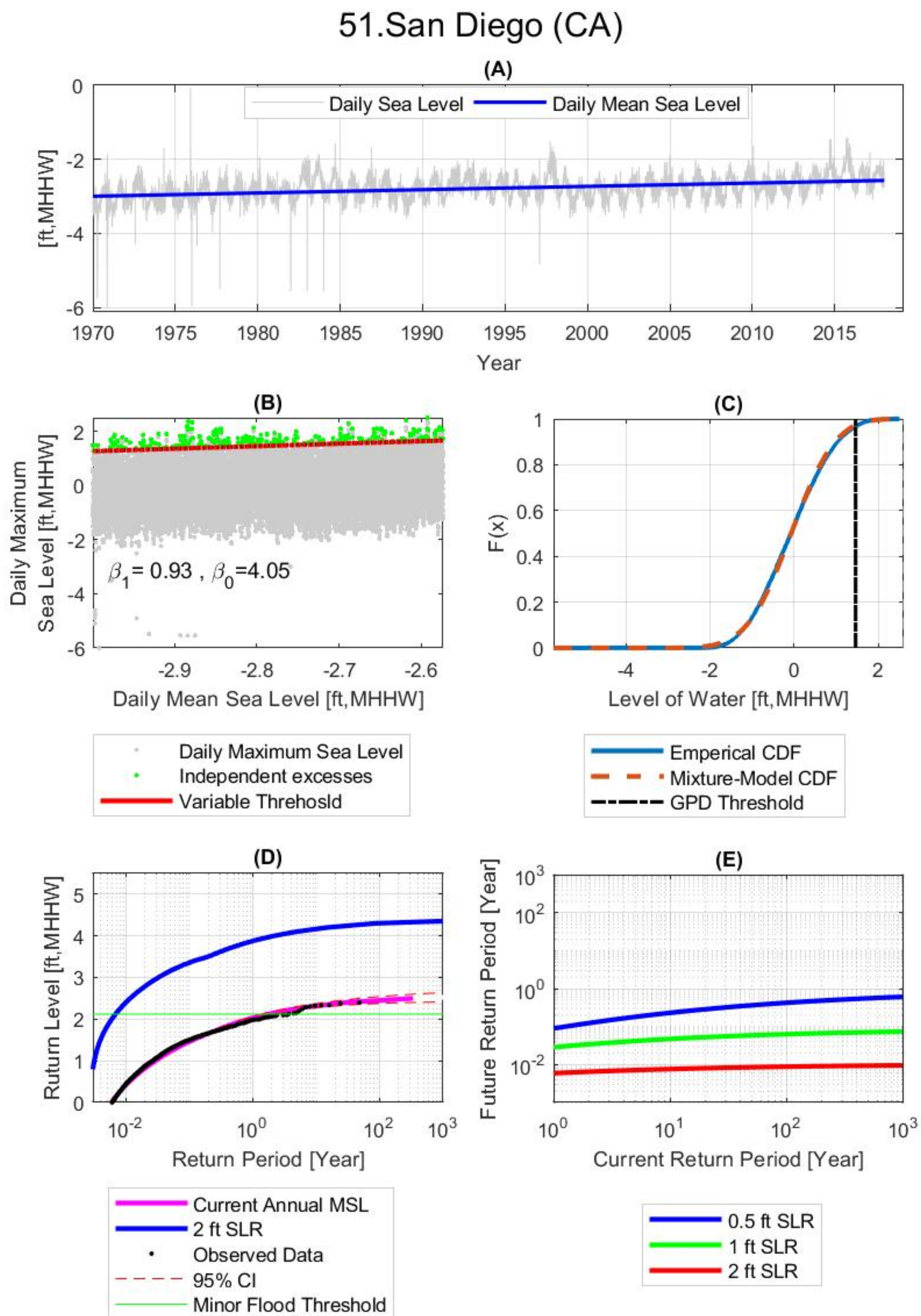

Figure A52. San Diego (CA) station

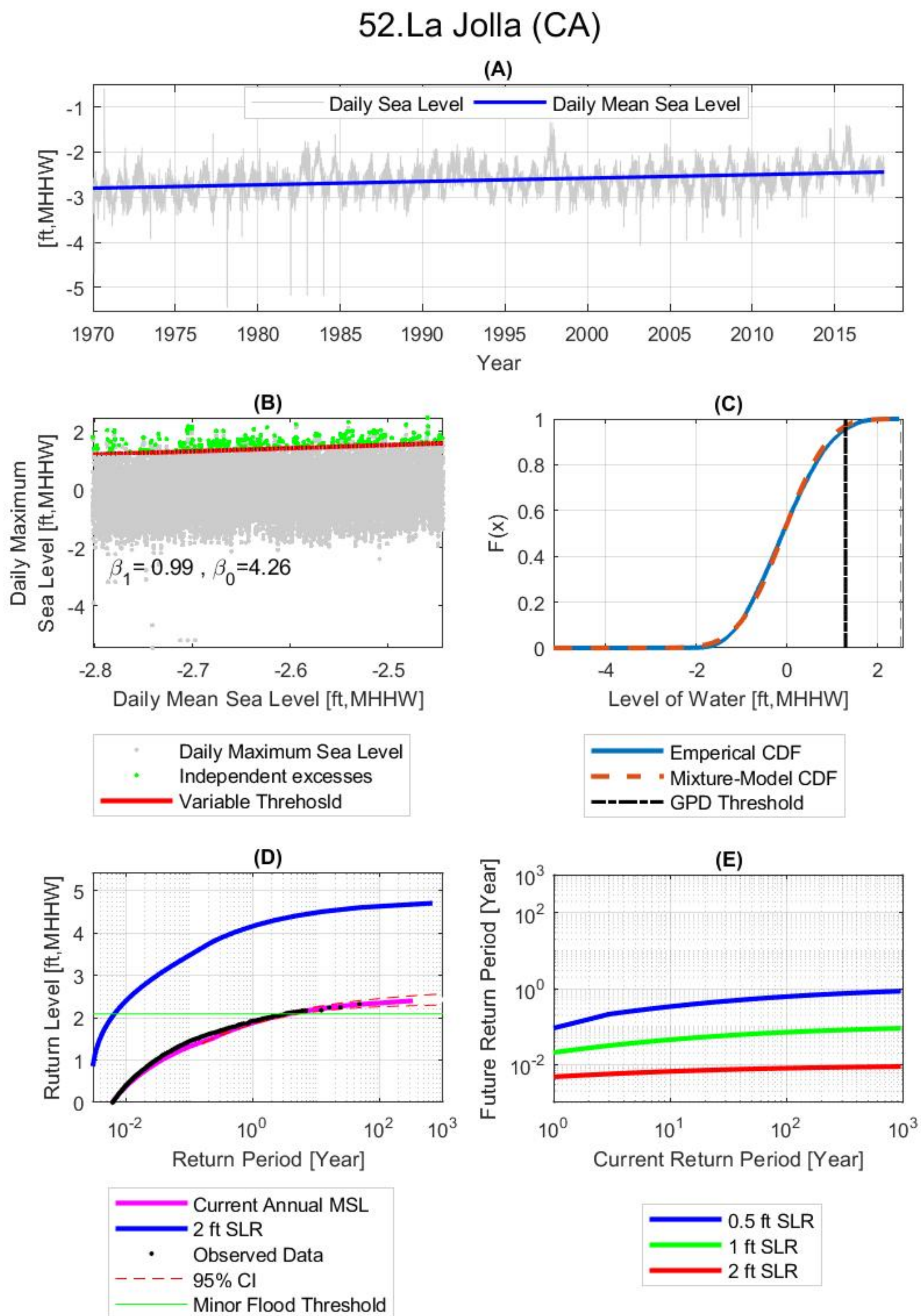

Figure A53. La Jolla (CA) station

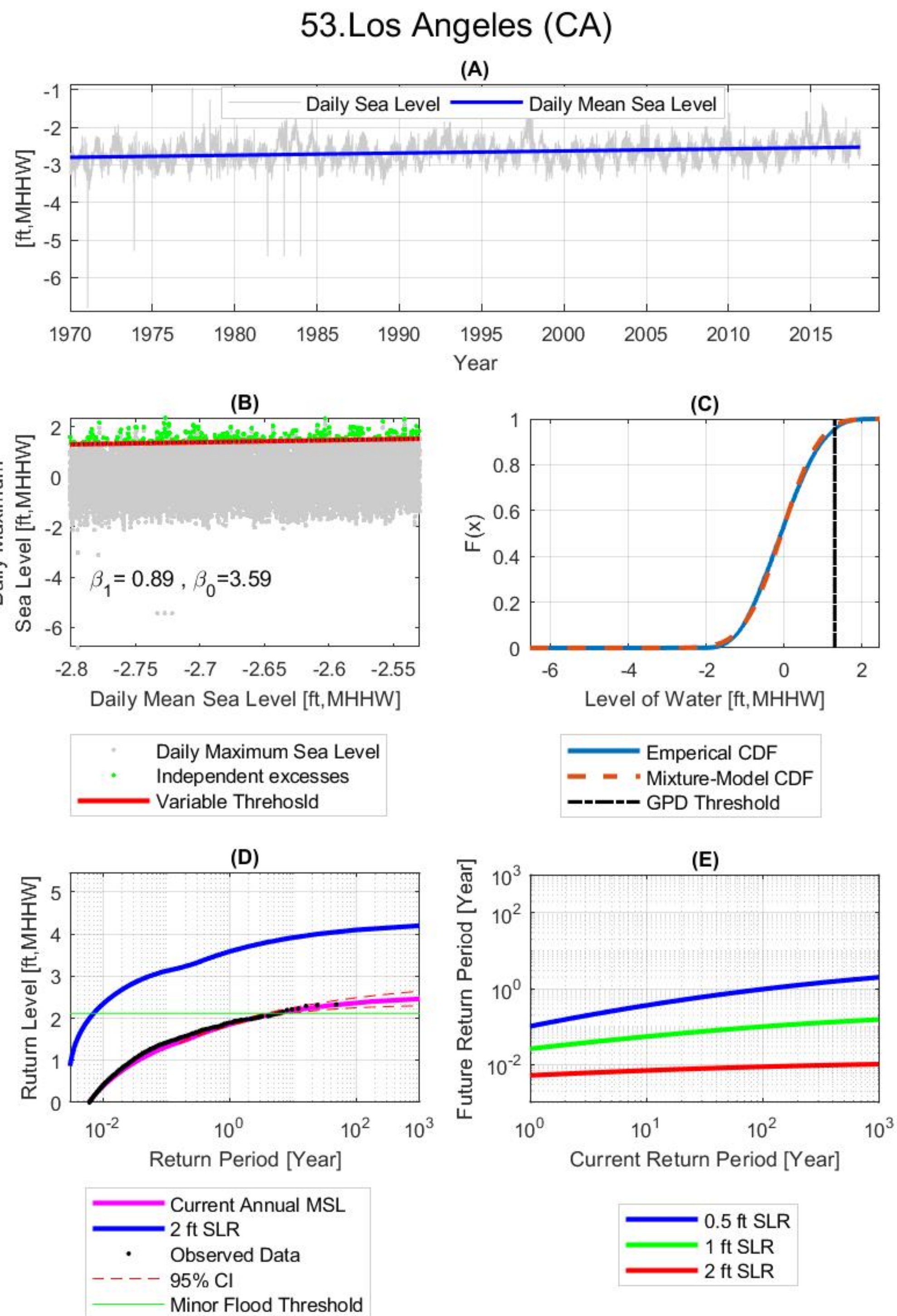

Figure A54. Los Angeles (CA) station

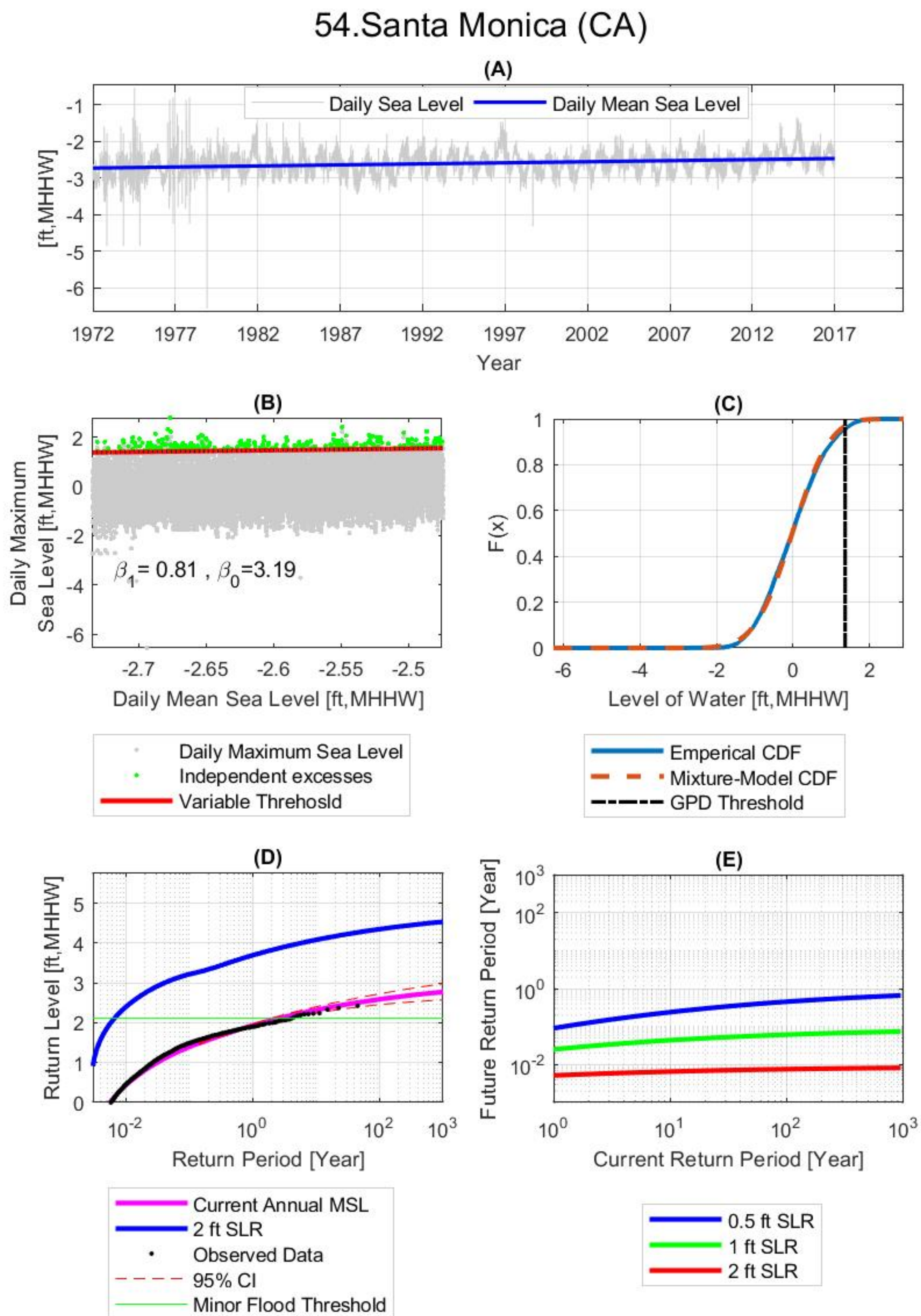

Figure A55. Santa Monica (CA) station

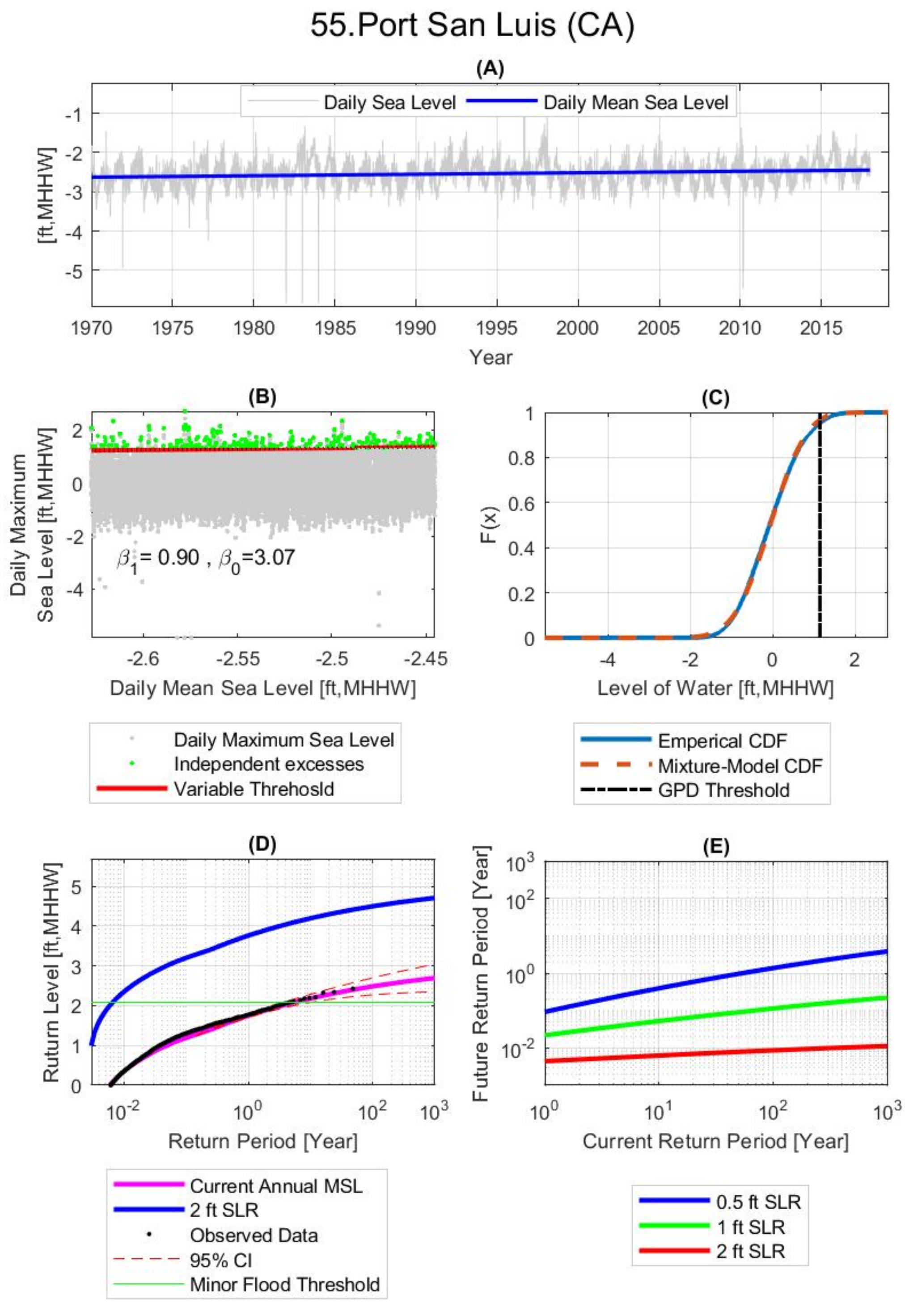

Figure A56. Port San Luis (CA) station

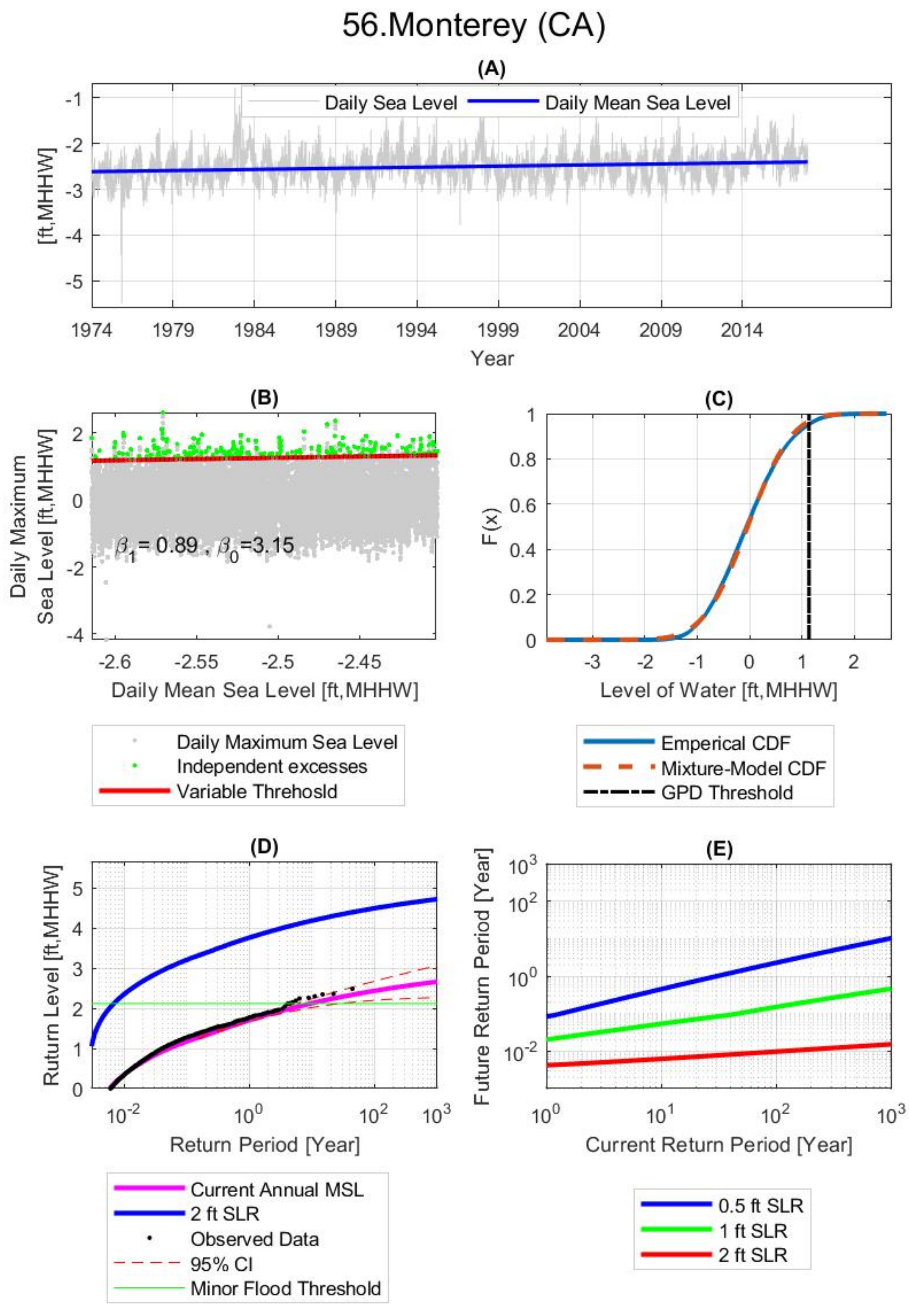

Figure A57. Monterey (CA) station

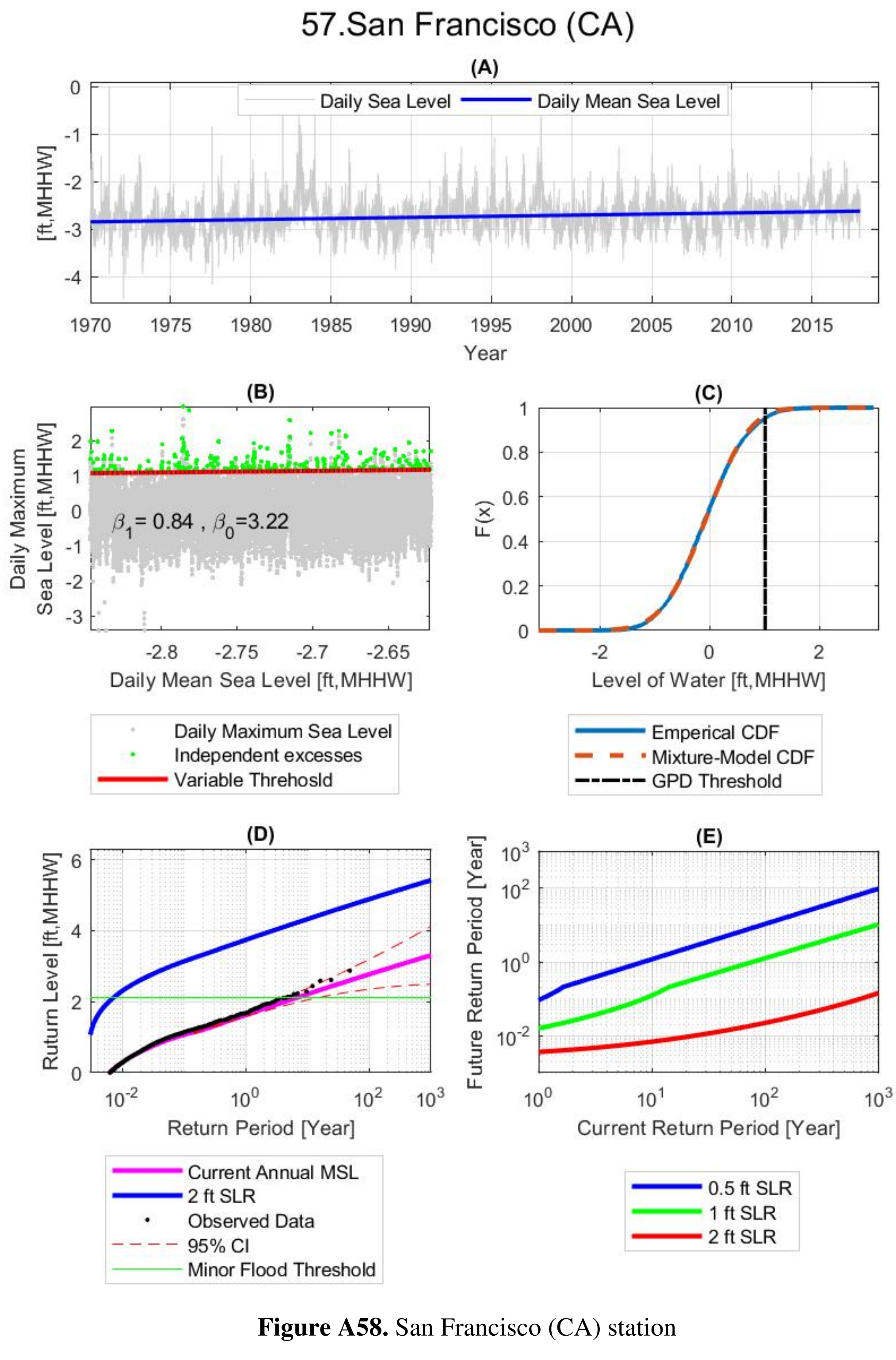

Figure A58. San Francisco (CA) station

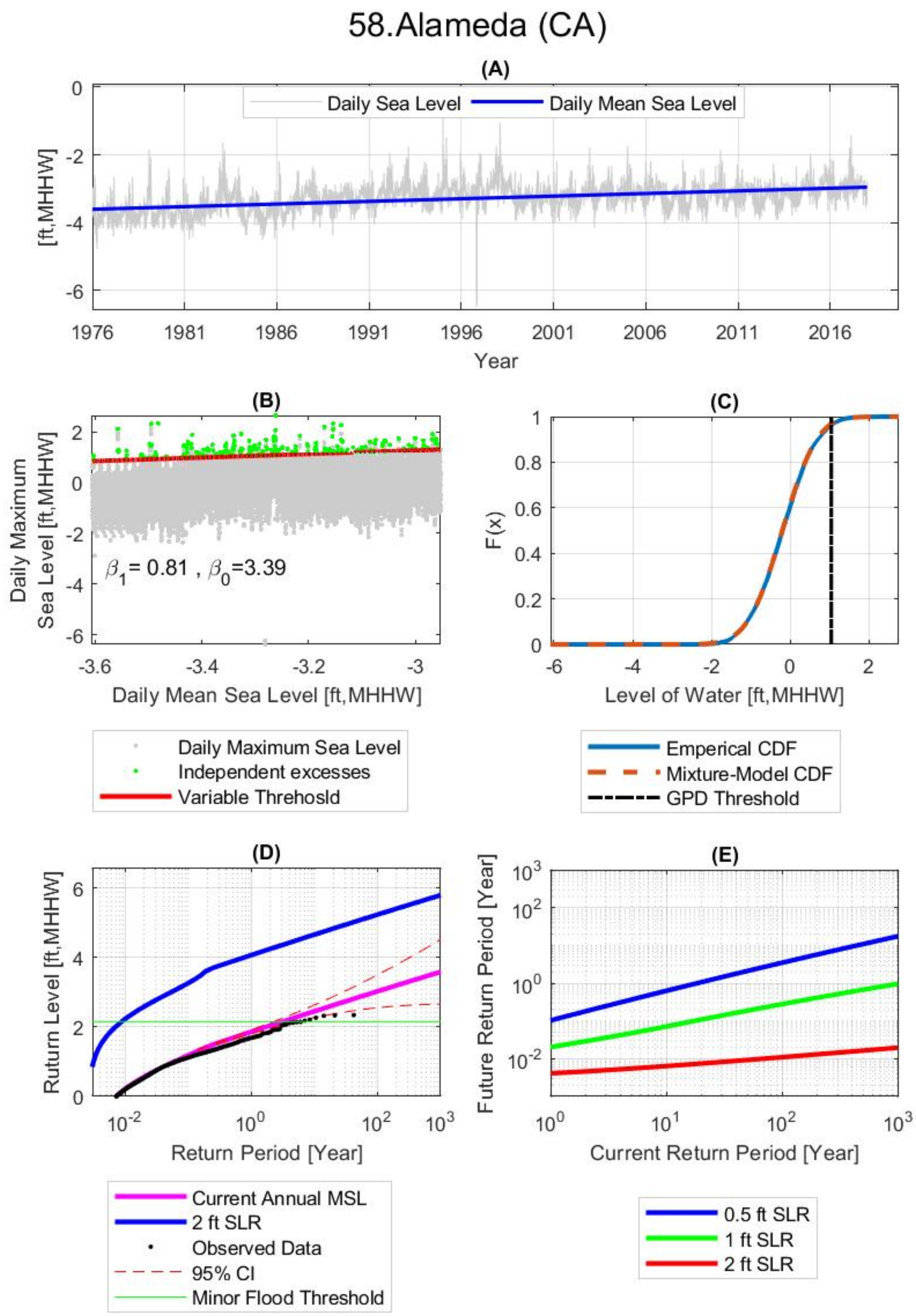

Figure A59. Alameda (CA) station

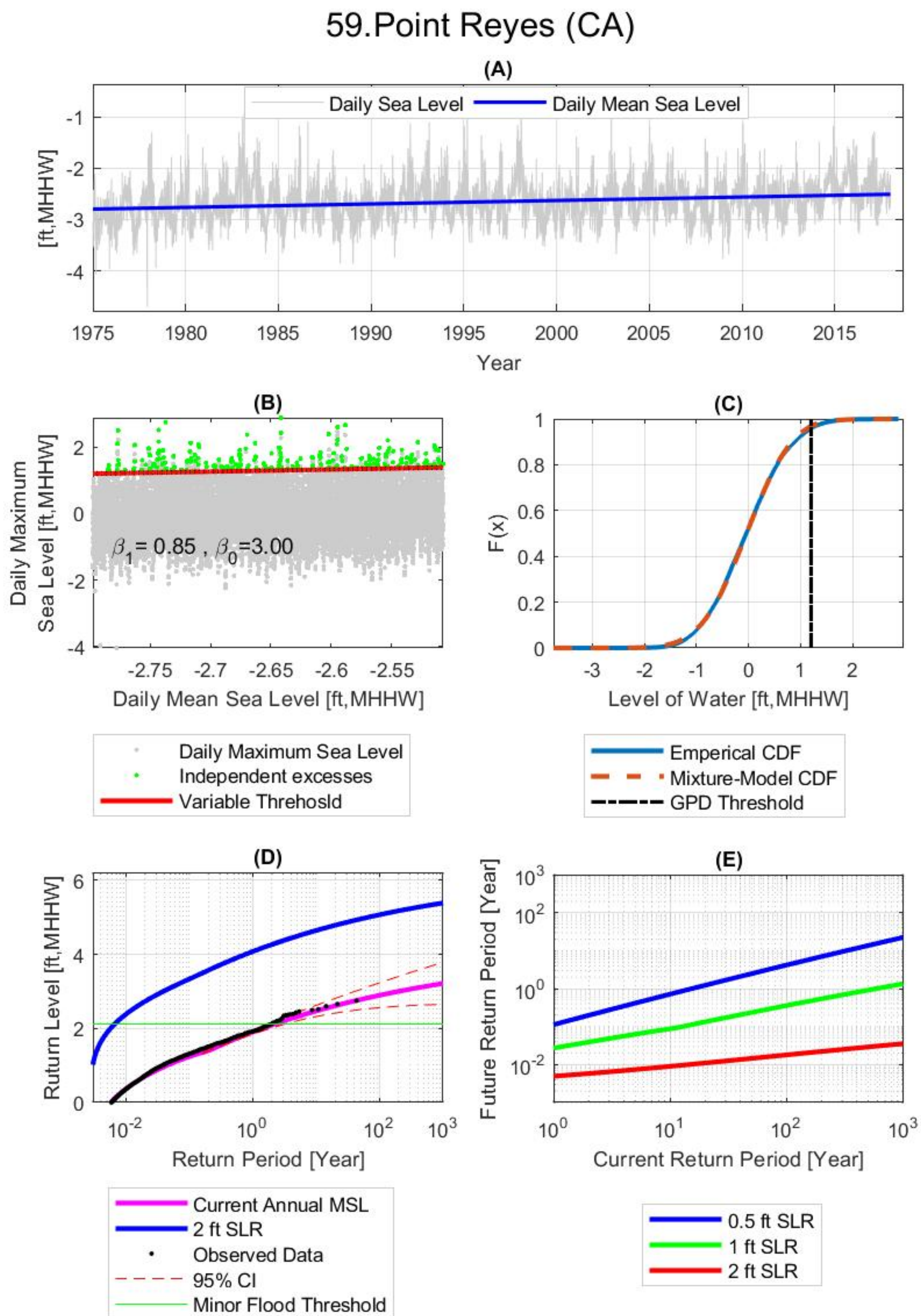

Figure A60. Point Reyes (CA) station

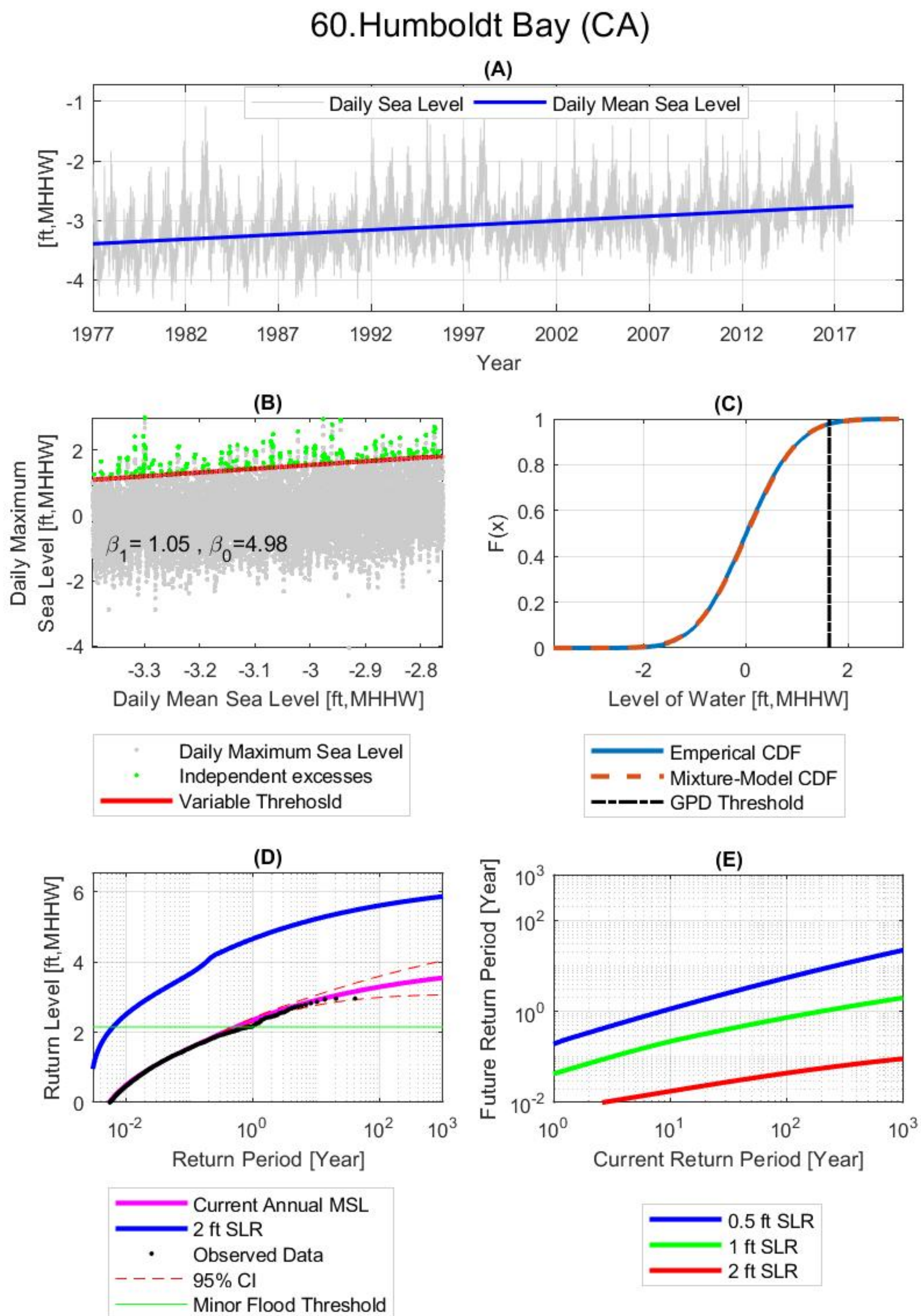

Figure A61. Humboldt Bay (CA) station

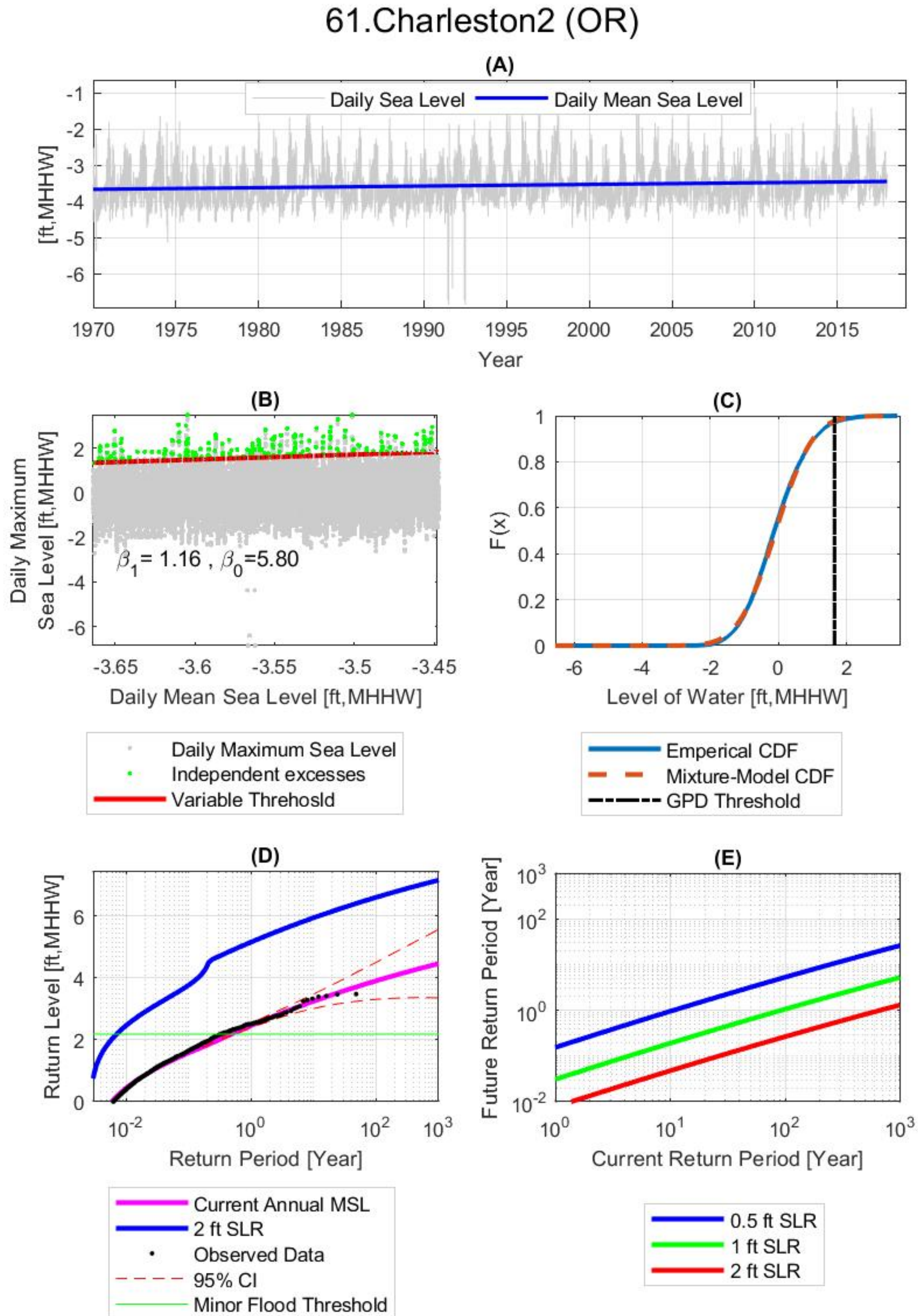

Figure A62. Charleston2 (OR) station

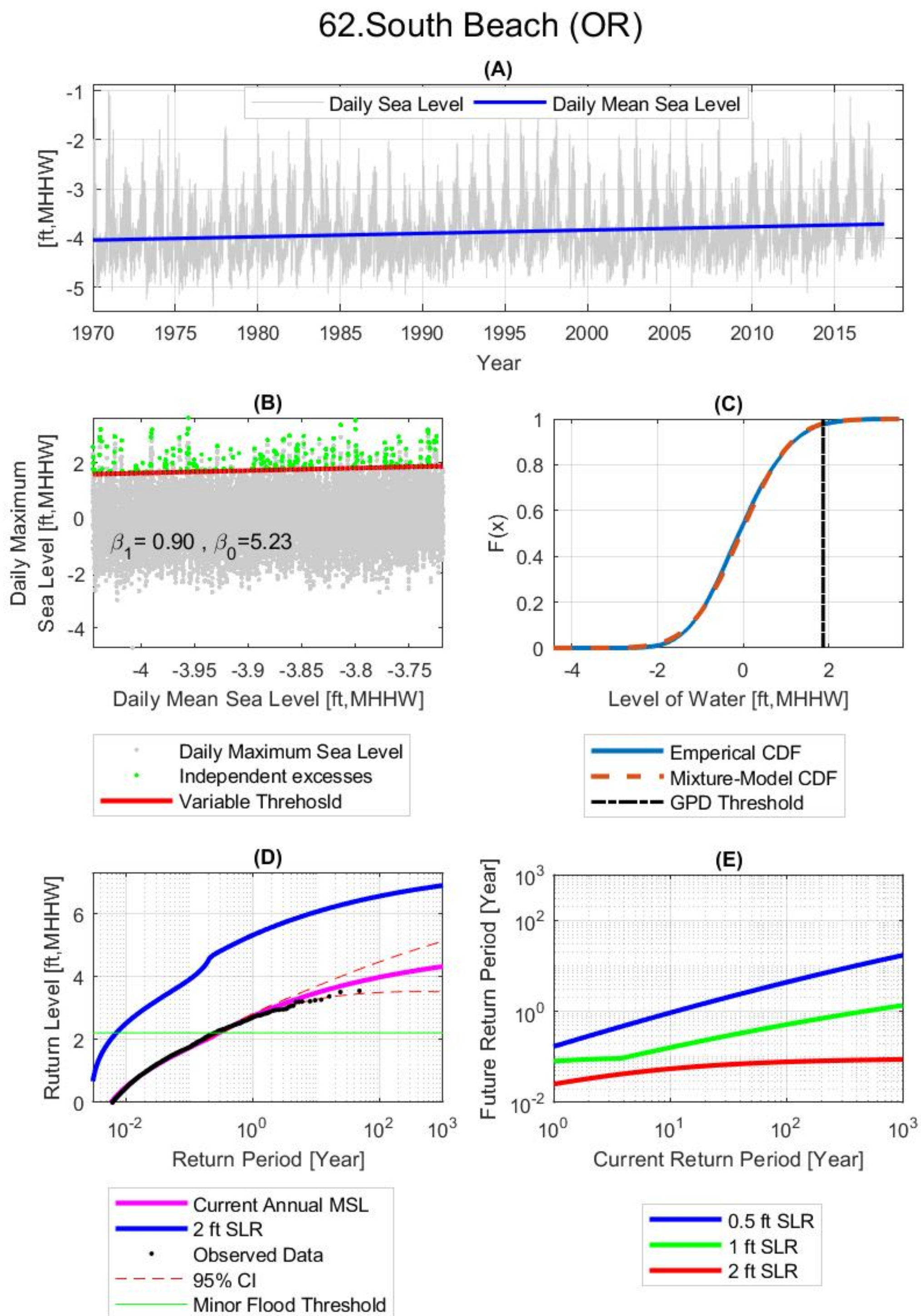

Figure A63. South Beach (OR) station

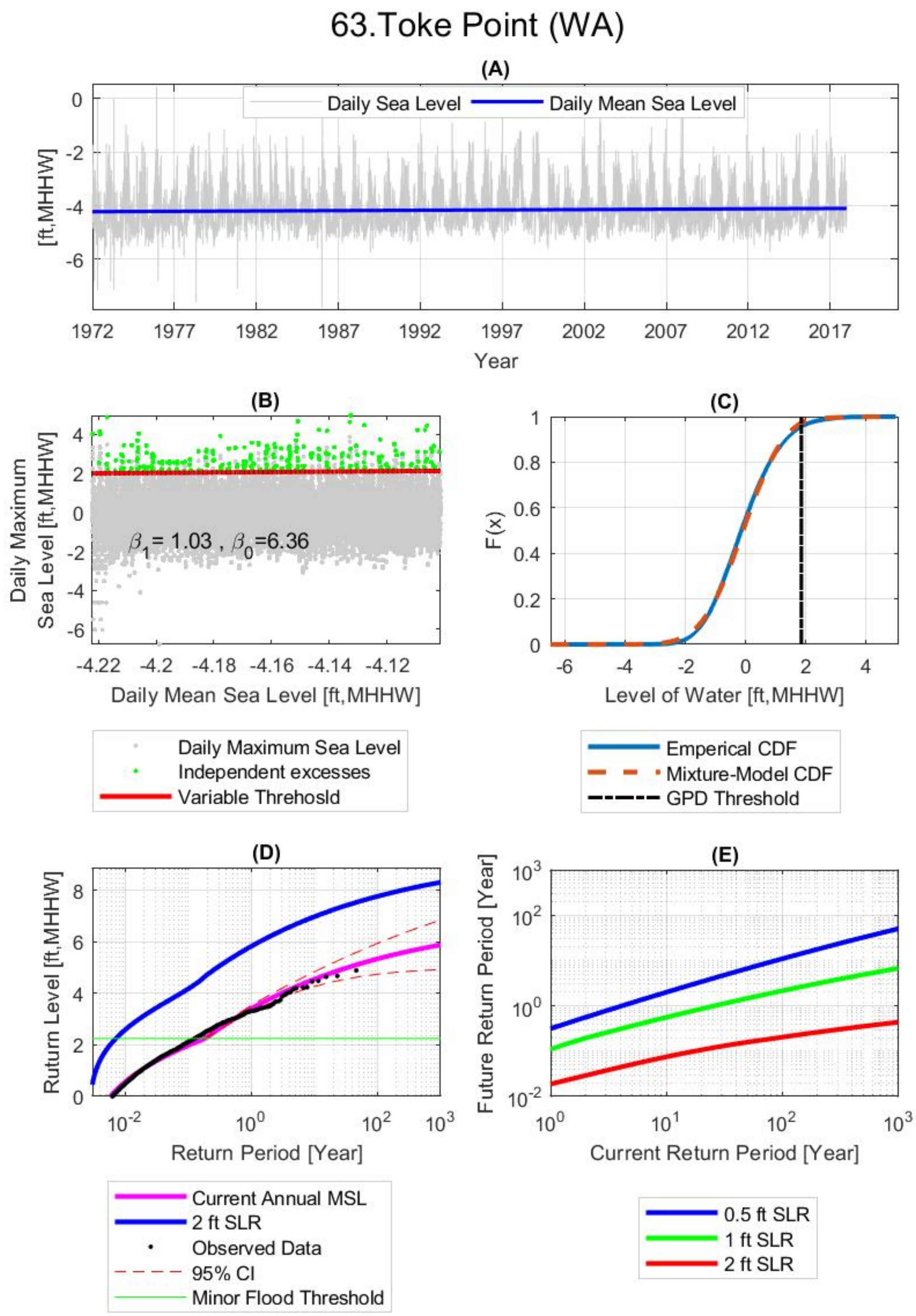

Figure A64. Toke Point (WA) station

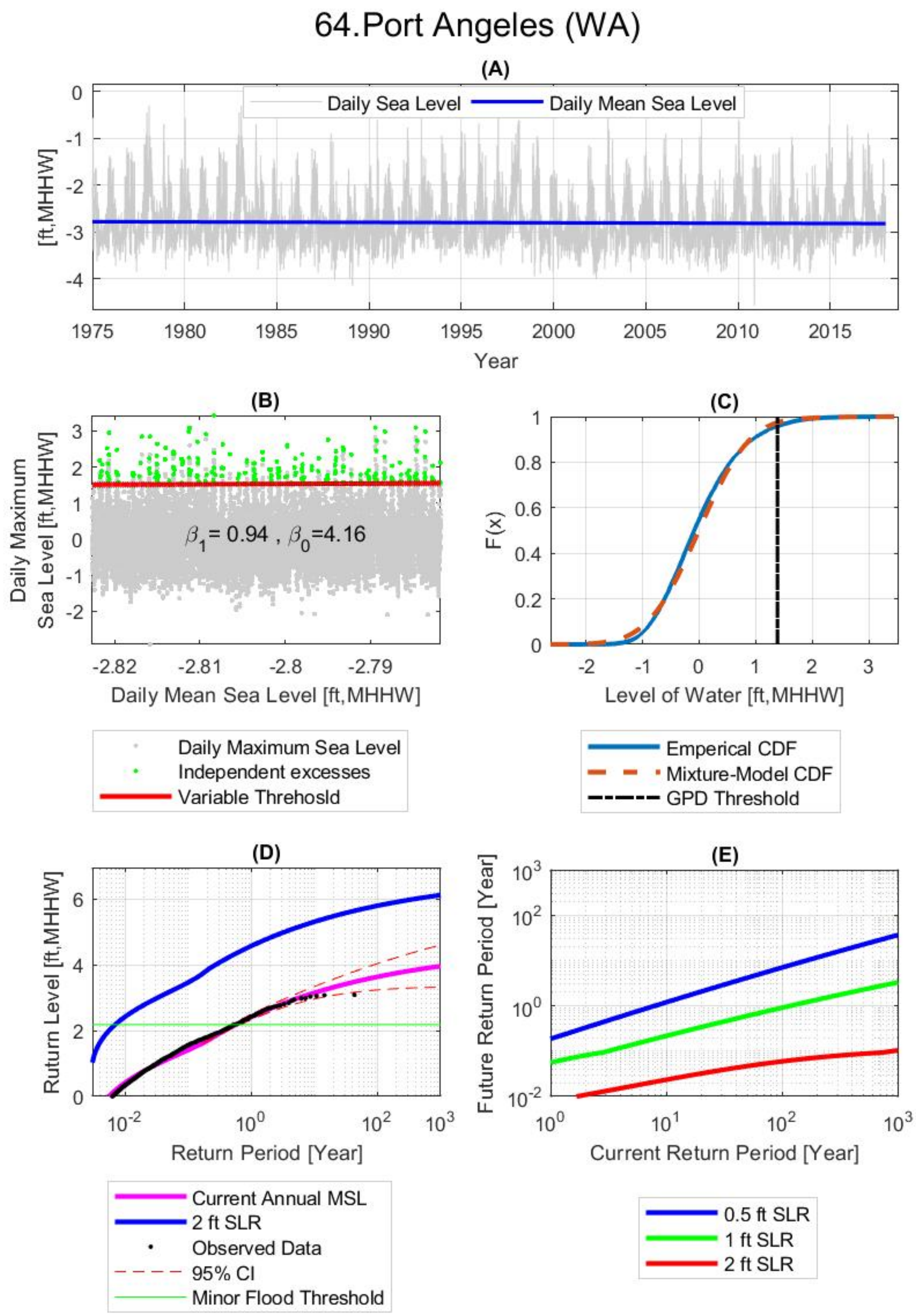

Figure A65. Port Angeles (WA) station

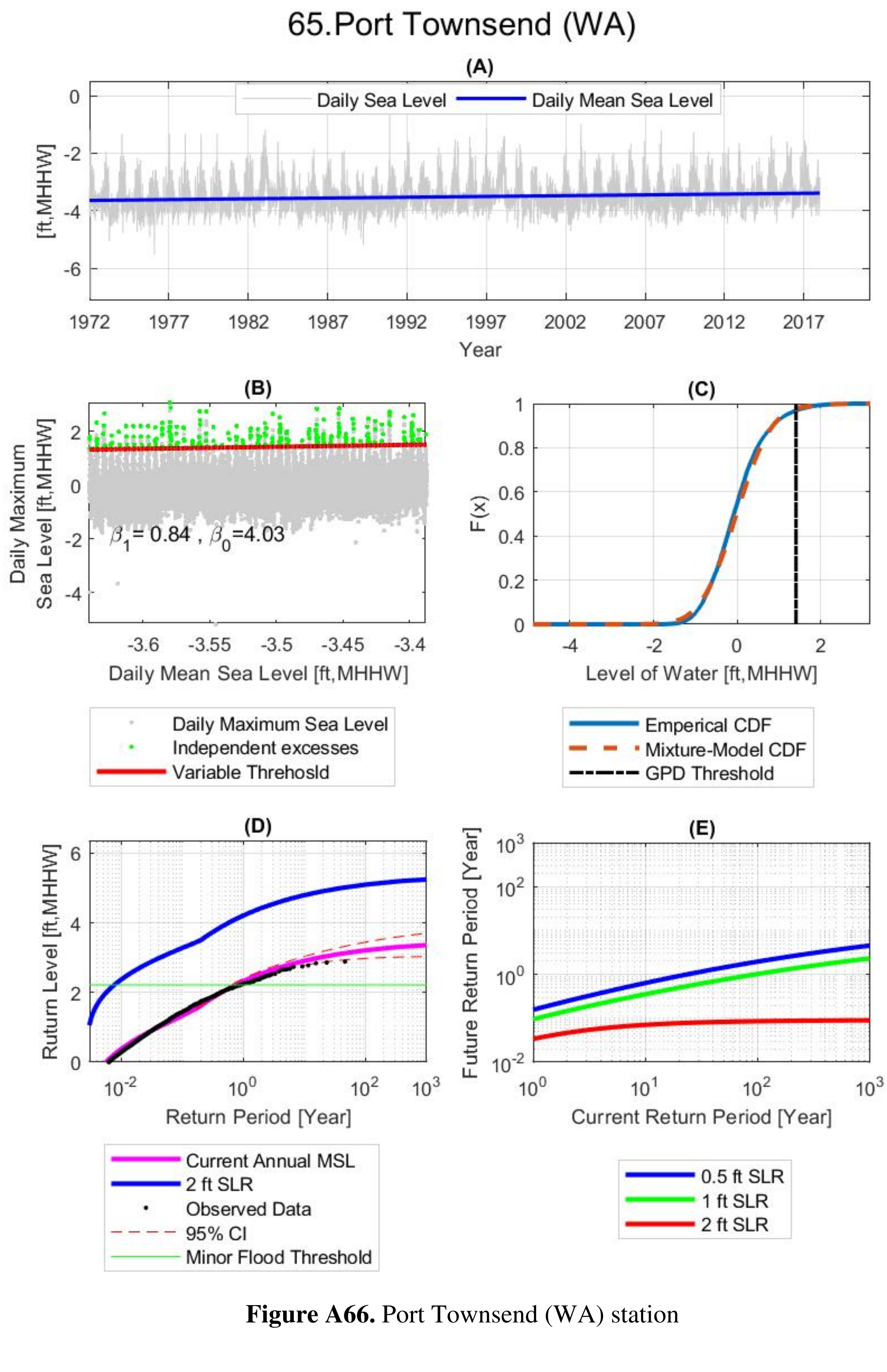

Figure A66. Port Townsend (WA) station

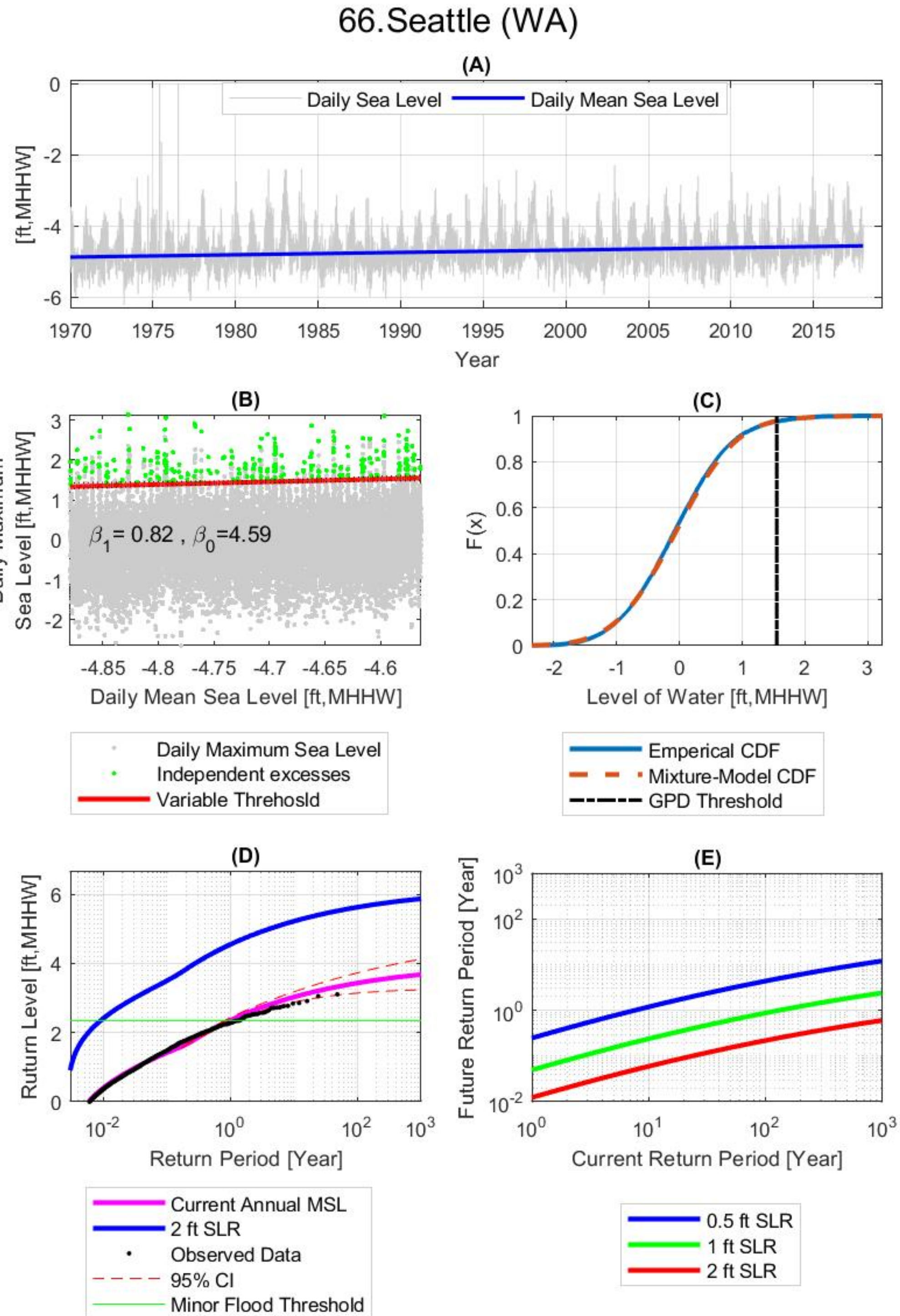

Figure A67. Seattle (WA) station

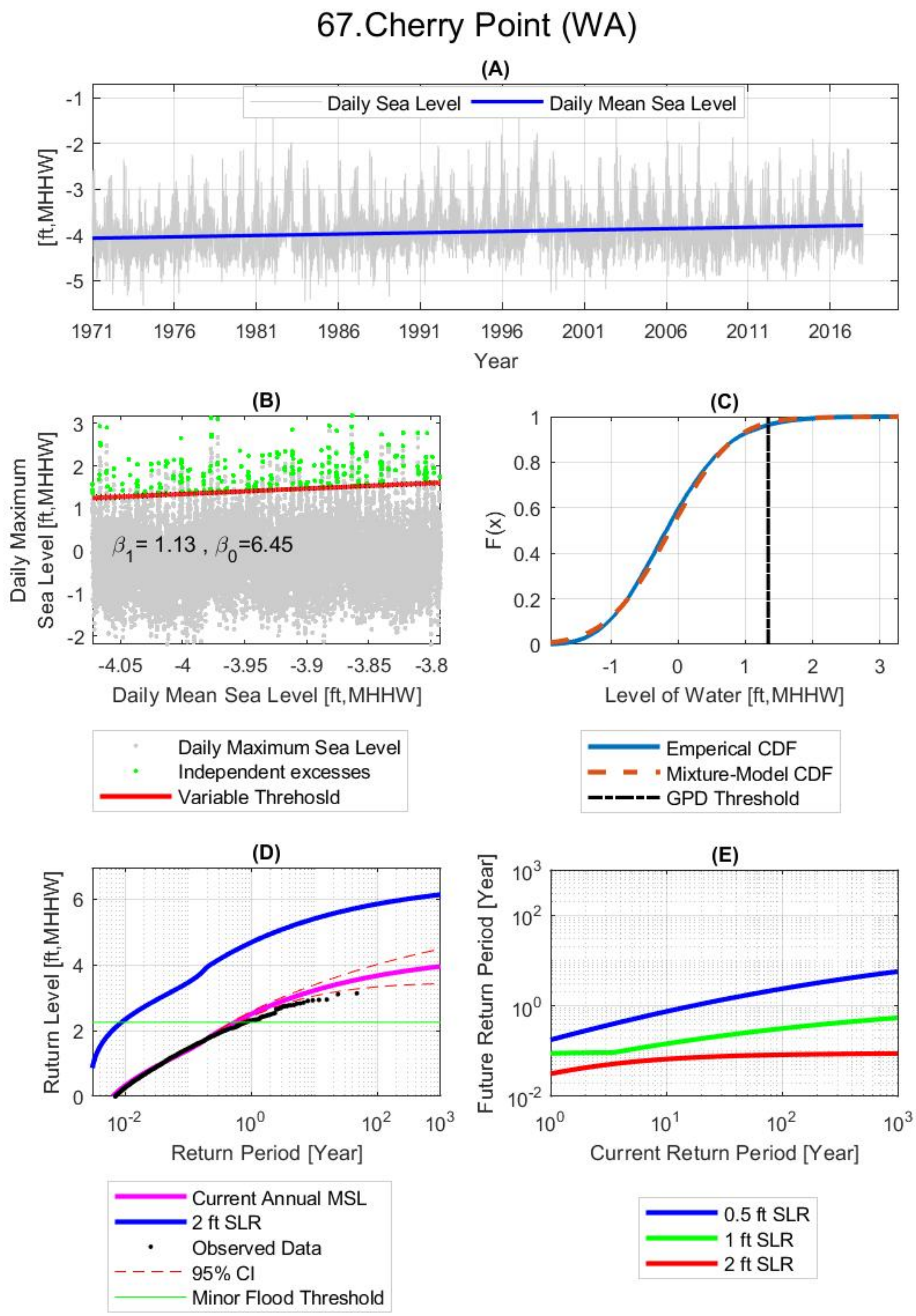

Figure A68. Cherry Point (WA) station

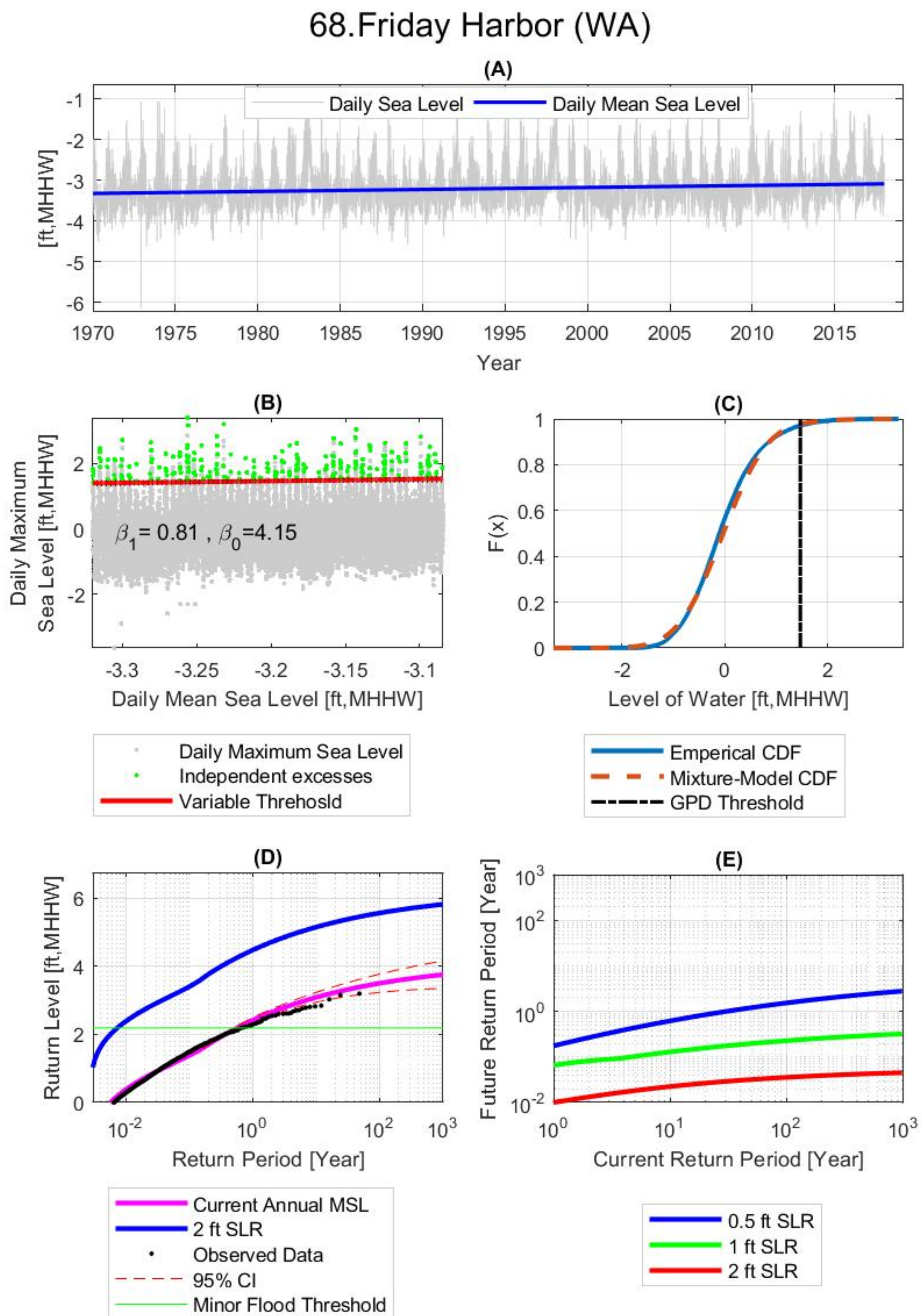

Figure A69. Friday Harbor (WA) station

Table A1. Summary of mixture model parameters (Feet above MHHW)

Station	Station ID	α (CI)	ξ (CI)	φ	μ	σ
Bar Harbor, ME	8413320	0.41 (0.36, 0.49)	-0.14 (-0.25, -0.06)	0.016	-0.09	1
Portland, ME	8418150	0.36 (0.31, 0.42)	-0.05 (-0.16, 0.05)	0.017	0	0.89
Boston, MA	8443970	0.37 (0.31, 0.44)	0.07(-0.05, 0.19)	0.016	-0.01	0.91
Woods Hole, MA	8447930	0.32 (0.27, 0.38)	0.19(0.08, 0.35)	0.021	0.01	0.57
Nantucket Island, MA	8449130	0.35 (0.28, 0.38)	-0.01 (-0.03, 0.18)	0.020	0.02	0.55
Newport, RI	8452660	0.36 (0.3, 0.4)	0.11(-0.04, 0.18)	0.019	0.02	0.67
Providence, RI	8454000	0.4(0.34, 0.46)	0.14(0.03, 0.26)	0.020	0.01	0.73
New London, CT	8461490	0.37 (0.32, 0.43)	0.13(0.01, 0.24)	0.022	0.02	0.58
Bridgeport, CT	8467150	0.38 (0.33, 0.45)	0.15(0.03, 0.27)	0.021	-0.03	0.81
Montauk, NY	8510560	0.37 (0.31, 0.43)	0.16(0.03, 0.28)	0.022	0.05	0.59
Battery, NY	8518750	0.43 (0.37, 0.5)	0.11(0.01, 0.21)	0.019	0.04	0.76
Bergen Point, NY	8519483	0.47 (0.4, 0.55)	0.08(-0.02, 0.18)	0.018	0.07	0.78
Sandy Hook, NJ	8531680	0.44 (0.38, 0.51)	0.06(-0.04, 0.15)	0.019	0.02	0.8
Atlantic City, NJ	8534720	0.44 (0.38, 0.51)	0.02(-0.08, 0.12)	0.019	0	0.78
Cape May, NJ	8536110	0.36 (0.31, 0.43)	0.05(-0.07, 0.18)	0.019	0.02	0.73
Reedy Point, DE	8551910	0.32 (0.28, 0.38)	0.03(-0.08, 0.13)	0.019	0.02	0.72
Lewes, DE	8557380	0.42 (0.36, 0.5)	0.07(-0.05, 0.19)	0.019	0.02	0.73
Cambridge, MD	8571892	0.29 (0.25, 0.34)	0.04(-0.06, 0.14)	0.021	0.09	0.59
Tochester Beach, MD	8573364	0.35 (0.28, 0.37)	-0.03 (-0.01, 0.2)	0.024	0.08	0.61
Baltimore, MD	8574680	0.31 (0.27, 0.36)	0.11(0.02, 0.21)	0.021	0.05	0.66
Annapolis, MD	8575512	0.29 (0.25, 0.34)	0.1(0 , 0.19)	0.020	0.05	0.63
Solomons Island, MD	8577330	0.26 (0.22, 0.31)	0.06(-0.03, 0.23)	0.019	0.12	0.6
Washington, D.C.	8594900	0.34 (0.28, 0.4)	0.2(0.1, 0.35)	0.017	0.01	0.72
Wachapreague, VA	8631044	0.4(0.39, 0.56)	0.06(-0.08, 0.19)	0.018	0.01	0.71
Kiptopeke, VA	8632200	0.44 (0.37, 0.53)	-0.03 (-0.15, 0.1)	0.016	0.02	0.62
Lewisetta, VA	8635750	0.31 (0.27, 0.36)	0.03(-0.07, 0.12)	0.017	0.06	0.6
Sewell point, VA	8638610	0.52 (0.49, 0.68)	-0.01 (-0.12, 0.1)	0.016	0.03	0.67
Chesapeake Bay Bridge, VA	8638863	0.57 (0.49, 0.69)	-0.04 (-0.18, 0.06)	0.016	0.04	0.69
Duck, NC	8651370	0.43 (0.36, 0.51)	-0.02 (-0.14, 0.1)	0.017	0.06	0.69
Oregon Inlet, NC	8652587	0.27 (0.23, 0.31)	0.03(0.1, 0.33)	0.020	0.07	0.48
Beaufort, NC	8656483	0.29 (0.24, 0.34)	0.02(-0.1, 0.14)	0.015	0.01	0.56
Wilmington, NC	8658120	0.26 (0.21, 0.3)	0.05(-0.05, 0.2)	0.015	0.02	0.5
Springmaid Pier, SC	8661070	0.33 (0.28, 0.39)	-0.04 (-0.15, 0.06)	0.016	-0.03	0.77
Charleston, SC	8665530	0.29 (0.23, 0.32)	0.05(-0.01, 0.18)	0.015	0	0.71
Fort Pulaski, GA	8670870	0.28 (0.24, 0.33)	0.03(-0.06, 0.13)	0.014	-0.02	0.8
Fernandina Beach, FL	8720030	0.32 (0.28, 0.38)	-0.04 (-0.13, 0.05)	0.015	-0.03	0.73
Vaca Key, FL	8723970	0.19 (0.14, 0.19)	0.05(0.03, 0.23)	0.014	0.06	0.39

Key West, FL	8724580	0.16 (0.14, 0.19)	0.04(-0.04, 0.13)	0.013	0.02	0.4
Naples, FL	8725110	0.23 (0.19, 0.27)	0.2(0 .07, 0.34)	0.018	0.04	0.47
Fort Myers, FL	8725520	0.24 (0.19, 0.28)	0.29(0.2, 0.52)	0.017	0.03	0.52
St. Petersburg, FL	8726520	0.27 (0.21, 0.3)	0.16(0.08, 0.35)	0.019	0.03	0.53
Cedar Key, FL	8727520	0.26 (0.22, 0.3)	0.3(0 .22, 0.48)	0.021	0.01	0.69
Apalachicola, FL	8728690	0.31 (0.26, 0.37)	0.3(0 .16, 0.44)	0.019	0.06	0.53
Panama City, FL	8729108	0.28 (0.19, 0.28)	0.29(0.14, 0.45)	0.018	0.1	0.51
Pensacola, FL	8729840	0.22 (0.18, 0.27)	0.37(0.28, 0.63)	0.016	0.07	0.51
Grand Isle, LA	8761724	0.22 (0.16, 0.27)	0.38(0.26, 0.67)	0.016	0.12	0.53
Sabine Pass, TX	8770570	0.27 (0.22, 0.34)	0.28(0.12, 0.44)	0.015	0.06	0.56
Galveston Pier 21, TX	8771450	0.33 (0.28, 0.39)	0.24(0.07, 0.32)	0.017	-0.05	0.61
RockPort, TX	8774770	0.22 (0.2, 0.3)	0.17(0.04, 0.33)	0.030	0.17	0.65
Port Isabel, TX	8779770	0.2(0.16, 0.24)	0.26(0.11, 0.41)	0.013	0.07	0.48
San Diego, CA	9410170	0.25 (0.26, 0.35)	-0.29 (-0.42, -0.23)	0.029	-0.06	0.83
La Jolla, CA	9410230	0.32 (0.27, 0.38)	-0.32 (-0.42, -0.22)	0.013	-0.07	0.78
Los Angeles, CA	9410660	0.23 (0.24, 0.33)	-0.22 (-0.36, -0.16)	0.029	-0.06	0.77
Santa Monica, CA	9410840	0.25 (0.22, 0.3)	-0.29 (-0.23, -0.09)	0.029	-0.01	0.77
Port San Luis, CA	9412110	0.25 (0.24, 0.34)	-0.16 (-0.27, -0.05)	0.029	-0.05	0.69
Monterrey, CA	9413450	0.23 (0.22, 0.32)	-0.1(-0.26, -0.02)	0.029	-0.04	0.66
San Francisco, CA	9414290	0.27 (0.22, 0.32)	-0.02 (-0.13, 0.11)	0.013	-0.07	0.63
Alameda, CA	9414750	0.24 (0.24, 0.34)	-0.1(-0.19, 0.04)	0.029	-0.07	0.66
Point Reyes, CA	9415020	0.27 (0.23, 0.32)	-0.09 (-0.25, 0)	0.029	-0.03	0.69
Humboldt Bay, CA	9418767	0.39 (0.32, 0.46)	-0.15 (-0.3, -0.04)	0.012	0.03	0.78
Charleston2, OR	9432780	0.39 (0.34, 0.51)	-0.11 (-0.22, 0.07)	0.029	-0.08	0.86
South Beach, OR	9435380	0.42 (0.41, 0.62)	-0.15 (-0.33, -0.01)	0.029	-0.06	0.93
Toke Point, WA	9440910	0.58 (0.66, 0.92)	-0.16 (-0.27, -0.04)	0.015	-0.07	1.07
Port Angeles, WA	9444090	0.39 (0.43, 0.61)	-0.11 (-0.3, -0.06)	0.029	-0.03	0.7
Port Townsend, WA	9444900	0.45 (0.47, 0.66)	-0.22 (-0.4, -0.17)	0.029	-0.03	0.67
Seattle, WA	9447130	0.53 (0.44, 0.62)	-0.22 (-0.33, -0.11)	0.014	-0.05	0.77
Cherry Point, WA	9449424	0.49 (0.41, 0.63)	-0.22 (-0.41, -0.19)	0.029	-0.08	0.76
Friday Harbor, WA	9449880	0.49 (0.45, 0.61)	-0.27 (-0.31, -0.12)	0.030	-0.07	0.71

APPENDIX B

SUPPORTING INFORMATION FOR CHAPTER 4: HIGHER FREQUENCY OF COMPOUND COASTAL-RIVERINE FLOODING UNDER CLIMATE CHANGE ALONG THE U.S. COASTS

Tables B1 presents a summary of information for the paired coastal and riverine stations including latitude and longitude.

Table B2 presents a summary of information about univariate and bivariate analysis including the return period (RP) of major coastal and riverine flooding under current condition, the selected copula, and the joint return period (JRP) of compound major coastal-riverine flooding.

Figures B1-1 to B1-26 presents the comparison between fitted generalized Pareto distribution (GPD) and empirical cumulative distribution function (CDF) along with Q-Q plot for (right panels) sea water levels and (left panels) river discharge.

Figures B2-1 to B2-26 illustrates the flow duration curve for simulated and observed river discharge along with statistical information including Nash–Sutcliffe coefficient of efficiency, Mean relative error (MRE), Kling-Gupta efficiency (KGE), and percent bias (PBIAS), which are estimated as follows:

$$NSE = 1 - \frac{\sum_{t=1}^{T}(Q_{sim}^{t} - Q_{obs}^{t})^2}{\sum_{t=1}^{T}(Q_{obs}^{t} - \bar{Q}_{obs})^2}$$

where Q_{sim}^{t} is simulated discharge, Q_{obs}^{t} is observed discharge at time *t* and $\bar{Q}_{obs}$ is the mean of observed discharges.

$$MRE = \frac{1}{n}\sum_{t=1}^{n}\left|\frac{Q_{sim}^{t} - Q_{obs}^{t}}{Q_{obs}^{t}}\right|$$

where n is the number of observations.

$$KGE = 1 - \sqrt{(r-1)^2 + (\frac{\sigma_{sim}}{\sigma_{obs}} - 1)^2 + (\frac{\mu_{sim}}{\mu_{obs}} - 1)^2}$$

Where σ_{sim} is the standard deviation in simulations, σ_{obs} is the standard deviation in observations, μ_{sim} is the simulation mean, and μ_{obs} is the observation mean (i.e. equivalent to $\bar{Q}_{obs}$)

$$PBIAS = \frac{\sum_{t=1}^{n}(Q_{sim}^{t} - Q_{obs}^{t})}{\sum_{t=1}^{n} Q_{obs}^{t}} \times 100$$

Figures B3-1 to B3-26 present marginal distribution based on generalized Pareto Distribution (GPD) for (top left panel) extreme river discharges, (bottom right panel) extreme sea water levels (SWL); (top right panel) joint return period of extreme paired data based on the selected copula. The dashed red line shows the major flood threshold and corresponding univariate return period in the top left and top right panels. The red square (top right panel) shows the JRP of compound major flooding under current conditions. The figure is not provided for the stations with no significant dependence structure between high SWLs and river dicharges.

Figures B4-1 to B4-26 illustrate (left panel) the changes in joint return period (JRP) of compound major flooding, (right panel) the risk of failure (RF) due to compound major flooding over a 30-year design lifetime.

Table B1. Summary of information for the paired coastal and riverine stations

Coastal Station	Lat	Long	Riverine Station	USGS Station Number	Lat	Long
Boston	42.4	-71.1	Charles River	01104500	42.4	-71.2
New London	41.4	-72.1	Shetucket River	01122500	41.7	-72.2
BridgePort	41.2	-73.2	Housatonic River	01205500	41.4	-73.2
Battery	40.7	-74.0	Saddle River	01391500	40.9	-74.1
Reedy Point	39.6	-75.6	Brandywine Creek	01481500	39.8	-75.6
Baltimore	39.3	-76.6	Dead Run	01589330	39.3	-76.7
Annapolis	39.0	-76.5	Western Branch Patuxent River	01594526	38.8	-76.7
Washington DC	38.9	-77.0	Potomac River	01646500	38.9	-77.1
Sewell point	36.9	-76.3	James River	02037500	37.6	-77.5
Duck	36.2	-75.7	Blackwater River	02049500	36.8	-76.9
Oregon Inlet	35.8	-75.5	Tar River	02083500	35.9	-77.5
Beaufort	34.7	-76.7	Neuse River	02091814	35.3	-77.3
Wilmington	34.2	-78.0	Northeast Cape Fear River	02108000	34.8	-77.8
Charleston	32.8	-79.9	Edisto River	02175000	33.0	-80.4
Fort Pulaski	32.0	-80.9	Savannah River	02198500	32.5	-81.3
Fernandina Beach	30.7	-81.5	Saint Marys River	02231000	30.4	-82.1
Apalachicola	29.7	-85.0	Apalachicola River	02359170	29.9	-85.0
Panama City	30.2	-85.7	Econfina Creek	02359500	30.4	-85.6
Pier 21	29.3	-94.8	Buffalo Bayou	08074000	29.8	-95.4
Rock Port	28.0	-97.0	Mission River	08189500	28.3	-97.3
Santa Monica	34.0	-118.5	Santa Clara River	11109000	34.4	-118.7
North Spit	40.8	-124.2	Mad River	11481000	40.9	-124.1
Charleston 2	43.3	-124.3	Umpqua River	14321000	43.6	-123.6
South Beach	44.6	-124.0	Siletz River	14305500	44.7	-123.9
Toke Point	46.7	-124.0	Willapa River	12013500	46.7	-123.7
Seattle	47.6	-122.3	Green River	12113000	47.3	-122.2

Table B2. Summary of information about the univariate and bivariate analysis

Coastal Station	Selected Copula	Tau	Univariate Analysis		Bivariate Analysis
			RP Major coastal flooding [yr]	RP Major Riverine flooding [yr]	JRP_compound major flooding [yr]
Boston	Gumbel	0.18	96	172	526
New London	Galambos	0.16	66	97	349
Bridge Port	Galambos	0.16	71	11	214
Battery	Joe	0.11	62	8	335
Reedy Point	Galambos	0.15	79	41	408
Baltimore	Gumbel	0.16	83	113	460
Annapolis	Gumbel	0.12	87	32	472
Washington	Galambos	0.30	20	48	115
Sewell point	Gumbel	0.11	79	19	309
Duck	Joe	0.11	108	30	990
Oregon Inlet	Independence	0.03	103	11	N/A
Beaufort	Gumbel	0.11	109	28	499
Wilmington	Gumbel	0.16	318	20	884
Charleston	Joe	0.14	276	43	999
Fort Pulaski	Independence	0.06	245	48	N/A
Fernandina Beach	Tawn	0.27	271	11	833
Apalachicola	Independence	0.02	22	11	N/A
Panama City	Independence	-0.03	37	79	N/A
Pier 21	Galambos	0.27	33	60	210
Rock Port	Gumbel	0.24	43	13	N/A
Santa Monica	Independence	-0.09	N/A	39	N/A
North Spit	Tawn	0.17	N/A	27	N/A
Charleston 2	Tawn	0.18	N/A	110	N/A
South Beach	Tawn	0.11	N/A	75	N/A
Toke Point	Gumbel	0.17	85	39	911
Seattle	Independence	0.03	N/A	12	N/A

Boston - Charles River

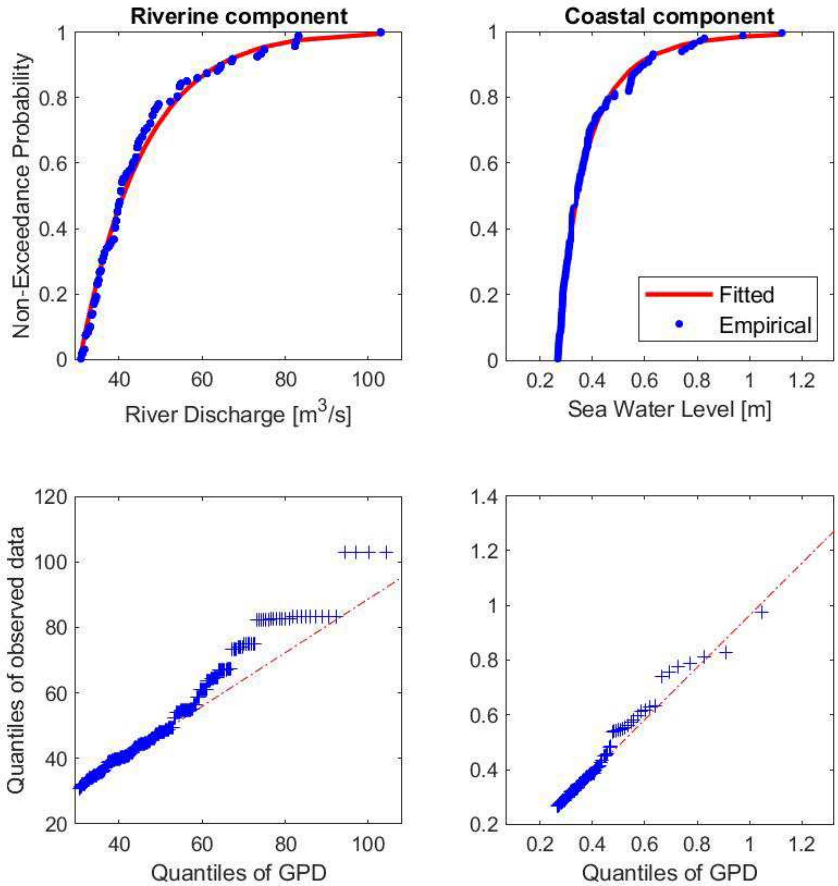

Figure B1-1

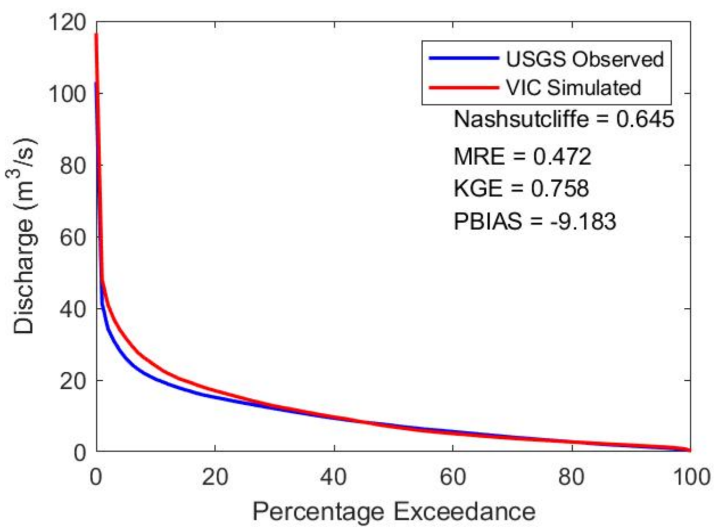

Figure B2-1

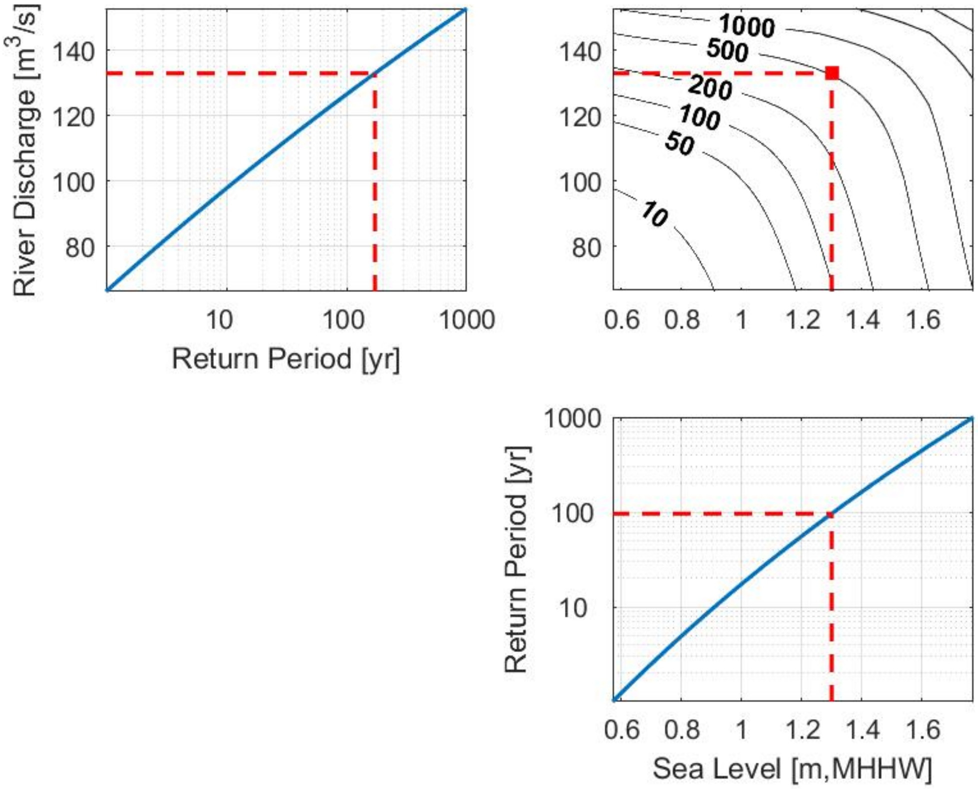

Figure B3-1

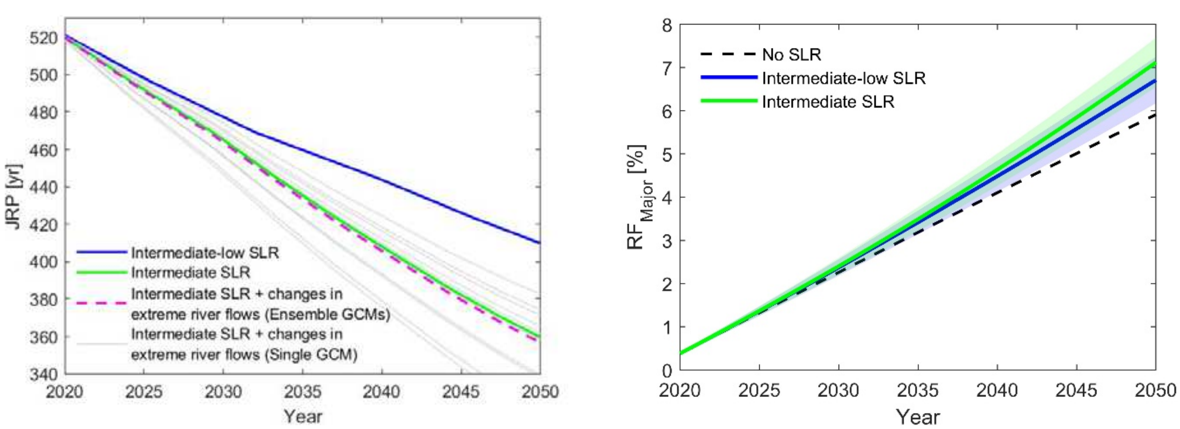

Figure B4-1

New London - Shetucket River

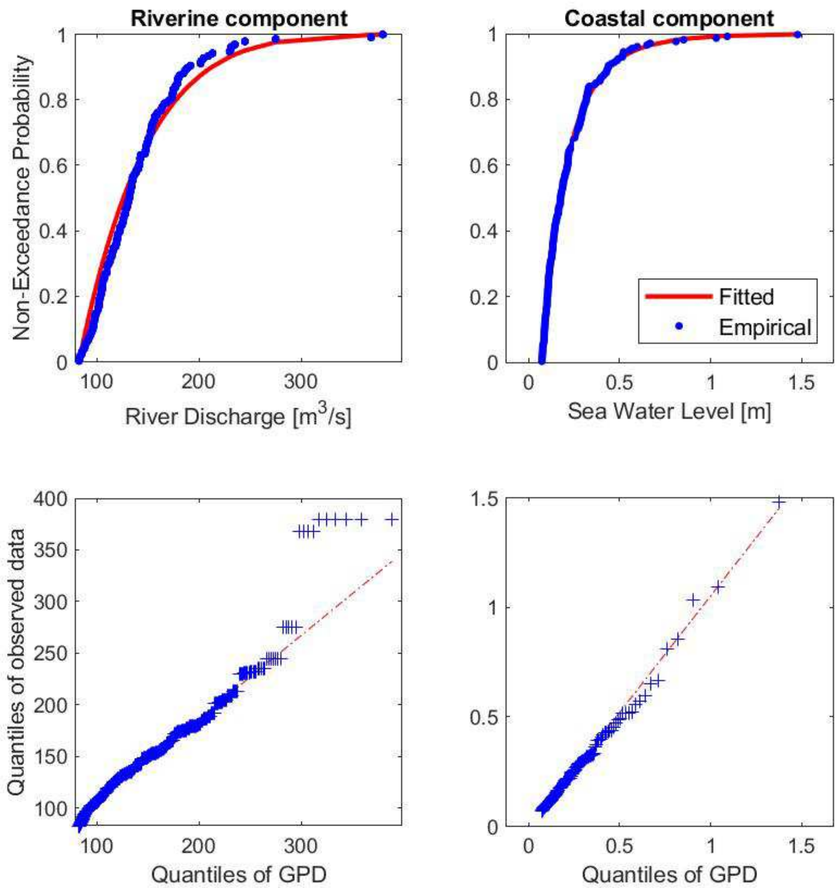

Figure B1-2

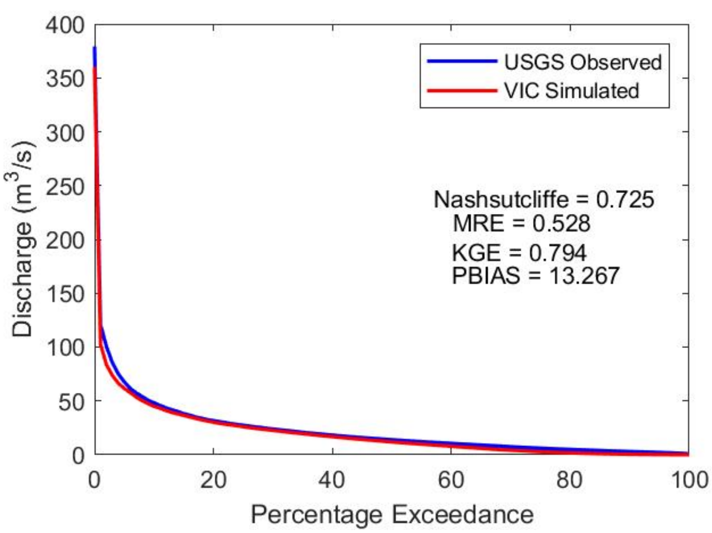

Figure B2-2

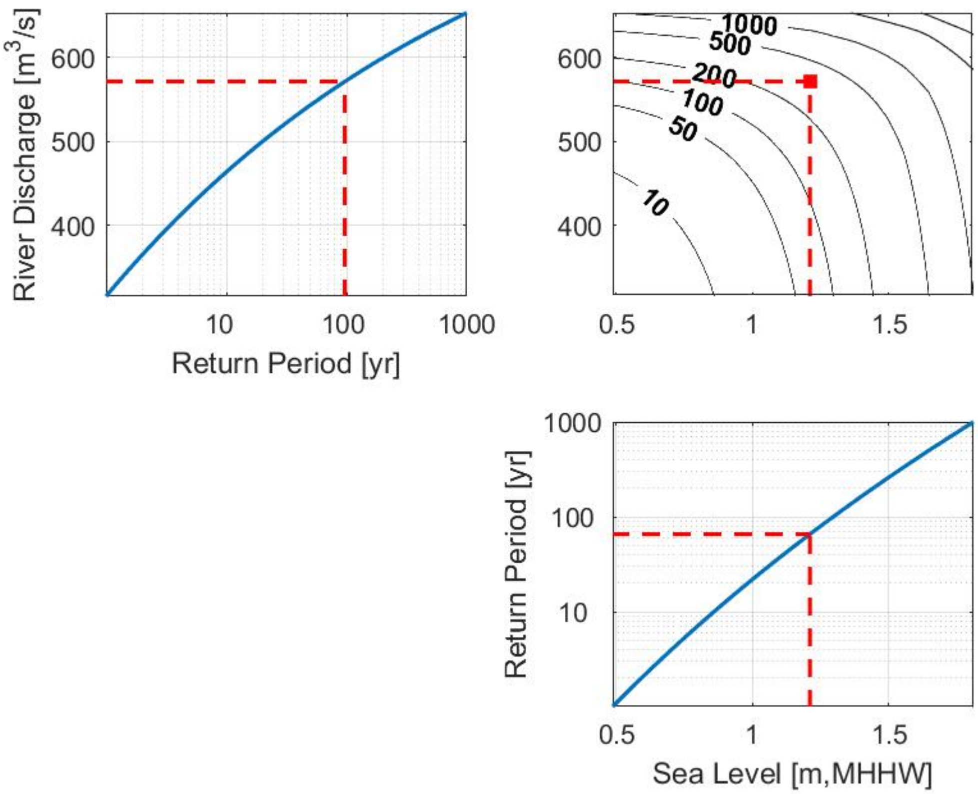

Figure B3-2

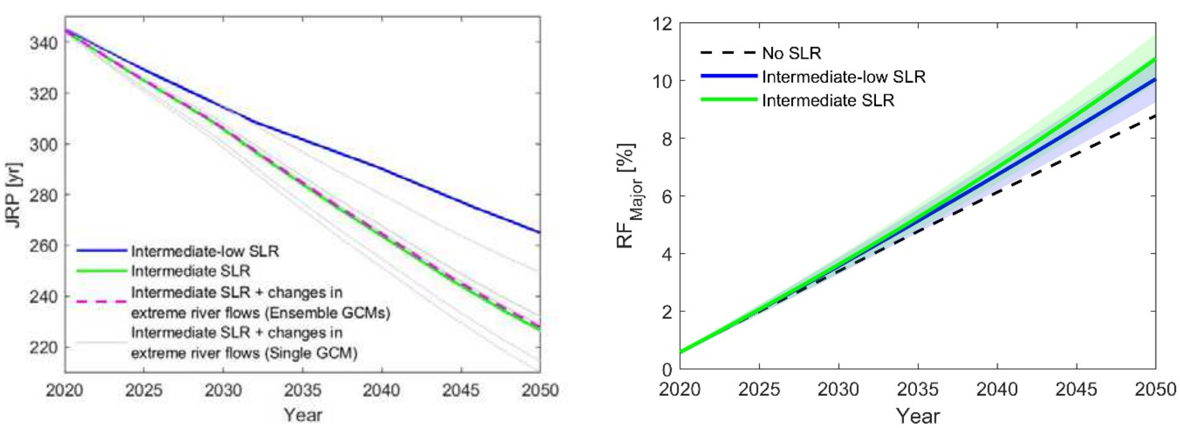

Figure B4-2

Bridge Port - Housatonic River

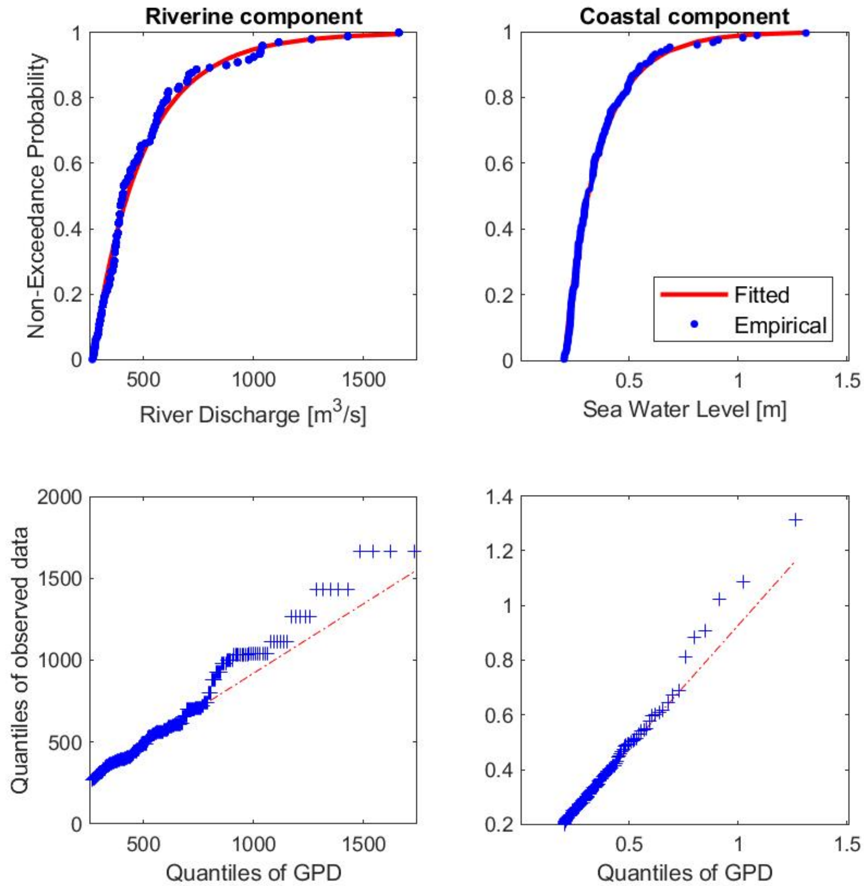

Figure B1-3

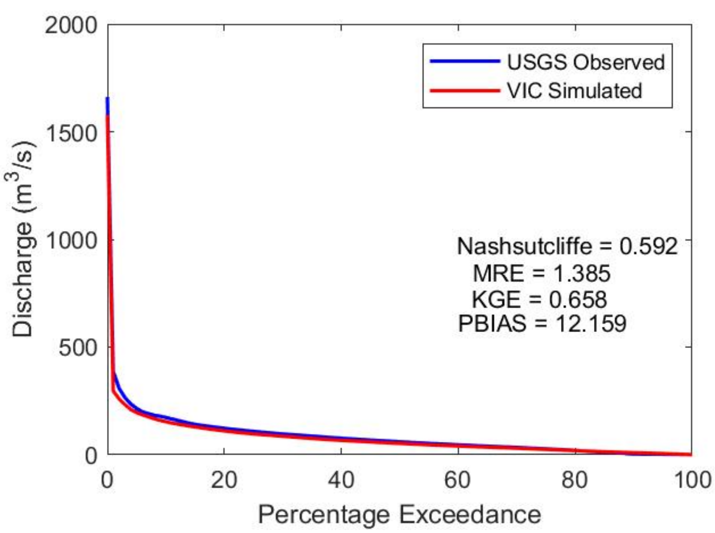

Figure B2-3

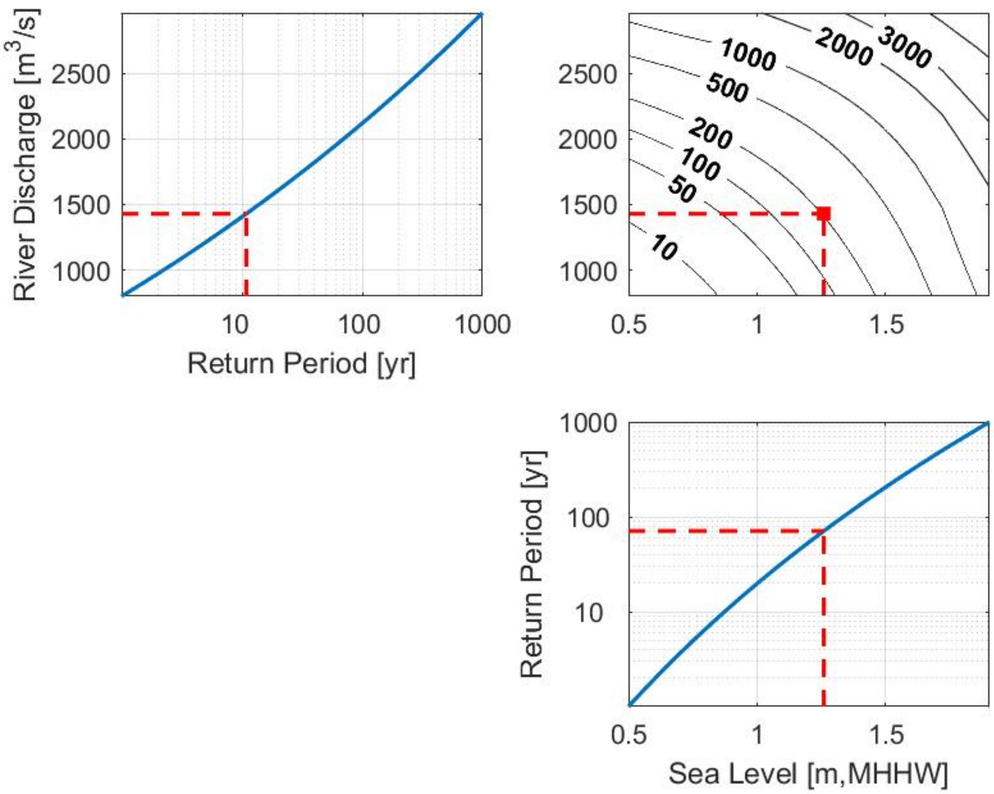

Figure B3-3

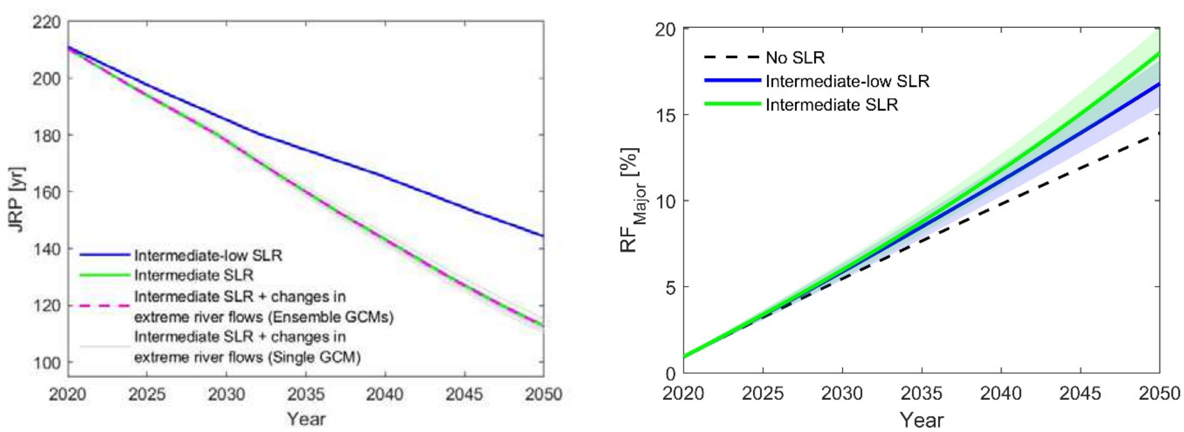

Figure B4-3

Battery - Saddle River

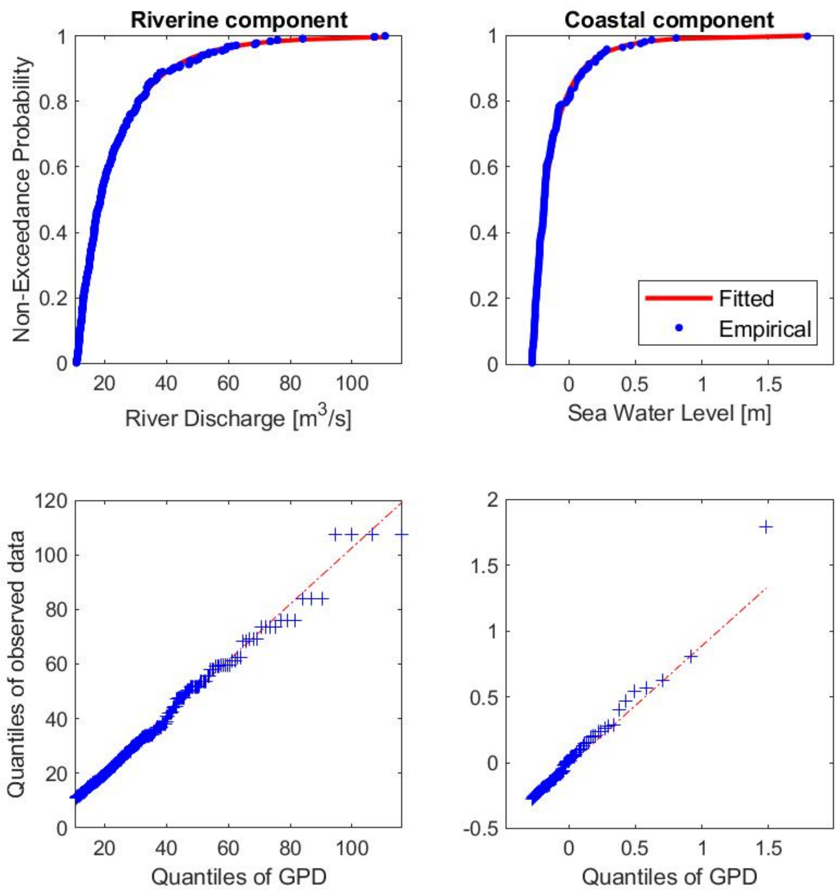

Figure B1-4

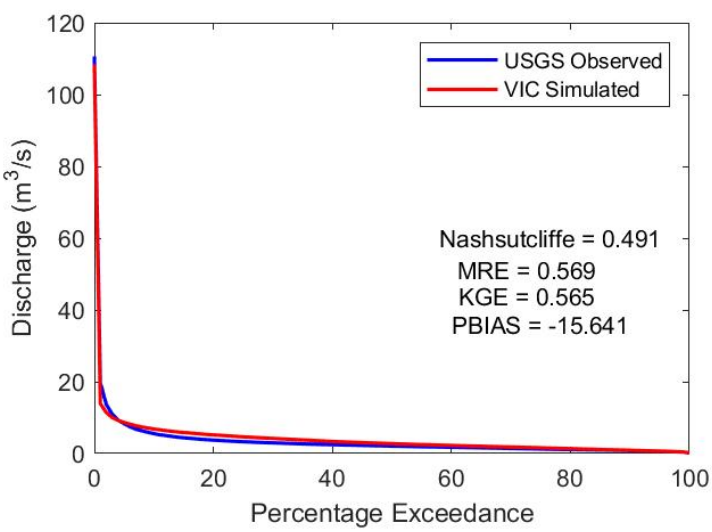

Figure B2-4

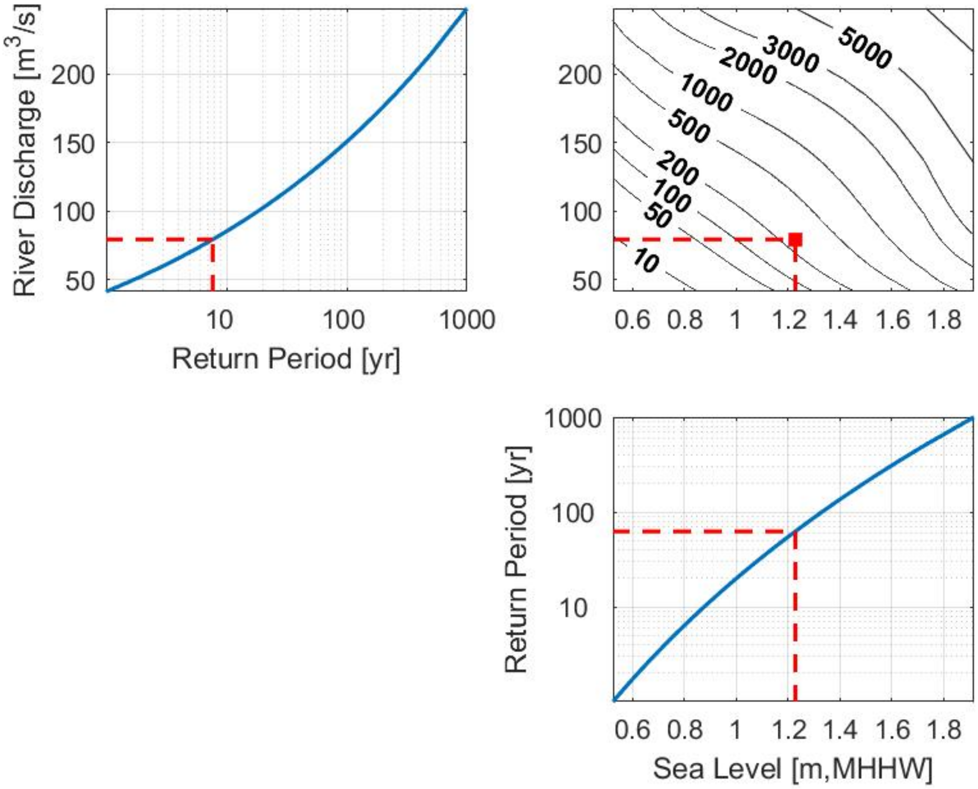

Figure B3-4

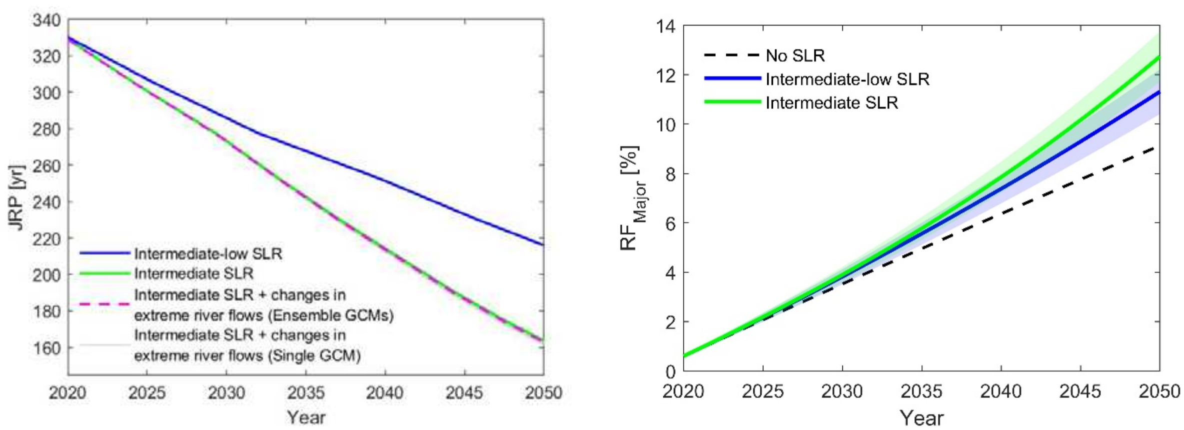

Figure B4-4

Reedy Point - Brandywine Creek

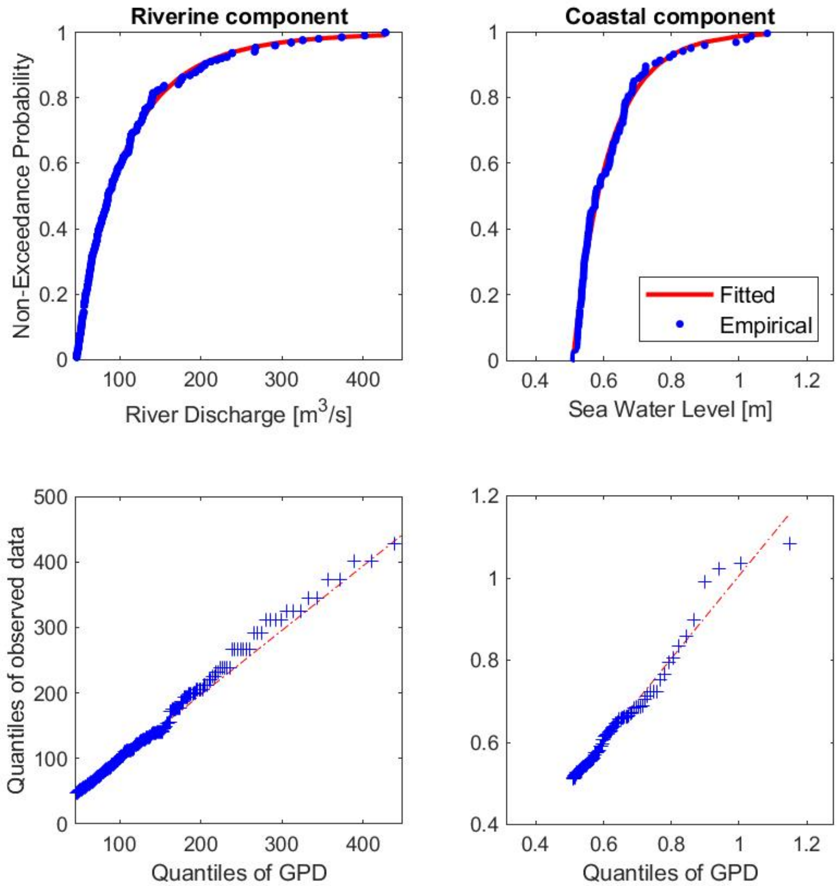

Figure B1-5

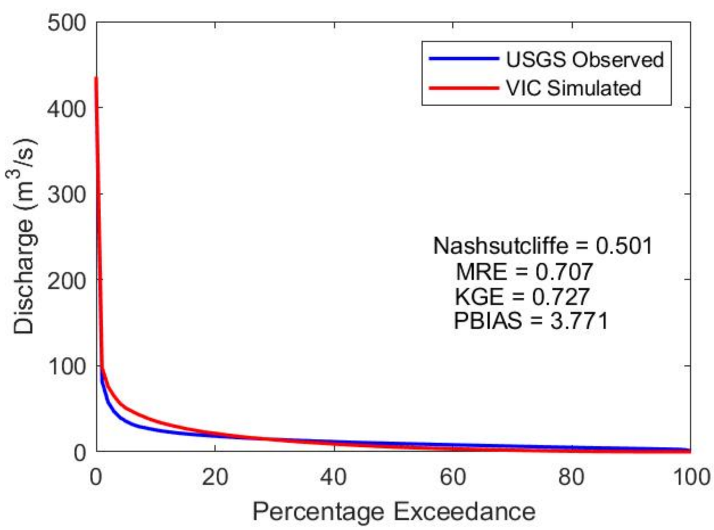

Figure B2-5

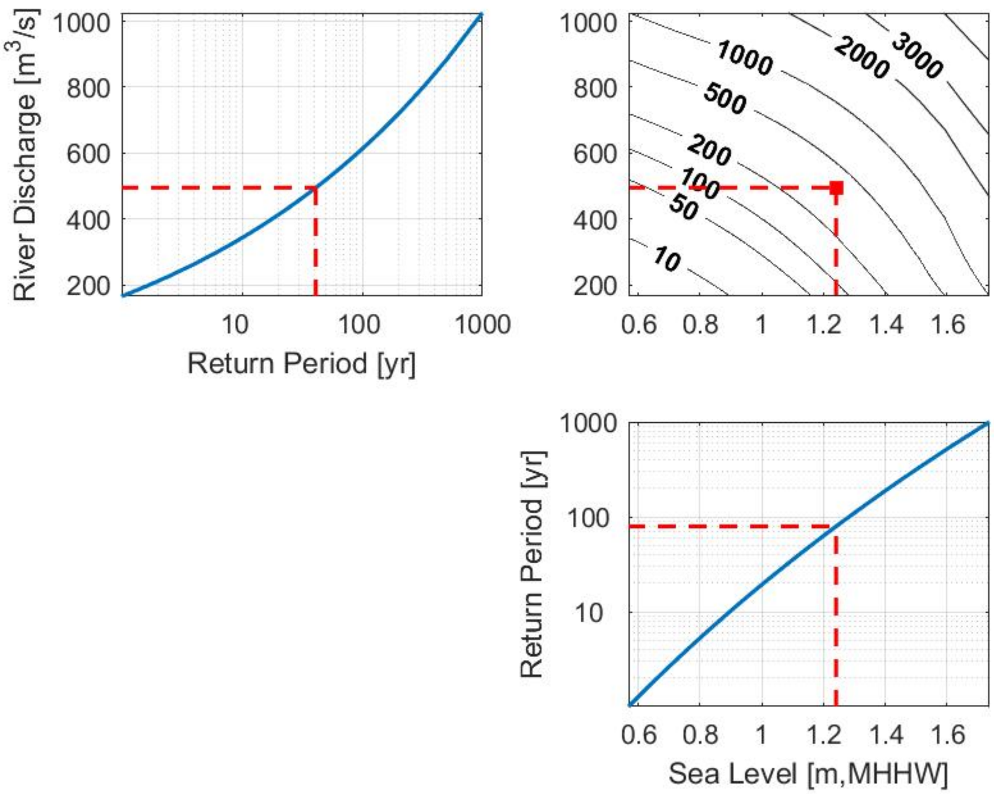

Figure B3-5

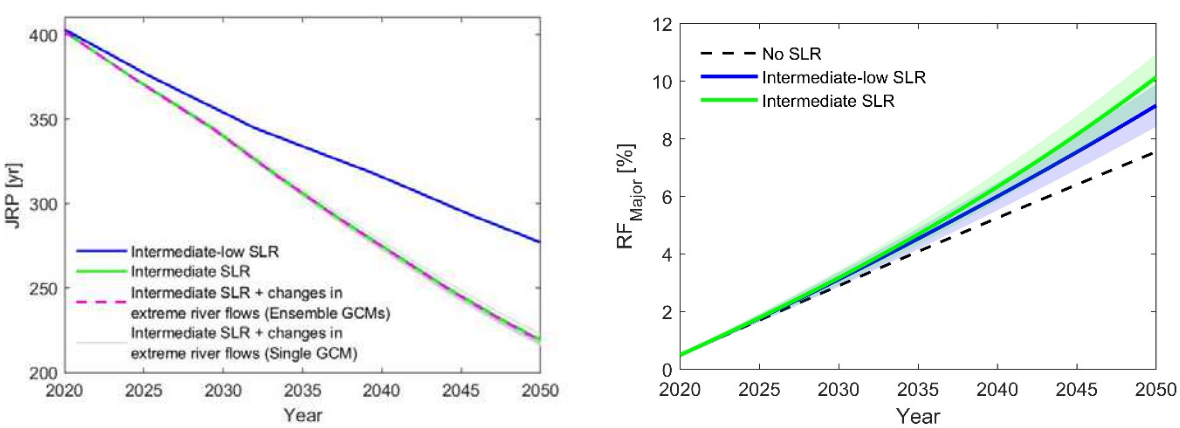

Figure B4-5

Baltimore - Dead Run

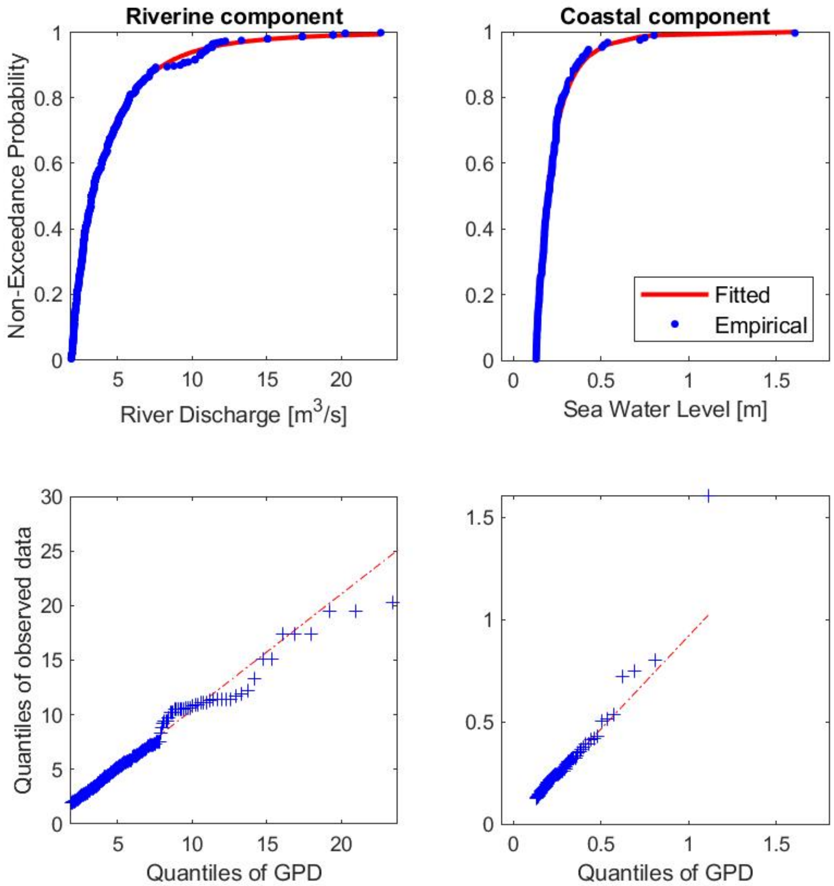

Figure B1-6

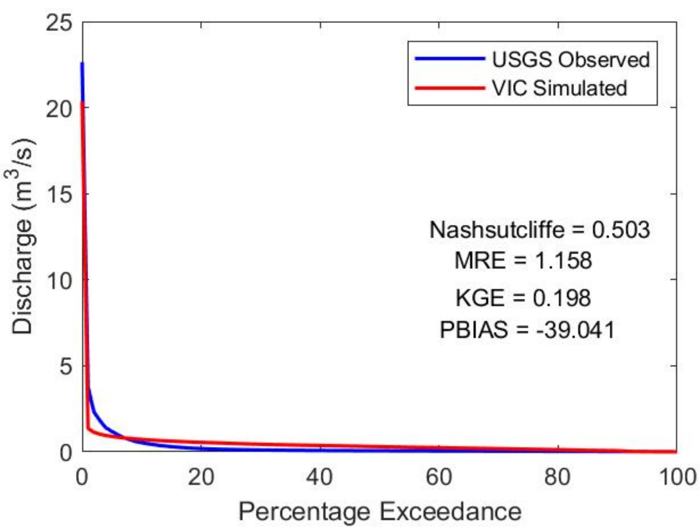

Figure B2-6

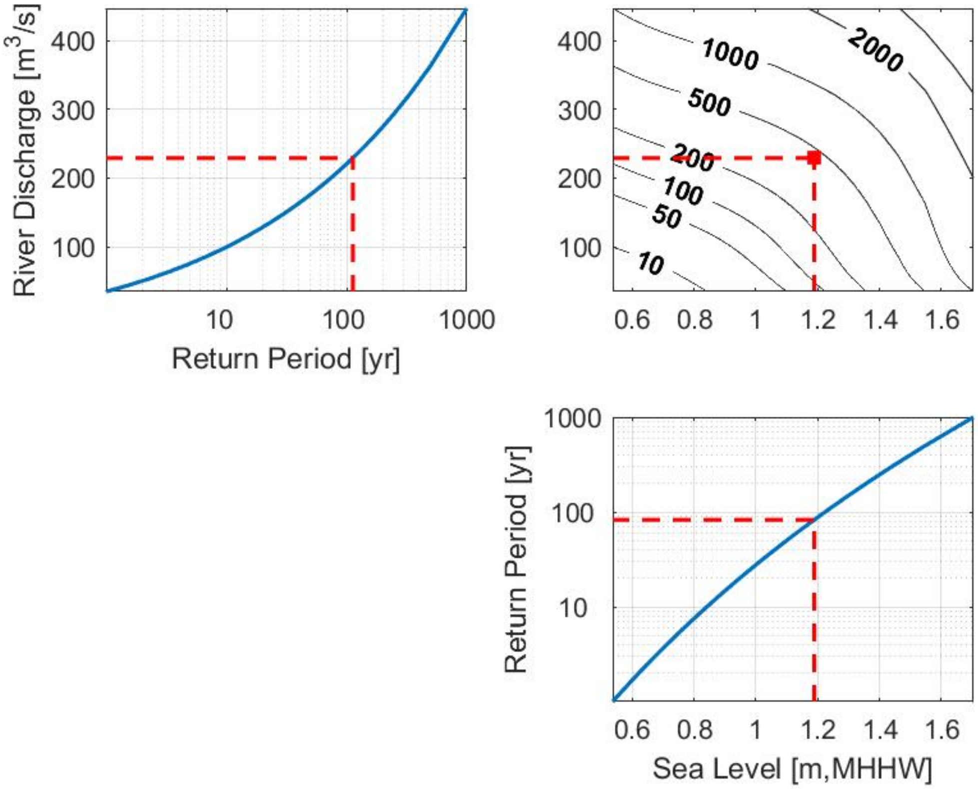

Figure B3-6

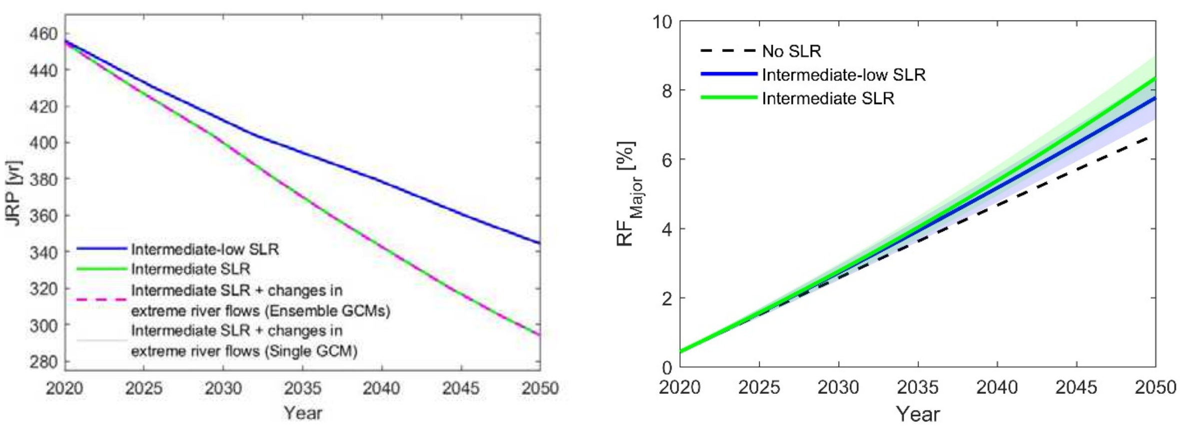

Figure B4-6

Annapolis - Western Branch Patuxent River

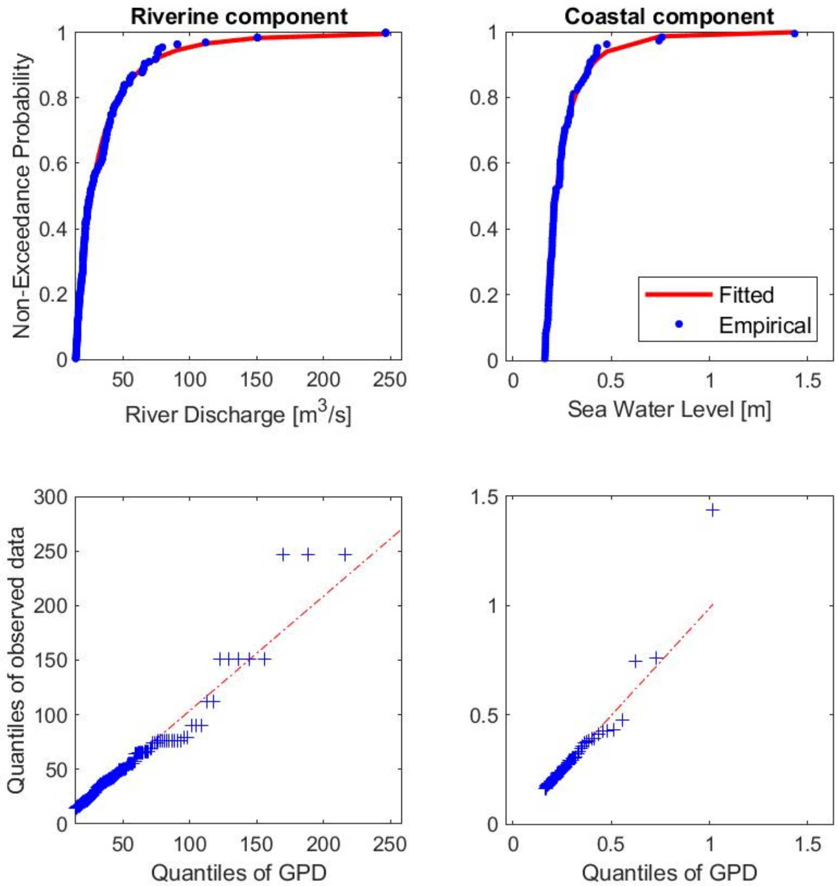

Figure B1-7

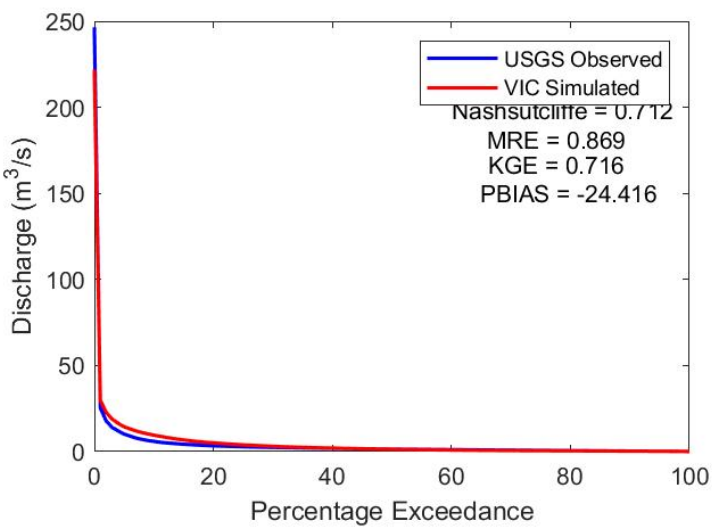

Figure B2-7

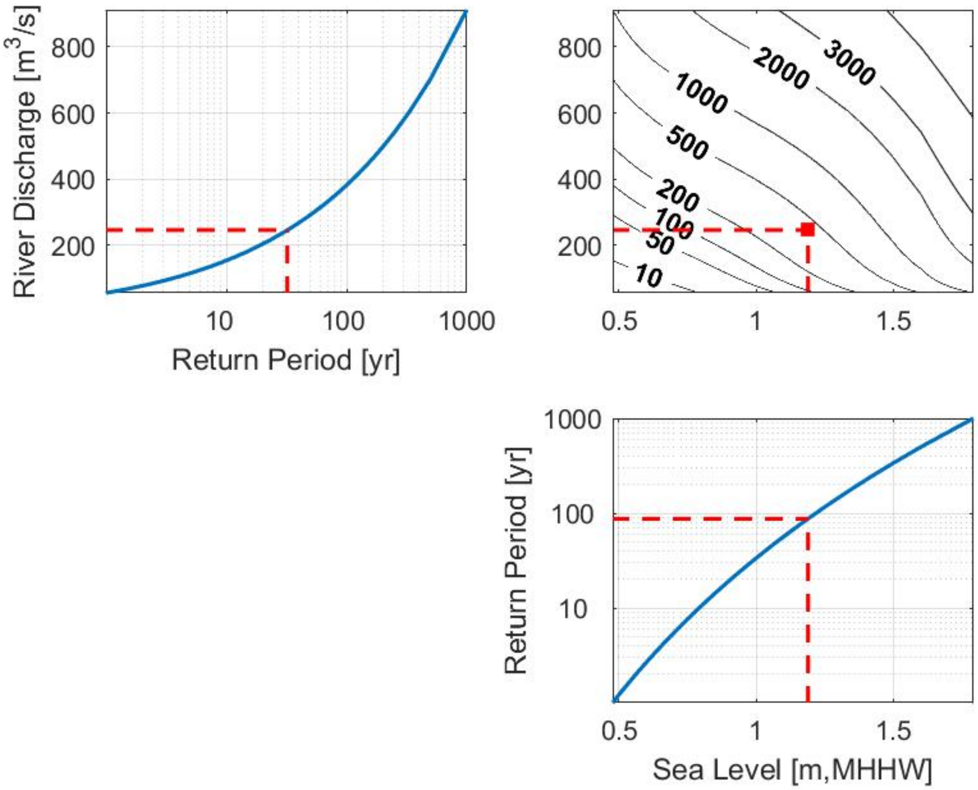

Figure B3-7

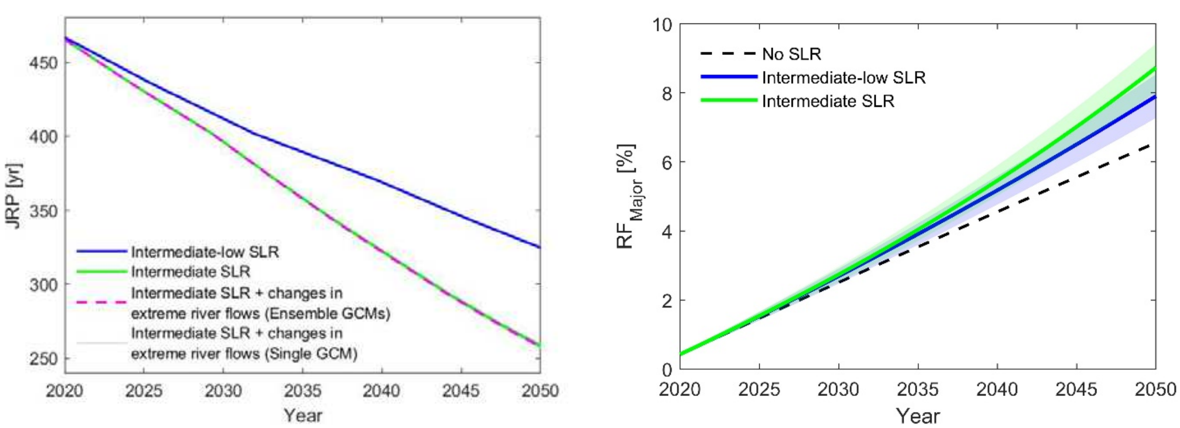

Figure B4-7

Washington D.C. - Potomac River

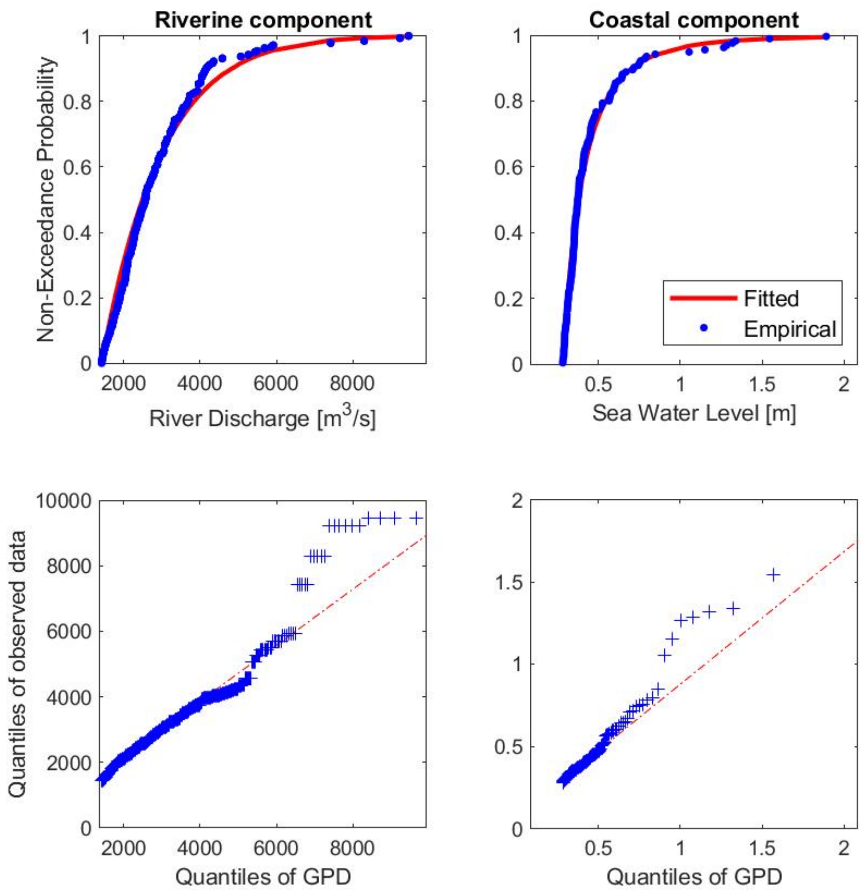

Figure B1-8

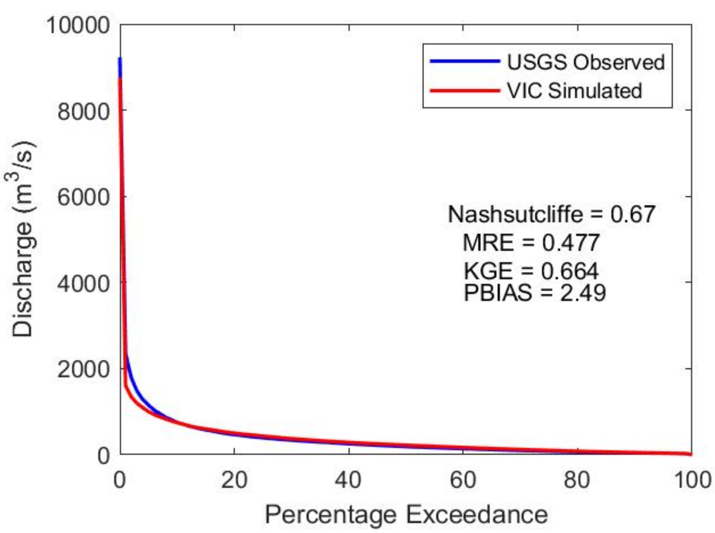

Figure B2-8

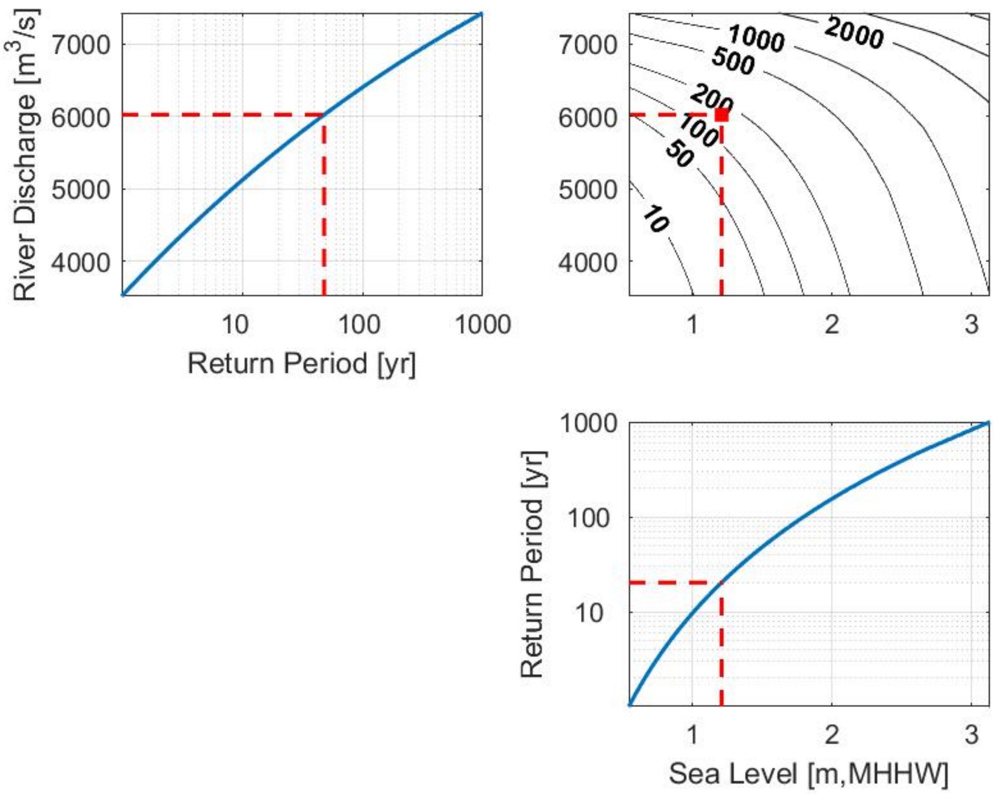

Figure B3-8

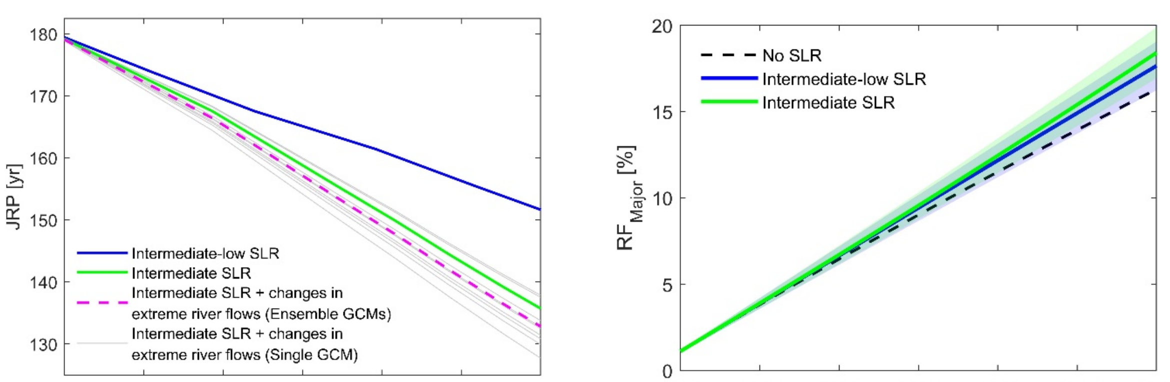

Figure B4-8

Sewell point - James River

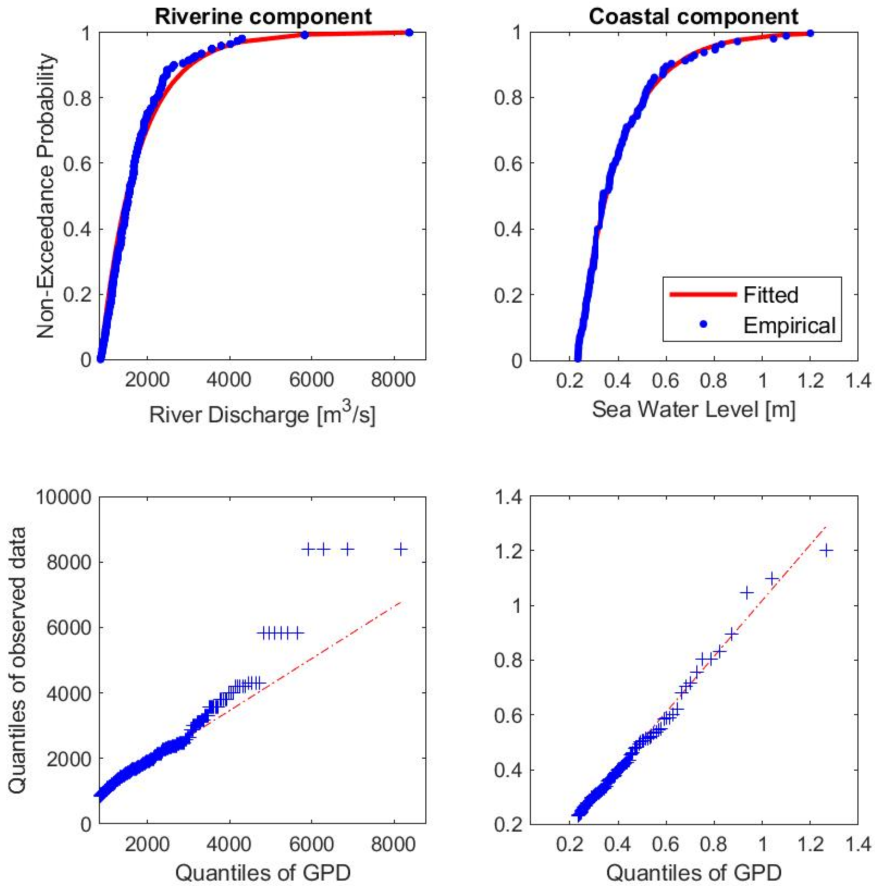

Figure B1-9

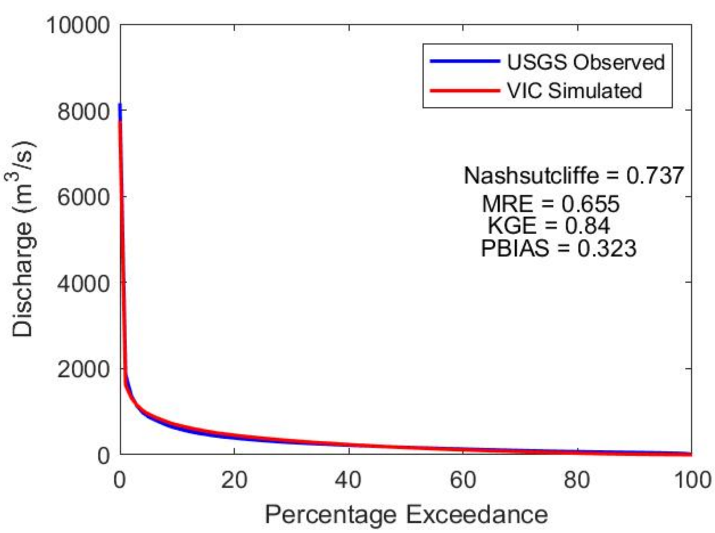

Figure B2-9

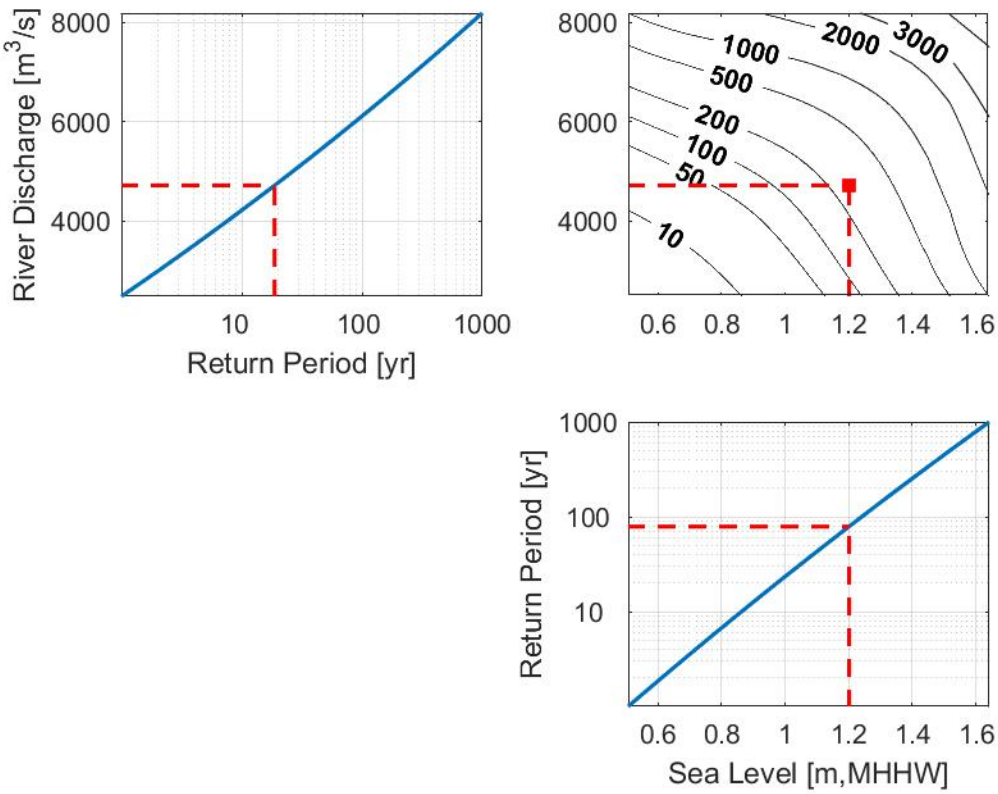

Figure B3-9

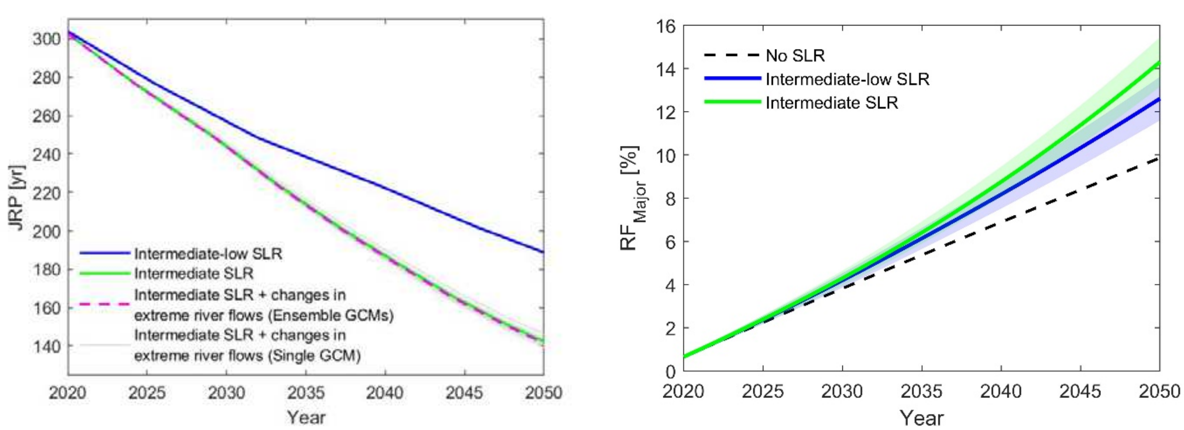

Figure B4-9

Duck - Blackwater River

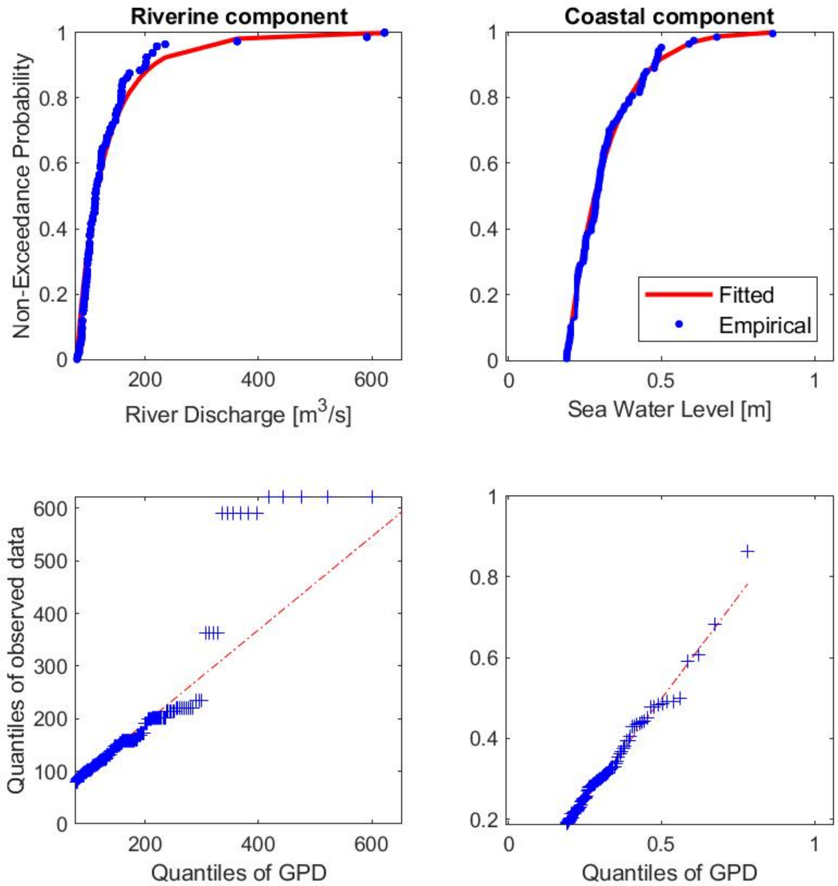

Figure B1-10

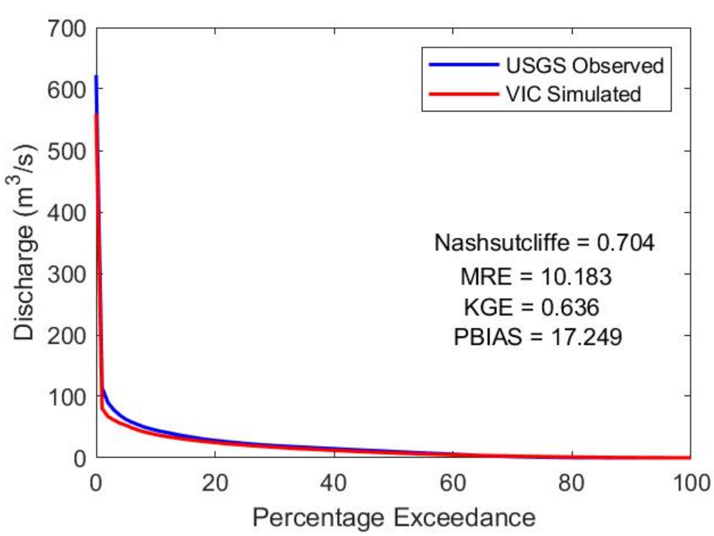

Figure B2-10

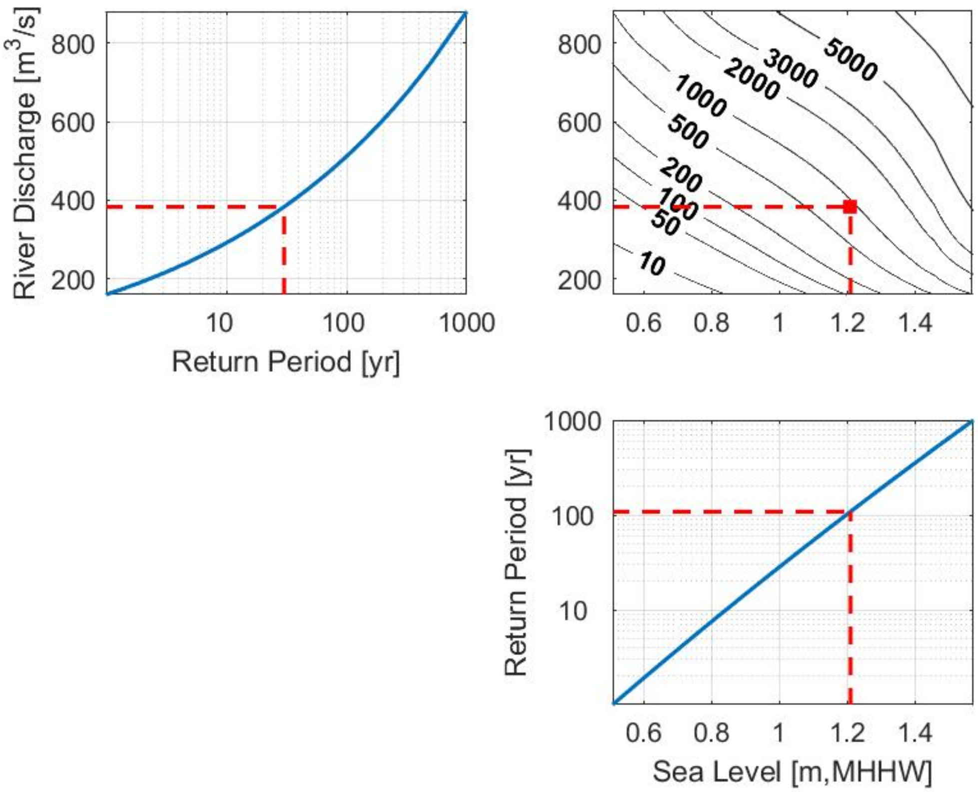

Figure B3-10

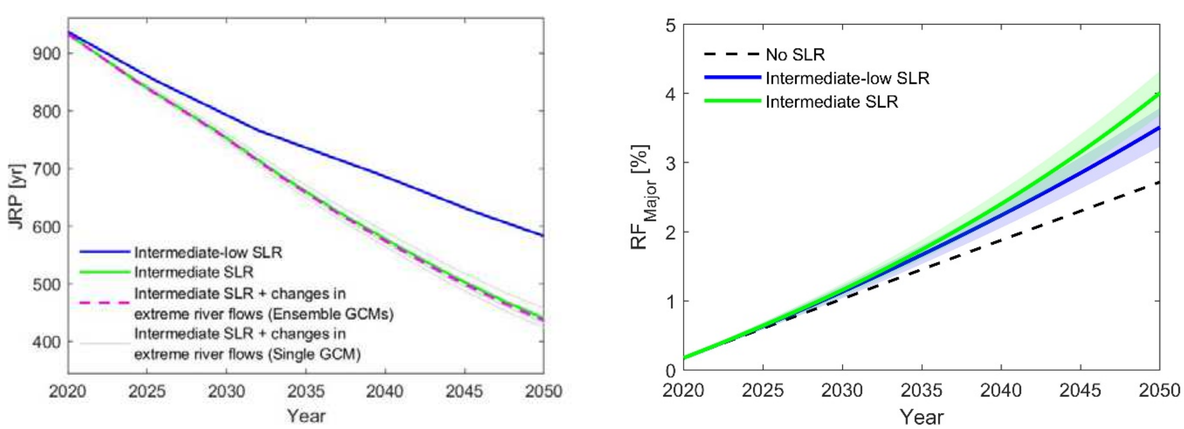

Figure B4-10

Oregon Inlet - Tar River

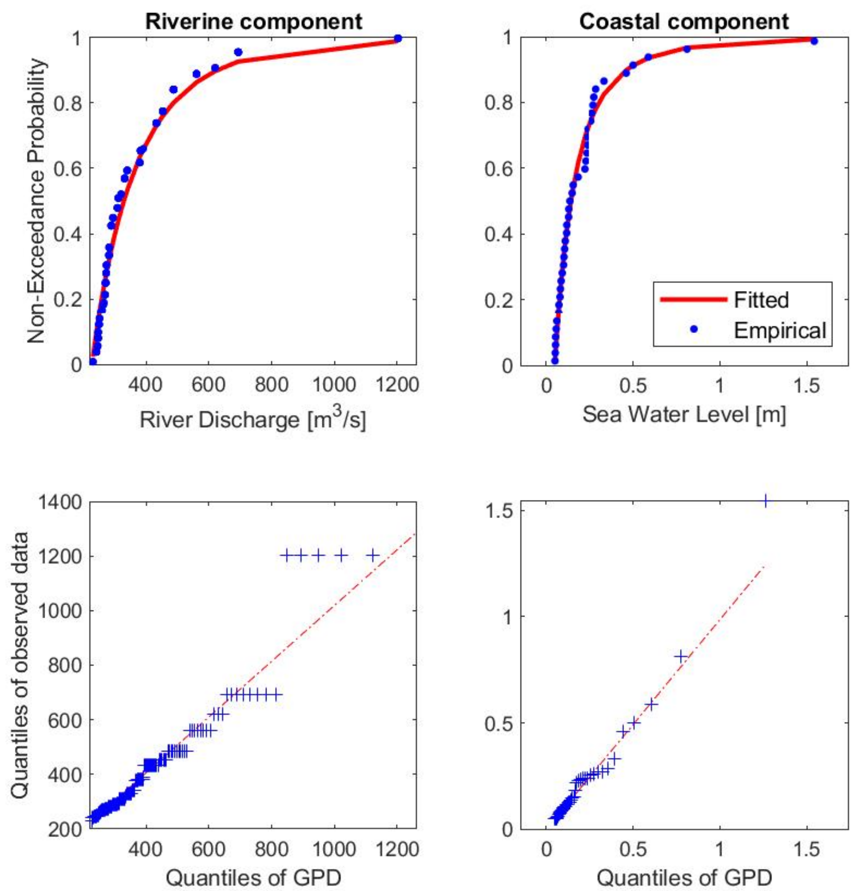

Figure B1-11

Beaufort - Neuse River

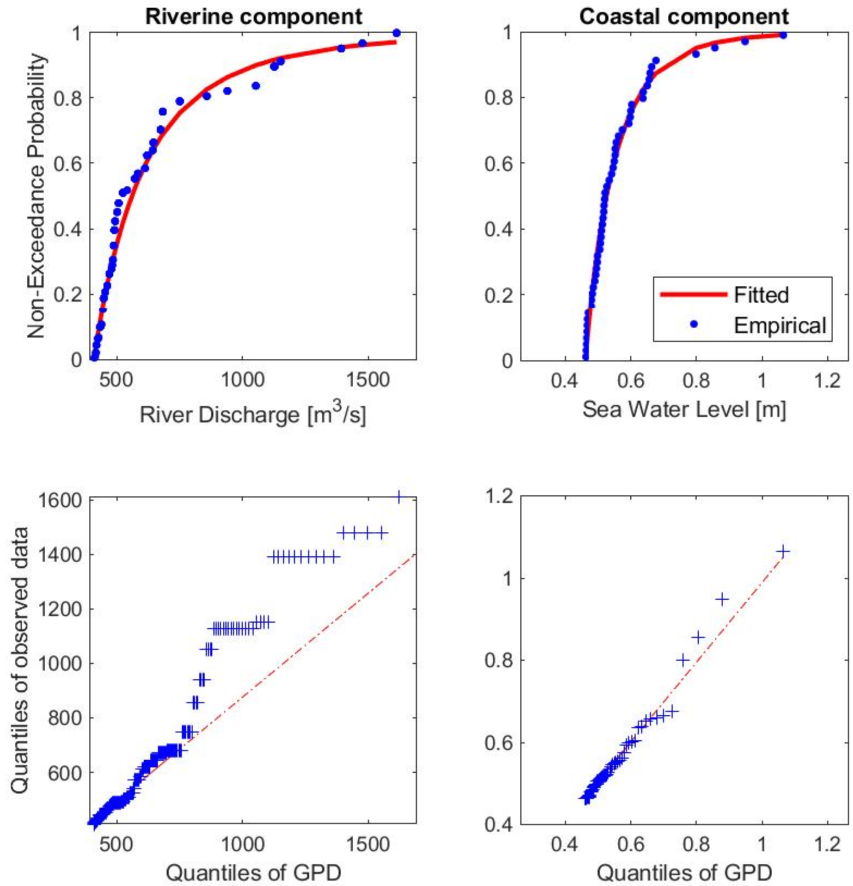

Figure B1-12

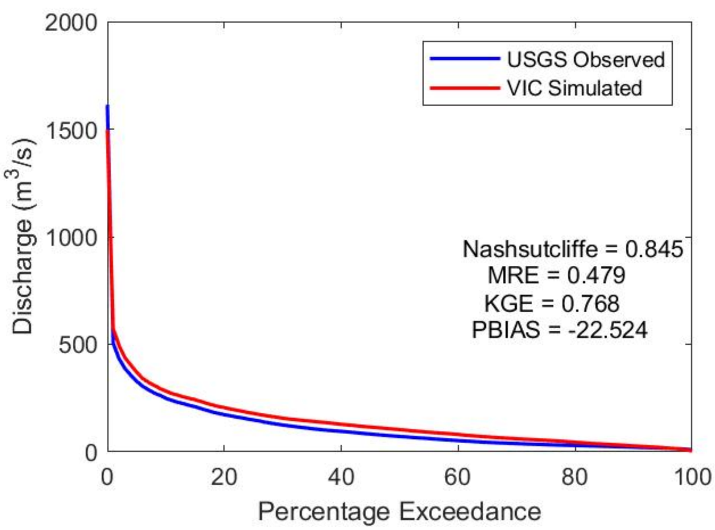

Figure B2-12

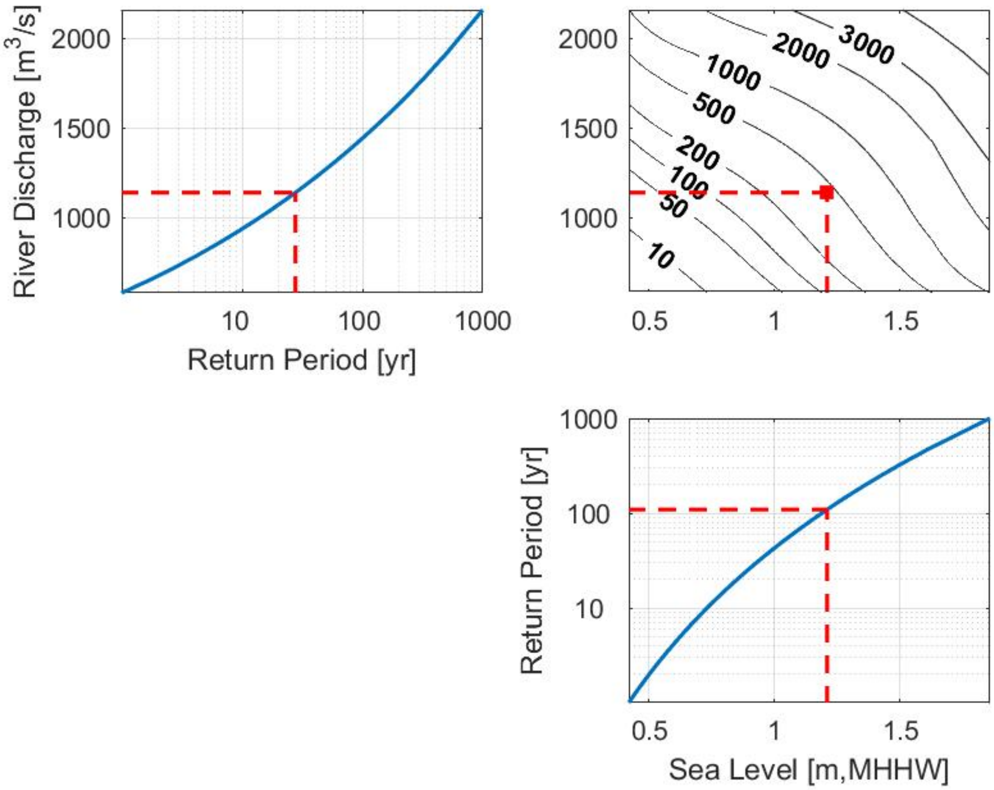

Figure B3-12

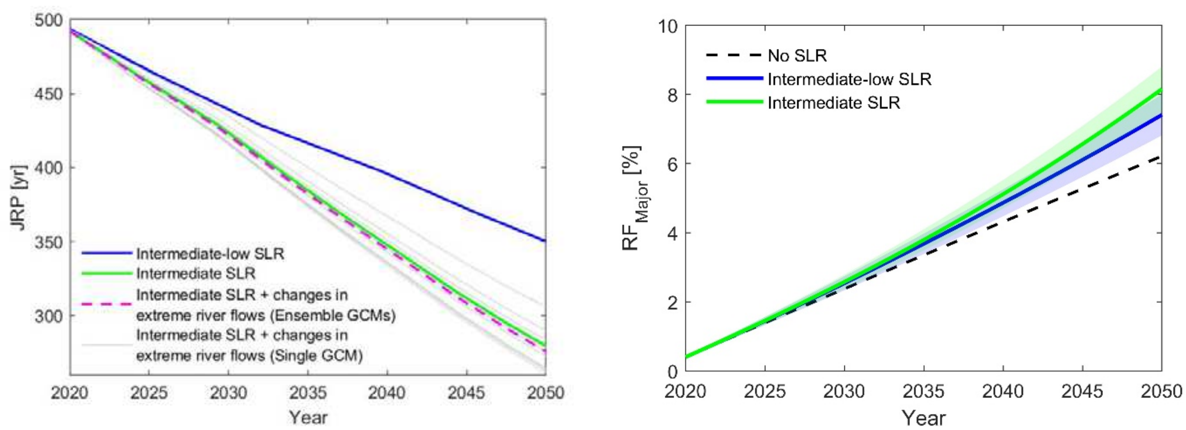

Figure B4-12

Wilmington - Northeast Cape Fear River

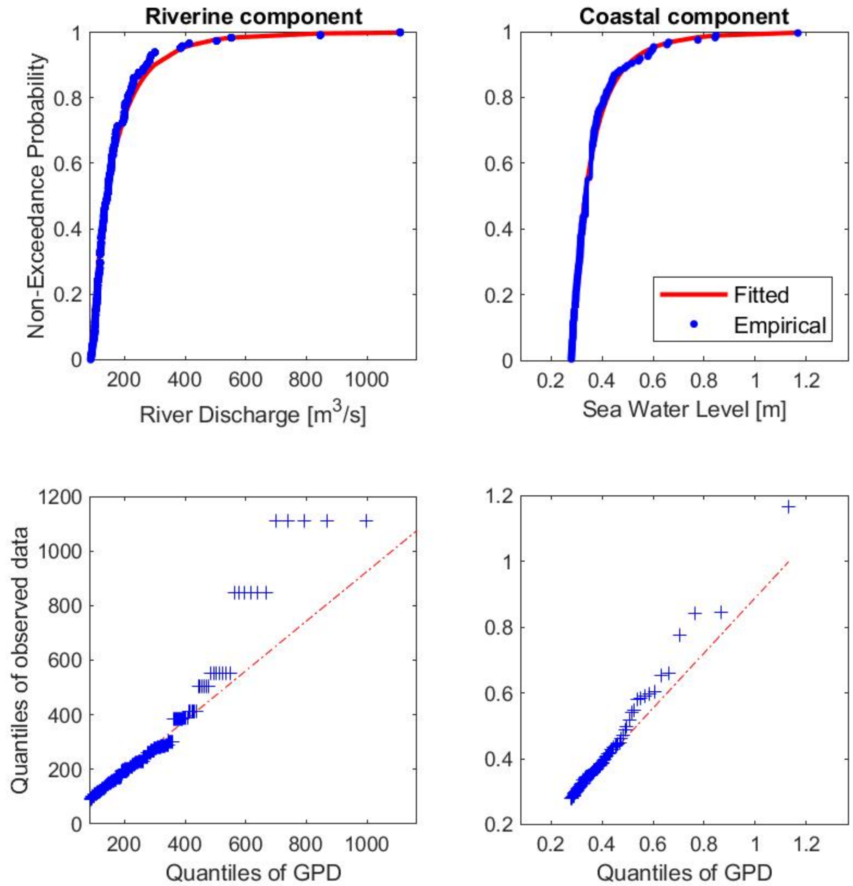

Figure B1-13

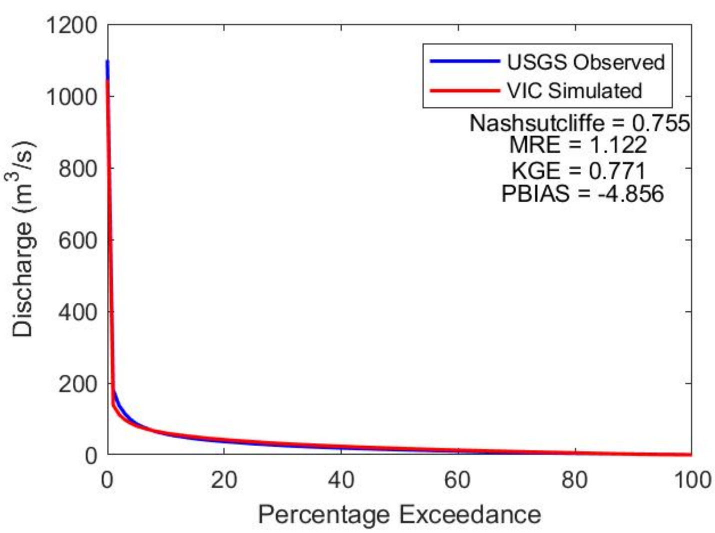

Figure B2-13

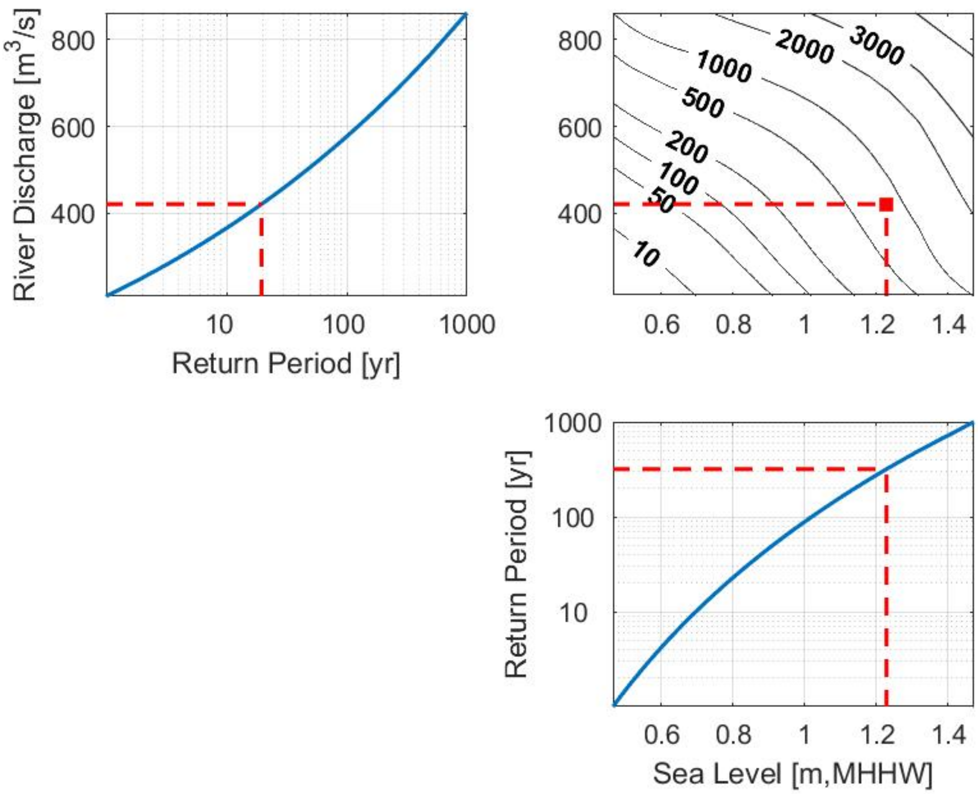

Figure B3-13

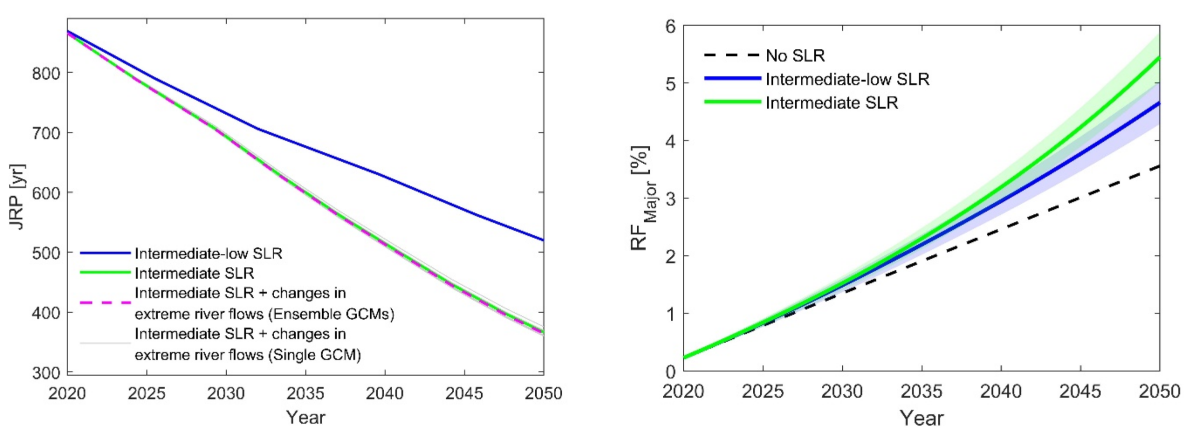

Figure B4-13

Charleston - Edisto River

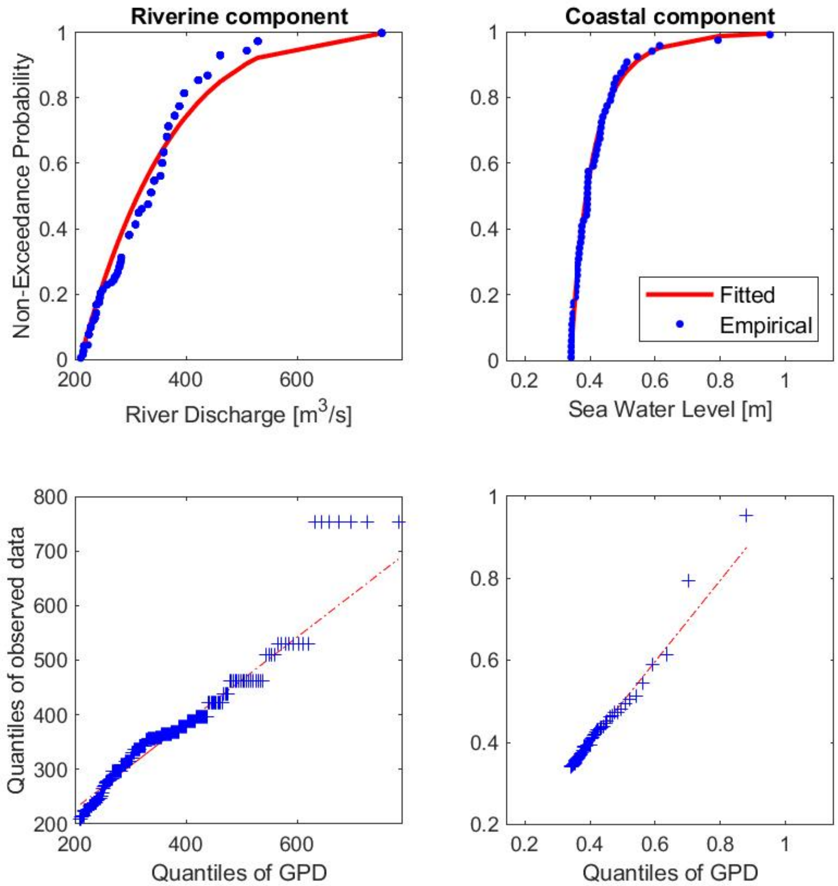

Figure B1-14

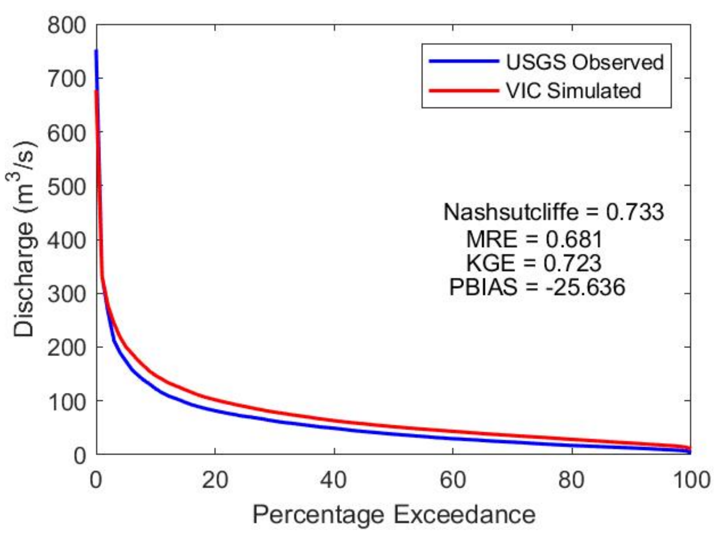

Figure B2-14

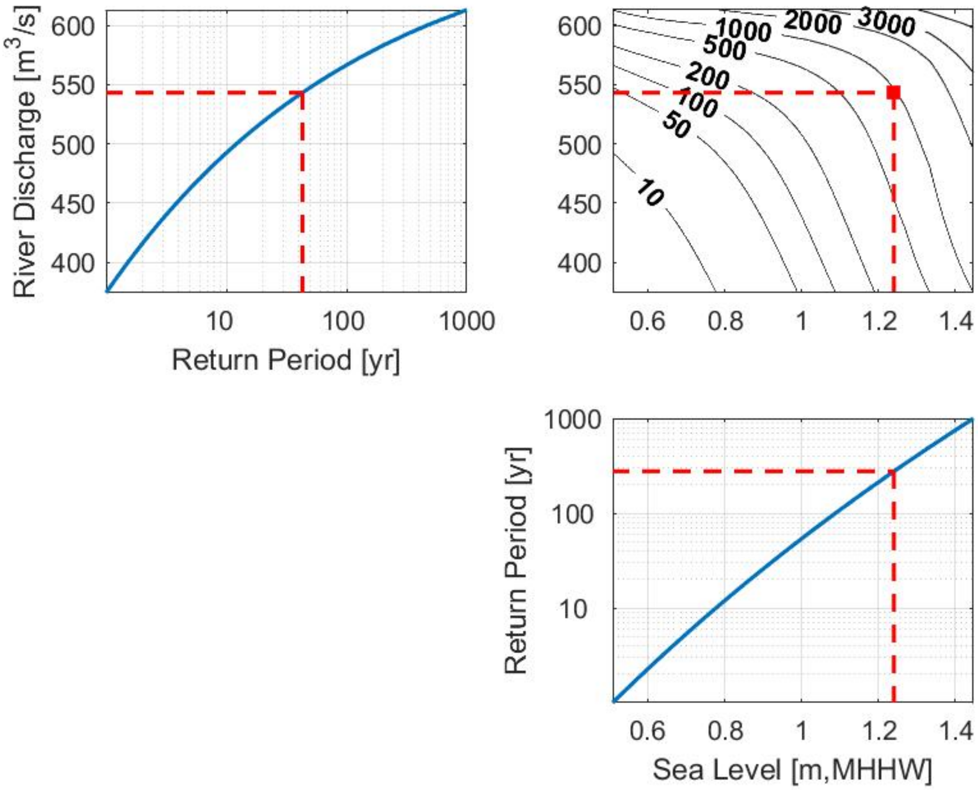

Figure B3-14

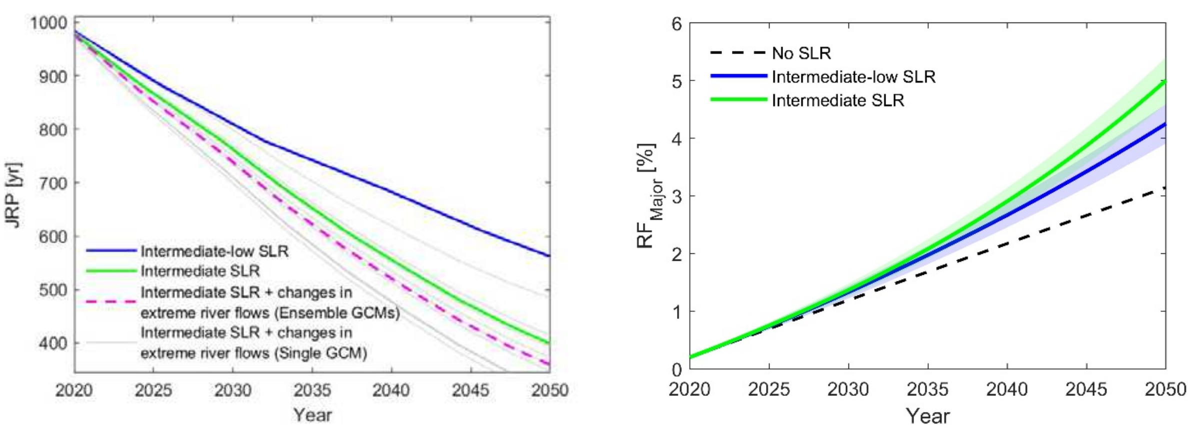

Figure B4-14

Fort Pulaski - Savannah River

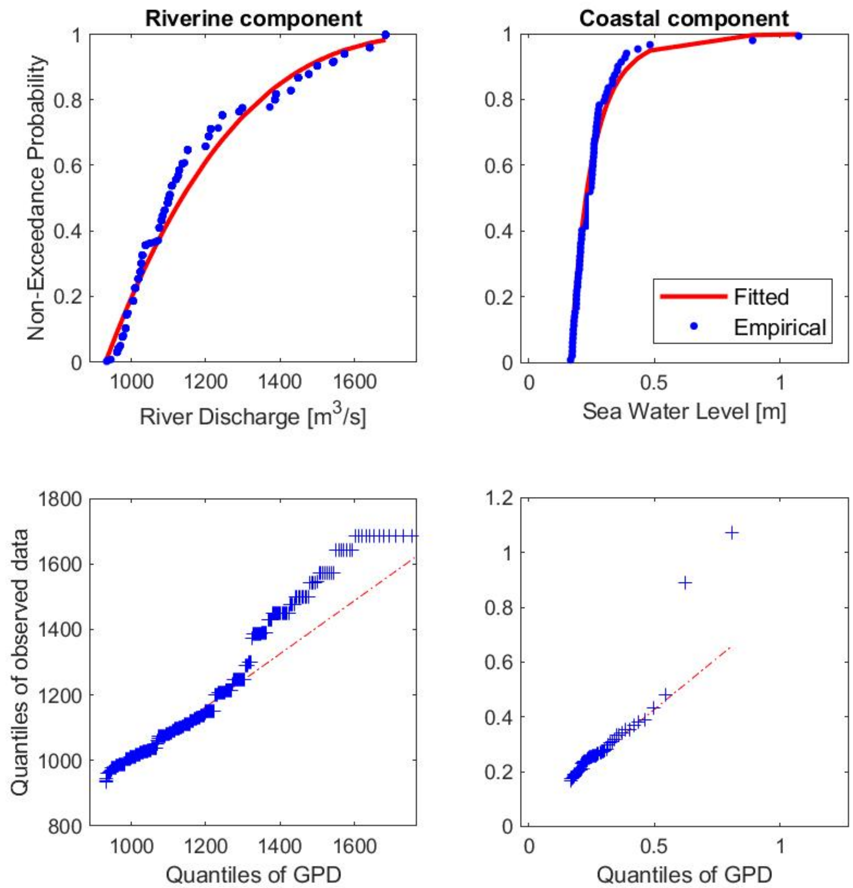

Figure B1-15

Fernandina Beach - Saint Marys River

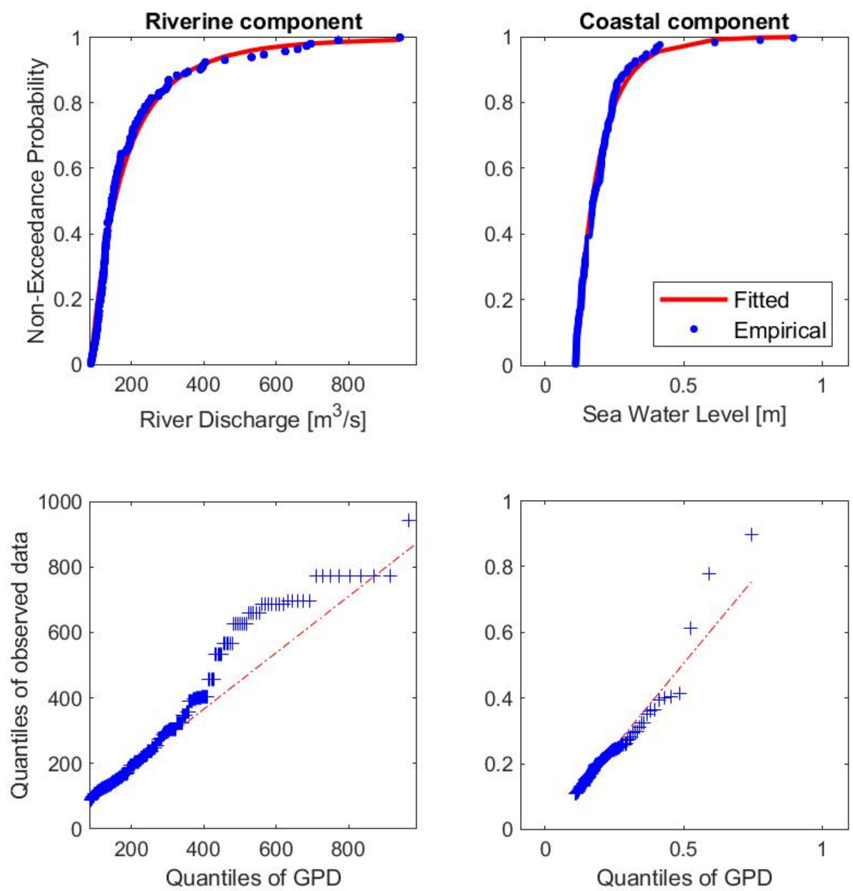

Figure B1-16

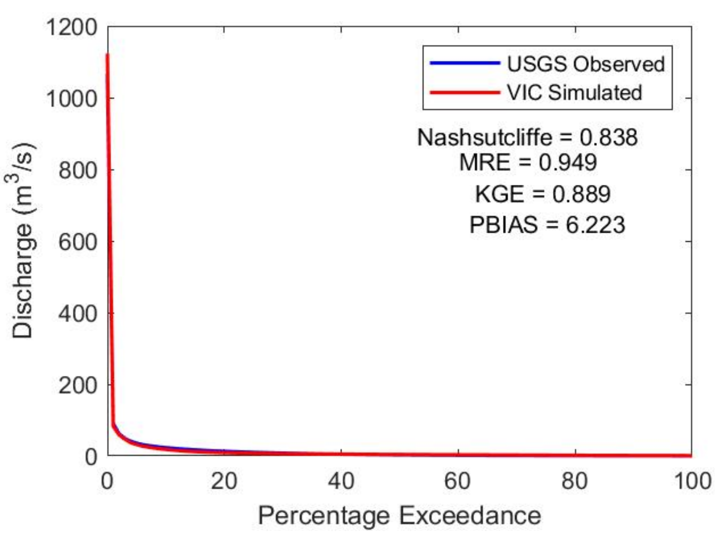

Figure B2-16

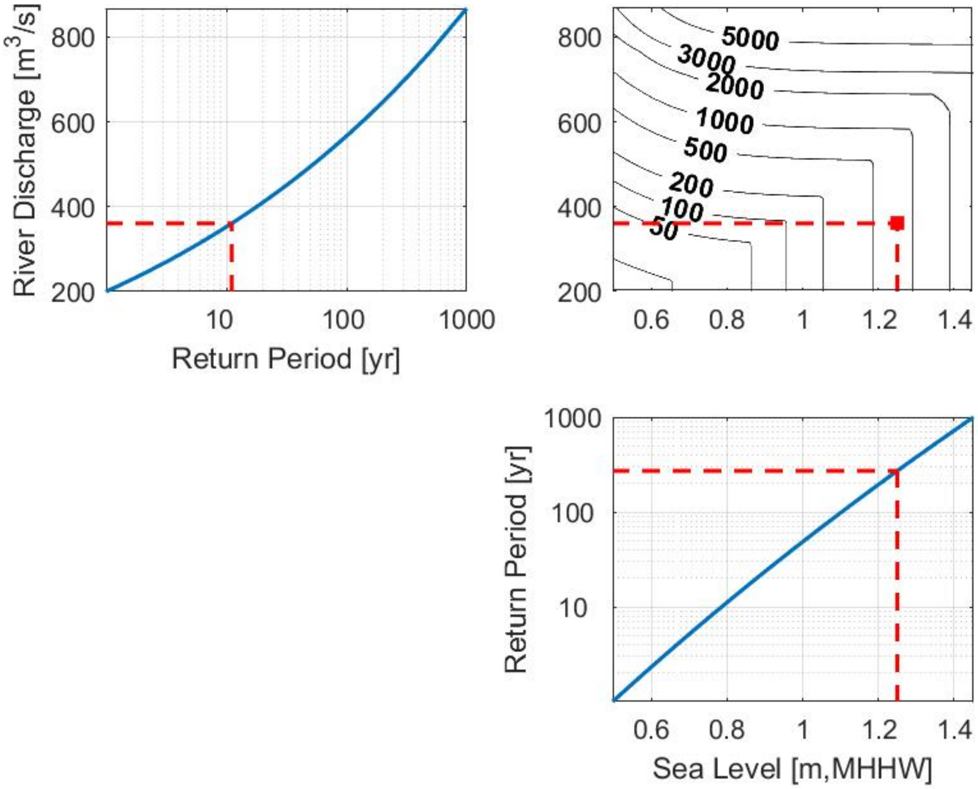

Figure B3-16

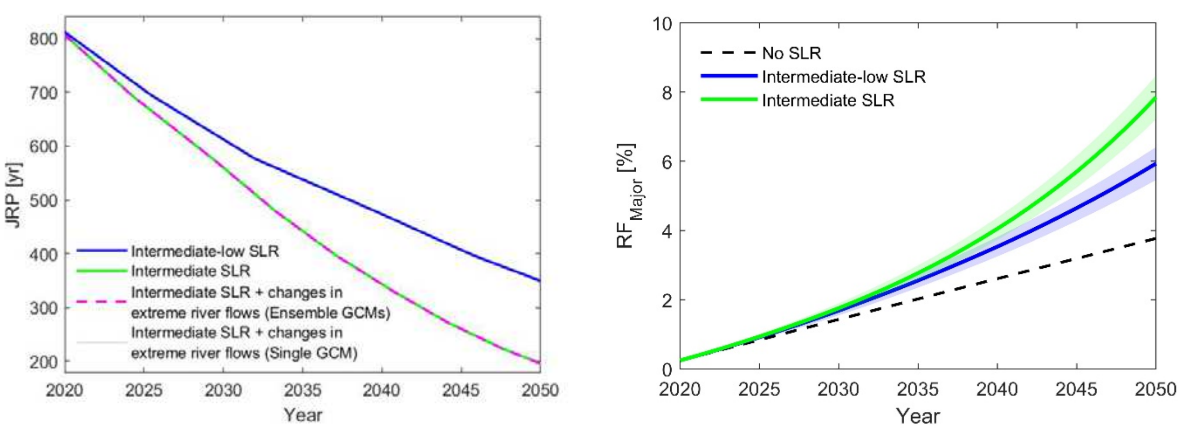

Figure B4-16

Apalachicola - Apalachicola River

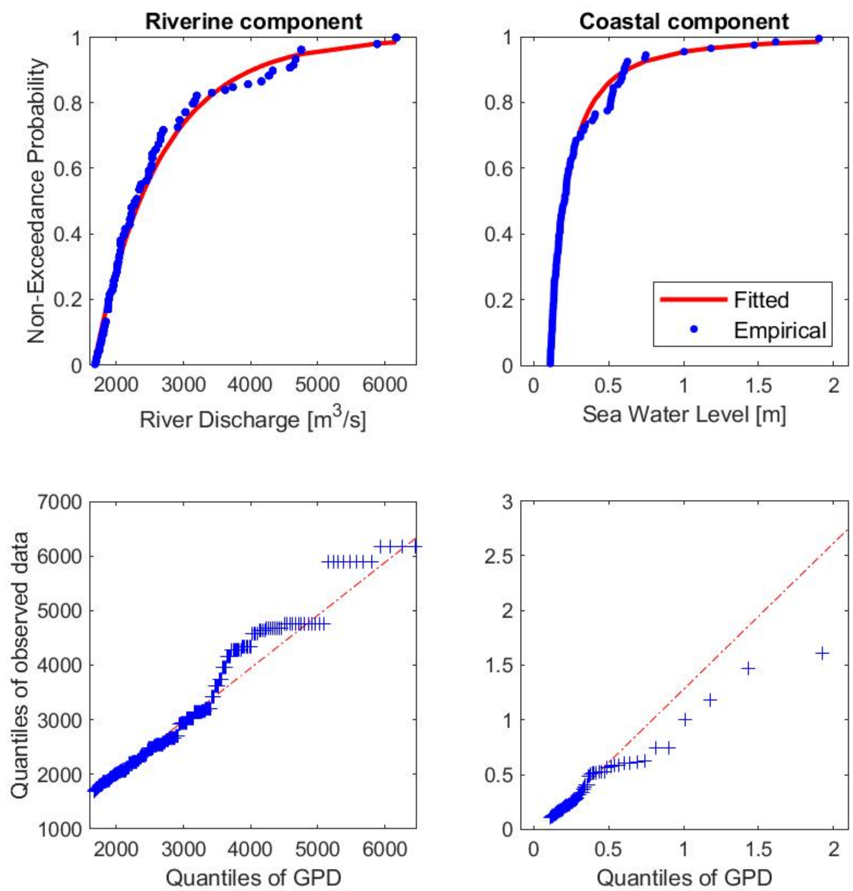

Figure B1-17

Panama City - Econfina Creek

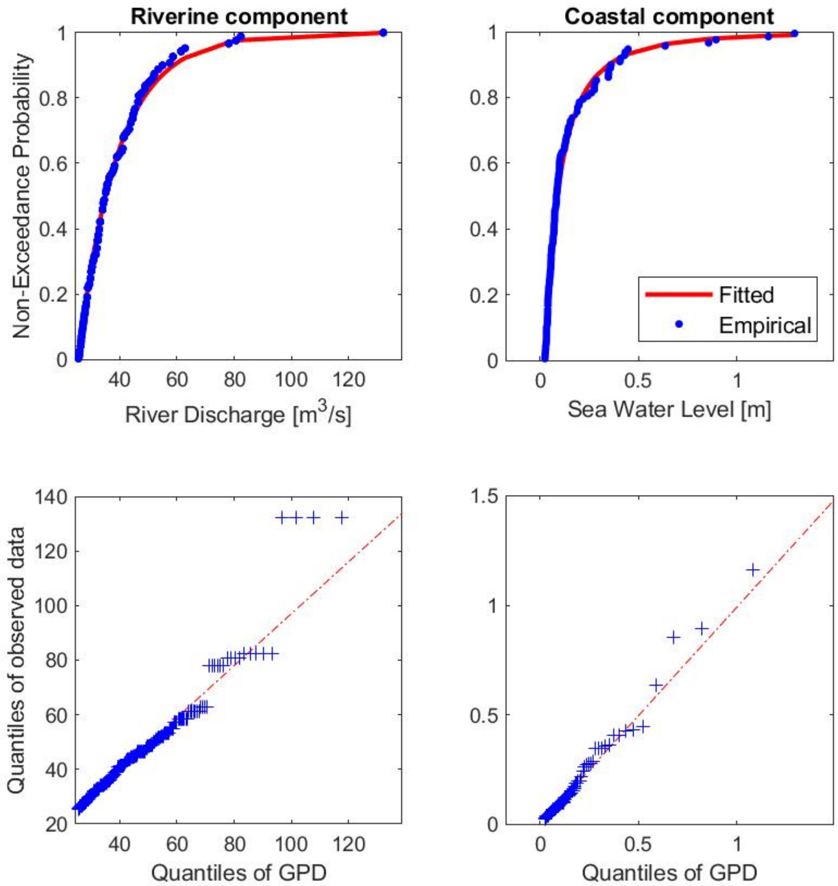

Figure B1-18

Pier 21 - Buffalo Bayou

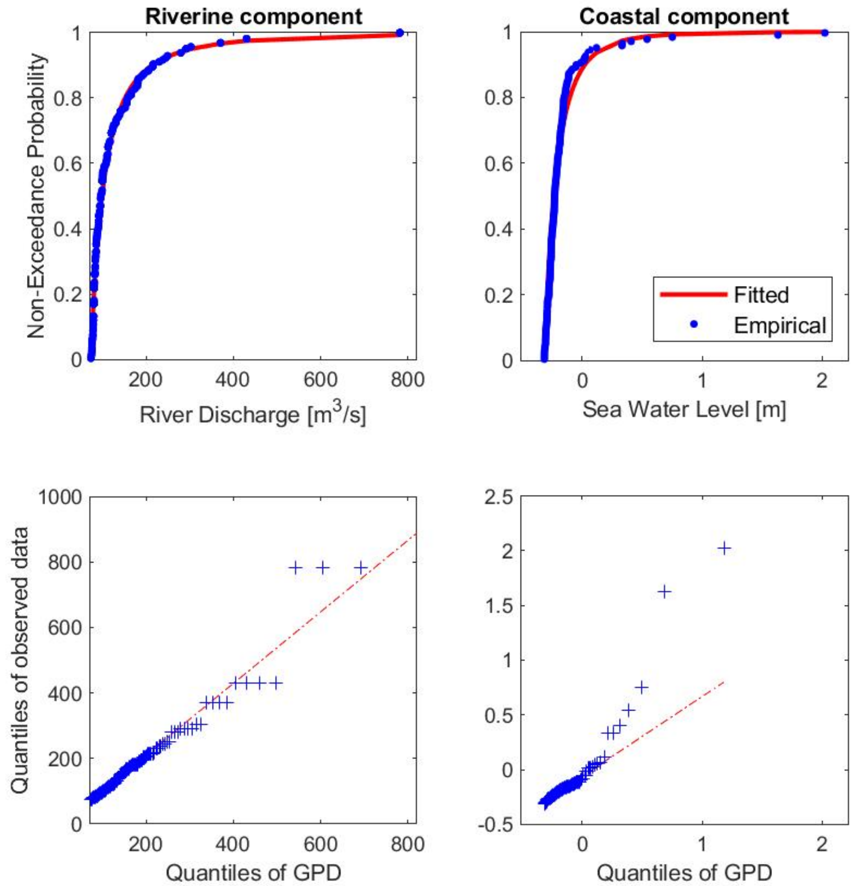

Figure B1-19

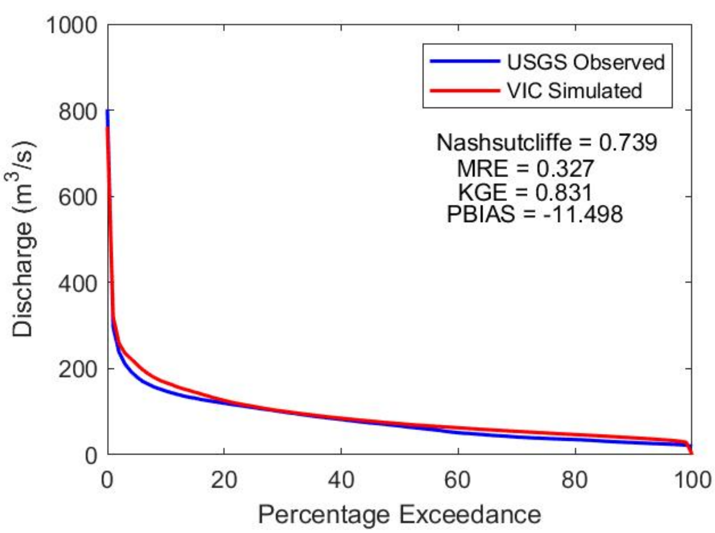

Figure B2-19

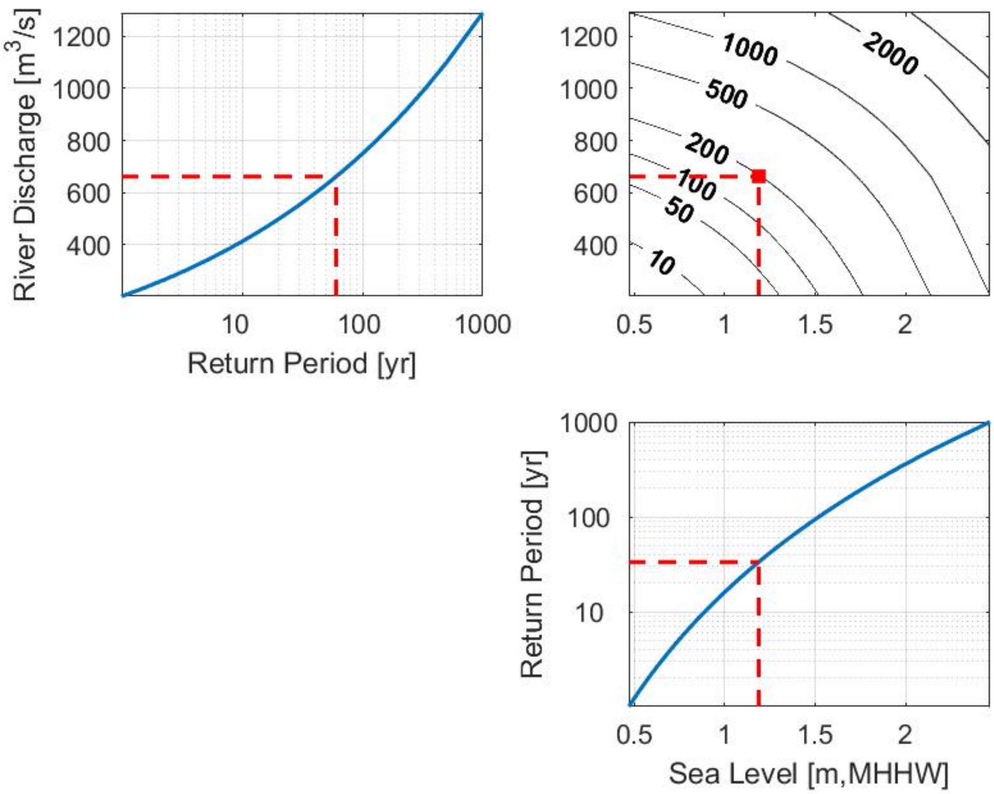

Figure B3-19

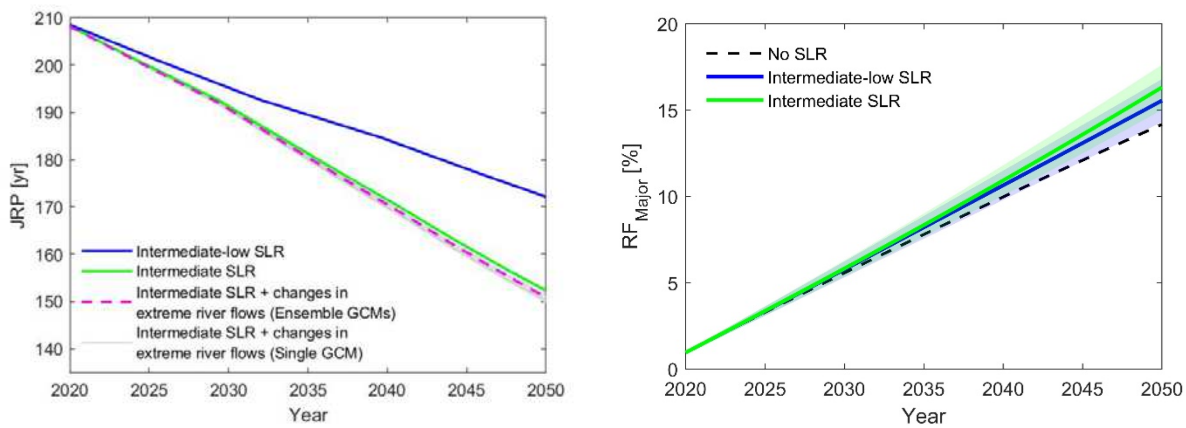

Figure B4-19

Rock Port - Mission River

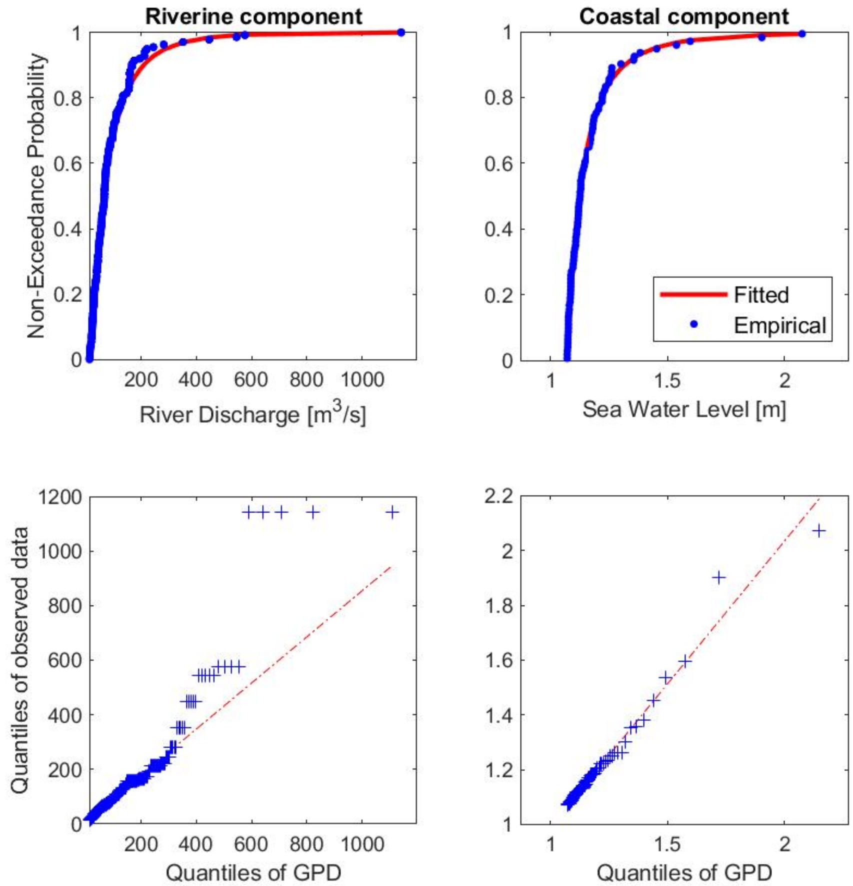

Figure B1-20

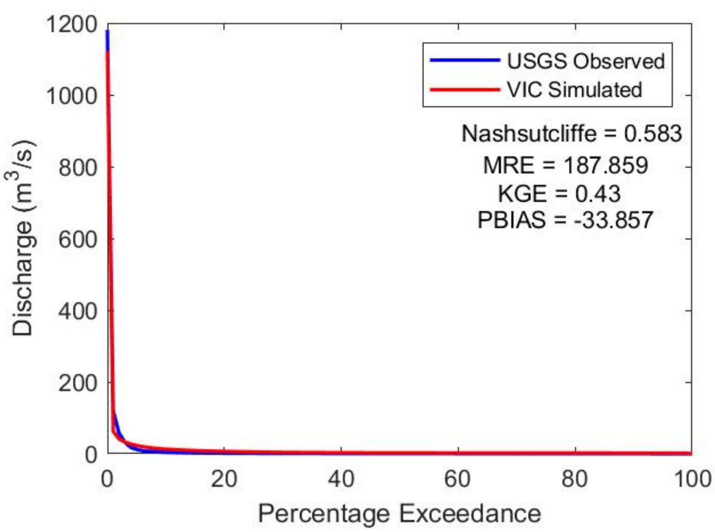

Figure B2-20

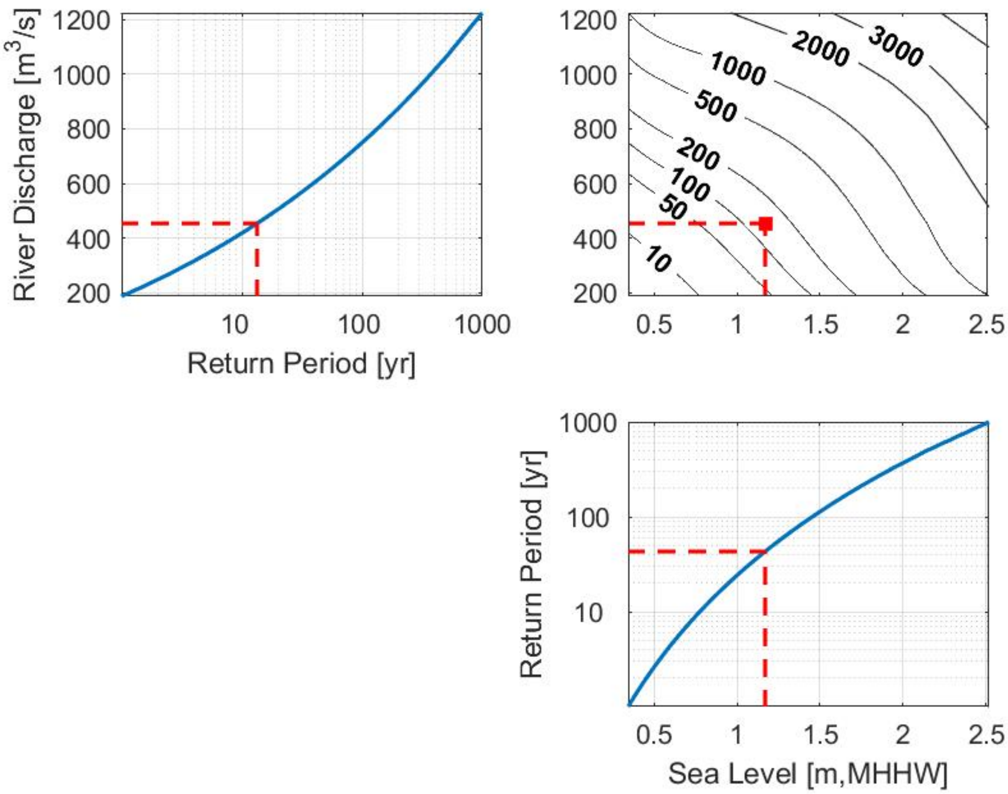

Figure B3-20

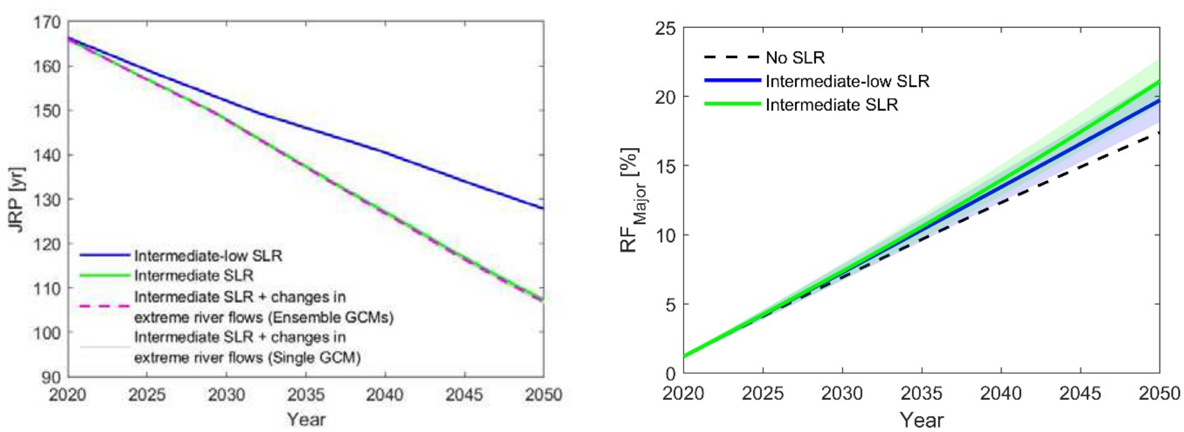

Figure B4-20

Santa Monica - Santa Clara River

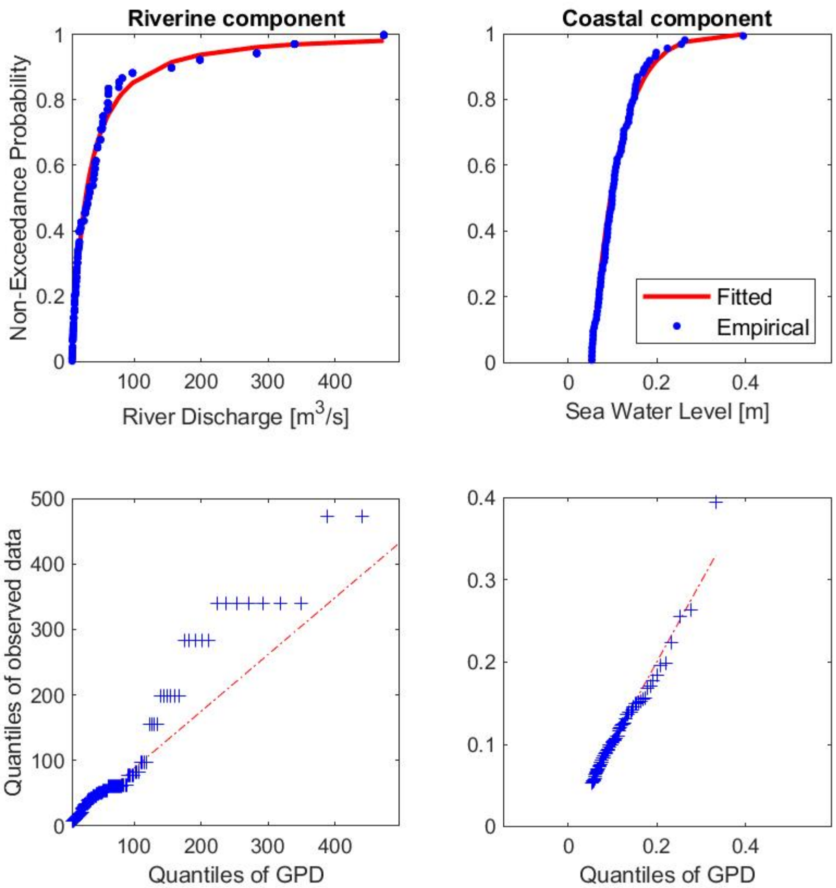

Figure B1-21

North Spit - Mad River

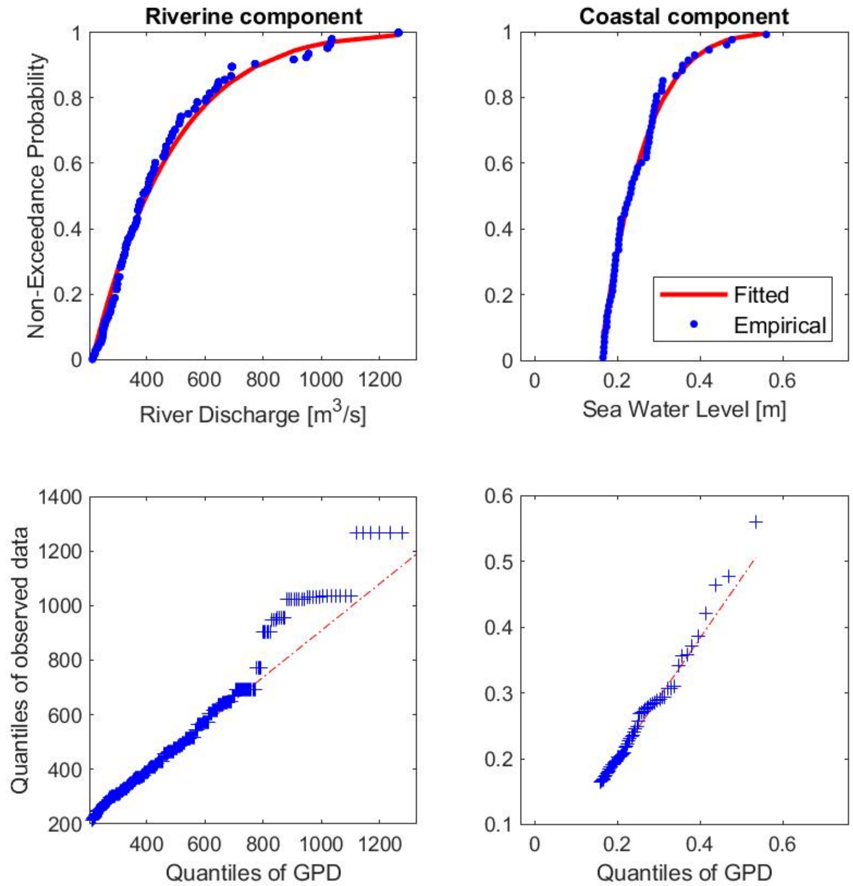

Figure B1-22

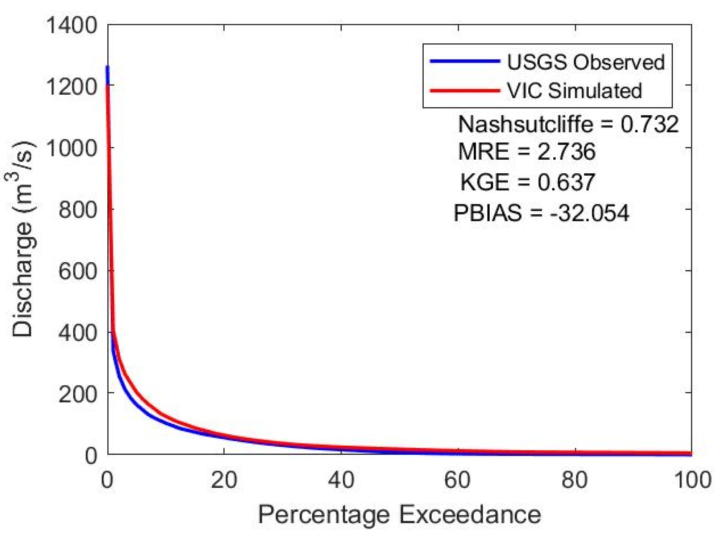

Figure B2-22

Charleston 2 - Umpqua River

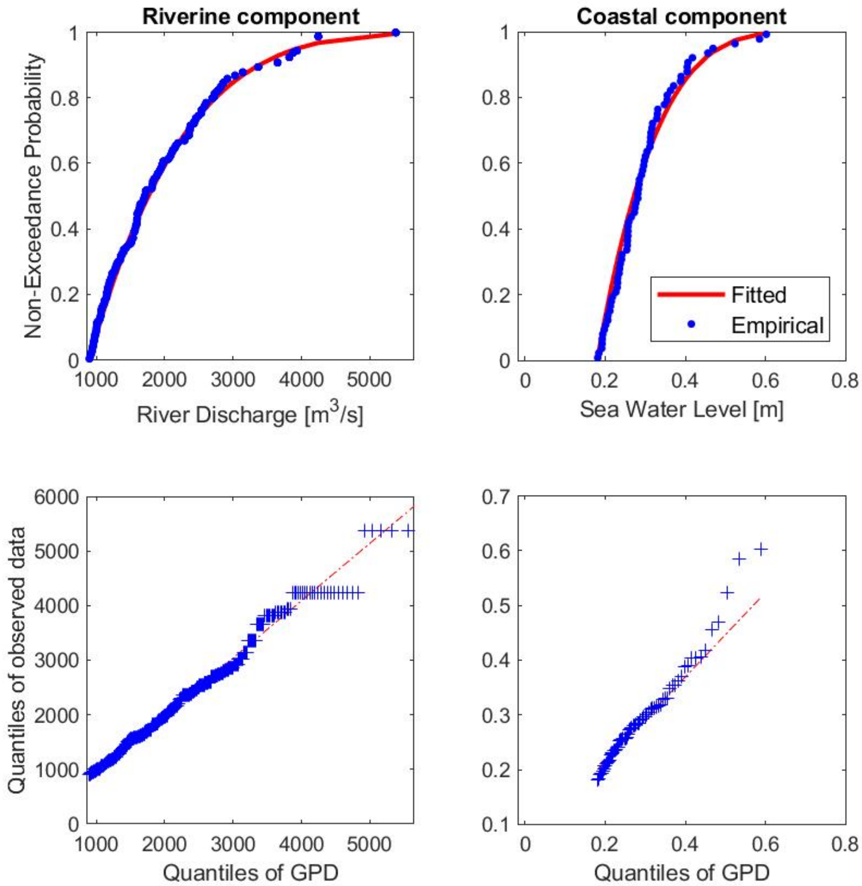

Figure B1-23

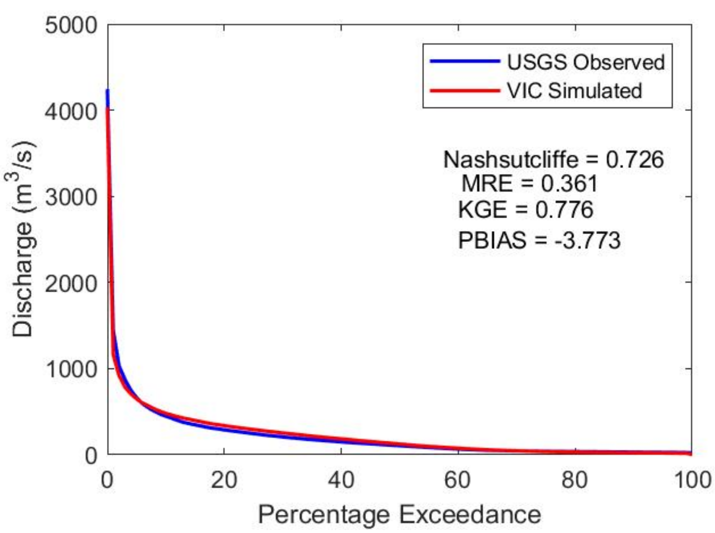

Figure B2-23

South Beach - Siletz River

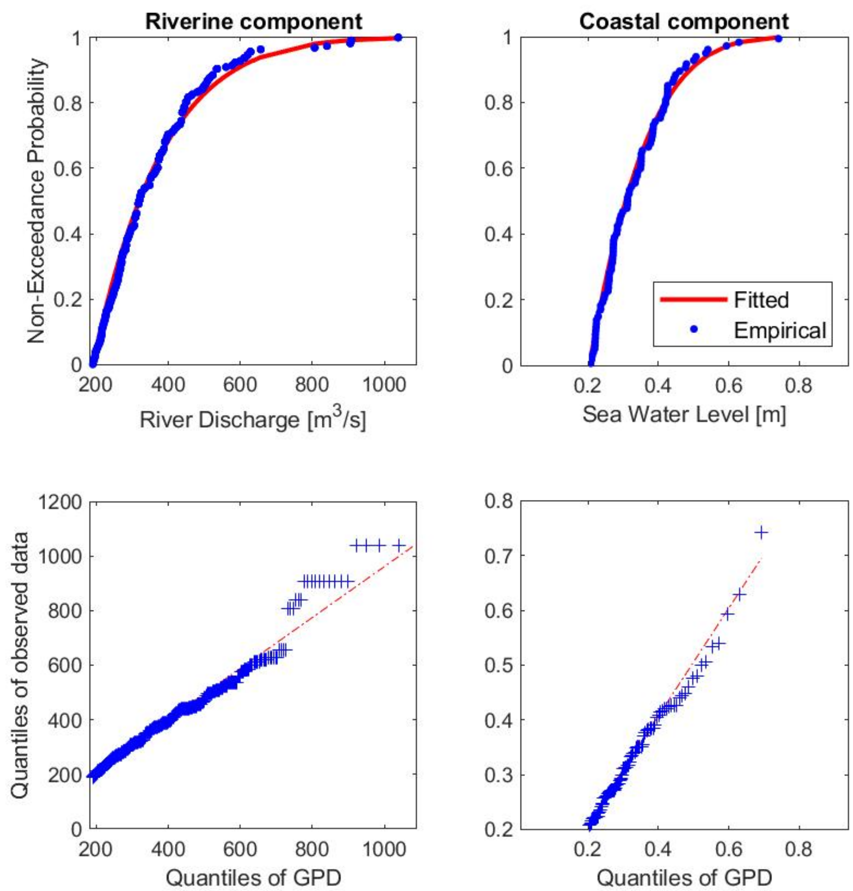

Figure B1-24

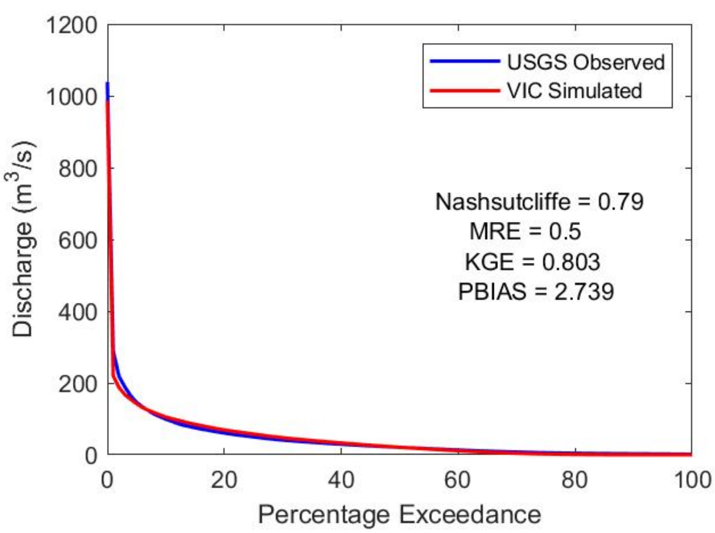

Figure B2-24

Toke Point - Willapa River

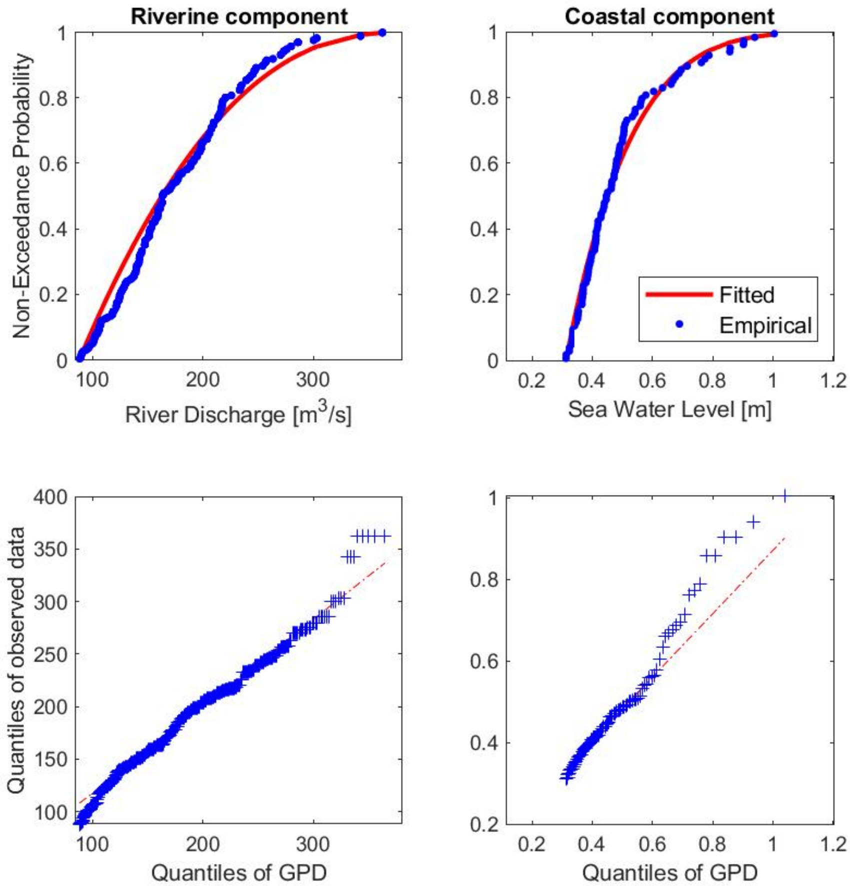

Figure B1-25

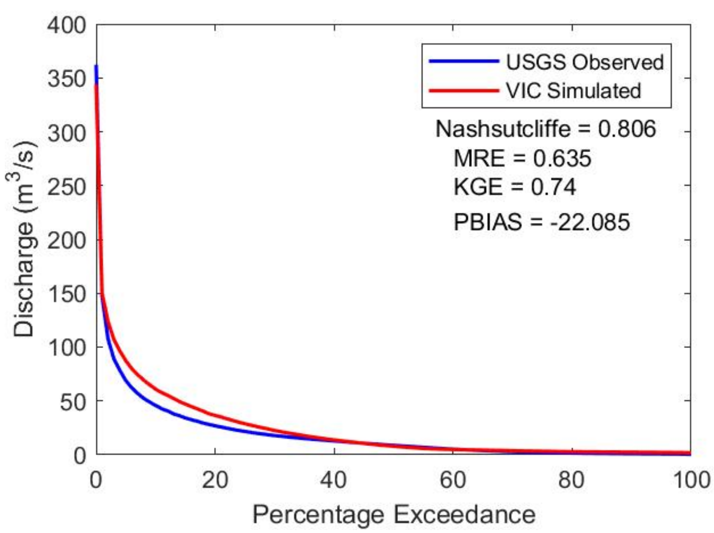

Figure B2-25

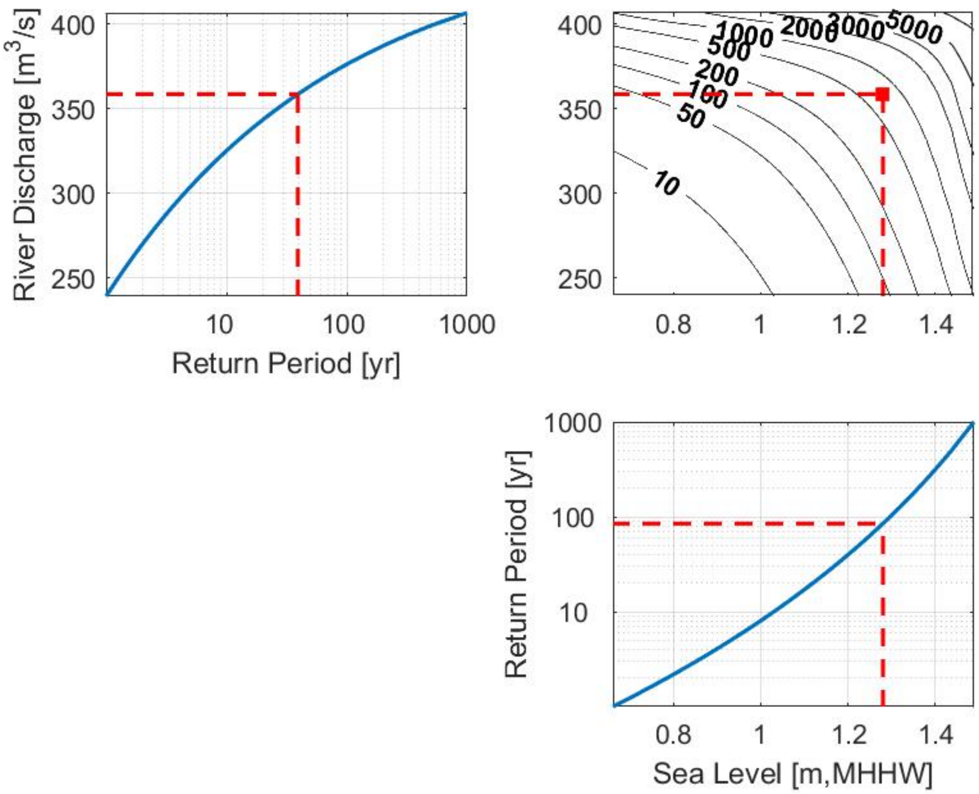

Figure B3-25

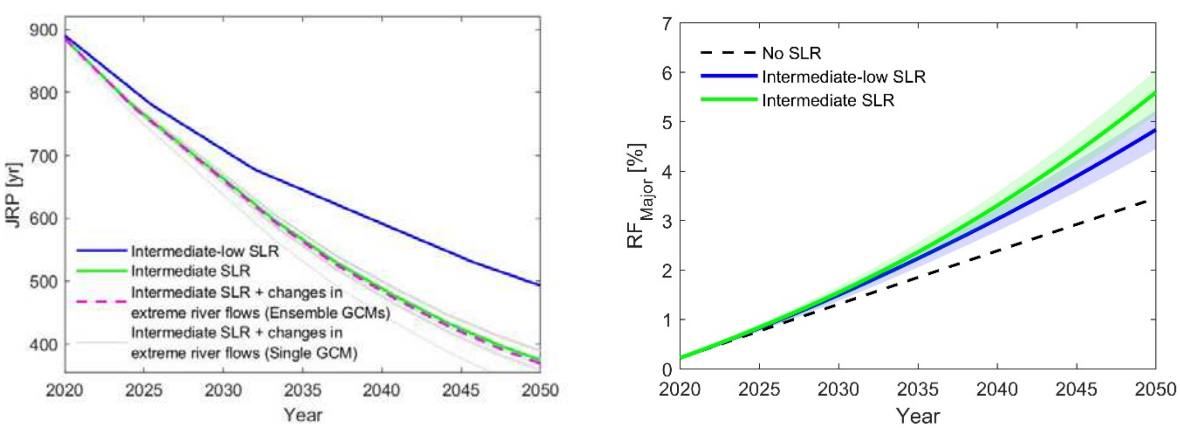

Figure B4-25

Seattle - Green River

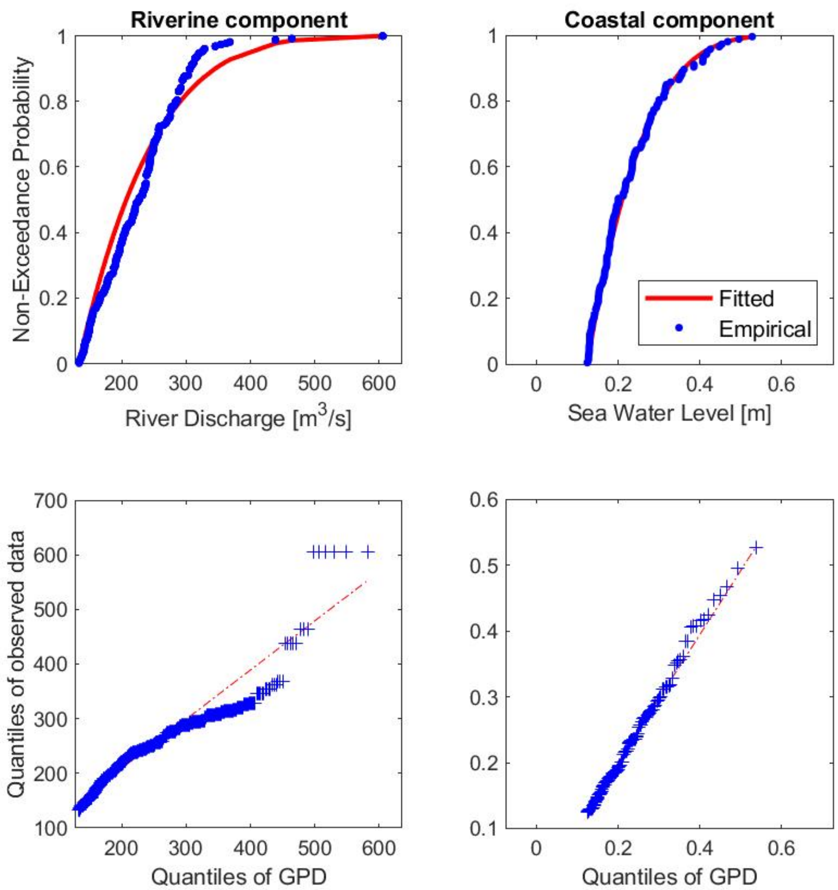

Figure B1-26

APPENDIX C

SUPPORTING INFORMATION FOR CHAPTER 5: GREEN STORMWATER INFRASTRUCTURE IN NEW YORK CITY: COMPLEMENTARY OR SUBSTITUTIVE?

C1. Storm scenarios

C1.1. Univariate Extreme Value Analysis

Extreme Value Analysis (EVA) was used with observed rain data to assign return periods to rain events. Hourly continuous observed rain data from all rain gauges within 15.5 miles of Central Park, plus others on Long Island (16 total) were downloaded from NOAA's National Climatic Data Center (NCDC 2016). Rain gauge years of operation vary, but the entire 16 rain gauge dataset covers a whole period of record from 1948 to 2013. All station-years of data were pooled together, and a sliding time window was used to sum the rain total depth for a specific duration time by moving hour by hour over the entire rain record.

EVA was performed separately for 1,3, and 24 hours rain durations. For each duration, the "peak" rain totals were identified throughout the record. "Peak" rain totals are the maximum rain totals for the duration, with no overlapping events allowed. Two common EVA distributions were tested, the Generalized Extreme Value (GEV) distribution and the Generalized Pareto Distribution (GPD). The GEV distribution was applied to annual maximum peak rain totals or the maximum rain totals for a duration in a given year. The GPD was applied to Peaks Over Threshold (POT) data, within the period of record.

Rain totals for each return period duration were used to create Intensity-Duration-Frequency (IDF) curves. Intensity is defined by the rain total divided by the duration, and frequency is defined by the return period.

C1.2. Bivariate Extreme Value Analysis

The joint probability of extreme precipitation and surge were quantified to create the scenario of compound flooding. The analysis only looks at compound events conditioned on the occurrence of extreme precipitation, as opposed to compound events conditioned on the occurrence of extreme surge, because this study is primarily a study of urban flooding.

Hourly rain data from all rain gauges in a radius of 15.5 miles around the Battery tide gauge site (14 total) were used to estimate the joint probability of extreme precipitation and storm surge. These gauge data were then averaged to estimate a spatial average. This focuses the analysis on synoptic rain events, as opposed to localized convective rain events, as the former are much more likely to be accompanied by storm surge (Wahl et al. 2015a). Hourly continuous storm surge data were used for the whole period of record (1928-2012) from the Battery tide gauge. The storm surge value was obtained from total water level by subtracting astronomical tide data created using harmonic analysis (Pawlowicz et al. 2002). We use the maximum surge during the rain event, departing from methods used in the Wahl et al. (2015) study that used maximum surge within a window of ±1 day, because the relatively small NYC sewersheds have very short recession times (e.g., minutes-to-hours).

Copula method was used to estimate the joint probability of compound extreme precipitation and surge (Salvadori et al. 2007, 2011, 2016a). Copulas are a powerful tool to analyze the dependence structure between multiple variates and to construct the multivariate probability distribution. The Multivariate Copula Analysis Toolbox (MvCAT) was used to perform joint probability analysis with a large set of 26 candidate copula models (Sadegh et al. 2017) and select the best copula model to fit the observed data. Return periods associated with co-occurring extreme precipitation and surge were calculated and the highest-likelihood event for each return period based on joint probability density were chosen.

C1.3. Offshore Sea Level Forcing for Tide and Storm Surge

All storm scenarios in this study are essentially forms of compound events, either including only rain and tide, or including rain, tide, and surge. The coupling of rain and these offshore water levels occurs through provision of time series of hourly offshore water level as open boundary conditions (OBCs) for the H&H model. Spatially and temporally varying water level data, from pre-existing regional hydrodynamic model simulations, were utilized for these OBCs. The use of the model results, from the New York Harbor Observing and Prediction System (NYHOPS), captures the spatial variation in tides around the city (Long Island Sound and Jamaica Bay have much larger tide ranges than Manhattan; Orton et al. 2016), as well as the non-linear enhancement of tide range by SLR in Long Island Sound (Kemp et al. 2017).

C1.4. Accounting for Climate Change

Climate change was represented for the 2050s time horizon with the high-end (90th percentile) estimates of future changes in sea level and rain intensity.

C1.4.1. Future precipitation

Two approaches were used to construct rain time series in a future climate, where the approach depends on the present-day time series. In both cases, we find realistic rain time series from the large catalog of historical simulations.

For rain intensities coinciding with present-day extreme events (greater than 5-yr return period), published IDF curves (Castellano and Degaetano 2017) were used. Rain time series for those future rain events were constructed identically to the present-day scenarios, namely the catalog of dynamically downscaled rain simulations was searched for time series matching the intensity and duration.

For a priori specified durations such as 1 in/hr, and generally common events, a quantile-matching approach was adopted to determine intensity scaling. The approach scales current quantiles to future quantiles. A recent downscaled climate simulation produced at the National Center for Atmospheric Research (NCAR, Liu et al. 2017) was used to provide future downscaled rain over the NYC region, and compare that with our historical downscaled rain catalog. The changes indicated by the Liu et al. (2017) dataset were used to "scale" precipitation time series like what the Liu et al. (2016) simulations indicate.

C1.4.2. Future sea level

For the future climate in the 2050s, a SLR projection of 30 inches above a baseline at 2000-2004 is applied. This is the NPCC 90th percentile projection (Horton et al. 2015). With this projection, the 2050s sea level is projected to be 29.1 inches NAVD88. This mean sea level is simply superimposed upon the offshore boundary condition water levels of tide or tide and surge. It should be noted that the "present-day" simulations incorporate a projection of the year 2018 mean sea level which is 1.7 inches NAVD88.

C2. Green Infrastructure System

Rain gardens (i.e., right-of-way bioswales, tree pits, bioretention) are vegetated or landscaped depressions designed with an engineered soil layer. These technologies promote infiltration of storm- water runoff into the underlying soil as well as increased evapotranspiration. In addition to direct rainfall, stormwater runoff from surrounding im- pervious surfaces, such as sidewalks and rooftops, can be directed into the rain garden to infiltrate into the ground or be taken up by plants.

Green roofs consist of a top vegetative layer that grows in an engineered soil on roof tops, which sits on top of a drainage layer. A green roof can be "intensive" with thicker soils that support a wide variety of plant growth, or "extensive" with a light layer of soil and minimal vegetation. Runoff is captured, stored on the roof, and slowly released through a drainage mat or is lost through evapotranspiration.

Permeable pavements (i.e., pervious concrete, porous asphalt) use a range of materials and techniques to allow water seepage through paving materials into the ground. Some pavement technologies include an underdrain to help drain the system where poor soils are present. Permeable paving can be used instead of traditional impermeable concrete or asphalt allowing for the use of parking/ driving areas for stormwater management.

Site-scale detention systems have similar functions to centralized storage tanks and tunnels but capture smaller volumes, up to tens of thousands of gallons of water. Site-scale detention systems can be deployed by both public and private entities and are typically placed underground. These systems are primarily implemented to store and slowly release stormwater into an existing sewer system. However, in some cases captured stormwater is retained and either allowed to infiltrate into native soils or used for either irrigation or other suitable purposes. Site-scale storage strategies examined in this study include subsurface drainage, blue roof, and rainwater harvesting systems.

Subsurface detention systems provide temporary, underground storage of stormwater runoff. However, these systems generally include capabilities for controlled infiltration. Additional detention volume can be gained via an open-bottom that can incorporate perforated pipe and stormwater chambers. These systems are primarily designed with a layer that stores water until it can infiltrate into the ground or it is slowly released into the sewer system. There are several types of subsurface detention systems including storage vault, gravel bed, perforated pipe and stormwater chamber systems. The choice of stormwater management system depends on site conditions and the preferences of developers for proposed projects. In this study, the design of subsurface systems was informed by the DEP's criteria and several other factors such as the available footprint area onsite, sewer elevation, and the pretreatment system.

Blue roofs temporarily store stormwater with various types of detention systems located on the roofs of buildings. Unlike green roofs, blue roofs do not have vegetation and are only used to capture rainwater. While blue roofs have similar hydrologic effects as green roofs, their co-benefits are limited. On the other hand, blue roofs have lower maintenance requirements than green roofs.

Cisterns and rain barrels are watertight receptacles designed to catch and store stormwater from roofs and other impervious surfaces for rainwater harvesting. Cisterns are often larger than rain barrels and can be located underground, at ground level, or on an elevated stand. Rain barrels are connected to the existing downspout of a roof and reuse the stormwater for watering plants and other landscaping or non-potable purposes.

C3. Stormwater Intervention Scenarios

C3.1. IS1: Current and Planned Distributed Infrastructure to 2035

C3.1.1. Combined sewer interventions

Combined sewer interventions included additional storage volume to reduce CSOs through publicly funded green infrastructure as well as existing regulated private on-site rules for combined sewer and those currently under evaluation. The storage volume of each added node was computed based on the constructed and planned GI dataset for NYC combined sewer subcatchments obtained from NYC DEP. Fig. S2 illustrates the location of GI assets that are implemented or planned and added to the H&H model with associated storage volume.

C3.1.2. Separate Storm Sewer Infrastructure

Distributed green practices in separate storm sewer areas were determined based on the municipal separate storm sewer systems (MS4) onsite retention rules that DEP is currently evaluating. These potential regulations would require privately developed or redeveloped lots of a certain size to capture 1.5 inches of rainfall. These are similar requirements as discussed above in combined sewers, however, these requirements lead to the implementation of green infrastructure within MS4 areas. Based on these stormwater rules under current evaluation, the total disturbed acres between 2021-2035 is estimated to be 1,105 acres. The storage volume that would be required to capture up to 1.5 inches of rainfall over the disturbed 1,105 acres was estimated to be 45 MG for the separate storm sewer systems.

This storage volume was distributed across the NYC systems based on the percent of total available MS4 area within each sewershed. First, the spatial distribution of new development or redevelopment acres was determined using MS4 area within each sewershed. Furthermore, the disturbed areas across the NYC sewersheds were compared to development patterns by water bodies to corroborate the procedure. The amount of MS4 area within the watershed boundary for each water body was determined using maps of watershed boundaries obtained from NYC green infrastructure 2018 annual report (NYC 2018). Finally, the required storage volume in each sewershed was determined by multiplying the total disturbed acres by 1.5 inches rainfall depth.

The estimated storage volume was evenly distributed across MS4 areas using the 100 ft by 100 ft grid in the respective sewersheds.

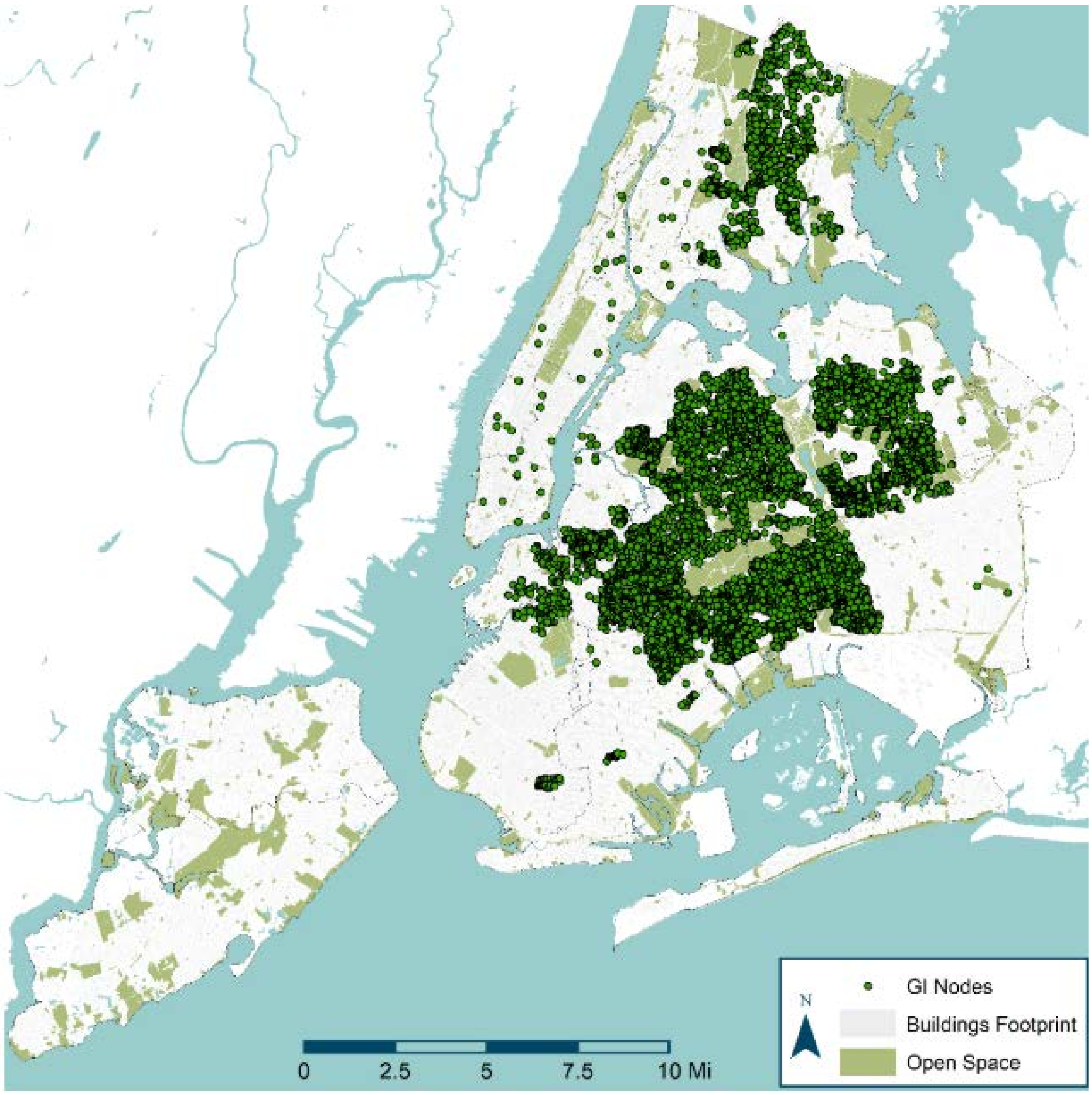

Figure C1. Map of the green infrastructure assets with known geospatial location

C3.3. Planned distributed infrastructure to 2050 and cloudburst systems (IS3)

C3.3.1. Combined Sewer Infrastructure

If the onsite water management threshold is lowered from 20,000 to 15,000 square ft, it is estimated that 2,280 acres citywide would be required to capture 1.5 inches of rainfall events, over the period of 2036-2050. The additional storage volume to accommodate this requirement is approximately 92.9 MG. This additional storage capacity was distributed across the city according to 1) the estimated disturbed land within the watershed boundaries of NYC water bodies of disturbed land; and 2) percentages of combined sewer area within each waterbody for each sewershed.

C3.3.2. Separate Storm Sewer Infrastructure

Lowering the onsite water management threshold in MS4 regions was investigated as well. The total amount of new/redevelopment that meets this criterion is estimated at a rate of 79 acres per year. Thus, an additional 1,185 acres are predicted to be developed from 2036 to 2050. Management of onsite water according to the regulations would require an additional 48.3 MG of storage across NYC. This estimated storage was distributed to sewersheds using the procedures described for onsite water management in IS1.

C3.3.3. Cloudburst Systems

Two different locations were selected to model cloudburst management. In the South Jamaica Houses, cloudburst management was applied to two blocks in the housing projects. The proposed project is estimated to manage 38,400 ft^3 of stormwater runoff for approximately 6 acres of the housing development. The second cloudburst management system was applied in the Astoria neighborhood, located southeast of Queensbridge Park in the Bowery Bay. The proposed project is estimated to manage 53,000 ft^3 of stormwater runoff.

C4. Co-Benefit Analysis

C4.1. Unit Volume Ratios for Different Intervention Technologies

A typical cross-section of green infrastructure contains a ponding layer above the ground surface, a media layer at the top of the intervention, with a storage layer directly beneath. By multiplying the depth of each layer by the porosity it is possible to determine what the storage of each intervention type is on a per area basis. Table C1 shows the volume to surface area ratios for prevailing green infrastructure systems in NYC.

Equation S1-1 and S1-2 show how to find the unit volume (V_U) of storage from various layers for different infrastructure interventions.

$$V_U = \sum \left(D_{layer} * \eta_{layer}\right) \tag{C1-1}$$

where $\boldsymbol{D_{layer}}$ and $\boldsymbol{\eta_{layer}}$ are depth and porosity of each layer, respectively.

$$V_U = SA * P * n \tag{C1-2}$$

where SA is the surface area of the roof, P is the rainfall depth, and n is the efficiency.

Subsurface Detention Systems have a unit volume ratio estimated to be 0.54-1.5 ft^3/ft^2 depending on the type of subsurface detention. The characteristics of the general subsurface of the system were assumed to have a depth of 4 ft with a gravel media porosity of 0.3. These were input into S1-1 to find the Volume/Area ratio to be 1.2 ft^3/ft^2.

For **Rain Gardens**, Equation S1-1 was used with the design specifications for open-graded stone and engineered soil. The depths of various layers in the system were determined from the design specifications as 3 ft and 1.5 ft for open-graded stone base and engineered soil, respectively. The porosity for these storage layers were assumed to be 0.3 and 0.33 for open-graded stone base and engineered soil, respectively. The summation of the characteristics of the different layers were input into Equation S1-1 to find the unit volume storage to be 1.9 ft^3/ft^2.

The unit volume ratio for **green roofs** was characterized using Equation S1-1 with the design specifications for engineered soil, available ponding, and moisture retention fabric. The depth of the engineered soil media and moisture retention fabric were assumed to be 4 inches and 0.25 inches, respectively. The porosity for these storage layers were assumed to be 0.33 and 0.385, respectively. The ponding layer was assumed to be 1 inch. The summation of the characteristics of the different layers were input into Equation S1-1 to find the unit volume storage to be 0.2 ft^3/ft^2.

Blue roofs' unit volume ratio were characterized using Equation S1-1 with the design specifications for gravel storage layer and ponding: There is no media layer for blue roofs hence the volume was determined based on gravel storage depths and available ponding allowed above the roof. According to structural analysis and building code, the required storage layer depths of a blue roof are a minimum of 2 inches and a maximum of 4 inches. Additional assumptions included a gravel storage layer of 3 inches with porosity of 0.3 and a ponding layer of 1 inch. The summation of the characteristics of the different layers were input into Equation C1-1 to find the unit volume storage to be 0.16 ft^3/ft^2.

The unit volume ratio for **rainwater harvesting** systems comes from the expected height of rainwater harvesting systems in NYC. A traditional 60-gallon barrel has a 2 ft diameter. Tanks for rainwater harvesting systems in NYC typically range in size from 300 to 1000 gallons but can be as small as 55 gallons and as big as 10,000 gallons. The amount of water that can be harvested varies on the size of the roof and was calculated using Equation C1-2. For estimations of available volume, NYCDEP assumes capturing the first inch of rainfall and an efficiency of 0.75.

The **permeable pavement** unit volume ratio was characterized using Equation C1-1 for permeable pavements including a surface layer, a choker course, and a base or sub-base layer. There are three types of surface layers: permeable pavers, pervious concrete, and porous asphalt. The depths of these layers depend on the type and feasibility for the system. The depth of the open graded base layer was assumed to be 4 ft. The porosity of the base layer was assumed to be 0.33. The unit volume of storage was determined to be 1.32 ft^3/ft^2.

Table C1**.** The volume to surface area ratios for prevailing green infrastructure systems in NYC.

Green Infrastructure Type	Volume/Area Ratio (ft^3/ft^2)
Blue Roof	0.16
Green Roof	0.2
Permeable Pavement	1.32
Rain Garden	1.9
Rainwater Harvesting	4
Subsurface Detention Systems	1.2

C4.2. Green Infrastructure Calculator Co-benefit Equations

Urban Heat Island Mitigation

Thermal properties of common urban surfaces can lead to warmer air temperatures. By using natural surfaces that are cooler and reflect more solar radiation, green infrastructure can help reduce urban heat island effects (UHIE). UHIE was calculated as the percent reduction of heat absorption capacity provided by changing the underlying surface material and distributed across the sewershed. The NYC Green Infrastructure Co-benefits Calculator calculated the percent reduction of UHIE from the difference in albedo of the initial paved area and the added albedos of the components of the green infrastructure project (Yamamoto 2006). This co-benefit is calculated for the following practices: Green Roof, Porous Concrete, and Rain Garden. These practices are chosen because they are replacing darker asphalt that is on roofs and sidewalks. The following equation shows the way UHIE is measured.

$$UHIE\ reduction(\%) = UHIE\ Reduction\ Factor(\%) * \frac{Area\ of\ practice}{Sewershed\ Area}$$

The area of practice changes per scenario and the sewershed area is the total area of the sewer- shed that the practice is being added to. Table C2 shows the UHIE Reduction Factor for each practice.

Table C2. The urban heat island effects (UHIE) Reduction Factor

Practice	UHIE Reduction Factor (%)
Green Roof	12
Porous Concrete	44
Rain Garden	14

Reduced Wastewater Treatment (WWT)

By reducing the amount of runoff that enters the sewer system, green infrastructure reduces the amount of water reaching NYC's treatment plants, thereby reducing the amount of chemicals, energy, and costs associated with treating that water. The calculation of the reduced treatment needs was based on the saved money from the amount of untreated water removed. This co-benefit is seen throughout all the infrastructure interventions. The following equation shows the monetary value of wastewater treatment needs.

$$\text{Reduced WWT}\left(\$/_{yr}\right) = 0.6 * 0.0003 * Annual\ Volume\ Controled * 7.48052$$

Where 0.6 is the portion diverted from treatment plant, $0.0003 is the treatment cost per gallon, 7.48052 is the conversion from cubic ft. to gallons.

Carbon Sequestration

Carbon Sequestration is associated only with practices that have vegetated surfaces to promote natural interactions with the environment. The only practices in this study that fit this criteria are Rain Gardens and Green Roofs. Below equations are the Carbon Sequestration equations for Rain Gardens and Green Roofs, respectively.

$$CD_{\text{Sequestered}}(Rain\ Garden) = (SH_{rate} * SH_{area} + S_{rate} + SH_{area}) * ({}^{CO_2}/_{C})_{rate}$$

$$CD_{\text{Sequestered}}(Green\ Roof) = (GR_{rate} * GR_{area}) * ({}^{CO_2}/_{C})_{rate}$$

Where $CD_{\text{Sequestered}}$ refers to carbon dioxide sequestered per year (lbs/year), SH_{rate} is Shrub and Herbaceous Carbon Sequestration Rate (lbs/sq. ft.*year), SH_{area} is shrub and herbaceous area (sq. ft.), S_{rate} is soil carbon sequestration rate (lbs/sq. ft.*year), GR_{rate} is green roof carbon sequestration rate (lbs/sq. ft.*year), GR_{area} is green roof area (sq. ft.), $({}^{CO_2}/_{C})_{rate}$ is equivalence rate of atomic weight from C to CO2=2.67. Table C3 shows the sequestration rate values for the different interventions.

Table C3. The sequestration rate values for the different interventions

Infrastructure Intervention Sequestration Rate (lb C/year/ft2)	Annual Capture Ratio
Soil Sequestration Rate	0.14
Shrub and Herbaceous Sequestration	0.02
Green Roof Sequestration Rate	0.07

Improved Air Quality

The analysis of improved air quality involves the pollutant reduction of 5 different pollutants: ozone, PM10, NO2, SO2, and CO. Only infrastructure interventions with vegetative surfaces reduce pollutant concentrations through various mechanisms. The only technologies for this study that improve the air quality by reducing air pollutant concentrations are green roofs and rain gardens. The following equations show the way air pollutant reduction is measured for rain gardens and green roofs.

$$P_{r,x} = RG_{area} * RG_{RR}$$

Where $P_{r,x}$ denotes "x" type of pollutant removed (lb removed/yr), RG_{area} is rain garden area (sq. ft.), and RG_{RR} is Reduction Rate of "x" pollutant from rain garden.

$$P_{r,x} = GR_{area} * GR_{RR}$$

Where $P_{r,x}$ denotes "x" type of pollutant removed (lb removed/yr), GR_{area} is rain garden area (sq. ft.), and GR_{RR} is Reduction Rate of "x" pollutant from rain garden.

Stormwater Jobs

Stormwater Jobs refer to the amount of jobs that are supported each year from the construction and maintenance of infrastructure interventions. The following are the interventions where information on maintenance and construction costs were found: Blue Roof, Green Roof, Porous Asphalt, Porous Concrete, and Rain Garden. The following equation shows the characterization of number of jobs per implementation of each intervention type.

$$\text{Jobs supported } \left({}^{jobs}/_{yr}\right) = \left(Construction\ Cost\ \left({}^{1}/_{ft^2}\right) + Maintenance\ Cost\ \left({}^{1}/_{yr * ft^2}\right) * years\right) * \frac{Area\ of\ intervention}{Salary\ of\ Stormwater\ Worker}$$

Where, years is the number of years that each intervention requires maintenance (25 years), Salary of stormwater worker- \$58,824 in 2012 according to the NYCDEP Co-benefits Calculator, Area of intervention is variable based on input for each sewershed and scenario. Table C4 shows the construction and maintenance costs for the various interventions.

Table C4. The construction and maintenance costs for the various interventions

Intervention	Maintenance Cost per year (\$/sq.ft.)	Construction Cost (\$/sq.ft)
Blue Roof	1	16
Green Roof	1	21
Porous Asphalt	1	20
Porous Concrete	1	20
Rain Garden	1.46	120